UNIVERSITY OF LIVERPOOL

Investigating the role of human umbilical mesenchymal stromal cells as therapies in a model of renal IRI in different mouse strains

Thesis submitted in accordance with the requirements of the University of Liverpool for the degree of Doctor in Philosophy

By Ioana-Roxana Martinas

March, 2023

Abstract

Acute kidney injury (AKI), a common complication in hospitalised patients, has been associated with a high mortality rate as well as progression to chronic kidney disease and end-stage renal failure. AKI does not have a distinct pathophysiology as the disease can be brought about by different insults from nephrotoxicity and sepsis to surgical procedures. Regardless of the initial cause, AKI is characterised by a reduction in blood flow to the kidneys and subsequent hypoxia, processes which are associated with inflammation and immune system activation. Macrophages are highly versatile cells of the immune system, ubiquitous in all tissues, and have been identified to play a central role in both the injury phase and the subsequent resolution of inflammation in animal models of kidney disease. Despite recent advances in medical treatment, currently, there is no cure for AKI, and the disease is managed with fluid therapy, dialysis and ultimately, transplantation.

Over the last two decades, extensive research done within the fields of regenerative medicine and pre-clinical research has proposed mesenchymal stromal cells (MSCs) as the main therapy for the treatment of various inflammatory diseases, including AKI. MSCs have become an attractive tool for cell-based therapies due to their potent immunosuppressive and immunomodulatory functions with effects on both innate and adaptive immune cells, including monocytes and macrophages. Nevertheless, the precise mode of action of these therapies is still largely unknown.

The work in this thesis aimed to characterise and compare the injury response to bilateral renal ischaemia-reperfusion injury (IRI), and on this basis, characterise and compare the regenerative response to cellular therapies following bilateral renal IRI in three different mouse strains.

Throughout all the experiments within this thesis I have demonstrated that bilateral renal IRI leads to strain-dependent responses. I have employed a series of experiments that assessed renal function, weight, macrophage levels in kidneys and spleens, and cytokine levels in plasma and kidneys to characterise and compare the effect that bilateral renal IRI has on three different mouse strains – BALB/c, C56BL/6 albino and CD1. Importantly, the application of human umbilical cord (hUC) MSC therapies failed to result in an efficacious response in ameliorating kidney injury, regardless of mouse strain. Despite this observation, I was able to

demonstrate that hUC-MSC treatment can marginally modulate macrophages in kidney and spleen, and influence cytokine levels in the kidney. However, these effects were not replicated across the three strains and displayed high inter-strain variability. Further work is required into the mode of action of MSCs so as to better replicate the results seen in pre-clinical studies and to translate these into the clinic.

Acknowledgements

I would like to express my gratitude to my supervisors, Dr. Bettina Wilm, Dr. Patricia Murray and Dr. Neill Liptrott, for offering me the opportunity to undertake this work. Their confidence in me as well as their guidance, expertise and encouragement have been invaluable and have helped shape me not only academically but also personally. I am fortunate to have been able to work under their supervision and mentorship, and their feedback and constructive criticism have been essential in helping me develop not only as a professional but also as an individual.

The work and data produced in this thesis is the result of much collaboration, between not only my supervisors but also the wider research team at the University of Liverpool. I would like to express my gratitude to Dr Rachel Harwood for taking the time to teach me how to perform the key techniques that I have used throughout this thesis at the beginning of my PhD, such as the GFR measurements, the surgical procedure and dissection. I would also like to thank Dr Thomas Wilm for the constant support and guidance he has given me throughout my PhD, from teaching me key techniques on fluorescence microscopy to our collaboration on several experiments where we divided the work in order to increase efficiency and implement the 3Rs.

Furthermore, this research would not have been possible without Dr Tamiris Borges Da Silva, Dr Ana Muniz Garcia, and Dr Francesco Amadeo who have prepared the MSCs and PBS samples for IV injection (described in this work) on the day of the R-IRI surgery while I was performing the surgery, as the cells had to be administered within 3h of collection.

My heartfelt thanks also go to Dr Sandra Cachinho and Dr Christopher Law from the Cell Sorting and Isolation Facility at the University of Liverpool for helping me come up with a gating strategy and subsequently analyse my flow cytometry samples as I was not able to complete the training to use the facilities due to the imposed COVID-19 restrictions. Chapter 4 would not have been possible without them.

I would also like to thank the animal technicians at the Biomedical Sciences Unit, University of Liverpool – Edyta Kijak, Katharine Gittins, Sarah Roper and Esther Mokori – for their continuous help and support with the surgical procedure as well as their dedication to the animals' wellbeing.

I would also like to thank Louise, Katherine and Tamiris who have been an integral part of this journey for their friendship, continuous encouragement, and comfort. There have been some many moments when I have wanted to give up but you have always been ready to provide a shoulder to lean on and invaluable advice that have helped me reach the finish line.

Finally, I would like to thank my mother who has always been my strongest advocate, an unwavering source of support and inspiration throughout my life. I am grateful for the sacrifices you have made to ensure my happiness and success, as well as your unconditional love and continuous confidence in me. Thank you for instilling in me the belief that I can be anything I want as long as I put my mind to it, that anything is possible with hard work and determination. Mum, I would not be here today if it were not for your endless support. This thesis is dedicated to you.

Table of Contents

List of Figures

List of tables

Abbreviations

A

alb – albino

AKI – acute kidney injury

ATP – adenosine triphosphate

B

BUN – blood urea nitrogen

b.w. – body weight

C

CKD – chronic kidney disease

COPD – chronic obstructive pulmonary disease

D

DC – dendritic cells

DCT – distal convulated tubule

DMSO – dimethyl sulfoxide

E

ECM – extracellular matrix

ESRD – end-stage renal disease

eNOS – endothelial nitric oxide synthase

F

FBS – foetal bovine serum

FGF – fibroblast-growth factor

G

GFR – glomerular filtration rate

GVHD – graft versus host disease

H

HGF – hepatocyte growth factor

HLA-G – human leukocyte antigen-G

hUC-MSC – human umbilical-cord mesenchymal stromal cell

I

IRI – ischaemia-reperfusion injury

ICAM-1 – intercellular adhesion molecule-1

IDO – indoleamine 2,3-dioxygenase

IL – interleukin

iNOS – inducible nitric oxide synthase

IRI – ischaemia-reperfusion injury

K

KIM-1 – kidney injury molecule-1

M

Mϕ – macrophage

MCP-1 – Monocyte chemoattractant protein-1

MMP – matrix metalloprotease

MSC – mesenchymal stromal cell

N

NGAL – neutrophil gelatinase-associated lipocalin

NAG – N-acetyl-ß-D-glucosaminidase

NF-κβ – nuclear factor κβ

NK cells – natural killer cells

O

Oct4 – octamer-binding transcription factor 4

P

PDGF – platelet-derived growth factor

PFA – paraformaldehyde

PGE2 – prostaglandin E2

R

R-IRI – renal ischaemia-reperfusion injury

RRT – renal replacement therapy

S

sCr – serum creatinine

SEM – standard error of the mean

Sox2 – SRY-box 2

STAT – signal transducer and activator of translation

T

TGF – transforming growth factor

U

UUO - unilateral urethral obstruction

V

VEGF – vascular endothelial growth factor

VCAM-1 – vascular cell adhesion molecule-1

Chapter 1

Introduction

1. Introduction

1.1. Anatomy and physiology of the renal system

Mammals have two bean-shaped kidneys located posteriorly on either side of the vertebral column, between the peritoneum and the posterior abdominal wall, with the right kidney found slightly higher than the left due to the presence of the liver. The kidney is surrounded by three thin tissue layers (i.e., a renal fibrous capsule, an adipose capsule and the renal fascia) that protect the organ from damage and stabilise its position within the abdominal cavity. A sagittal section of the kidney shows two distinct areas (*Figure 1.1*): the renal cortex or the outer, and the renal medulla or inner portion of the kidney . Nephrons are the functional units of the kidneys, and extend from the renal cortex through to the renal medulla. They are divided into two main structures (*Figure 1.2*): the renal corpuscle and the renal tubule. The renal corpuscle is further subdivided into the glomerulus and the surrounding glomerular (Bowman's) capsule whose main function is blood plasma filtration. Blood and solutes flow into the kidneys through the renal artery which branches out into afferent arterioles that surround the glomerulus; from here, unfiltered fluids exit via the efferent arterioles which form the venous system of the kidney and branch out into peritubular capillaries. Fluid passes though the capillary network of the glomerulus and is filtered by the Bowman's capsule before passing through the renal tubule. The renal tubule is divided into three regions: the proximal convoluted tubule (PCT; attached to the glomerular capsule), the loop of Henle and the distal convoluted tubule (DCT, distal to the glomerulus). The glomerulus (and its surrounding capsule), the PCT and the DCT are located within the cortex whereas the loop of Henle extends into the renal medulla (i.e. descending limb of the loop of Henle) before returning to the renal cortex (i.e. ascending limb of the loop of Henle). The majority of nephrons (80-85%) have short loops of Henle which lie mostly within the renal cortex and extend a short distance into the renal medulla, whilst the remaining 15-20% extend much deeper into the medulla. The nephrons with shorter loops are known as cortical nephrons, whereas those that extend deeply into the medulla are known as juxtamedullary nephrons. The fluid that passes through the DCT, and has not been reabsorbed, flows into collecting ducts which then unite to form large papillary ducts that transport this excretory fluid through the renal pelvis and empties it into the ureter[1–3].

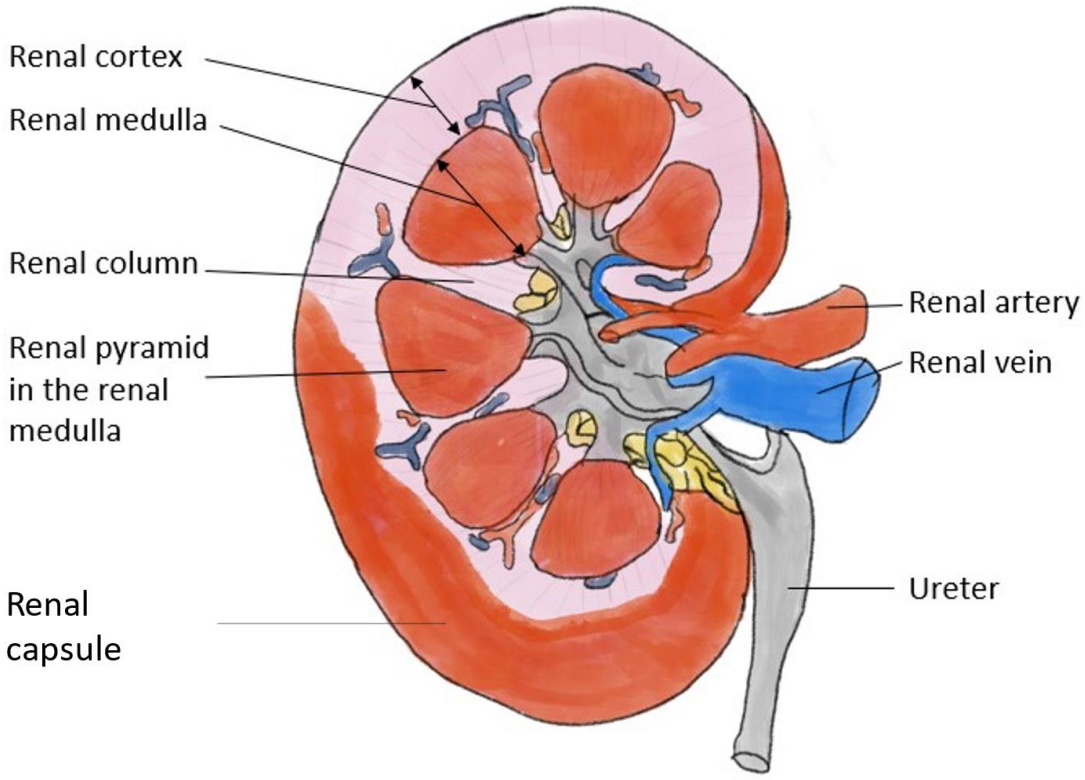

Figure 1.1: Frontal section of the kidney; adapted from Tortora et al. (2009), Principles of Anatomy and Physiology[2]

The kidneys are an integral part of the urinary system with the ureter, urinary bladder and the urethra. The main function of the kidneys is to filter blood plasma and remove metabolic waste products to produce urine. The kidneys filter water and most solutes through the glomerular capillaries and the glomerular capsule. The filtered fluid then flows along the renal tubule and the collecting duct where water and useful solutes are reabsorbed into blood and returned to the body. While fluid travels through the renal tubule, waste products (i.e., urea, creatinine and uric acid), ions and other by-product are secreted into the fluid and eventually excreted in urine (*Figure 1.2*). Through their excretory function, the kidneys help regulate blood volume and composition, and maintain body homeostasis. Water absorption/secretion by the kidneys maintains blood volume while regulation of ions (such as sodium, chloride and potassium) controls blood composition and pH. The kidneys also release the enzyme renin which activates the renin-angiotensin-aldosterone pathway and alters blood pressure while the production of the hormones calcitriol and erythropoietin regulates calcium homeostasis and red blood cell production, respectively[1–3].

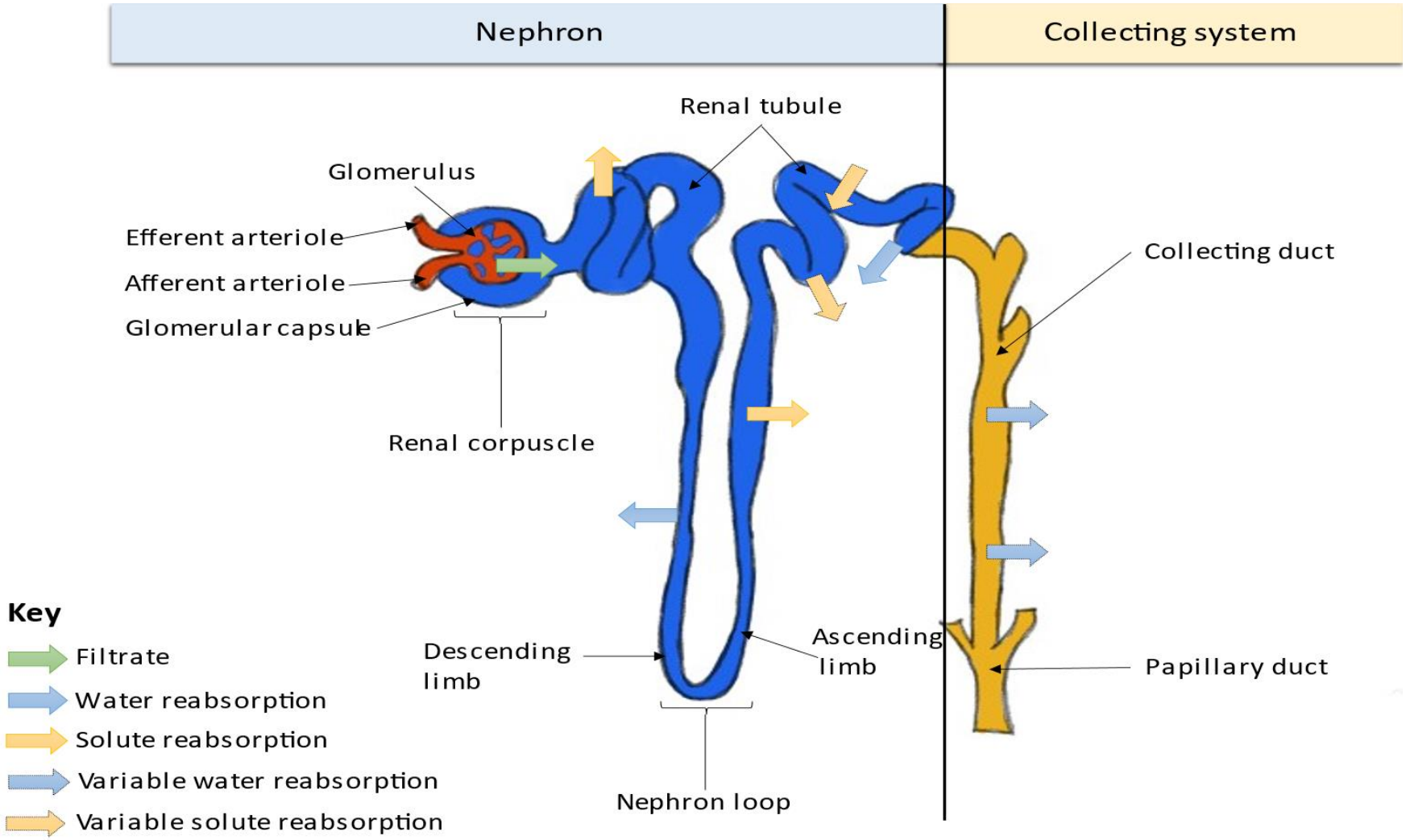

Figure 1.2: The Functional Anatomy of a Representative Nephron and the Collecting System; adapted from Martini and Nath (2012), Fundamentals of Anatomy and Physiology[3].

1.2. Biomarkers of acute kidney injury

In a clinical setting, AKI is detected by a sudden rise in serum creatinine (sCr) and blood urea nitrogen (BUN) levels, alongside a rapid decrease in glomerular filtration rate (GFR); GFR estimates how much blood is filtered by the kidneys in a minute[2–8]. Creatinine and urea are waste products of metabolism, filtered out of blood and excreted in urine in healthy kidneys; during injury, these two markers can be found in higher concentrations in serum as the kidney is unable to function properly and remove them through urine[9–11]. Both sCr and BUN are a are often used in the clinic, however, levels can vary widely with age, gender, exercise, diet, drug exposure and hydration status thus making them at times unreliable and unspecific[8,10]. In addition, neither sCR nor BUN are direct markers of tubular damage, but rather a marker of GFR. Furthermore, changes in sCR can only be measured when the kidneys have lost a significant percentage of their function (more than 50%) thus not allowing for early diagnosis of AKI while changes in BUN can also be observed in various conditions, unrelated to AKI, such as hypercatabolism or gastrointestinal bleeding[5,8,10,12–14].

Due to the limitations stated above, there is on-going research into the discovery and validation of better, more reliable and more sensitive biomarkers of kidney disease. The focus is currently on a panel of urinary biomarkers consisting of proteins such as kidney injury molecule-1 (KIM-1), clusterin, neutrophil gelatinase-associated lipocalin (NGAL) and N-acetyl-ß-D-glucosaminidase (NAG). These proteins are sensitive to changes in the kidney, and upregulated early during the injury phase. If validated, these markers would be preferable to serum markers as they would allow for rapid detection of kidney injury using non-invasive techniques[8,10,12,15].

1.3. Definition and classification of acute kidney injury

Acute kidney injury (AKI) is a common complication in hospitalised patients which affects approximately 15% of patients every year; it can rise up to 60% in critically ill patients[5,16–22]. AKI has been estimated to cost the NHS between £434 million and £620 million per year in the United Kingdom alone, and has been associated with a high in-hospital mortality rate ranging from 18% to 80%, as well as progression to chronic kidney disease (CKD) and end-stage renal disease (ESRD)[6,16,21–24]. AKI has been characterised as an abrupt and

sustained decline in renal function that leads to fluid overload, electrolyte imbalances, metabolic acidosis and deterioration of renal excretory function[5,17,23,25–27].

AKI has had different denominations and definitions throughout the years which has led to some discrepancies in research findings, and the need for standardisation. In 2004, the Acute Dialysis Quality Initiative (ADQI) group formulated the RIFLE (Risk, Injury, Failure, Loss, End-stage kidney disease) classification scheme (*Figure 1.3*) which allowed for the grouping of AKI based on severity and timing of the occurrence[28–30]. The RIFLE classification uses sCr, proportional changes in GFR and urine output (UO) to determine the severity of kidney injury. Nonetheless, the RIFLE classification also comes with some limitations. First, it is dependent on determining the baseline levels of sCr which are often unknown in clinical practice. Second, the RIFLE classification does not take into consideration neither the cause of AKI nor whether the patients are undergoing renal replacement therapy (RRT)[28,32,33].

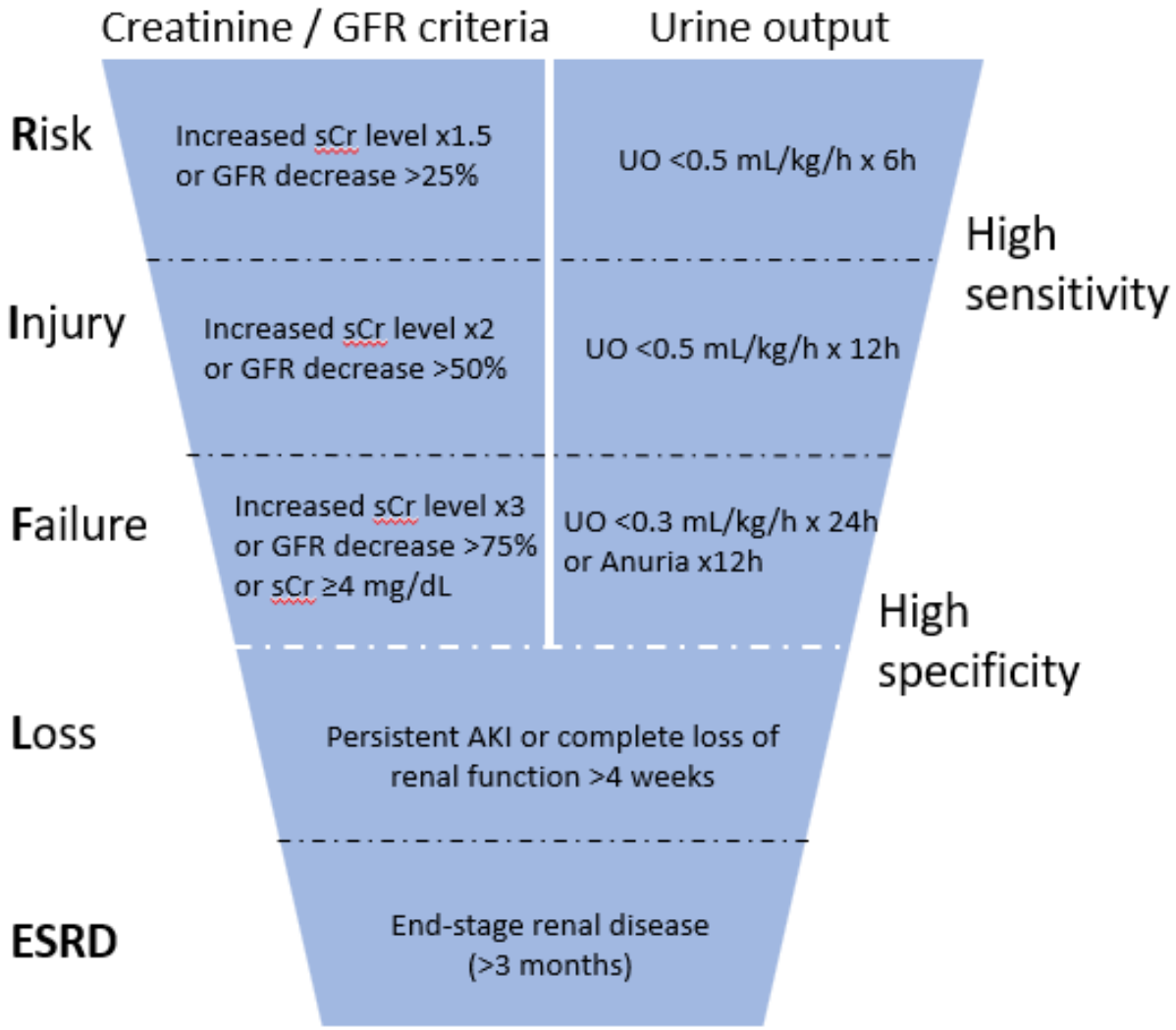

Figure 1.3: The RIFLE criteria. The ADQI defined the RIFLE criteria which classifies AKI into three stages: Risk, Injury, Failure, Loss and End-stage renal disease; figure was adapted from Lopes and Jorge (2013)[28]. Abbreviations: sCR – serum creatinine; UO – urine output.

As a result, in 2005, the Acute Kidney Injury Network (AKIN) attempted to address some of the limitations of the RIFLE classification by: 1) excluding GFR changes, and 2) not relying on baseline sCr. The AKIN criteria (*Table 1.1*) classifies the severity of AKI from stage 1 to 3, with 1 representing the lowest level of injury and the 'Risk' category, 2 representing the 'Injury' category and 3 representing the 'Failure' category of the RIFLE criteria[28,34].

Stage	Serum creatinine	Urine output
1	↑ sCr ≥26.5 µmol/L (≥0.3 mg/dL) or ↑sCr ≥150 - 200% (1.5 - 2×)	<0.5 mL/kg/h (>6 h)
2	↑ sCr >200 - 300% (>2 - 3×)	<0.5 mL/kg/h (>12 h)
3	↑ sCr >300% (>3×) or if baseline sCr ≥353.6 µmol/L (≥4 mg/dL) ↑sCr ≥44.2 µmol/L (≥0.5 mg/dL)	<0.3 mL/kg/h (24 h) oranuria (12 h)

Table 1.1: The AKIN criteria. The Acute Kidney Injury Network defined the AKIN criteria which classifies AKI into three stages, from 1 to 3; table was adapted from Lopes and Jorge (2013)[28]. Abbreviations: sCR – serum creatinine; UO – urine output.

In 2012, the Kidney Disease: Improving Global Outcomes (KDIGO) workgroup unified the RIFLE and AKIN criteria. The KDIGO classification stages the severity of AKI according to the AKIN criteria (*Table 1.2*) and defines it as either an increase in SCr to ≥1.5 times when compared to the baseline or an increase in SCr ≥0.3 mg/dL (≥26.5 µmol/L) over 48h[28,35].

Stage	Serum creatinine	Urine output
1	≥1.5 – 1.9x within 7 days or ≥26.5 µmol/L (≥0.3 mg/dL) within 48h	<0.5mL/kg/h for 6-12 hours
2	>2.0 – 2.9x	<0.5mL/kg/h for ≥12 hours
3	>3× or ≥4 mg/dL	<0.3mL/kg/h for ≥24 OR anuria for ≥12 hours

Table 1.2: The KDIGO classification. The Acute Kidney Injury Network defined the AKIN criteria which classifies AKI into three stages, from 1 to 3; table was adapted from KDIGO.org (2012)[35].

1.4. Pathophysiology and aetiology of acute kidney injury

AKI does not have a distinct pathophysiology as the disease can be brought about by different insults, including nephrotoxicity, sepsis and major surgery (more prevalent in high-income countries) or dehydration and infectious diseases (more prevalent in low-income countries). Furthermore, these distinct aetiologies can often co-exist within the same patient[5,19,20,27]. However, a commonality between these "injuries" is that they all lead to a reduction in blood flow to the kidneys (i.e. ischaemia) and subsequent hypoxia[36–38].

Classification of AKI is broadly defined by pre-renal, intrinsic and post-renal causes[5,39,40]. Pre-renal AKI or azotaemia is caused by hypoperfusion of the kidneys through

hypovolemia, reduced cardiac output or reduced effective circulatory volume, all of which lead to a decrease in GFR. As such, pre-renal AKI can be reversed if the underlying cause is promptly treated. Intrinsic renal failure or 'true AKI' is caused by a direct damage to the kidneys and can be further classified according to the primary site of injury: glomerulus, tubules, interstitium and vessels. Intrinsic AKI can be attributed to various insults brought by medication, systemic diseases or rheumatological illnesses. Post-renal AKI is caused by any obstruction in the urinary tract which stops urine flow such as an enlarged prostate, cancer or kidney stones.

1.5. Renal ischaemia-reperfusion injury triggers inflammation in the kidney

The kidney is highly susceptible to ischaemia/reperfusion injury, making renal IRI the leading cause of AKI, most often as a secondary response to surgical procedures, such as renal transplantation or cardio-pulmonary bypass surgeries[4,16,18,21,25–27].

Renal IRI is a complex process characterised by multi-factorial events[41,42]. Renal IRI is marked by a period of ischaemia which stops blood flow and oxygen to the organ, and leads to a drastic decrease in intracellular adenosine triphosphate (ATP) levels in epithelial cells. ATP depletion is accompanied by changes in the actin cytoskeleton and the displacement of adhesion molecules, such as β-integrins. This affects the polarity and integrity of renal epithelial and endothelial cells, and causes the desquamation of both viable and non-viable cells of the PCT brush border membrane as well as transtubular back-leak of filtrate as the tubular cell layer becomes permeable[4,10,50,17,43–49]. If the ischaemia period is long enough, cellular death occurs through both regulated and unregulated processes, such as apoptosis, pyroptosis and necrosis; in mouse models, an ischaemia period above 25min is thought to be severe enough to produce irreparable damage[4,10,54,27,42–44,49,51–53]. While all nephron structures can be affected by ischaemia, tubular epithelial cells of PCT (S3 segment located in the outer medulla) are particularly susceptible to hypoxic injury, with significant damage also brought to endothelial and smooth muscle cells[4,10,50,55,17,43–49]. Epithelial cells of the PCT have a high number of mitochondria and an increased metabolic rate, however, they also have a limited capacity for anaerobic glycolysis which makes them highly dependent on oxidative phosphorylation[14,43]. During injury, the S3 segment of the PCT is also highly affected by microvascular hypoperfusion and vascular congestion where endothelial cell dysfunction

promotes peritubular capillary rarefaction and a subsequent reduction in vascular density which further promotes hypoxia and leads to impaired renal haemodynamics[4,10,19,43,45,47,56–58].

At a cellular level, inflammation and immune system activation of both innate and adaptive branches underlie the pathogenesis of acute renal diseases, irrespective of their initial cause (**Error! Reference source not found.**)[19,20,55,59]. Animal models point towards multiple components of the innate system being responsible for kidney injury, including Toll-like receptors (TLRs), macrophages, dendritic cells (DCs) and neutrophils, among others. The hypoxic environment and cellular death due to ischaemia drive the release of damage-associated molecular patterns (DAMPs) from intracellular compartments, such as reactive oxygen species (ROS), interleukin (IL)-1α and heat-shock proteins (HSPs) as well as the intra-renal activation of hypoxic-inducible factors (HIFs)[19,20,27,41,43,54,55,57,60]. The release of DAMPs activates the innate system through an antigen-independent pathway: DAMPs stimulate TLRs on the cell surface of surviving renal cells and promote a pro-inflammatory environment. While apoptosis is the least immunogenic mode of cell death, both pyroptosis and necrosis are highly immunogenic causing local inflammation through the release of pro-inflammatory cytokines (e.g., interferon (IFN)-γ, tumour necrosis factor (TNF)-α, IL-1β, IL-6) and chemokine upregulation (e.g., monocyte chemoattractant protein (MCP)-1, IL-8, stromal cell-derived factor (SDF)-1)[16,20,27,41,52,54,55,59,61,62].

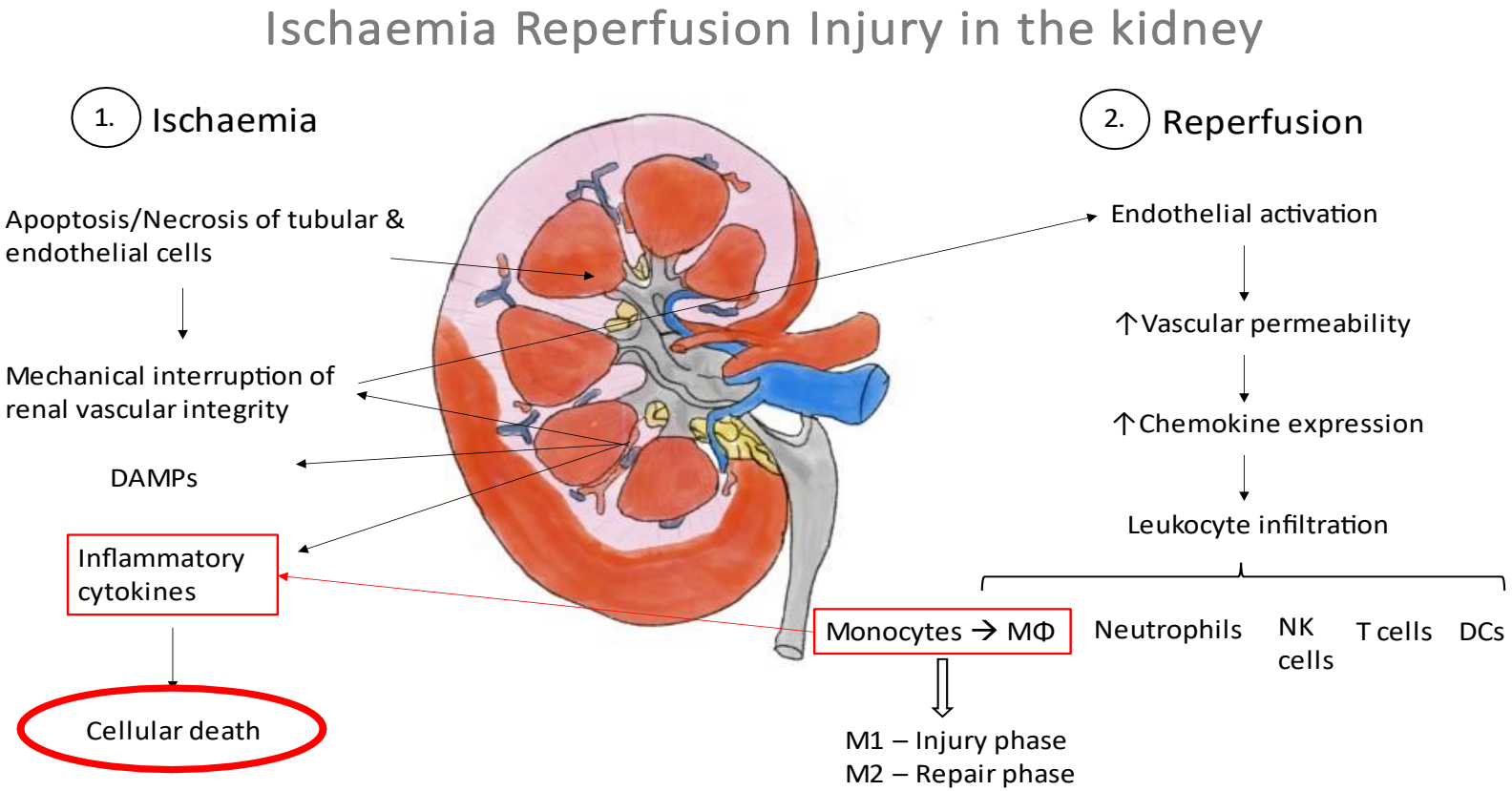

Figure 1.4: Mechanisms of ischaemia-reperfusion injury mediated inflammation in the kidney. IRI in the kidney can be divided into two distinct episodes: the ischaemia phase and the reperfusion phase. Ischaemia is associated with tubular and endothelial cell death which has negative effects on renal vasculature and causes the release of damage-associated molecular patterns and inflammatory cytokines. The reperfusion phase will, in turn, increase vascular permeability and chemokine expression necessary to bring leukocytes into the damaged kidneys; these inflammatory leukocytes cause further cell death by exacerbating the inflammatory milieu.

With the reperfusion of the injured kidney, blood and oxygen are restored to the tissue, activating the endothelium and increasing both vascular permeability and chemokine expression (**Error! Reference source not found.**)[16,49,63]. These changes, in concert with an increase in oxygen free radicals, HIFs and pro-inflammatory factors, promote immune cell infiltration to the damaged kidney and exacerbate organ dysfunction and injury[16,17,20,49,52,55,57,59,60,63]. Neutrophils and natural killer (NK) cells are first to home to the injured kidney via chemotaxis, followed by monocytes which differentiate into macrophages, and T-cells; immune cell transmigration in the interstitium is facilitated by the increased microvascular permeability that describes the post-ischaemic kindey[16,27,55,60]. In the initial phase of injury, neutrophils enter the renal interstitium and bind to the vascular endothelium through selectins and integrins to promote further organ damage through the secretion of proteases, TNF-α and ROS. *In vivo* IRI models of kidney injury indicate that necrotic tubular cells can prime neutrophils to form neutrophil extracellular traps which have been linked to progressive kidney damage and multi-organ dysfunction[27]. In the kidney, HIF activation in tubular cells has been shown to induce macrophage infiltration of the interstitium within 24 hours after injury where they cause further tissue injury and death through the release of pro-inflammatory cytokines and chemokines, and activation of caspases and ROS generation[17,20,43,48,52,55,57,60,61,64]; *in vivo* studies suggest that tubular injury peaks at day 2-3 following IRI, followed by resolution of the inflammatory phase[52,57,60]. The injury phase is estimated to last approximately 3 days and it is characterised by upregulated cellular death and inflammation. The inflammatory milieu that describes the injured kidney works in concert with the different forms of cell death to create a feedback loop that promotes organ damage and dysfunction[54,59,60].

Following the injury phase, there is a period of recovery and regeneration with a decrease in inflammatory markers and cellular death, and an increase in the proliferation of surviving cells[15,65,66]. Depending on the severity of the injurious stimuli this process might not be enough to restore full function of the organ, reaching what has been characterised as a 'point of no return' of irreversible damage and progressive atrophy[15]. In unilateral models, this period is also associated with a compensatory hypertrophy of the contralateral kidney[15].

1.6. The kidney has an intrinsic regenerative ability

Previous studies point towards the kidney being able to intrinsically regenerate after an episode of AKI (if damage is not too high) through a repair process whose mechanisms are not completely understood[67,68]. While the kidney shows limited capacity for regeneration when compared to other organs such as the liver, it still has a remarkable capacity for structural remodelling and repair following an insult. However, there is still a debate on whether regeneration is due to cellular dedifferentiation or to an endogenous population of stem cells[44,69–72]. Previously, this intrinsic regenerative ability of the kidneys was attributed to renal epithelial cells capable of repopulating the injured kidney and restoring kidney architecture through mitogenesis and dedifferentiation[42,44,50,71–73]. The renal papilla is a niche for adult kidney stem cells that have the capacity to repopulate and regenerate the kidney after an episode of transient ischaemia through their plastic phenotype[42,44,50,71–74]. More recently though, Lazzeri and colleagues reported that following a mild episode of AKI, most surviving tubular epithelial cells undergo hypertrophy and only a small subsection of kidney cells have the capacity to proliferate[66]. These renal progenitor cells, which are lineage-restricted to specific segments of nephrons, show increased survival in response to injury and the ability to replace approximately 50% of cells lost through injury thus restoring some of the lost tubular architecture and renal function[15,44,66,70,71].

However, as kidneys are unable to completely restore the functional integrity of nephrons or generate new nephrons, repeated episodes of AKI will lead to further nephron loss and injury which is ultimately associated with CKD and ESRD[16,67,68]. As a result, a single episode of AKI puts patients at risk of future episodes of AKI which consequently increases the risk of developing chronic kidney disease and end stage kidney failure[19,20]. Recently, studies performed in fish have shown that some species are capable of neonephrogenesis (i.e. generate new nephrons) leading to possible new therapeutic avenues to explore[70].

1.7. Macrophages in renal ischaemia-reperfusion injury

Macrophages are highly versatile cells, ubiquitous in all tissues, that play important roles in the pathophysiology of diseases, such as cancer, metabolic and fibrotic disorders, and autoimmune illnesses. Macrophages are essential in both organogenesis and normal

development and maintenance of tissue homeostasis where they promote tissue remodelling and repair through phagocytosis and infection control[16,75–79]. Ontogenically, there are two distinct types of macrophages: tissue-resident macrophages and monocyte-derived macrophages. The majority of tissue-resident macrophages are derived from progenitor cells in the embryonic yolk sac, and are recruited to tissues before birth where populations are maintained locally[80]. A transcriptional analysis of tissue-resident macrophages indicates that these cells have activated both tissue-specific and shared gene profiles, depending on the tissue of origin[80,81]. Circulating blood monocytes derived from bone marrow give rise to monocyte-derived macrophages in inflamed and cancerous tissues[80]. The current body of literature suggests that monocyte-derived macrophages are one of the main perpetrators of renal injury regardless of the initial cause where they play critical roles in both the injury phase and the subsequent resolution of inflammation[16,17,52,57,82,83]. Liposomal clodronate depletion studies of monocytes and macrophages during the initial phase of injury show an amelioration of kidney damage and a decrease in BUN and sCr levels, while their depletion during the recovery phase leads to a reduction in cellular proliferation and a delay in tissue repair[17,52]. It is important to note that liposomal clodronate will also deplete neutrophils and $CD11c^+$ DCs, the other type of mononuclear phagocytes alongside macrophages[17,52,76,84].

While not abundant in a normal, healthy kidney, macrophage numbers rise significantly within 24 hours of injury induction[57,77,82]. Monocytes enter the damaged kidney in response to chemokine and pro-inflammatory factors which are released into the bloodstream in response to injury, and differentiate into macrophages that surround the injured tubules to initiate an early innate immune response[16,52,57,82,83,85,86]. Macrophage populations are heterogenous but can be classified into two main groups: M1 and M2 macrophages, however, this is quite an oversimplification due to the functional crossover between different types of macrophages as well as their ability to exist in various intermediate states. Macrophages are highly plastic cells, capable of altering their phenotypic profile based on cues received from their microenvironment making their characterisation increasingly more complex; in the injured kidney, tubular epithelial cells release molecules capable of mediating macrophage polarisation, and evidence suggests that dominance of one phenotype over the other is critical in influencing disease progression[19,52,91,57,61,64,86–90]. Whereas M1 macrophages play a major role in the early stage of kidney injury, M2 macrophages are involved in the late injury

phase characterised by tubular cell repair, proliferation and fibrosis[19,52,64,92–94]. M1 and M2 responses can stimulate T cells towards a Th1 and Th2 phenotype, respectively, which in turn will stabilise macrophage responses in an auto-amplifying circuit[75,76,78,95,96]. Macrophages can also be classified based on their preference for arginine metabolism: M1 cells produce high levels of inducible nitric oxide synthase (iNOS/NOS2) to kill pathogens whereas M2 cells produce ornithine and polyamines to help with wound healing[75,76,83,89,90,93,95,97].

M1 or classically activated macrophages are induced by IFN-γ, alone or in combination with cytokines (e.g., TNF-α, GM-CSF) or microbial products, such as lipopolysaccharide (LPS)[19,52,64,78,79,86,86,91,98,99]. In the context of AKI, tissue injury leads to the local infiltration of blood monocytes which, through local environmental stimuli released by damaged cells, such as GM-CSF, IGF-1 and M-CSF, maturate into phagocytic M1 macrophages[16,19,52,88]. These pro-inflammatory macrophages promote the removal of apoptotic and necrotic cells, and further contribute to the local inflammatory milieu through the release of cytokines that promote cellular death[16,19,52,77,88]. With the removal of noxious stimuli, the pro-inflammatory state is replaced by a wound healing state characterised by the presence of M2 macrophages[16,19,79,83,87,92–94,99,100]. M1 macrophages express opsonic receptors and are characterised by their high expression of IL-12, IL-23 (humans) and toxic intermediates, such as iNOS/NOS2 and ROS which promote oxidative stress and induce severe damage to the injured kidney[19,52,86,90,93,94,101]. Classically activated macrophages have a high capacity to present antigen, reflective of Th1 immune responses with strong microbicidal and tumoricidal activity through the generation of chemokines (IP-10, MIP-1α, MCP-1) and pro-inflammatory cytokines (IL-1β, IL-6, IL-1, TNF-α)[16,52,99,102,103,61,78,86,86,91,93,97,98].

M2 or alternatively activated macrophages are indicative of the proliferative phase of kidney recovery where they stimulate angiogenesis, tissue remodelling and repair. Animal models of kidney injury indicate that macrophages switch towards an M2 phenotype, capable of activating the Wnt7b signalling pathway to directly promote kidney repair through its effects on epithelial cells, on day 6 following injury induction; the Wnt7b signalling pathway plays a crucial role during kidney development by regulating cellular proliferation, differentiation and death, as well as cell-fate decisions[16,19,99,100,103,52,61,79,87,92–94,97]. Large numbers of M2 macrophages can be found in fibrotic areas: these cells stimulate fibrosis

through the release of pro-fibrotic molecules, such as TGF-β, platelet-derived growth factor (PDGF), fibroblast-growth factor 2 (FGF-2) and MMP-9, that promote epithelial-to-mesenchymal transition, endothelial-to-mesenchymal transition and myofibroblast proliferation, and the subsequent ECM overproduction and collagen deposition. Furthermore, these cells are capable of transdifferentiation into collagen-producing fibrocytes that directly contribute to a fibrotic environment[16,20,61,78,86,93,94,104,105]. M2 macrophages are typically activated through the JAK-STAT6 signalling pathway that acts through the IL-4 receptor and its ligands, IL-4 and/or IL-13[64,91,94,99]. Alternatively activated macrophages express non-opsonic receptors that promote Th2 responses[16,61,78,93]. With a diverse functional repertoire, M2 macrophages are currently classified into three distinct subphenotypes: M2a, M2b and M2c[52,78,86,93,99,106,107]. M2a are induced by IL-4 and IL-13 released from Th2 cells, basophils and mast cells, and are characterised by a high production of anti-inflammatory cytokines (e.g., IL-10, TGF-β) and a low production of pro-inflammatory cytokines (e.g., IL-12, TNF-α, IL-6)[78,79,86,91,93,97,107]. M2b are induced by immune complexes, IL-1R and TLR agonists through interactions with the Fc gamma receptor on their surface, and are characterised by high production of both anti- and pro-inflammatory cytokines; M2b macrophages are critical in promoting a Th2 phenotype and humoral immune responses, and provide LPS protection in mouse models of disease[19,78,86,93,107,108]. M2c are induced by glucocorticoids, TGF-β and IL-10, and are characterised by a high scavenger activity and their ability to induce regulatory T cells[86,93,107].

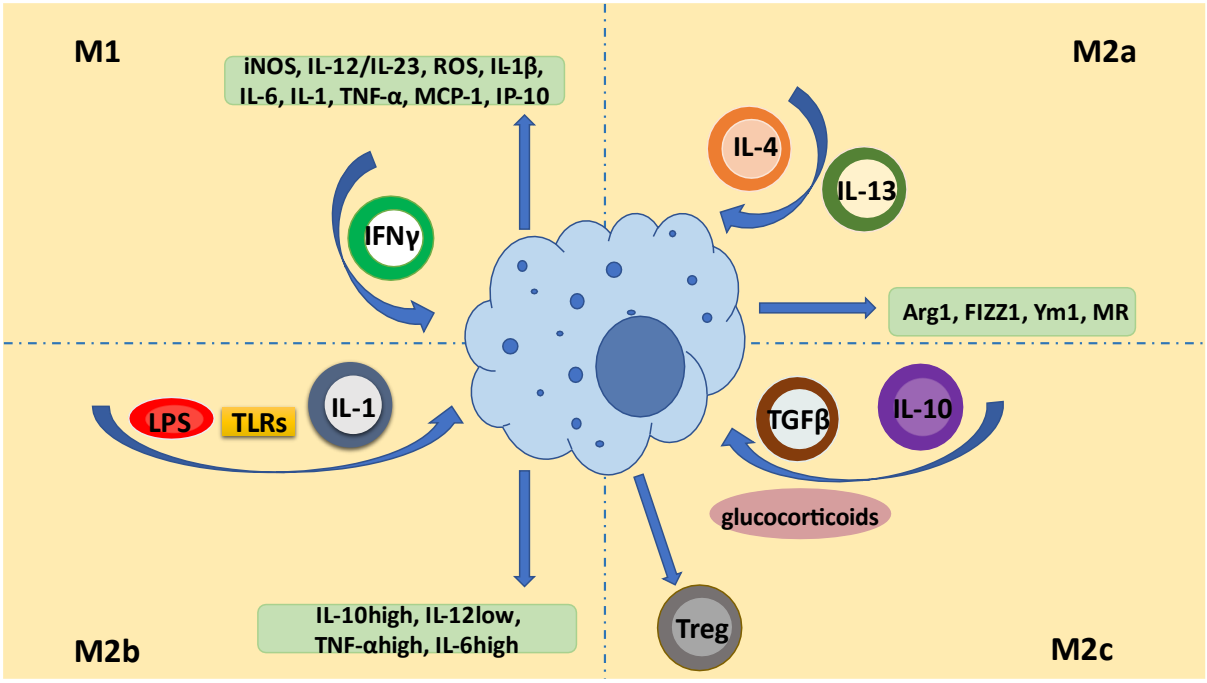

Figure 1.5: Macrophage polarisation states. Macrophages are a highly heterogenous and plastic population that can adopt different functional programs in response to signals received from their environment. M1 macrophages are induced by IFN-γ and release iNOS, IL-12/IL-23, ROS, IL-1β, IL-6, IL-1, TNF-α, MCP-1 and IP-10 in their environment. M2a macrophages are induced by IL-4 and IL-13 and release Arg1, FIZZ1, Ym1 and MR in their environment. M2b macrophages are induced by LPS, TLRs and IL-1 and release IL-10^{high}, IL-12^{low}, TNF-α^{high} and IL-6^{high} in their environment. M2c macrophages are induced by glucocorticoids, TGF-β and IL-10, and stimulate T_{REG} production.

As previously described, macrophages form a highly plastic and heterogenous population capable of dynamically switching their phenotype and function based on signals received from their local environment (*Figure 1.5*) through the spatiotemporal regulation of different transcription and post-transcription factors, such as nuclear factor-κβ (NF-κβ), signal transducer and activator of translation 1 (STAT1) and STAT6, and interferon regulatory factors[19,52,91,97,57,61,64,86–90]. Their dynamic functionality along with their ability to exist in a variety of intermediate states makes identifying markers for macrophage characterisation *in vivo* increasingly difficult[89,97]. A transcriptional analysis comparing the gene profiles of *in vivo* M1 and M2 macrophages against *in vitro* M1 and M2 macrophages, respectively, shows high discrepancies between the two groups, depending on their environment: while these cells share some genes and pathways between *in vitro* and *in vivo* signatures, there are also many genes that have opposite signatures[97].

1.8. Animal models of acute kidney injury

A range of animal models can be used in pre-clinical research to study kidney disease such as sepsis models generated through exposure to various endogenous or exogenous toxins, kidney ischaemia-reperfusion models, toxin-induced AKI models and urinary tract obstruction models, and much of our knowledge of AKI is based on research conducted on these animals as renal biopsy is rarely performed in the acute phase of the disease[6,105,109,110]. The kidney is highly susceptible to ischaemia-related injury which is one of the main causes of AKI[6,50,109]. While it is possible to study some of the effects of kidney IRI using cell culture or ex-vivo models, animal models are still the preferred method as they allow for the investigation of whole-organ and whole-body responses to injury, and analysis of the pathophysiology of AKI, from the injury phase to the ensuing recovery and regenerative phases associated with IRI[6,73,109,111–113]. Experimental models of AKI using ischaemia-reperfusion have been used in animals to mimic the effects of R-IRI seen in the clinic, with the warm ischaemia model being the most conventional one[6,109,114]. The ischaemia model can be generated through three common methods – bilateral clamping of the renal arteries, unilateral clamping, and unilateral clamping with contralateral nephrectomy – with the choice of model depending on the research question to be answered[6,105,109,110]. For example, the bilateral renal ischaemia-reperfusion injury (R-IRI) model is commonly used to investigate human AKI pathophysiology where hypoperfusion usually affects both kidneys, while unilateral models allow for the investigation of the effects of uraemia and azotaemia in kidney disease[110,111].

Animal models of renal IRI include smaller and larger species, both with their advantages and disadvantages. Mice are commonly used in pre-clinical models as they are readily available, easy to breed and their smaller size provides an advantage when investigating therapeutic strategies. Furthermore, these animals can be genetically manipulated to mimic a plethora of human conditions[6,109,115]. Both BALB/c and C57BL/6 strains are commonly used in pre-clinical models of disease as these two strains are characterised by a Th2 profile and a Th1 profile, respectively, making them ideal for research into conditions were the immune system plays an active role, however, not much research has been conducted using the CD1 strain[25,95,121–126,96,97,106,116–120]. The BALB/c strain T-cells

release IL-4 during infection which readily activates M2 macrophages while their macrophages produce ornithine in response to antigen stimulation; this makes BALB/c mice an unsuitable model for studying Th1 autoimmune diseases[96,97,127]. The BALB/c strain is also highly susceptible to *Listeria* and *Leishmania* infections due to their Th2 profile[96,97,127]. The C57BL/6 strain T-cell release IFN-γ during infection and activate M1 macrophages while their macrophages produce NO when stimulated with LPS. In contrast, C57BL/6 mice are more resistant to *Leishmania* infections[97,127,128]. These divergences in immune response patterns make the choice of mouse strain paramount when designing an experimental design as it will heavily influence the research data generated. Larger rodents such as rats are also commonly used in pre-clinical research as they are a larger size than mice and thus easier to surgically manipulate[110,129]. Larger animals such as pigs and sheep are preferred for transplantation models due to their size and anatomical similarities to humans; however, their larger size also comes with an increase in the costs of husbandry which limits their laboratory use[6,109,110,130].

Animal models of kidney disease also come with some significant limitations. First, the bilateral R-IRI model does not replicate the most severe AKI injuries as it is not possible to provide dialysis to experimental animals. As a result, these models are constrained by the requirement that the injury be severe enough to cause significant kidney damage while remaining minor enough to prevent early animal death from acute uremia[111]. Secondly, experimental research conducted on mice has shown that age, sex and strain drastically impact the response to kidney damage, with male and older animals showing a higher degree of injury in addition to impaired recovery[6,109]. Furthermore, the degree of injury varies with temperature during ischaemia as well as the ischaemic period[15]. Thirdly, these pre-clinical models are frequently performed on young, healthy and genetically inbred strains whereas patients suffering from AKI often present with multiple comorbidities such as hypertension, diabetes or cardiovascular disease and are characterised by genetic variability[114,131,132]. Based on the foregoing, the choice of animal model is highly important when trying to simulate a disease and test for the effect of therapies on said model.

1.9. The relationship between kidneys and spleen during sterile inflammation

The spleen is the largest secondary lymphoid organ, with both local and systemic effects on immune cell responses. The spleen has a complex structure and is one of the

primary organs of the reticuloendothelial system, a reservoir of monocytes, macrophages and DCs. However, only splenic monocytes show high displacement to inflammatory sites whereas macrophages and DCs are primarily sessile[76,84,133]. The spleen presents with four distinct macrophage populations: one population of macrophages specific to the white pulp with phagocytic functions, two macrophage phenotypes specific to the marginal zone that specialise in defence against blood-borne pathogens, and red pulp macrophages with homeostatic and metabolic functions[2,76,134–136]. The red pulp also contains a population of 'reservoir monocytes' capable of mobilising to inflamed organs during acute inflammatory disease[76,133,137].

While extensive research has been done into cytokine production and immune cell activation in the kidney following AKI induction, not many studies have explored the role of extrarenal organs in AKI[138]. Nevertheless, from research conducted in other disease models, such as myocardial infarction and stroke, mobilisation of spleen monocytes is crucial in sterile inflammatory responses with active roles in both injury and repair phases[84,133,139]. The spleen is an organ that has not been investigated extensively in relation to AKI, and most research has been focused either on sepsis-associated AKI or CKD[140,141]. Current research points towards contrasting results in the role of the spleen in AKI. Bilateral renal IRI has been shown to lead to an increase in several pro-inflammatory cytokines in spleen and points towards the spleen playing a central role in AKI through the release of the anti-inflammatory cytokine IL-10. Splenic IL-10 is released from macrophages, B cells and T cells in response to injury and is responsible for downregulating the levels of the pro-inflammatory cytokine IL-6 in serum, kidneys and liver[138].

1.10. The role of acute kidney injury in chronic kidney disease

While recovery of renal function is possible following an episode of AKI, multiple studies have shown that patients are still at risk of developing CKD and ESRD later in life[15,36,69,105,142–145]. CKD is defined as "abnormalities of kidney function or structure present for more than 3 months"[7,146] and is clinically diagnosed by proteinuria (>30 mg/day or >30 mg/g creatinine), an estimated GFR of less than 60 mL/min/1.73 m^2 or persistent haematuria[146–148]. Globally, CKD is one of the leading causes of morbidity and mortality with a prevalence between 8% - 16%, and is a known contributor to cardiovascular disease and

AKI[58,149–152]. CKD is characterised by a chronic inflammatory state with altered immune and oxidative stress responses, progressive cellular damage and fibrosis linked to permanent loss of function and ESRD[144,150,153–155].

Analogous to AKI, CKD does not have a distinct pathophysiology and can develop from a variety of processes that damage the kidney. Regardless of the initial insult, several distinct mechanisms stand out as crucial for the progression to and development of ESRD[105,153,154]. CKD is associated with an increase in tubular cells exhibiting G2/M cell-cycle arrest which upregulate the release of profibrotic cytokines, and stimulate the fibroblast proliferation and extracellular matrix deposition[105,147]. Furthermore, there is also an increase in cellular senescence which occurs early in the injury phase and has been linked to the promotion of mitotic arrest[105,144]. The kidney's outer medulla is particularly susceptible to hypoxia due to a loss of microvasculature integrity and an increase in fibrosis. Renal pericytes are of particular importance in this context; these cells stabilise renal microvasculature during homeostasis whereas during injury they directly contribute to renal fibrosis as they migrate from their perivascular locations and change into a myofibroblastic phenotype responsible for collagen deposition[104,105].

There is increasing evidence that AKI and CKD are closely related and promote one another, although the underlying pathophysiological mechanisms have not been uncovered yet[15,105,147]. According to the KDIGO group, stage 1 (mild) AKI has been linked to an increase in mortality as some patients never recover full kidney function even in the presence of no proteinuria and normal sCr levels[105,142,145,156]. Whereas young and healthy adults suffering from stage 1 or stage 2 AKI can often recover full kidney function that is not the case for older patients who also suffer from other underlying conditions such as diabetes, myocardial infarction and hypertension[157–159]; these elderly patients often do not make a full recovery due to maladaptive renal repair processes that lead to a progressive loss of kidney function[144]. Current research shows that microvasculature rarefaction, tubular cell loss and cellular senescence, mechanisms associated with maladaptive repair processes in AKI are major risk factors in progression to CKD. While the precise link between AKI and CKD has not been elucidated, a growing body of literature has shown that survivors of AKI are at risk of developing proteinuria and progressive CKD when compared to non-AKI patients[105]. Bucaloiu

et al. (2012) have shown that patients who fully recover after an episode of AKI are twice as likely to develop CKD[145]. The outcomes are increasingly dire for patients that suffered from severe AKI requiring dialysis as this has been associated with a 28-fold increase in the risk of developing CKD and a high risk of ESRD[155,160–162]. In addition, CKD can also be a precursor to AKI as high levels of proteinuria and low GFR are major risk factors for AKI. Furthermore, CKD patients often experience a range of acute illnesses associated with an increase in hospital stays and procedures that further promote kidney injury and subsequent AKI[155,162–164].

As the prevalence of both AKI and CKD increases, it becomes increasingly vital to better comprehend the pathogenesis of kidney injury and all the clinically significant outcomes following an episode of AKI, identify the patients who are most at risk for severe complications, and develop novel treatment plans to improve their care.

1.11. Renal replacement therapies

Despite recent advances in medical treatment, currently, there is no cure for AKI, and the disease is managed with fluid therapy, dialysis and ultimately, transplantation[16,19,20,25,165]. Diagnosis and treatment of AKI within 72 hours of commencement is critical and can determine the long-term outcomes of the disease. Nevertheless, most patients are diagnosed after significant damage to the kidney has already occurred so there is a dire need for early diagnostic tools as well as the development of effective therapeutic regimens that could enhance kidney repair and prevent kidney fibrosis[16,19,20,25,166].

Renal replacement therapy (RRT) comprises of dialysis and transplantation, and it is estimated to be administered to about 5% of patients in the intensive care unit (ICU) where in-hospital mortality is typically above 50%[167–169]. RRT modalities are used to correct fluid imbalance and remove waste products from the body[167–169]. Dialysis can be divided into two categories: 1) haemodialysis which uses a dialysis machine to filter blood externally, and 2) peritoneal dialysis which uses the peritoneum as a filter to remove toxins from the body[168,169]. Renal transplantation is performed using either deceased or living donor organs but it also carries risks such as long-term morbidity due to immunosuppressive therapies which are used to reduce the probability of organ rejection[169,170]. Nevertheless, there is a severe shortage of transplant-eligible kidneys: in 2018, there were approximately 5,500 people on the national renal transplant waiting list (NHS Blood and Transplant) with an estimated 3,000 kidney

transplants performed per year[149,169]. However, in 2020, transplant activity across the globe was affected by the COVID-19 pandemic where it saw a marked decrease in the number of performed transplants and an increase in the number of patients on the waiting list as all non-emergency surgeries were cancelled[171–173]. At the same time, in 2020 there was a change in organ donation law in England where adults are now automatically considered for organ donation unless they specifically 'opt-out'[174]. There is also a focus on decreasing the number of discarded organs that have been deemed un-transplantable by maintaining and improving organ quality during the retrieval process[175,176].

As mentioned previously, RRT increases the risk for long-term dialysis, as well as CKD and ESRD[155,160–162,167]. As a result, some patients may choose to refuse RRT due to the strain it can bring on their bodies and may opt for conservative management of the disease which focuses on managing the symptoms of kidney disease (e.g., nausea, poor appetite, anaemia), maintaining quality of life and making preparations for end-of-life care[168,169,177]. Therefore, there is a dire need for novel strategies to prevent AKI and subsequent CKD, therapies that are able to modulate and promote the endogenous repair capacity of the kidney, modulate the immune system towards an anti-inflammatory role, and reduce scarring and loss of functional kidney cells.

1.12. Mesenchymal stromal cells as regenerative therapy in acute kidney injury

1.12.1. Mesenchymal stromal cells - characterisation

Over the last two decades, extensive research has been done within the fields of regenerative medicine and pre-clinical research using mesenchymal stromal cells (MSCs) as the main therapy for the treatment of various haematological disorders, inflammatory and autoimmune diseases[178–180]. MSCs are multi-potent cells capable of self-renewal and multi-lineage differentiation (e.g., osteoblasts, chondroblasts, adipocytes, stromacytes, or neurons) both *in vitro* and *in vivo* animal implant models[10,16,19,43,78,181–183]. MSCs can be isolated from almost all tissues, both adult and foetal, including bone marrow (BM), adipose tissue, umbilical cord (UC), placenta or peripheral blood. Some sources, such as adipose tissue and UC, are more easily accessible and abundant whereas BM procurement, for example, involves a more invasive and painful procedure[26,181–186]. Several studies have compared MSCs isolated from different tissue-origin niches, and while there are similarities in phenotype, there are

also distinct differences in gene expression, surface antigen expression, secretion of bioactive molecules, and their subsequent immunomodulatory and angiogenic properties[116,180,183,184,187,188]. In addition, the activity of MSCs can be influenced by long-term culture: in a study conducted by Baksh and colleagues (2007), MSCs isolated from UC were preferable to those isolated from BM as they showed both a higher proliferative capacity and a higher expression of CD146, a proangiogenic marker[183,187,189]. As a result, it is important to carefully consider the tissue source of MSC as well as the duration of culture when examining their clinical applications so as to achieve the desired effect. At the moment, there is no consensus on which tissue origin provides the best source of cells for clinical application, however, this will most likely be dependent on the disease model[183].

When grown in culture, MSCs form a heterogeneous population of fibroblast-like cells, capable of retaining their multi-potency for up to 40 cell divisions[181,183,184]. MSCs are positive for CD29, CD44, CD73, CD90, CD105, and negative for hematopoietic markers (i.e. CD31, CD34, CD45, CD54) and CD14 (marker for cells of myeloid origin)[78,178,181–183,186,190]. Whereas MSCs are not as highly plastic as embryonic stem cells, they present with a lower risk of tumour formation, and are more readily isolated and propagated[182].

Early studies to assess the biodistribution of cells suggested that MSCs exert their effects by engrafting in the injured organs (regardless of the route of administration) where they either stimulate cellular proliferation or differentiate into functional cells to repopulate the damaged organ[191,192]. However, most of these initial studies were performed by using fluorescent dyes as MSC cell label that can be easily taken up by phagocytic cells, such as macrophages, when MSCs die and be distributed throughout the body[191–193]. This was later confirmed in biodistribution studies using luciferase reporter genes which demonstrated that most MSCs accumulate and die in the lungs of animals when administered through IV injection, with very little systemic distribution to other organs, such as the kidneys, liver and spleen. Other routes of administration have been used, such as intramuscular, intraarticular and intradermal, however, these do not lead to systemic biodistribution either[23,44,71,117,101,194–202]. In contrast, biodistribution studies using an intra-arterial route of administration show that MSCs can bypass the pulmonary vasculature and home to the injured organs, however,

usage of this route also runs the risk of MSCs getting trapped in the capillaries with thrombus formation, and ultimately death from vascular occlusion[21,26,47,98,179,183,199–201].

MSCs have become an attractive tool for cell-based regenerative therapies due to their low expressions of both MHC I and MHC II molecules, as well as the absence of CD40, CD80 and CD86 – T cell co-stimulatory molecules; these qualities allow MSCs to evade the immune system and exert their potent immunosuppressive and immunomodulatory functions with effects on both innate and adaptive immune cells[25,101,178,181–184,186,190]. As MSCs do not home to injured organs, it is thought that their effects are due to the soluble molecules they release in their secretome, capable of regulating processes, such as angiogenesis, tissue repair, immune function, and fibrosis amongst others (Table 1.3)[157,183,185,187,190,203]. MSCs constitutively express a multitude of receptors and signalling substances: pro-angiogenic molecules, such as IL-8, hepatocyte growth factor (HGF) and vascular endothelial growth factors (VEGF), such as VEGF-A, VEGF-B and VEGF-C, cell fate / transcription factors such as SRY-box 2 (Sox2) and octamer-binding transcription factor 4 (Oct4), cellular adhesion molecules, such as vascular cell adhesion molecule-1 (VCAM-1) and intercellular adhesion molecule-1 (ICAM-1), and immune-stimulatory molecules such as monocyte chemoattractant protein-1 (MCP-1), IL-6, indoleamine 2,3-dioxygenase (IDO), TGF-β and prostaglandin E2 (PGE2)[6,16,206–211,22,26,45,187,188,197,204,205]. In addition, analysis of the secretome released by MSCs using mass spectroscopy showed distinct differences in protein composition depending on physiological condition of the tissue i.e. the environment which MSCs are introduced into leads to the release of regulatory substances that match the primary needs of the tissue[209]. In support of this hypothesis, several research studies have shown that MSC preconditioning leads to the release of immune-modulatory molecules while hypoxia preconditioning leads to the release of various growth factors[119,181,183,190,212–214].

Immune cell type	MSC effect	MSC secretome
Innate immune system		
Monocyte / Macrophage	Stimulate macrophage polarisation towards an M1 or M2 phenotype	IDO/NO, PGE2, cyclooxygenase 2
DC	Inhibit DC cell activity, proliferation, differentiation and maturation.	PGE2
NK cell	Inhibit NK activity, proliferation and maturation	IDO/NO, PGE2
Adaptive immune system		
B cell	Inhibit B cell activity, proliferation, differentiation and maturation.	IDO/NO
T cell	Inhibit T cell activity, proliferation, differentiation and maturation. Stimulate the generation of T_{REG} cells	IDO/NO

Table 1.3: The effect of MSCs on the innate and adaptive immune system through the release of molecules in their secretome.

In vitro, MSCs interact with both monocytes and antigen-presenting cells (i.e., macrophages and DCs). MSCs can stimulate macrophages either towards an M1 pro-inflammatory phenotype or towards an M2 anti-inflammatory phenotype depending on the initial activation status of the monocytes and/or macrophages through the action of cyclooxygenase 2 and IDO expression[78,92,98,181,215,216]. MSC-primed macrophages have also been shown to inhibit Th1, and stimulate the production of regulatory T (T_{REG}) cells[204,216–218]. MSCs have been shown to also inhibit the maturation of DCs through the action of PGE2 while their co-culture led to a decrease in TNF-α and an increase in IL-10[204,219–221] . MSC co-culture with lymphocytes (i.e., T and B cells) inhibits their proliferation and inhibits their activity through the activity of IDO (humans) or NO (rodents). MSCs can also induce T-cell death through the Fas/FasL apoptotic pathway and promote the upregulation of T_{REG} cells: apoptotic cells are engulfed by circulating macrophages which leads to the release of TGF-β and the subsequent increase in T_{REG} lymphocytes[82,101,178,197,212,220–223]. MSCs have also been shown to have direct effects on NK cells: MSCs inhibit the expression of NK activating receptors on the cell surface, leading to a decrease in their proliferation and cytotoxic activity as well as inhibited IFN-γ production through the action of IDO and PGE2[203,211].

1.12.2.Efficacy of Mesenchymal Stromal Cells as regenerative therapy in kidney injury

Pre-clinical models of AKI show that MSCs are able to ameliorate renal injury and improve renal function through a decrease in the levels of sCr and BUN[21,23,26,47,149,191–193,224–228]. At a cellular level, MSC therapy has been shown to preserve the structural integrity of the kidney in response to injury through a decrease in both tubular cell death and intratubular cast formation. MSC treatment was also able to promote the proliferation of kidney tubular cells while increasing cellular regeneration and survival. In addition, MSC therapy was able to stimulate angiogenesis and reduce damage to the vasculature following renal injury. It is important to note, however, that these studies have not shown consistency in the types of cells used, administered doses and experimental design[21,23,26,47,149,191–193,224–228].

MSCs, administered through IV injection, do not engraft in the damaged kidney but rather travel to the lungs where they die through apoptosis within 24 hours[23,98,117,196,198,229]. As these cells are still capable of ameliorating the effects of AKI, the question of how they are able to exert these effects arises. It has been shown that CD68+ macrophages surround the dying cells, and these macrophages release IL-10, a powerful anti-inflammatory cytokine[23]. Clearance of apoptotic cells by phagocytes plays central roles during development, tissue remodelling and homeostasis, and modulation of immune responses. Efferocytosis, conducted by professional (i.e., macrophages, immature DCs) and nonprofessional phagocytes (i.e., epithelial, smooth muscle, stromal cells), is both anti-immunogenic and anti-inflammatory with effects on leucocytes, particularly antigen-presenting cells. Clearance of apoptotic cells by activated macrophages leads to resolution of inflammation, the secretion of leucocyte protease inhibitors, a decrease in pro-inflammatory cytokines (e.g., IL-1β, IL-8, GM-CSF, IL-1, IL-12, TNF-α), and an increase in anti-inflammatory molecules (e.g., PGE2, IL-10) through TGF-β production[122,230,231]. In addition, other studies have shown that MSCs do not need to interact with cells in order to exert their effects: MSC-conditioned media can increase cell survival and ameliorate the degree of injury in multiple AKI animal models, suggesting endocrine/paracrine factors might be involved[45,106,229]. Whether these effects are due to the proteins MSCs are known to express or to their release of extracellular vesicles (ECVs) remains to be shown. Multiple studies conducted have demonstrated that the therapeutic effects of MSCs can be delivered through the actions of ECVs. Bruno *et* al. (2009) have shown that treatment with MSCs-released ECVs is able to improve disease outcome in

a glycerol-induced model of AKI, in SCID (severe combined immunodeficiency) mice (i.e., that lack mature B and T cells)[232] whereas Cao *et al.* (2020) have shown that MSC-ECVs injection enhanced the mitochondrial function on tubular cells and promoted amelioration of kidney function in a unilateral IRI mouse model[227]. Furthermore, several studies have indicated that MSC-conditioned media can increase the survival of endothelial cells, promote an anti-inflammatory M2 macrophage phenotype, promote tissue repair and recovery, and a subsequent reduction in fibrosis[45,64,106,149,229].

Study	Animal, age, sex, weight, group size	Model	Type of MSC, route of administration, time of administration	Experimental endpoint	Effect
Behr *et al*. (2007)[47]	Sheep, female, adult, n = 5	60min bilateral R-IRI	autologous BM-MSC, 50 × 10^6 (1.5 million MSCs per kilogram), IA injection, 60min following injury induction	day 7 following injury induction	no change in renal function no change in ischaemic renal lesions no change in cell proliferation no change in apoptosis no changes in TNF-α, VEGF-α, Bcl-2, caspase
Bi *et al.* (2007)[229]	C57/BL6 mice, female, 10 - 12 weeks, 18 - 20 g, n = 12	cisplatin model	BM-MSC from C57/BL6 male mice, 2 × 10^5, IP injection, 24h after injury induction	day 2, day 3 and day 6 following injury induction	↓ tubular necrosis ↑ survival ↑ proliferative cells
Bruno *et al.* (2009)[232]	SCID mice, male, 7 - 8 weeks, n = 8	rhabdomyolyses model	extracellular vesicles released by human BM-MSC, IV injection 3 day after injury induction	day 4, day 5, day 8 and day 15 following injury induction	↓ tubular damage (day 5) ↓ tubular necrosis (day 5) ↑ proliferative cells (day 4 and day 5)
Cao *et al.* (2010)[21]	Sprague–Dawley rats, female, 200 ± 20 g, n = 6	60min bilateral R-IRI	human UC-MSCs, 10^6, left carotid artery injection, 16h following reperfusion	day 3 following injury induction	4.8x ↓ sCr 3.6x ↓ BUN ↓ IL-1β ↓ caspase-3 ↑ proliferative cells (+36%)
Cao *et al.* (2020)[227]	FVB mice, male, 6 - 8 weeks, n = 5	50min bilateral R-IRI with	extracellular vesicles released by human placenta-derived MSC, IV injection	day 3, day 5 and day 7 following injury induction	↓ sCr ↓ BUN ↓ KIM-1 (day 5)

		contralateral nephrectomy			↓ TNF-α, PCR (day 7) ↓ caspase 8, PCR (day 7)
Chen *et al.* (2011)[192]	Sprague–Dawley rats, male, adult, 275-300 g, n = 8	60min bilateral R-IRI	autologous ADMSCs, 10^6, intra-renal injection immediately after injury induction & IV injection, 6h and 24h after injury induction	72h following injury induction	↓ sCr ↓ BUN ↑ angiogenesis ↓ oxidative stress ↓ endothelial damage
da Silva *et al.* (2015)[228]	Wister rats, female, adult, 250 - 300 g, n = 7	UUO model	BM-MSC from male Wistar rats, 10^6, abdominal vein injection after total ligation of left ureter	day 7 and day 14 following injury induction	↓ TNF-α, PCR (day 7) ↓ collagen, PCR (day 7) ↓ fibrosis, PCR (day 7) ↑ tubular proliferation (day 14) ↓ caspase 3 (day 14)
Feng *et al*. (2010)[26]	Fisher rats, male, age?, n = 7 - 9	38min bilateral R-IRI	adult male rat ADRCs, 5 × 10^6, IA injection, 20min following injury induction	2h, 24h, 72h and 7 days following injury induction	↑ survival (90%) ↓ sCr (+50%), day 4 ↓ tubular necrosis (72h) ↓ intratubular cast formation (72h) ↑ Ki-67$^+$ proliferative cells (12h) 25x ↓ CD68$^+$ cells (72h) ↓ CXCL2, PCR (2h and 24h) ↓ IL-6, PCR (2h and 24h)
Hauser *et al.* (2010)[106]	SCID BALB/c mice, male, 23 ± 6 g, n = 6 - 8	rhabdomyolyses model	human AFSCs and BM-MSCs, 350,000, IV injection	day 3, day 5, day 8 and day 21 following injury induction	↓sCr (+ day 5 following treatment) ↓BUN (+48h following treatment)

					↓ tubular necrosis ↓intratubular cast formation ↑ proliferative cells ↑ VEGF
Imberti *et al.* (2007)[191]	C57BL6/J, female, 2 months, n = 6	cisplatin model	BM-MSC from C57BL6/J male mice, 2 × 10^5, IV injection, 24h following injury induction		↑ tubular regeneration ↑ tubular proliferation ↓ apoptosis ↓ BUN
Morigi *et al.* (2004)[225]	C57BL6/J mice, female, 2 months, n = 12	cisplatin model	BM-MSC from male C57BL6/J mice, 2 × 10^5, IV injection, 24h after injury induction	day 4, day 7, day 11, and day 29 following injury induction	↓ BUN (day 4 and day 5) ↓ tubular damage (day 4) ↓ tubular cast formation (day 4) ↓ focal cell loss (day 4) ↑ Ki-67$^+$ proliferative cells (day 11)
Morigi *et al.* (2008)[224]	NOD-SCID mice, female, 2 months, n = 9	cisplatin model	human BM-MSC, 5 × 10^5, IV injection, 24h after injury induction	day 4 following injury induction	↓ BUN (day 3 and day 4) ↑ tubular proliferation ↓ peritubular capillary damage ↑ survival (34% by day 14)
Morigi *et al.* (2010)[193]	NOD-SCID mice, female, 2 months, n = 11	cisplatin model	human UC-MSC, 5 × 10^5, IV injection, 24h after injury induction	day 4 following injury induction	↓ BUN (day 3 and day 4) ↓ tubular necrosis / apoptosis ↓ peritubular capillary damage ↑ survival (86%) ↓ oxidative damage

					↑ tubular proliferation
Németh *et al*. (2009)[117]	C57/BL6 mice, male, 42 - 44 weeks, n = 14	caecal ligation puncture	C57/BL6, BALB/c or FVB/NJ BM-MSC, 1 million, IV injection, 1h and 24h following injury induction	24h following injury induction	↓sCr ↓BUN ↓ organ damage with 24h MSC injection ↑ glycogen storage in liver ↓ apoptotic / necrotic cells in spleen ↓ TNF-α, serum (24h) ↓IL-6, serum (24h) ↑IL-10, serum (3 – 12h)
Ren *et al.* (2008)[122]	BALB/c, sex ?, 8 weeks, n = 6	LPS injury model	human apoptotic PMN, 10 × 10^6, IV injection, 1h, 3h, 6h and 24 h following injury induction	3 weeks following injury induction	↑ survival (80%) ↓ organ damage (lung, liver, heart, kidney) ↓ IL-12, TNF-α, and IFN-γ serum (1.5h after treatment)
Rota *et al.* (2018)[149]	athymic rats, male, 200–250 g, n = 7	adryamycin model	human BM-MSCs, UC-MSCs, kPSCs, 1.5 × 10^6, IV injection, time of administration ?	28 days following injury induction	↓ glomerular podocyte injury ↓ endothelial cell injury ↓ fibrosis ↑ M2 macrophages
Santeramo *et al*. (2017)[23]	immunodeficient rats, male, 8 - 9 weeks, n = 6	cisplatin model	human $CD133^+$, 10^6, IV injection, day 2 and day 7 following injury induction	2 weeks following injury induction	↓ FITC-sinistrin $t_{½}$, day 7 ↓ sCr, day 7 ↓ BUN, day 7 ↓ mean luminal area ↓ fibrosis

Table 1.4: MSC used in pre-clinical studies of kidney injury. Abbreviations: ADRC – adipose-derived regenerative cell, AFSC – amniotic fluid stem cell, g – gram, HO – heme oxygenase, IA – intra-arterial, IP – intra-peritoneal, IV – intra-venous, kPSC - kidney perivascular stromal cell, PMN - polymorphonuclear neutrophils, UUO – unilateral urethral obstruction

A search was conducted as part of this study in the www.ClinicalTrials.gov database for registered trials using MSC therapy. In January 2023, there were 538 clinical trials conducted around the world using MSC therapies for the treatment of various diseases, with 29 studies focusing on kidney disease. The search included studies in all the stages ('not enrolling', 'recruiting', 'terminated' and 'completed') and the following terms were used: 'MSC', 'mesenchymal stromal cell', 'mesenchymal stem cell', 'kidney injury', 'kidney disease', 'nephropathy', 'renal', 'CKD', 'chronic kidney disease', 'AKI' and 'acute kidney injury'. While MSC therapies have shown promising results in pre-clinical models, their translation to the clinic has not yielded conclusive results on the merit of these treatments. Phase I clinical trials assessing the safety of MSCs in various disease models have found these therapies to be safe when given to humans[157,195,233–237]. However, when assessing the effects of MSC therapy on disease outcomes, the results were not as positive. A phase II and a phase III clinical trials showed that intravenous infusions of allogeneic MSCs were effective in reducing fistulas in patients with Crohn's disease[235,236], whereas a phase II clinical trial using MSCs for the treatment of chronic obstructive pulmonary disease (COPD) showed no significant differences in patients' quality-of-life following therapy. Preliminary data from a phase I clinical trial testing the safety and efficacy of MSC therapy in patients that are at high risk of developing AKI after cardiac surgery suggests that both length of hospital stay and readmission rates were reduced by 40% with a 20% reduction in the number of patients that developed AKI in the treatment group when compared to the control[157]. However, a phase II clinical trial to determine the efficacy of MSC treatment in reducing the recovery time from AKI after cardiac surgery found no differences between the therapy and placebo groups[237].

Therefore, understanding the mechanisms by which MSCs as cellular therapies confer protection, and promote repair and regeneration is a critical aspect of developing efficacious therapeutic interventions.

1.13. Aims

When shaping an experimental design, the choice of animal species and strain is highly important as it will influence how well the set scenario to test one's hypothesis is simulated. In addition, multiple studies throughout the years have shown variability in research data due to differences in genetic backgrounds[36,128,238–240]. The primary focus of this thesis was the

detailed characterisation of three different mouse strains: BALB/c, C57BL/6 alb and CD1 to detect whether there are any differences in how these three strains respond to nearly identical experimental conditions, and whether these differences are statistically and biologically significant. Both BALB/c and C57BL/6 alb are two inbred strains with mice in each strain nearly identical to each other whereas CD1 mice are an outbred strain generated to maintain maximal heterozygosity. Using techniques such as GFR measurements and cytofluorimetric analysis, we have aimed to:

(1) assess the impact of R-IRI on renal function in three different mouse strains;

(2) compare the impact of R-IRI on renal function between three different mouse strains.

Expanding on this narrative, we have considered the myriad of data pointing towards MSCs regenerative capabilities in kidney disease, and we have endeavoured to:

(1) assess the impact of regenerative medicine therapies on renal function in three different mouse strains following R-IRI;

(2) compare the impact of regenerative medicine therapies on renal function in three different mouse strains following R-IRI.

Finally, the multitude of literature available points towards MSCs exerting their regenerative functions through immune system modulation, and as such we have aimed to:

(1) assess the effect of R-IRI on spleen and kidney macrophages, in three different mouse strains;

(2) determine the effect of regenerative medicine therapies on spleen and kidney macrophages, in three different mouse strains following R-IRI;

(3) determine the effect of regenerative medicine therapies on pro- and anti-inflammatory cytokine levels in BALB/c mice.

Guiding these multifaceted experiments, the overarching hypotheses of this study were:

(1) There are significant differences in how animals from different strains respond to bilateral R-IRI.

(2) MSC therapy ameliorates kidney injury, regardless of strain, through their effects on macrophages.
(3) MSC therapy stimulates macrophages towards an M2 anti-inflammatory phenotype.
(4) MSC therapy leads to an increase in anti-inflammatory cytokines and a decrease in pro-inflammatory cytokines.

Chapter 2
Materials & Methods

2. Methodology

2.1. Animals

All *in vivo* experiments within this thesis were conducted at the University of Liverpool in accordance with UK Animal Scientific Procedure Act (ASPA), 1986 (Project Licences: PPL 70/8741 and PP3076489), and were approved by the Home Office in agreement with EU directive 2010/63/EU. All animal procedures were performed by an individual holding a personal licence.

Male mice were housed in pathogen-free individually ventilated cages, under standard conditions with a 12-hour light/dark cycle and *ad libitum* access to food and water; all animals were acclimated for 1 week prior to the start of experiments.

Male BALB/c and CD1 mice were procured from Charles River Laboratories (Margate, UK). Albino C57BL/6 mice (B6NTyrc-/BrdCrCrl) mice had been purchased from Charles River (Italy) in November 2018 and subsequently used to establish an in-house colony at the University of Liverpool, Biomedical Sciences Unit (BSU). Ten to thirteen weeks old BALB/c and C57BL/6 alb mice were used for *in vivo* experiments, whereas CD1 mice were eight to nine weeks old. BALB/c and C57BL/6 alb weighed between 20 – 27g, while CD1 weighed between 28 – 38g. The CD1 mice used in the experiments were younger and weighed significantly more than the other two strains at the start of the experiments because CD1 is an outbred strain that grows to bigger sizes than the other two strains used. *In vivo* experiments were conducted in three different animal strains to determine whether strain differences influence response to R-IRI and/or cell therapy. These experiments have only focused on male mice to generate more consistent data as female mice experience hormonal fluctuations which can introduce variability in the results.

2.2. Experimental design

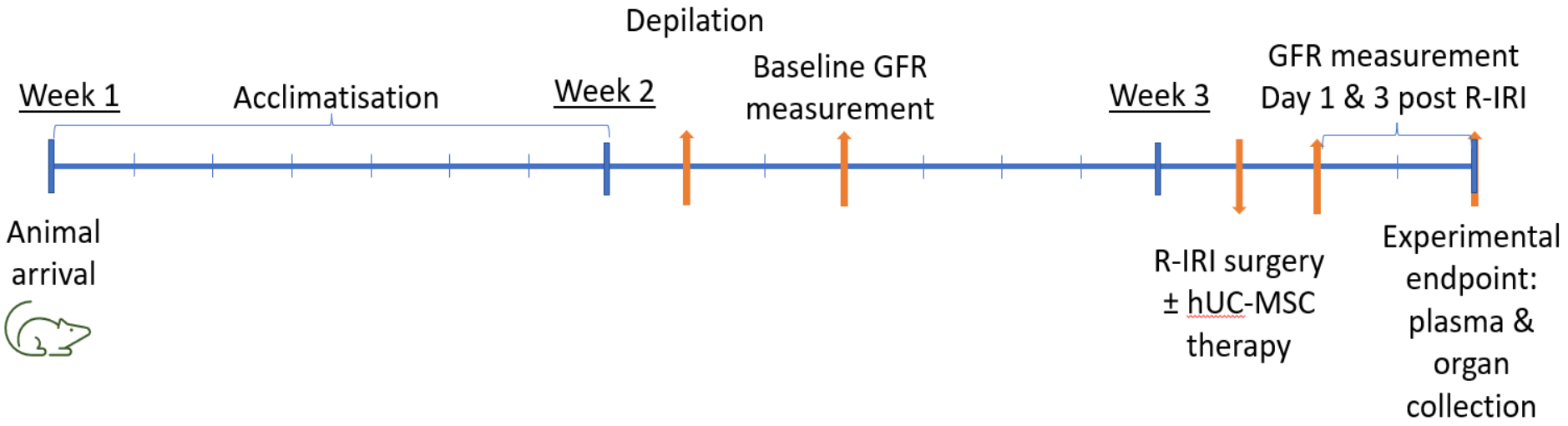

Figure 2.1: Schematic of AKI model experimental design.

In brief, the experiments began at week 1 with animal arrival (Figure 2.1). The animals were given 1 week to acclimatise to their new environment, and at the beginning of week 2 *in vivo* experiments start. First, the animals were anaesthetised with oxygenated isoflurane, shaved, and depilated on the area where the transcutaneous devices were placed. 24-48 hours following depilation, baseline GFR measurements that assess renal function were taken. In week 3, the animals underwent R-IRI surgery to induce an acute kidney injury, and were given cellular therapies immediately following surgery. Renal function was assessed at day 1 and day 3 post-operatively. Following GFR measurements on day 3, the animals were culled with collection of plasma and organs.

Animals were culled before the day 3 experimental end-point (and excluded from the analysis) if they showed no clearance of FITC-Sinistrin on day 1 as this was indicative of no renal function (GFR = 0); previous experiments have shown that these animals do not survive until the experimental end-point and most often were in extreme distress due to the effects of renal failure. Furthermore, animals were also excluded from analysis if they suffered significant blood loss during surgery or if the rectal temperature probe was dislodged during surgery.

2.3. Surgical model of acute kidney injury

Eight to thirteen weeks old mice were anaesthetised with 3% oxygenated isoflurane in an anaesthetic box. Following induction of anaesthesia, animals were transferred to a nose cone (2% ± 0.2% oxygenated isoflurane) and administered sub-cutaneous baytrill, buprenorphine and 0.5mL 0.9% saline by an animal technician. The animals were then shaved, and iodine and alcohol were used to sterilise the shaved area. The animals were transferred to a heat pad (Far Infrared Warming Pads, Physiosuite, Kent Scientific) in prone position; temperature of the heat pad was set to 37^{o}C, and a rectal probe was used to maintain a constant body temperature. Surgery commenced after 30 minutes from the induction of anaesthesia. Kidneys were reached through dorsal incisions in the skin and muscle (Figure 2.2), and gently pushed out of the body cavity; fat was removed from around the pedicles. Acute kidney injury was induced through bilateral clamping of renal pedicles with an atraumatic microaneurysm clamp (Schwartz, Interfocus, Linten) which was applied using microaneurysm forceps. Successful clamping was indicated by a uniform change in the organ's

colour, from pink/red to dark red/purple. Kidneys were clamped for 27.5min and the clamps were removed to allow for organ reperfusion; this was indicated by the change of the kidneys' colour back to red. We have employed a 30min pre-clamping time followed by a 27.5min clamping time due to previous optimisation experiments performed in the B. Wilm lab that showed refinement of these times decreases the variability associated with the bilateral R-IRI model and leads to a degree of injury severe enough without breaching the severity limits covered within the animal licence[241].

Following clamp removal, the kidneys were gently pushed back into the body cavity using a damp cotton bud. 6.0 Vicryl sutures (CliniSorb, CliniSut sutures) were used to close the muscle layer of the incision with a continuous suture, followed by skin closure with a horizontal mattress suture. Animals were placed for 30min in a ventilated heated chamber (32°C) for recovery before being transferred to clean cages. Animals in the sham group underwent all the same steps in the surgical model, except for the clamping of the renal pedicles.

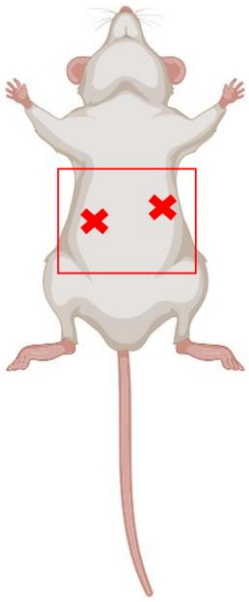

Figure 2.2: Schematic of IRI surgery model. Representative image of a mouse, laid in prone position for the IRI surgery. The red rectangle represents the area which was shaved for surgery while the two x's represent the incision points; the right x is higher than the one on the left as the right kidney is slightly located higher than the left kidney due to the presence of the liver on the right.

Animals were closely monitored throughout the procedure by both the researcher and an animal technician, and surgery was performed in a staggered manner on 3 mice at once. All mice were anaesthetised individually using separate nose cones attached to an anaesthetic 'splitter'. Rectal temperature was maintained between 36.5°C and 37.5°C throughout the procedure, using a rectal probe and a heating pad with a feedback-regulated system[1].

2.4. Cell Preparation & Administration

Human umbilical cord-derived MSCs (hUC-MSCs) were provided by NHS Blood and Transplant (NHS-BT) at passage 2. On receipt, the cells were expanded to passage 5, aliquoted and cryo-preserved in liquid nitrogen. One week prior to surgery, cells were taken out of cryo-storage and seeded in 10cm culture dishes. The cells were cultured in MEM-α medium (Gibco™, UK, Cat. Number 32561029) supplemented with 10% foetal bovine serum (FBS; Sigma, Germany, Cat. Number F2442). The cells were incubated at 37°C in a 5% CO_2 humidified atmosphere, and the medium was changed every 2-3 days until the cells reached 90% confluence. On the day of the surgery, the cells were prepared for IV administration. The media was aspirated and discarded; the dishes were washed twice with 3mL of sterile Dulbecco's phosphate-buffered saline (PBS; Sigma, Germany), and then were incubated with 1mL PBS and 500mL TrypLE select enzyme (Gibco, UK, Cat. Number 12563011), for 3 minutes at 37°C, 5% CO_2. Following incubation, 2mL of warm medium was added to the dishes, and the suspension was collected in a 15mL canonical tube and centrifuged for 3 minutes at 1500rpm or 400g. The supernatant was discarded, and the cells were resuspended in ice-cold sterile PBS. An automated cell counter was used to count the cells, and the cells were suspended at a volume of 2,500 cell/µL. The cells were aliquoted in separate microcentrifuge tubes for each individual animal and were kept on ice until the time of administration.

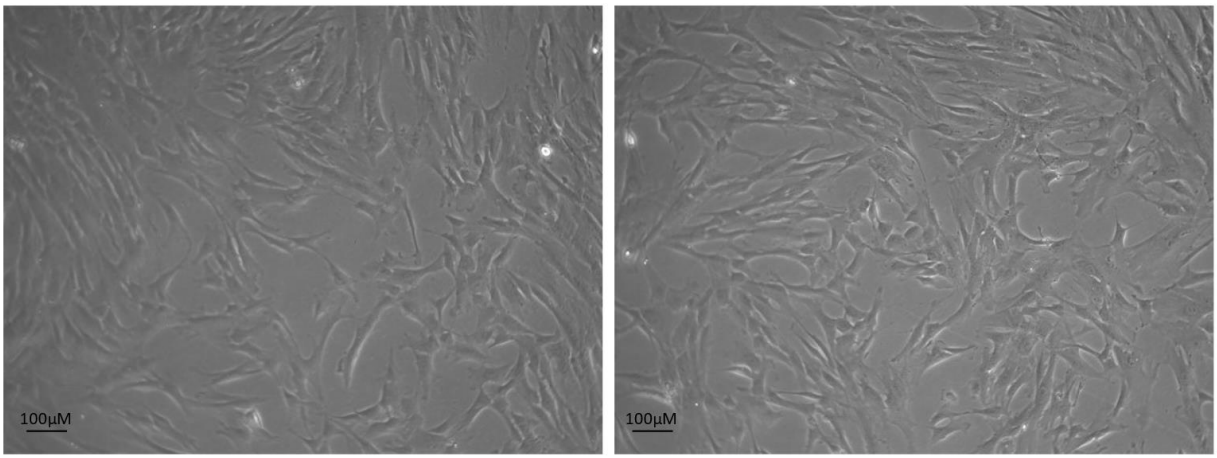

Figure 2.3: hUC-MSC morphology at passage 7. Representative Bright Field images of hUC-MSCs showing an elongated spindle-shaped morphology, typical of a fibroblast cell. Scale bar is 100 µM.

We have chosen to use hUC-MSCs received from NHS-BT due to multiple reasons:

(1) A Doctoral student in the B. Wilm lab had characterised these cells and demonstrated the adipogenic and osteogenic differentiation of these cells[326].
(2) Preliminary work from a Doctoral student in the B. Wilm showed that these cells are capable of ameliorating kidney injury[267].

It is important to note that at the time of these experiments, a Doctoral student in the B. Wilm lab was comparing the effect of BM-MSCs, UC-MSCs and adipose-derived MSC in ameliorating kidney injury following bilateral R-IRI; this research has not yet been published.

2.5. Therapy administration

hUC-MSCs were harvested and aliquoted during the surgical session by other members of the B. Wilm lab; the cells were administered within 3 hours of harvesting so as to avoid cellular apoptosis. Prior to administration, the cells were taken off ice until they reached hand-warm temperature; this was done to avoid damage to the tail tissue during IV injection. The cells were administered immediately after the surgery (i.e., after the researcher had finished suturing the wounds) while the mice were still under anaesthesia. Animals were administered either 100µL PBS or 250,000 cells (in 100µL PBS) via IV injection into the tail vein.

Animals were grouped into cages and randomly allocated to treatment groups within each cage to minimise bias.

2.6. Injury assessment using a transcutaneous device

The glomerular filtration rate (GFR) measures kidney function and was assessed at baseline (prior to R-IRI induction), and on days 1 and 3 after R-IRI by administering FITC-Sinistrin into the tail vein; FITC-Sinistrin is a substance exclusively filtered through the glomerulus. The GFR was measured using a transcutaneous device (Medibeacon™, Mannheim) that measures the fluorescence signal given by FITC-Sinistrin clearance over a 90-minute period[242]. This device allowed for the measurement of GFR without any of the constraints of sCr or BUN assays[241,242]. The FITC-Sinistrin half-life (t½) clearance time was analysed through a 3-compartment linear fit model, using the Studio (V2, Medibeacon™,

Mannheim) software (Figure 2.5)[243]. The GFR was calculated from the FITC-Sinistrin t½, using the following equation, as per manufacturer's instructions[244]:

$$GFR\left[\frac{\mu L}{min}\ per\ 100g\ body\ weight\right] = \frac{14616.8(\mu L/100g\ body\ weight)}{t1/2(FITC - Sinitrin[min])}$$

Animals that showed no FITC-Sinistrin clearance at day 1 post-surgery (Figure 2.5C) had a flat curve (indicating a lack of excretion of the FITC-Sinistrin compound) and the software was unable to calculate a $t_{1/2}$. However, the FITC-Sinistrin $t_{1/2}$ formula for measuring GFR allows for the addition of animals that show no excretion (GFR = 0) to be included in the analysis.

At least 24 hours prior to the GFR measurements, the animals were anaesthetised with oxygenated isoflurane, shaved and depilated with Veet cream (Veet, UK) for 1 minute; the depilated area was approximately 3x3cm and covered the right dorsal side. For the measurement of FITC-Sinistrin clearance, animals were once again anaesthetised with oxygenated isoflurane and the transcutaneous device was applied on their back, on the depilated area, above the right kidney (Figure 2.4). A benchmark reading was taken for 5 minutes followed by intravenous (IV) injection of FITC-Sinistrin into the tail vein. During the 90-minute period when clearance of FITC-Sinistrin was measured, animals were housed individually, without any access to water.

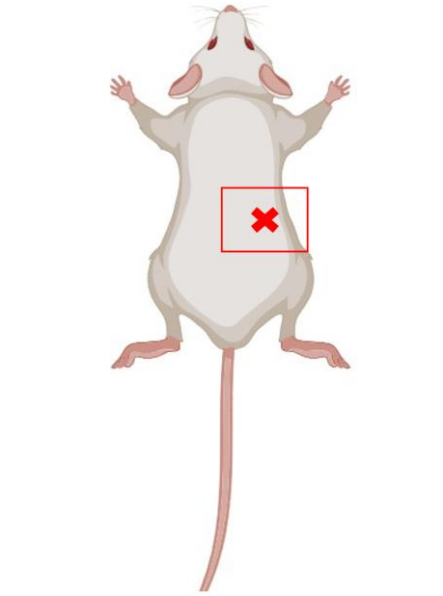

Figure 2.4: Schematic of GFR measurement procedure. Representative image of a mouse, laid in supine position for the GFR measurement procedure. The red rectangle represents the area which was depilated while the x represents the area where the GFR measurement device was placed.

Healthy animals were given a standard dose of 75µg/g body weight of FITC-Sinistrin, in line with manufacturer's instructions (approximately 100µL). For animals that had undergone surgery, the FITC-Sinistrin dose was lowered to 70% of the initial dose to avoid quenching which would make it difficult to measure the peak of the curve and would lead to inaccurate measurements.

We have relied on assessing GFRs using solely the transcutaneous devices due to three main reasons:

1. It has allowed for repeated assessments of renal function without culling of the animal.
2. sCr and BUN are both markers found in serum and are routinely used in the clinic to assess kidney injury. However, as one of the main aims of this thesis was to assess the impact of cellular therapies on the immune system, we had decided to forego these two assessments and measure cytokines in the plasma. Due to the nature of the experiments and the volume of blood needed to conduct them, we were unable to measure sCr and BUN in addition to cytokines.
3. Previous worked from a Doctoral student in the B. Wilm showed that the transcutaneous device provides an accurate measurement of kidney injury when compared to sCr and BUN level in serum[267].

A.

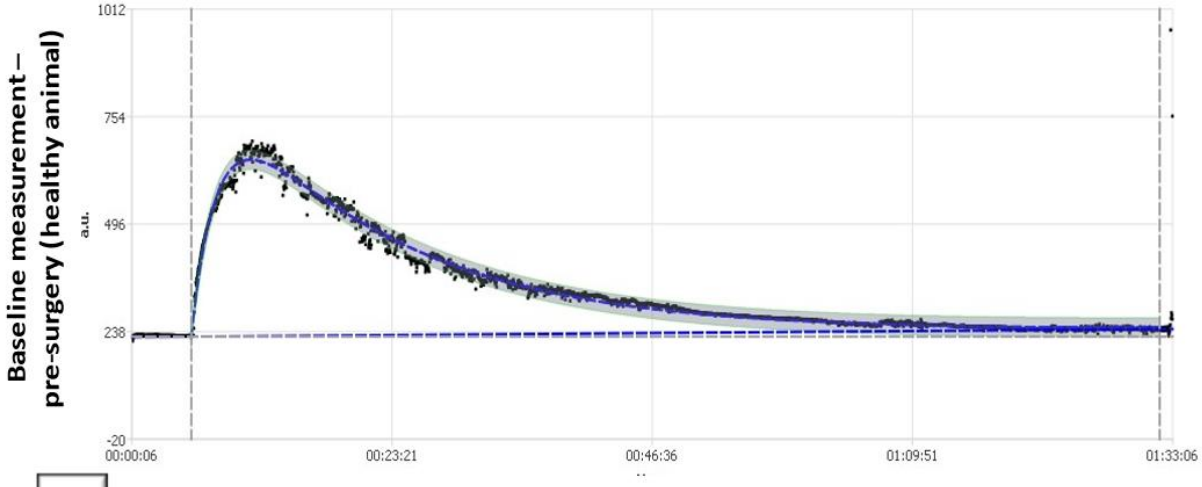
Baseline measurement – pre-surgery (healthy animal)
a.u.
1012
754
496
238
-20
00:00:06
00:23:21
00:46:36
01:09:51
01:33:06

B.

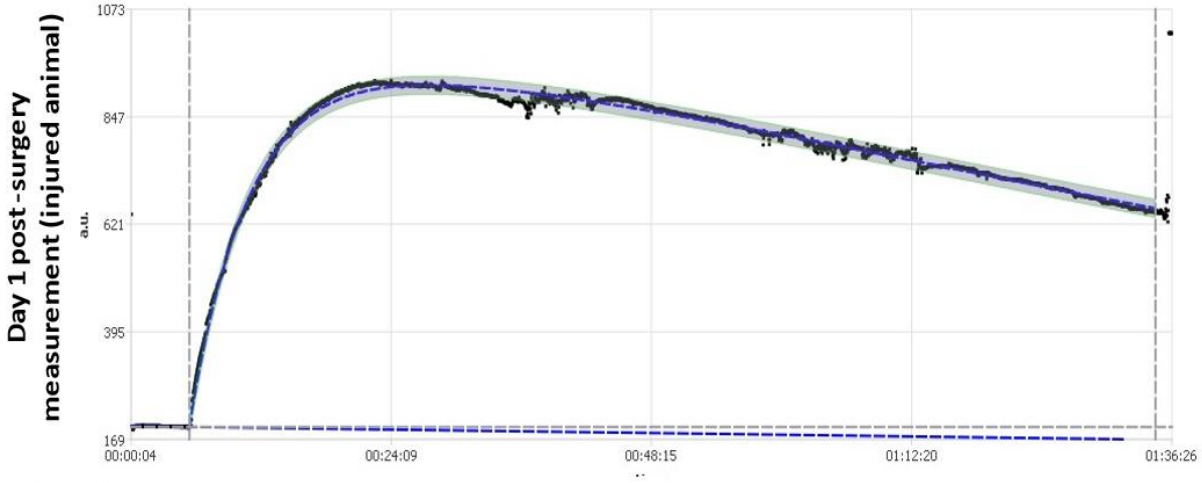
Day 1 post-surgery measurement (injured animal)
a.u.
1073
847
621
395
169
00:00:04
00:24:09
00:48:15
01:12:20
01:36:26

C.

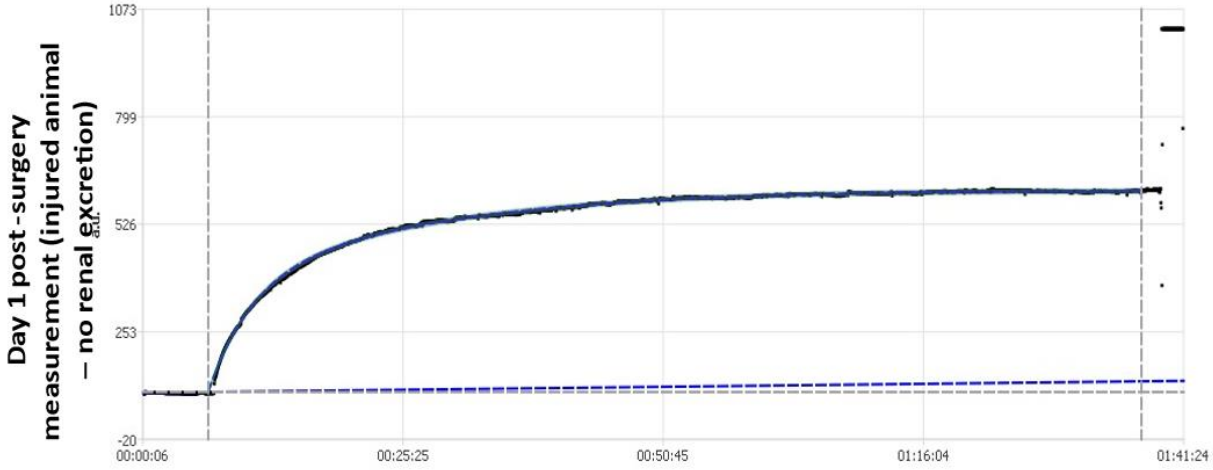
Day 1 post-surgery measurement (injured animal – no renal excretion)
a.u.
1073
799
526
253
-20
00:00:06
00:25:25
00:50:45
01:16:04
01:41:24

Figure 2.5: Transcutaneous assessment of FITC-Sinistrin clearance. (**A – C**) Examples of typical FITC-Sinistrin kinetic curves. (**A**) Baseline measurement of renal function on healthy animals, pre-surgery, indicating FITC-Sinistrin complete clearance within the 90-minute measurement period ($t_{1/2}$ = 11.39 minutes; GFR = 1254.52 µL/min/100g body weight (b.w.)); (**B**) Day 1 post R-IRI surgery measurement of renal function, indicating that the FITC-Sinistrin was not completely filtered by the kidney within the 90-minute measurement period ($t_{1/2}$ = 59.29 minutes; GFR = 245.72 µL/min/100g b.w.); (**C**) Day 1 post R-IRI surgery measurement of renal function, indicating no clearance of the FITC-Sinistrin within the 90-minute measurement period and complete renal failure ($t_{1/2}$ = unable to measure; GFR = 0 µL/min/100g b.w.). Black data points represent the raw data, while the blue line represent the 3-compartment linear fit model.

2.7. Organ collection and dissociation

The animals were culled on day 3 post-surgery by cardiac puncture under terminal isoflurane anaesthesia, followed by immediate cervical dislocation and organ collection of kidneys and spleens. Organs were washed with ice-cold PBS, cleaned of any residual fat and cut into small pieces. Individual organs were placed in C-tubes (Miltenyi Biotec, Germany, Cat. Number 130-093-237) containing 1.8mL Dulbecco's Modified Eagle's Medium (DMEM; Sigma-Aldrich, Germany, Cat. Number D5671), 20µL $CaCl_2$ (1M; Sigma-Aldrich, Germany, Cat. Number 10043-52-4), 20µL Dnase I from bovine pancreas (10mg/mL; Sigma-Aldrich, Germany, Cat. Number 11284932001), and 200µL Liberase DL enzyme (Sigma-Aldrich, Germany, Cat. Number 5466202001) stock solution; the Liberase DL stock solution was prepared by mixing 50mg Liberase powder with 15.5mL DMEM, and was stored at -20°C.

The organs were dissociated using the GentleMACS (Miltenyi Biotec, Germany) tissue dissociator. The C-tubes were placed on the GentleMACS and were minced using the Multi-E_01 program. This was followed by a 30-minute incubation period at 37°C with continuous rotation, and another run on the GentleMACS, Multi-E_02 program. Following dissociation, 10mL of ice-cold PEB buffer was added to the C-tubes in order to stop the enzymatic reaction; the PEB buffer was prepared on the day with 10g bovine serum albumin (BSA; Sigma-Aldrich, Germany, Cat. Number 9048-46-8), 480mL PBS and 8mL ethylenediaminetetraacetic acid (EDTA; Sigma-Aldrich, Germany, Cat. Number 60-00-4) at a concentration of 5mM. 1ml of the dissociated product was pipetted, transferred to a microcentrifuge tube and centrifuged at 400g for 10 minutes. The supernatant was carefully pipetted, aliquoted into microcentrifuge tubes and stored at −80°C in order to analyse for cytokine levels in kidney lysates.

Individual cell suspensions of the dissociated organs were each transferred to a 50mL Falcon tube using a 70µm cell strainer (Miltenyi Biotec, Germany, Cat. Number 130-098-462), and another 10mL of PEB buffer were added to the mixture. The cell suspension was centrifuged at 1400rpm for 10 minutes. The supernatant was discarded, and the cells were resuspended in 2mL ACK Lysing Buffer (Gibco™, UK, Cat. Number A1049201) for red blood cells (RBC) lysis; kidney cell suspensions were incubated for 2 minutes while those of spleens were incubated for 5 minutes. Following the incubation period, the tubes were filled with PEB buffer to stop the reaction and centrifuged at 1400rpm for 10 minutes.

2.8. Cytofluorimetric analysis of macrophages

Following RBC lysis, the supernatant was carefully aspirated, and the pellet was resuspended in flow cytometry staining buffer (Invitrogen, UK; cat. number 00-4222-26). 90µL of the resuspended cells were aliquoted to individual microcentrifuge tubes ($2x10^6$ cells per test tube) with 10µL of mouse FcR Blocking Reagent (Miltenyi Biotec, Germany, Cat. Number 130-092-575) and 1µL Viobility 405/452 Fixable Dye (Miltenyi Biotec, Germany, Cat. Number 130-109-812); the mixture was pulsed gently and incubated for 15 minutes at room temperature, in the dark. Following incubation, 1mL staining buffer was added and the tubes were centrifuged at 400g for 10 minutes. The supernatant was carefully aspirated, the pellet was resuspended in 100µL staining buffer, and purified antibodies were added to the tubes. The following antibodies were purchased from Invitrogen and were used to stain for macrophages (Table 2.1): F4/80 APC-eFluor 780 (Cat. Number 47-4801-82), CD86 PE-Cyanine7 (Cat. Number 25-0862-82), and CD163 APC (Cat. Number 17-1631-82). The isotype controls were Rat IgG2a kappa Isotype Control (eBR2a), APC-eFluor 780 (Invitrogen, Cat. Number 47-4321-82), Rat IgG2a kappa Isotype Control (eBR2a), PE-Cyanine7 (Invitrogen, Cat. Number 25-4321-82), and Rat IgG2a kappa Isotype Control (eBR2a), APC (Invitrogen, Cat. Number 17-4321-81). After 30 minutes incubation in the fridge, 2mL of staining buffer were added to the tubes and the solution was centrifuged at 400g for 10 minutes. The supernatant was gently aspirated, and the pellet was resuspended in 2mL of staining buffer and centrifuged once more at 400g for 10 minutes. Following this final round of centrifugation, the supernatant was discarded, and the cells were resuspended in 100µL IC Fixation Buffer (Invitrogen, UK, Cat. Number 00-8222-49). Samples were covered in aluminium foil and stored

in the fridge overnight. The samples were fixed prior to cytofluorimetric analysis as it was not possible to perform the analysis immediately due to the extended number of experiments carried out at the experimental end-point day (i.e., day 3 GFR measurements, cardiac puncture for blood collection, organ collection and dissociation followed by cellular staining of sample which took, in total, approximately 14 hours). The following day after cellular staining, the samples were resuspended in 1mL staining buffer with 20µL Dnase I to avoid cell-to-cell adhesion. Flow cytometry analysis was performed using a BD FACSCanto II with 80,000 acquired live events per sample. Data was acquired using the BD Cell Quest Software (BD Biosciences).

Antibody	**Clone**	**Isotype**	**Fluorochrome**	**Dilution**
F4/80	BM8	Rat IgG2a, kappa	APC-eFluor 780	0.5 µg/test
CD86	GL-1	Rat IgG2a, kappa	PE-Cyanine7	0.25 µg/test
CD163	TNKUPJ	Rat IgG2a, kappa	APC	0.25 µg/test
F4/80 Isotype control	eBR2a	Rat IgG2a kappa Isotype Control	APC-eFluor 780	0.5 µg/test
CD86 Isotype control	eBR2a	Rat IgG2a kappa Isotype Control	PE-Cyanine7	0.25 µg/test
CD163 Isotype control	eBR2a	Rat IgG2a kappa Isotype Control	APC	0.25 µg/test
Viobility Fixable Dye	-	-	405/452	1:100

Table 2.1: Antibodies used for cytofluorimetric analysis of macrophages.

2.9. Gating strategy used to sort F4/80$^+$CD86$^+$ and F4/80$^+$CD163$^+$ cells

In order to create an effective flow cytometry sorting strategy, the spleen of healthy mice was used as a positive control for the gating strategy used to sort M1-like (F4/80$^+$CD86$^+$) and M2-like (F4/80$^+$CD163$^+$) cells, as this organ is rich in macrophages. Compensation, to correct fluorescence spillover and remove background noise, was performed for all three different mouse strains used in the experiments.

While CD206 is the more common marker used to identify M2-like macrophages, we had to rely on the use of CD163 instead as we were unable to purchase CD206 in the APC fluorochrome (at the time of experiments, CD206 was not available for purchase at any of the suppliers in the APC fluorochrome). Due to the use of FITC-Sinistrin in our experiments to assess renal function following bilateral R-IRI, we were unable to utilise the FITC and PE channels of the flow cytometer: due to the severe level of injury and the inability of the

kidneys to filter and excrete the FITC-Sinistrin compound in the urine, this had accumulated in the injured tubules and interfered with the assessment of our results (see Supplementary Figure 1).

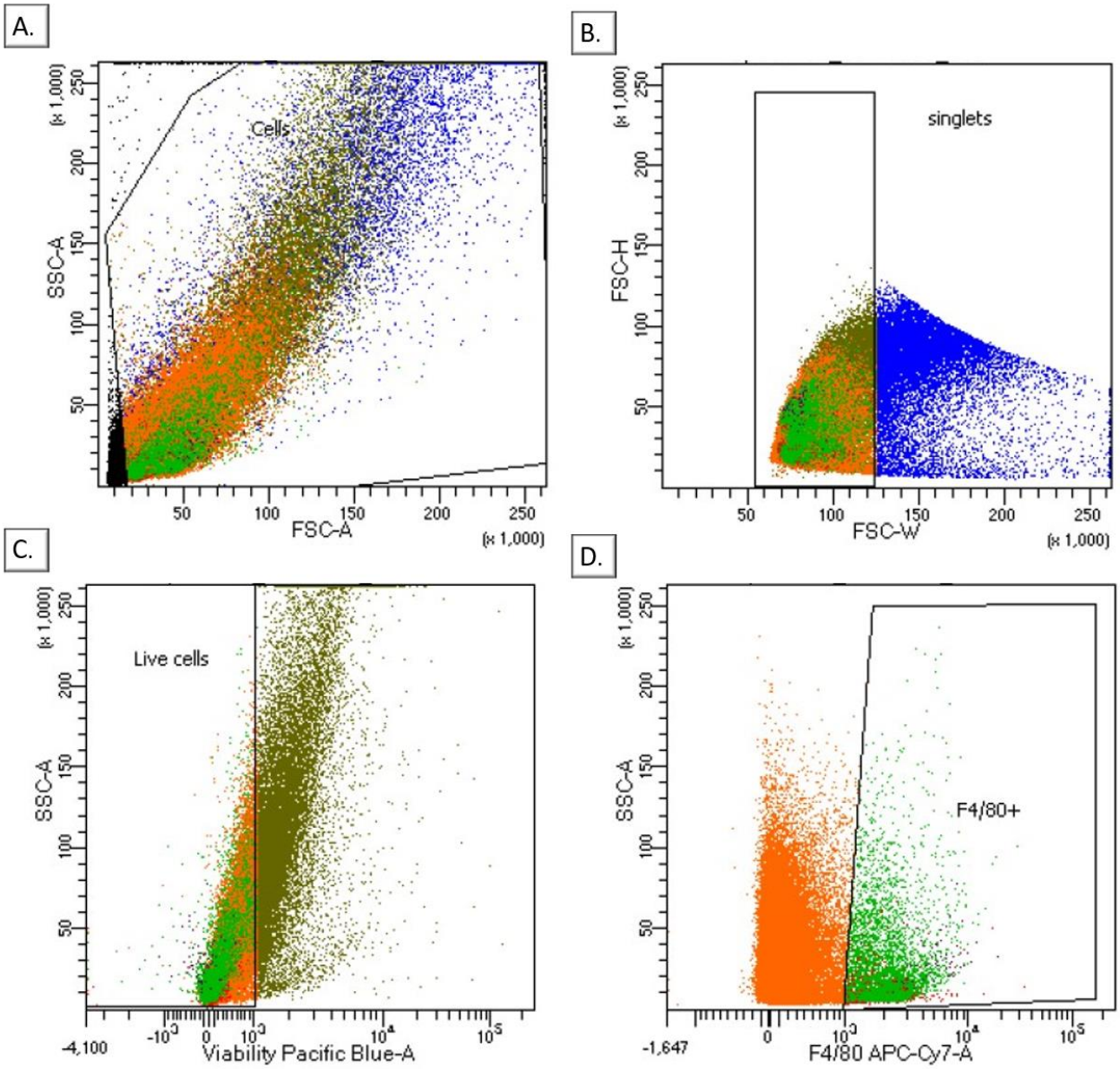

Population	#Events	%Parent	%Total
All Events	181,059	####	100.0
Cells	109,974	60.7	60.7
singlets	96,925	88.1	53.5
Live cells	80,000	82.5	44.2
F4/80+	5,425	6.8	3.0
CD86+	202	3.7	0.1
CD163+	3,535	65.2	2.0
Q1	1,341	37.9	0.7
CD86+CD163+	58	1.6	0.0
Q3	2,075	58.7	1.1
Q4	61	1.7	0.0

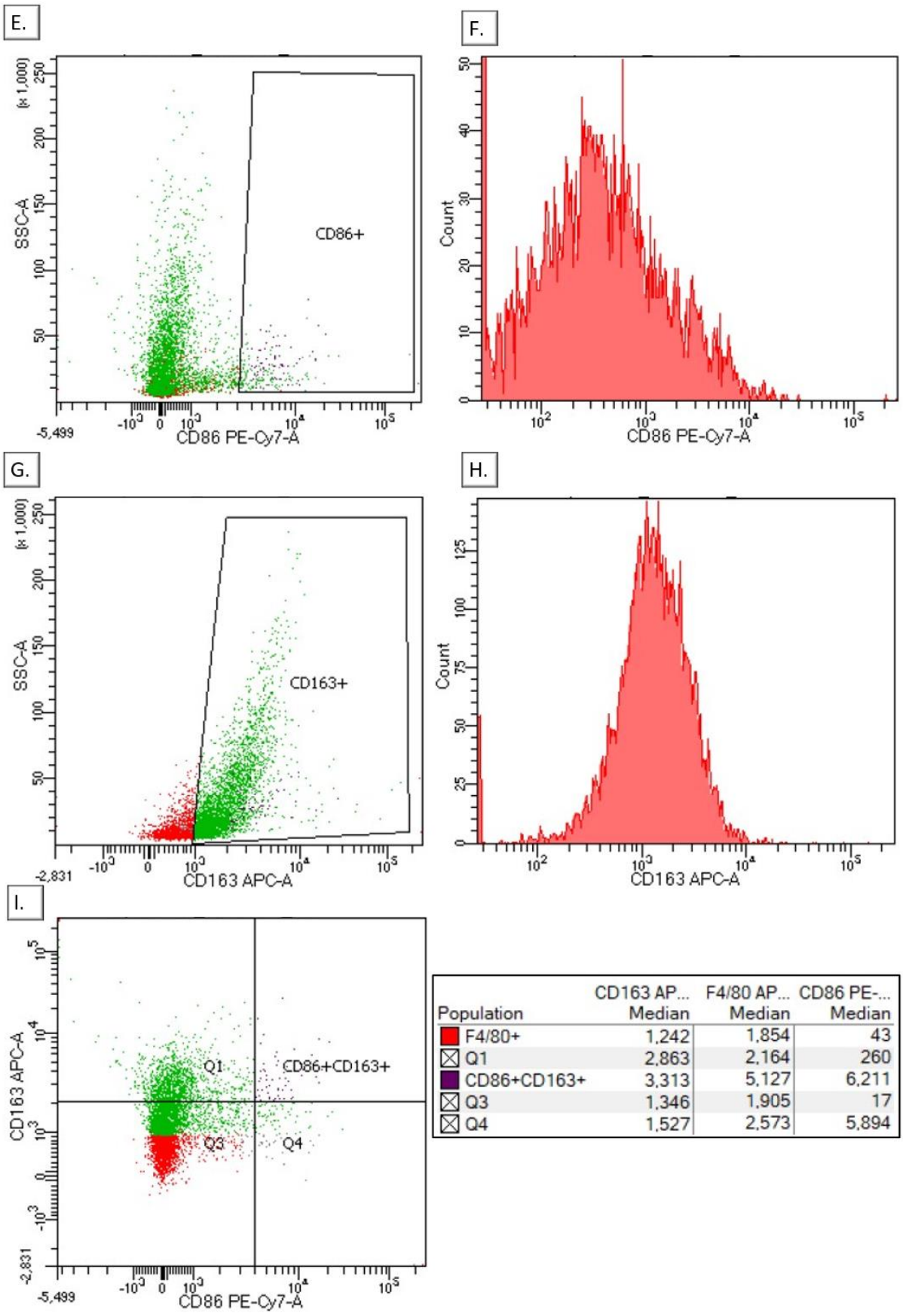

Population	CD163 AP... Median	F4/80 AP... Median	CD86 PE-... Median
F4/80+	1,242	1,854	43
Q1	2,863	2,164	260
CD86+CD163+	3,313	5,127	6,211
Q3	1,346	1,905	17
Q4	1,527	2,573	5,894

Figure 2.6: Gating strategy used to sort F4/80+CD86+ and F4/80+CD163+ cells in spleen lysates.

A dot plot showing Forward Scatter-Area (FSC-A) and Side Scatter –Area (SSC-A) was used to discriminate healthy and damaged or dying cells (Figure 2.6A). Next, a dot plot of Forward Scatter-Height (FSC-H) and Forward Scatter-Width (FSC-W) was used to discriminate singlets from doublets and clumps, which might represent a false positive signal (Figure 2.6B). This was followed by a dot plot of SSC-A and the signal from the excitation of cells with the 452nm laser (Pacific Blue) was used to discriminate between live and dead cells (Figure 2.6C). Next, a dot plot of SSC-A and the signal from the excitation of cells with the 635nm laser (APC-Cyanine7) was used to distinguish $F4/80^+$ cells in the live population (Figure 2.6D). To determine the population of M1-like macrophages from the $F4/80^+$ population, a dot plot of SSC-A and the signal from the excitation of cells with the 532nm laser (PE-Cyanine7) was used (Figure 2.6E). To determine the population of M2-like macrophages from the $F4/80^+$ population, a dot plot of SSC-A and the signal from the excitation of cells with the 647nm laser (APC) was used (Figure 2.6G). Finally, in order determine macrophage found in an intermediate state ($F4/80^+CD86^+CD163^+$), a dot plot of and the signal from the excitation of cells with the 532nm laser (PE-Cyanine7) and the signal from the excitation of cells with the 647nm laser (APC) was used (Figure 2.6I).

2.10. Cytokine analysis

Whole blood was collected through cardiac puncture into microfuge heparinised tubes (Vetlab Supplies, UK). Cells were removed from plasma by centrifugation for 10 minutes at 1,000g at 4°C. The supernatant or the plasma was removed, aliquoted into microcentrifuge tubes and stored at −80°C until they were analysed. Cytokine levels in plasma and kidney lysates were determined using the Mouse Premixed Multi-Analyte Kit (R&D Systems – a Bio-Techne® brand, Cat. Number LXSAMSM), a flexible magnetic bead-based assay, and measured on Bioplex 200 (Bio-Rad Bio-plex analyser) as per manufacturer's instructions. Samples were analysed in triplicate for presence of the following analytes: MCP-1, IL-1β, IL-6, IL-13, M-CSF, IFN-γ, IL-4, IL-10, IL-17E/IL-25, and TNF-α. Due to limited funds we were only able to perform a preliminary analysis of cytokine levels in a single strain – BALB/c.

Analyte	Role
MCP-1	Pro-inflammatory chemokine – manages leukocyte recruitment to the site of inflammation[19,20,57,63,94,116,187,245–247]
IL-1β	Pro-inflammatory cytokine produced by monocytes, macrophages and kidney cells during injury[25,52,61,63,86,248]
IL-6	Cytokine with both pro- and anti-inflammatory roles[63,78,91,249,250]
IL-13	Anti-inflammatory cytokine associated with M2 macrophage polarisation[52,86,90,93,107,251,252]
M-CSF	Pro-inflammatory cytokine capable of activating monocytes and macrophages [17,63,85,93,97,253–255]
IFN-γ	Pro-inflammatory cytokine associated with M1 macrophage activation[61,215]
IL-4	Anti-inflammatory cytokine associated with M2 macrophage polarisation[53,55,61,116,204]
IL-10	Anti-inflammatory cytokine capable of inhibiting leukocyte migration and pro-inflammatory cytokines release[117,256]
IL-17E/IL-25	Anti-inflammatory cytokine capable of promoting Th2 responses[257]
TNF-α	Pro-inflammatory cytokine produced by monocytes, macrophages and kidney cells during injury[15,122,256]

Table 2.2: Multiplex Cytokine Analysis of mouse plasma for common pro- and anti-inflammatory cytokines.

2.11. Statistical analysis

Data was assessed for variance and normality. Two-way ANOVA with either Sidak's multiple comparisons correction test (for comparisons between two groups) or Tukey's multiple comparisons correction test (for comparisons between three groups) were used to analyse FITC-Sinistrin t½, GFR and body weight data. Pearson's correlation was used to investigate the relationship between renal function and body weight. The coefficient of variation (%CV) was calculated from absolute GFR values to assess the variability in renal function following bilateral R-IRI or sham-operated procedure. All data are shown as mean (95% confidence interval) ± SEM.

Statistical analysis was performed using GraphPad Prism 8 for Windows (GraphPad, LLC). All data points represent individual animals and error bars represent mean ± SEM. Statistical significance is represented by values < 0.05.

A power calculation was previously performed in our lab to determine the number of animals per group needed for a clinically relevant amelioration of renal function on day 3 to 75% of the baseline GFR. This resulted in a n= 6 animals per groups, with $\alpha = 0.05$, $1 - \beta = 0.8$

and allocation ratio = 1^{267}. However, for the series of experiments in this thesis we had decided to increase the number of animals allocated to each group due to:

(1) The increased variability in animal responses from different strains following bilateral R-IRI (see section 3.5.7)
(2) The increased inter-strain variability following bilateral R-IRI.
(3) The variability in seen in the data also led to us needing a larger sample size to determine whether the effects seen were statistically significant.
(4) The attrition seen in the experiments due to surgery complications or animals exceeding the severity limits.
(5) The desire to reduce the margin of error around the estimates.

Chapter 3

Assessing the efficacy of regenerative medicine therapies in ameliorating renal function in different mouse strains following bilateral renal ischaemia-reperfusion injury

3. Assessing the efficacy of regenerative medicine therapies in ameliorating renal function in different mouse strains following bilateral renal ischaemia-reperfusion injury

3.1. Introduction

In the last two decades, extensive pre-clinical research has been performed assessing the efficacy and suitability of MSCs as therapy for the treatment of various inflammatory and autoimmune diseases[178–180].

In vivo models of kidney disease have shown that MSC therapy has renoprotective effects on the kidney and can ameliorate renal function in response to injury through a decrease in the levels of serum creatinine and blood urea nitrogen[21,25,225–229,258–260,26,106,149,191–193,207,224]. At a cellular level, MSC therapy has been shown to preserve the structural integrity of the kidney in response to injury by reducing both tubular apoptosis and necrosis, and intratubular cast formation. MSC treatment was also able to promote the proliferation of kidney tubular cells while increasing cellular regeneration and survival. In addition, MSC therapy was able to stimulate angiogenesis and reduce damage to the vasculature following renal injury. Studies to assess MSC-based mechanisms of action suggest that these cells exert their renoprotective effects through the release of molecules such as anti-inflammatory, anti-fibrotic and anti-apoptotic mediators capable of altering the local environment. MSCs can constitutively express biological factors such as IL-6, MCP-1 and PGE2 which have anti-inflammatory capabilities and are able to downregulate the activity of immune cells[92,204,211,216,219,223]. MSCs can also release pro-angiogenic molecules such as IL-8, HGF and VEGF that stimulate endothelial cells' proliferation and survival, matrix remodelling and monocyte chemotaxis[45,187,204–207].

Pre-clinical research into kidney disease can be conducted using a range of animal models, from ischaemia-reperfusion models to sepsis and toxin-induced AKI models, and most of the current knowledge of AKI originates from these animals as renal biopsy is not common practice in the acute phase of the disease[6,105,109,110]. While the bilateral renal IRI model is routinely used because it allows for the reproduction of human AKI pathophysiology, it also comes with its disadvantages around the variability of said model[110,111,261–263]. When it comes to the choice of animal, a range of animal models have been used to study AKI in pre-clinical

research, from smaller species, such as mice and rodents to larger ones, such as pigs depending on the research question posed[6,109,110,115,129,130]. Mice are frequently used in early pre-clinical research due to their small size, reduced propagation cost, and ease of breeding and genetic manipulation[6,109,115]. Nevertheless, multiple studies throughout the year have shown that age, strain and sex can have a significant impact on the response to kidney damage notwithstanding standardised experimental conditions[6,15,36,109,128,238–240].

3.2. Aims

The series of experiments in this chapter have focused on closely characterising mice from three different genetic backgrounds: BALB/c, C57BL/6 alb (inbred) and CD1 (outbred) strains by measuring their GFR and weight following bilateral renal IRI surgery or sham-operated procedure. BALB/c mice are characterised by a Th2 response whereas C57BL/6 alb are characterised by a Th1 response; these two strains are routinely used in pre-clinical research on conditions where the immune system plays a major role whereas CD1 mice are not as frequently described[25,95,121–126,96,97,106,116–120].

The *in vivo* experiments presented within this chapter had four main aims:

(1) assess the impact of R-IRI on renal function in three different mouse strains,

(2) compare the impact of R-IRI on renal function between three different mouse strains,

(3) assess the impact of regenerative medicine therapies on renal function in three different mouse strains following R-IRI, and

(4) compare the impact of regenerative medicine therapies on renal function in three different mouse strains following R-IRI.

3.3. Experimental Design

AKI was induced in healthy animals from three different mouse strains (BALB/c, C57BL/6 alb and CD1) through bilateral clamping of the renal pedicles which supply the kidney with blood (go to *2.3. Surgical model of acute kidney injury*).

Kidney injury following bilateral R-IRI was assessed using a transcutaneous device measuring the FITC-Sinistrin clearance time as it allowed for accurate longitudinal analysis of

kidney function without culling of the animals. Renal function was measured at baseline and at days 1 and 3 following bilateral R-IRI. Absolute values of FITC-Sinistrin clearance and GFR, as well as proportional (%) change in GFR were compared to baseline measurements. Percentage change in GFR in response to R-IRI were correlated with the 'RIFLE' criteria for AKI which classifies kidney injury into 3 grades of severity – Risk, Injury and Loss/Failure[28–30,143,264].

To assess the impact of hUC-MSC therapy on macrophage levels in the kidneys and spleen, mice were injected with 250,000 MSCs through the tail vein (in 100µL volume) immediately after surgery whereas control mice received 100µL PBS.

3.4. Statistical Analysis

Data was assessed for normality. Two-way ANOVA with Geisser-Greenhouse correction was performed as sphericity was not assumed i.e., did not assume that data were sampled from populations where the standard deviation were identical in all groups at all time points. Sidak's multiple comparisons correction test (for comparisons between two groups) and Tukey's multiple comparisons correction test (for comparisons between three groups), with individual variances computed for each comparison were used to analyse FITC-Sinistrin t½, GFR and body weight data. Pearson's correlation was used to investigate the relationship between renal function and body weight. The coefficient of variation (%CV) was calculated from absolute GFR values to assess the variability in renal function following bilateral R-IRI or sham-operated procedure. All data is shown as mean (95% confidence interval) ± SEM.

Statistical analysis was performed using GraphPad Prism 8 for Windows (GraphPad, LLC). All data points represent individual animals and error bars represent mean ± SEM. Statistical significance is represented by values < 0.05.

3.5. Results

One hundred BALB/c mice were used for the experiments: seventeen mice underwent sham-operated procedure and seventy-one mice underwent bilateral R-IRI surgery, with twenty-six mice receiving no therapy, twenty-four receiving $2.5x10^5$ hUC-MSC therapy and twenty-one receiving PBS. Ninety-five C57BL/6 alb mice were used for the experiments: seventeen mice underwent sham-operated procedure and seventy-eight mice underwent

bilateral R-IRI surgery, with twenty-nine mice receiving no therapy, twenty-five receiving $2.5x10^5$ hUC-MSC therapy and twenty-five receiving PBS. Sixty-eight CD1 mice were used for the experiments: fifteen mice underwent sham-operated procedure and fifty-three mice underwent bilateral R-IRI surgery, with fifteen mice receiving no therapy, nineteen receiving $2.5x10^5$ hUC-MSC therapy and thirteen receiving PBS; the CD1 group had less animals in the experiment due to time constraints and limited funding (Figure 3.14 and Figure 3.16). Due to surgery complications or to exceeding the severity limit, 13.25% BALB/c mice, 3.84% C57BL6/alb mice and 11.3% CD1 mice were culled before the day-3 experimental endpoint and excluded from the final results.

To test for normality, the baseline FITC-Sinistrin clearance time was plotted as a QQ plot which showed a normal distribution (Figure 3.1).

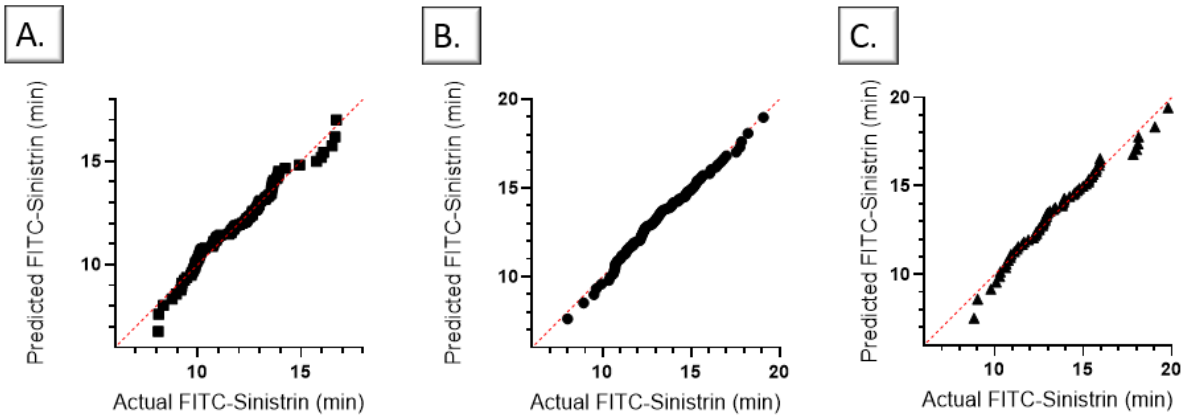

Figure 3.1: Normality plot. Normality or QQ plots of baseline FITC-Sinistrin clearance time from (A) BALB/c mice, (B) C57BL/6 alb mice and (C) CD1 mice.

3.5.1. The impact of R-IRI on BALB/c mice

AKI was induced in 26 healthy BALB/c mice, and injury level post-R-IRI was compared against 17 sham-operated (control) mice; 3 animals did not survive the study and were excluded from the analysis (Figure 3.2 and Figure 3.3).

Following bilateral R-IRI, BALB/c mice experienced a sharp decline in renal function on day 1 post-surgery, below 50% when compared to pre-surgery baseline measurements (Figure 3.2). On day 3 post-surgery, injured mice recovered a significant proportion of the renal function lost, while control animals showed a drastic increase in renal function following sham-operated procedure. Injured mice showed a statistically significant reduction in renal

function when compared to control animals, with a 0.01% chance of randomly observing an effect this large (or larger) in an experiment of this size (p value < 0.0001). It is important to note that injury levels after R-IRI showed a high degree of variability with proportional GFR change on day 1 widely scattered (4% - 50%) between loss and injury categories of the RIFLE classification system (Figure 3.2C).

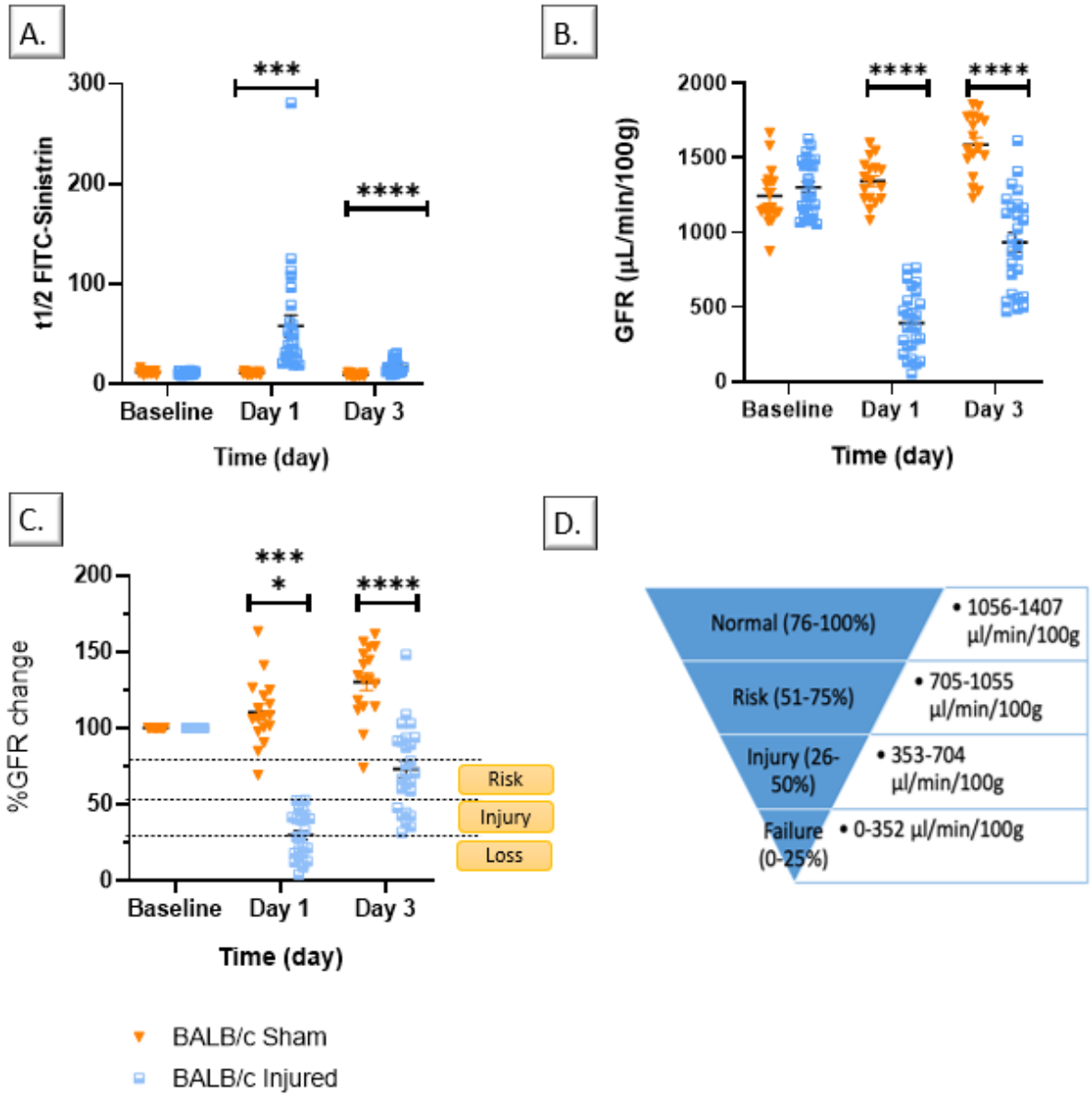

Figure 3.2: Changes in renal function in BALB/c mice following bilateral R-IRI. Renal function was assessed at baseline and on days 1 and 3 after R-IRI, and compared to sham-operated animals (with no R-IRI) by (A) FITC-Sinistrin half-life. (B) FITC-Sinistrin half-life was used, along with body weight, to calculate absolute changes in GFR after R-IRI. (C) Proportional change in GFR following R-IRI with 'RIFLE' criteria representation. (D) ADQI 'RIFLE' criteria. **n=29** injured mice and **n=17** sham-operated animals; n = 3 animal were excluded from the final results due

to either surgery complications or exceeding severity limits. All data points represent individual animals and error bars represent mean ± SEM. Significant differences between injured and sham-operated animals. ***p=0.0006 and ****p<0.0001.

When comparing changes in body weight in BALB/c mice following R-IRI, there was a steady decline in the injured group when compared to sham-operated animals (Figure 3.3). At the study end-point (day 3), injured mice had lost between 10% to 20% body weight when compared to their initial baseline (pre-surgery) measurement, while control animals had a mean weight loss of approximately 4% ($p < 0.0001$). There was no correlation between changes in renal function and changes in body weight following R-IRI.

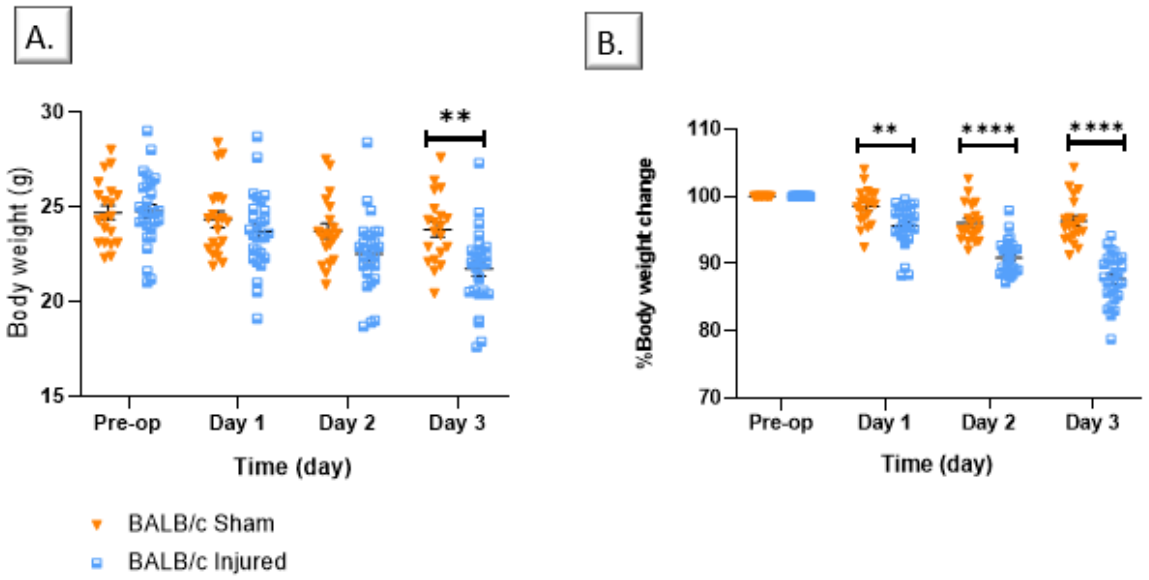

Figure 3.3: Changes in body weight in BALB/c mice following bilateral R-IRI. (A) Body weight was measured at baseline and on days 1, 2 and 3 after R-IRI, and compared to sham-operated animals (with no R-IRI). **(B)** Proportional change in body weight following R-IRI. **n=29** injured mice and **n=17** sham-operated animals; n = 3 animal were excluded from the final results due to either surgery complications or exceeding severity limits. All data points represent individual animals and error bars represent mean ± SEM. Significant differences between injured and sham-operated animals with: **p<0.005 and ****p<0.0001.

3.5.2. The impact of regenerative medicine therapies on BALB/c mice following R-IRI

Twenty-nine male BALB/c mice received 250,000 hUC-MSC through IV injection immediately after bilateral R-IRI, whereas twenty-four BALB/c mice received 100µL PBS; 8

animals did not survive the study and were excluded from the analysis (Figure 3.4 and Figure 3.5).

There were no differences in renal function between treatment and PBS groups following bilateral R-IRI (Figure 3.4). The effect of hUC-MSC treatment on proportional GFR change was considered not significant with an 86% chance of randomly observing an effect this large (or larger) in an experiment this size. At day 3 post-surgery, animals in both groups showed a recovery of renal function when compared to day 1, with mice in the hUC-MSC group displaying a higher degree of variability. Mice treated with PBS showed a slightly higher mean in proportional GFR change when compared to the hUC-MSC group (1% difference between means). Differences in proportional recovery of renal function following treatment were also analysed (Figure 3.4D): The PBS groups had a slightly higher mean of recovery than the hUC-MSC group (8% difference between means), however, there were no statistically significant changes between the two groups.

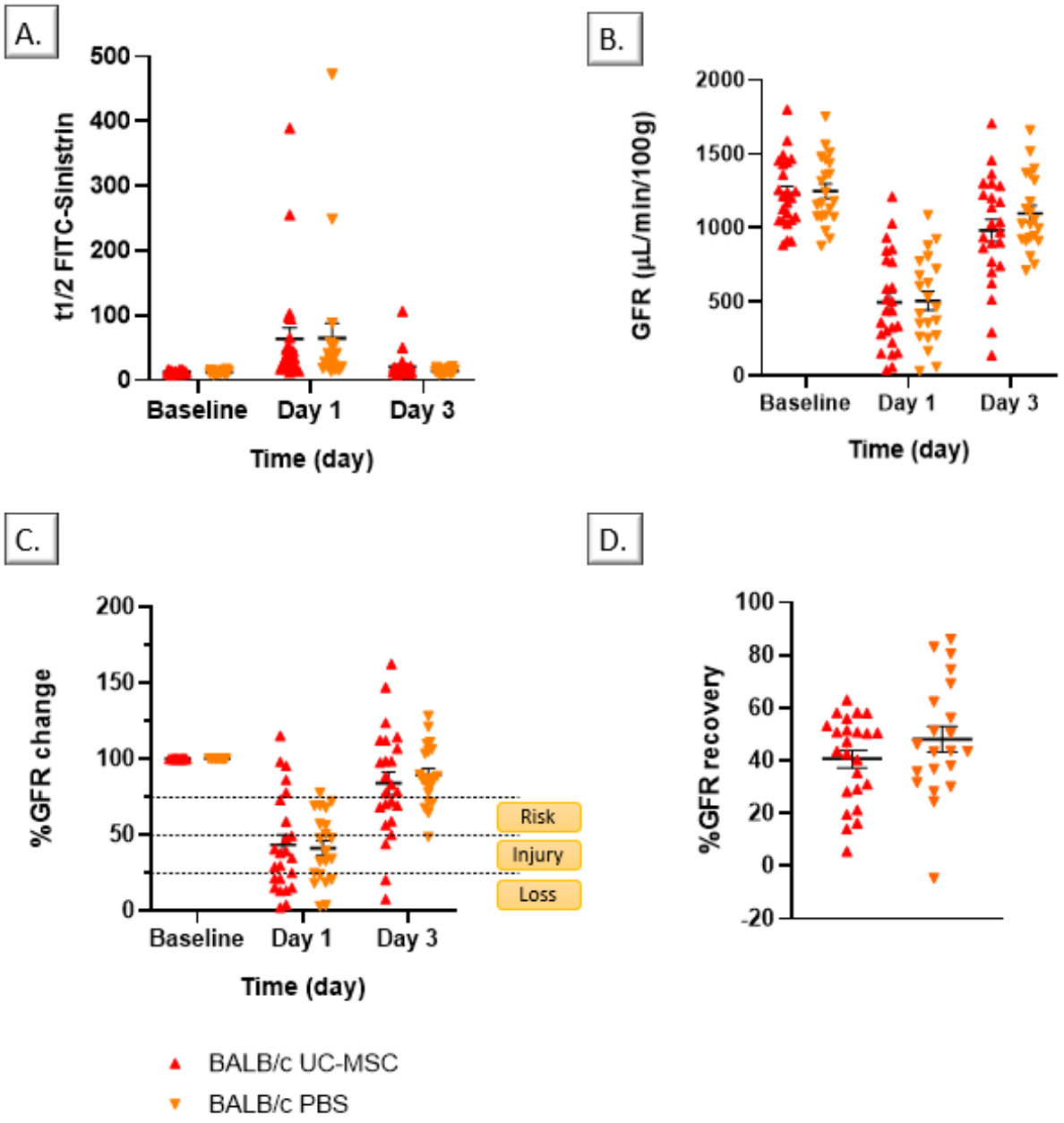

Figure 3.4: Changes in renal function in BALB/c mice in response to hUC-MSC therapy following bilateral R-IRI. Renal function of animals receiving hUC-MSC therapy was assessed by **(A)** FITC-Sinistrin half-life at baseline and on days 1 and 3 after R-IRI, and compared to animals that had received PBS. **(B)** FITC-Sinistrin half-life was used, along with body weight, to calculate absolute changes in GFR after R-IRI. **(C)** Proportional change in GFR following R-IRI with 'RIFLE' criteria representation. **(D)** GFR recovery rate following R-IRI. **n=29** hUC-MSC group and **n=24** PBS group; n = 8 animals were excluded from the final results due to either surgery complications or exceeding severity limits. All data points represent individual animals and error bars represent mean ± SEM (A-C). Wide lines represent the mean and short lines represent SEM (D).

When comparing changes in body weight following R-IRI between PBS and hUC-MSC treatments, there were no differences between the two groups (Figure 3.5). Mice showed a steady decrease in body weight post-surgery with an approximately 10% mean loss for both groups. As with changes in renal function, there was a high degree of variability in body weight following R-IRI, however, these were more pronounced on day 3 when compared to day 1.

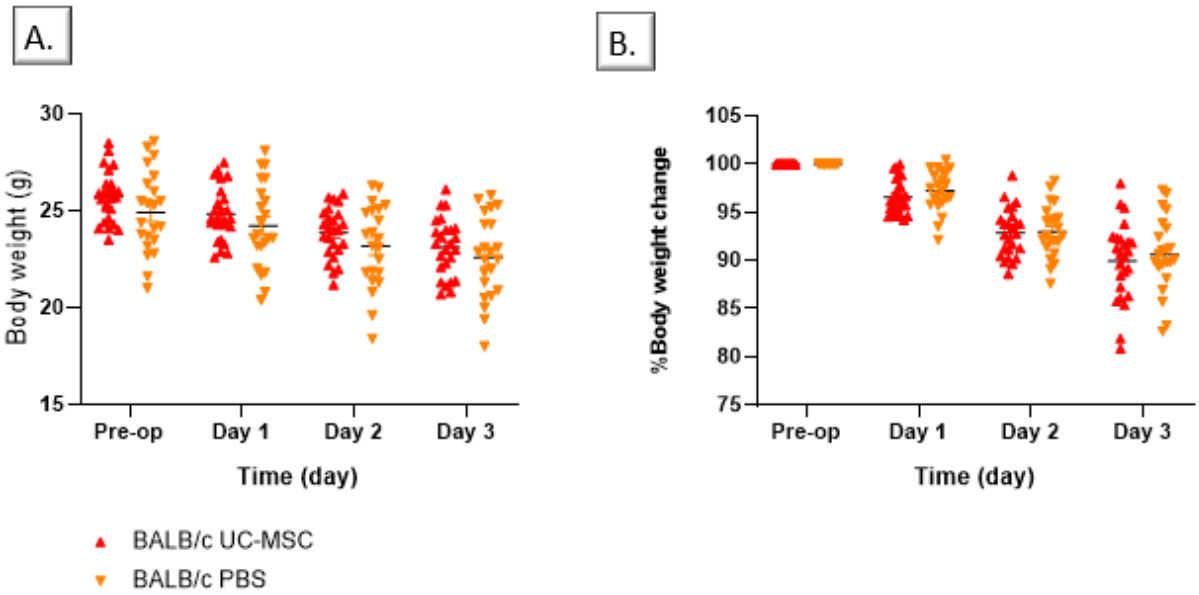

Figure 3.5: Changes in body weight in BALB/c mice in response to hUC-MSC therapy following bilateral R-IRI. (A) Body weight of animals receiving hUC-MSC therapy was measured at baseline and on days 1, 2 and 3 after R-IRI, and compared to animals that had received PBS. **(B)** Proportional change in body weight following R-IRI. **n=29** hUC-MSC group and **n=24** PBS group; n = 8 animal were excluded from the final results due to either surgery complications or exceeding severity limits. All data points represent individual animals and error bars represent mean ± SEM.

3.5.3. The impact of R-IRI on C57BL/6 alb mice

AKI was induced in 29 healthy C57BL/6 alb, and injury level post-R-IRI was compared against 17 sham-operated (control) mice; 2 animals did not survive the study and were excluded from the final analysis (Figure 3.6 and Figure 3.7).

Following bilateral R-IRI, C57BL/6 alb mice experienced a sharp decline in renal function on day 1 post-surgery, generally below 50% when compared to pre-surgery baseline measurements (Figure 3.6). On day 3 post-surgery, injured mice recovered a significant proportion of the renal function lost, while control animals showed a drastic increase in renal function following sham-operated procedure. Injured mice showed a statistically significant

reduction in renal function when compared to control animals, with a 0.01% chance randomly observing an effect this large (or larger) in an experiment of this size (p value < 0.0001). However, the injury levels after R-IRI showed a high degree of variability with proportional GFR change on day 1 widely scattered between loss and risk categories of the RIFLE classification system (Figure 3.6C).

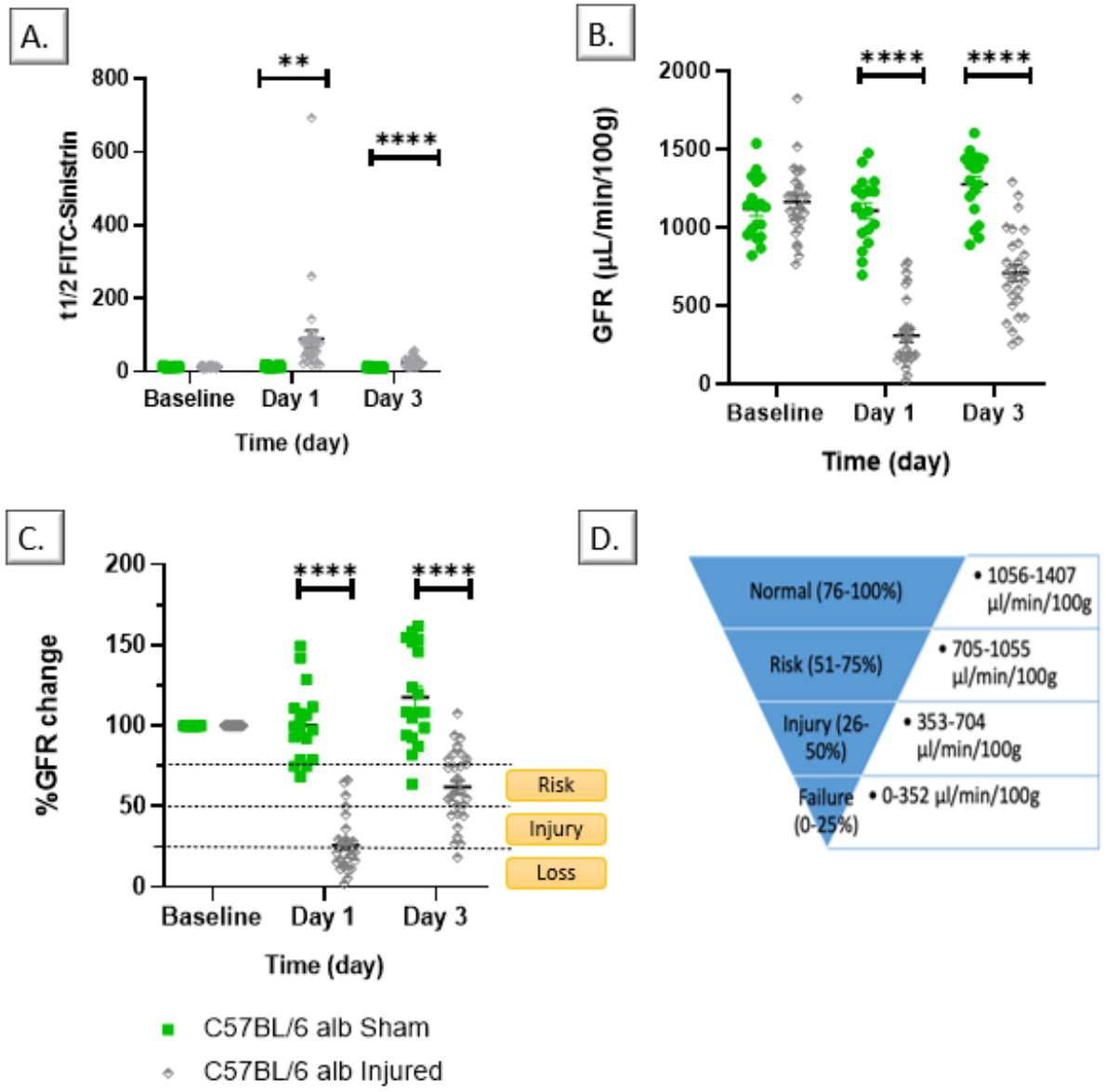

Figure 3.6: Changes in renal function in C57BL/6 albino mice following bilateral R-IRI. Renal function was assessed by **(A)** FITC-Sinistrin half-life at baseline and on days 1 and 3 after R-IRI, and compared to sham-operated animals (with no R-IRI). **(B)** FITC-Sinistrin half-life was used, along with body weight, to calculate absolute changes in GFR after R-IRI. **(C)** Proportional change in GFR following R-IRI with 'RIFLE' criteria representation. **(D)** ADQI 'RIFLE' criteria. **n=31** injured mice and **n=17** sham-operated animals; n = 2 animals were excluded from the final results due to either surgery complications or exceeding severity

limits. All data points represent individual animals and error bars represent mean ± SEM. Significant differences between injured and sham-operated animals with: **p=0.0089 and ****p<0.0001.

When comparing changes in body weight in C57BL/6 alb mice following R-IRI, there was a steady decline in the injured group when compared to sham-operated animals (Figure 3.7). At the study end-point (day 3), injured mice had lost between 7% to 15% body weight when compared to their initial baseline (pre-surgery) measurement, while control animals had a mean weight loss of approximately 3% ($p < 0.0001$). There was no correlation between changes in renal function and changes in body weight following R-IRI.

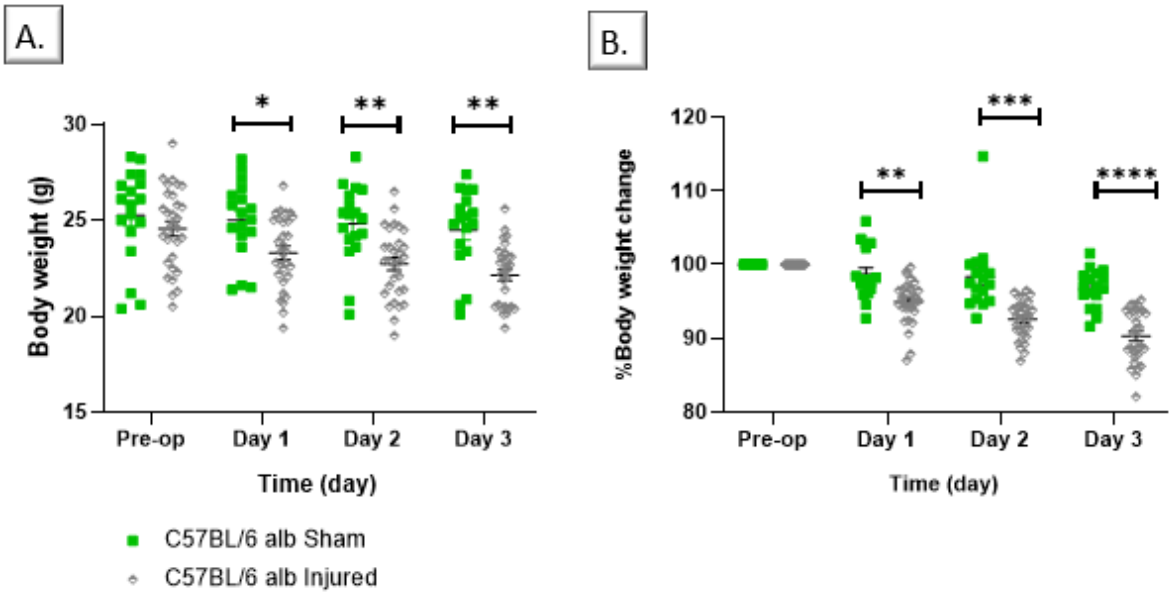

Figure 3.7: Changes in body weight in C57BL/6 albino mice following bilateral R-IRI. (A) Body weight was measured at baseline and on days 1, 2 and 3 after R-IRI , and compared to sham-operated animals (with no R-IRI). **(B)** Proportional change in body weight following R-IRI. **n=31** injured mice and **n=18** sham-operated animals; n = 2animasl were excluded from the final results due to either surgery complications or exceeding severity limits. All data points represent individual animals and error bars represent mean ± SEM. Significant differences between injured and sham-operated animals with: *p=0.0264, **p<0.0045, ***p=0.0005 and ****p<0.0001.

3.5.4. The impact of regenerative medicine therapies on C57BL/6 alb mice following R-IRI

Twenty-five male C57BL/6 alb mice received 250,000 hUC-MSC through IV injection immediately after bilateral R-IRI, and twenty-five C57BL/6 alb mice received 100µL PBS; 1

animal did not survive the study and was excluded from the analysis (Figure 3.8 and Figure 3.9).

There were no statistically significant differences in renal function between treatment and PBS groups following bilateral R-IRI (Figure 3.8). The effect of hUC-MSC treatment on proportional GFR change was considered not significant with an 31% chance of randomly observing an effect this large (or larger) in an experiment this size. At day 3 post-surgery, animals in both groups showed a recovery of renal function when compared to day 1. Mice treated with PBS showed a slightly higher mean when compared to the hUC-MSC group (3.96% difference between means). Analysis of the differences in proportional recovery of renal function following treatment revealed that while the PBS groups had a slightly higher mean of recovery than the hUC-MSC group (2.39% difference between means), there were no statistically significant changes between the two groups(Figure 3.8D).

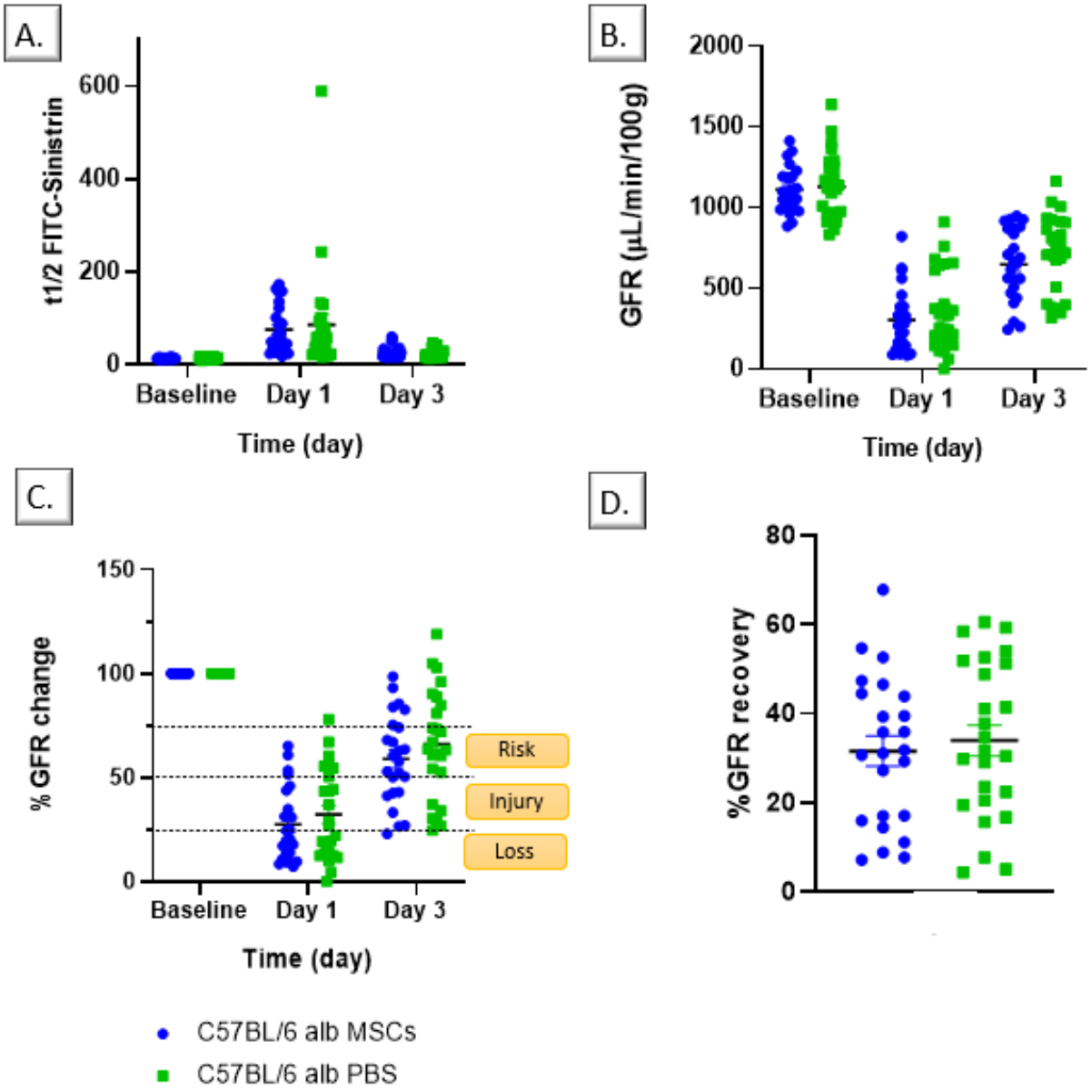

Figure 3.8: Changes in renal function in C57BL/6 albino mice in response to UC-MSC therapy following bilateral R-IRI. Renal function of animals receiving hUC-MSC therapy was assessed at baseline and on days 1 and 3 after R-IRI, and compared to animals that had received PBS by **(A)** FITC-Sinistrin half-life. **(B)** FITC-Sinistrin half-life was used, along with body weight, to calculate absolute changes in GFR after R-IRI. **(C)** Proportional change in GFR following R-IRI with 'RIFLE' criteria representation. **(D)** GFR recovery rate following R-IRI. **n=25** hUC-MSC group and **n=25** PBS group; n = 1 animal were excluded from the final results due to either surgery complications or exceeding severity limits. All data points represent individual animals and error bars represent mean ± SEM (A-C). Wide lines represent the mean and short lines represent SEM (D).

When comparing changes in body weight following R-IRI between PBS and hUC-MSC treatments, there were no differences between the two groups (Figure 3.9). Mice showed a steady decrease in body weight post-surgery with an approximately 5% mean loss by day 3 for both groups. As with changes in renal function, there is a high degree of variability in body weight following R-IRI, however, these were more pronounced on day 3 when compared to day 1, and more variable in the hUC-MSC group than in the PBS one.

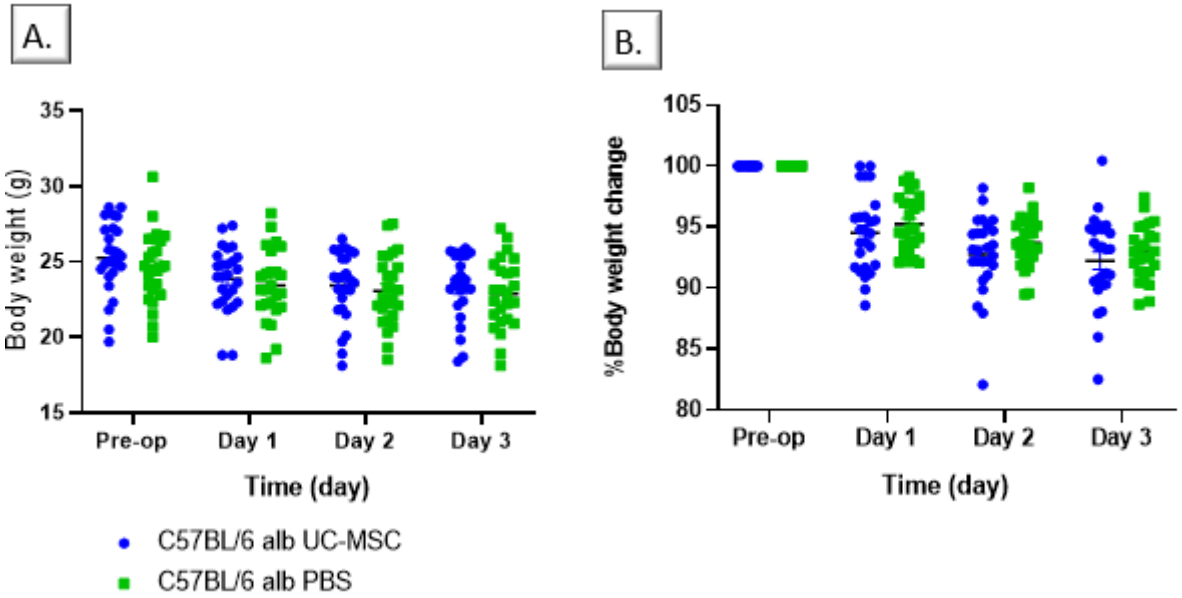

Figure 3.9: Changes in body weight in C57BL/6 albino in response to hUC-MSC therapy following bilateral R-IRI. (A) Body weight of animals receiving hUC-MSC therapy was measured at baseline and on days 1, 2 and 3 after R-IRI, and compared to animals that had received PBS. **(B)** Proportional change in body weight following R-IRI. **n=25** hUC-MSC group and **n=25** PBS group; n = 1 animal were excluded from the final results due to either surgery complications or exceeding severity limits. All data points represent individual animals and error bars represent mean ± SEM.

3.5.5. The impact of R-IRI on CD1 mice

AKI was induced in 15 healthy CD1 mice, and injury level post-R-IRI was compared against 15 sham-operated (control) mice; 2 animals did not survive the study and were excluded from the analysis (Figure 3.10 and Figure 3.11).

Following bilateral R-IRI, CD1 mice experienced a sharp decline in renal function on day 1 post-surgery, generally below 50% when compared to pre-surgery baseline measurements (Figure 3.10). On day 3 post-surgery, injured mice recovered a significant proportion of the lost renal function, while control animals showed a near recovery to

baseline levels following sham-operated procedure (mean %GFR = 94%). Injured mice showed a statistically significant reduction in renal function when compared to control animals, with a 0.01% chance randomly observing an effect this large (or larger) in an experiment of this size (p value < 0.0001). However, injury levels after R-IRI showed a high degree of variability with proportional GFR change on day 1 widely scattered between loss and injury categories of the RIFLE classification system (Figure 3.10C).

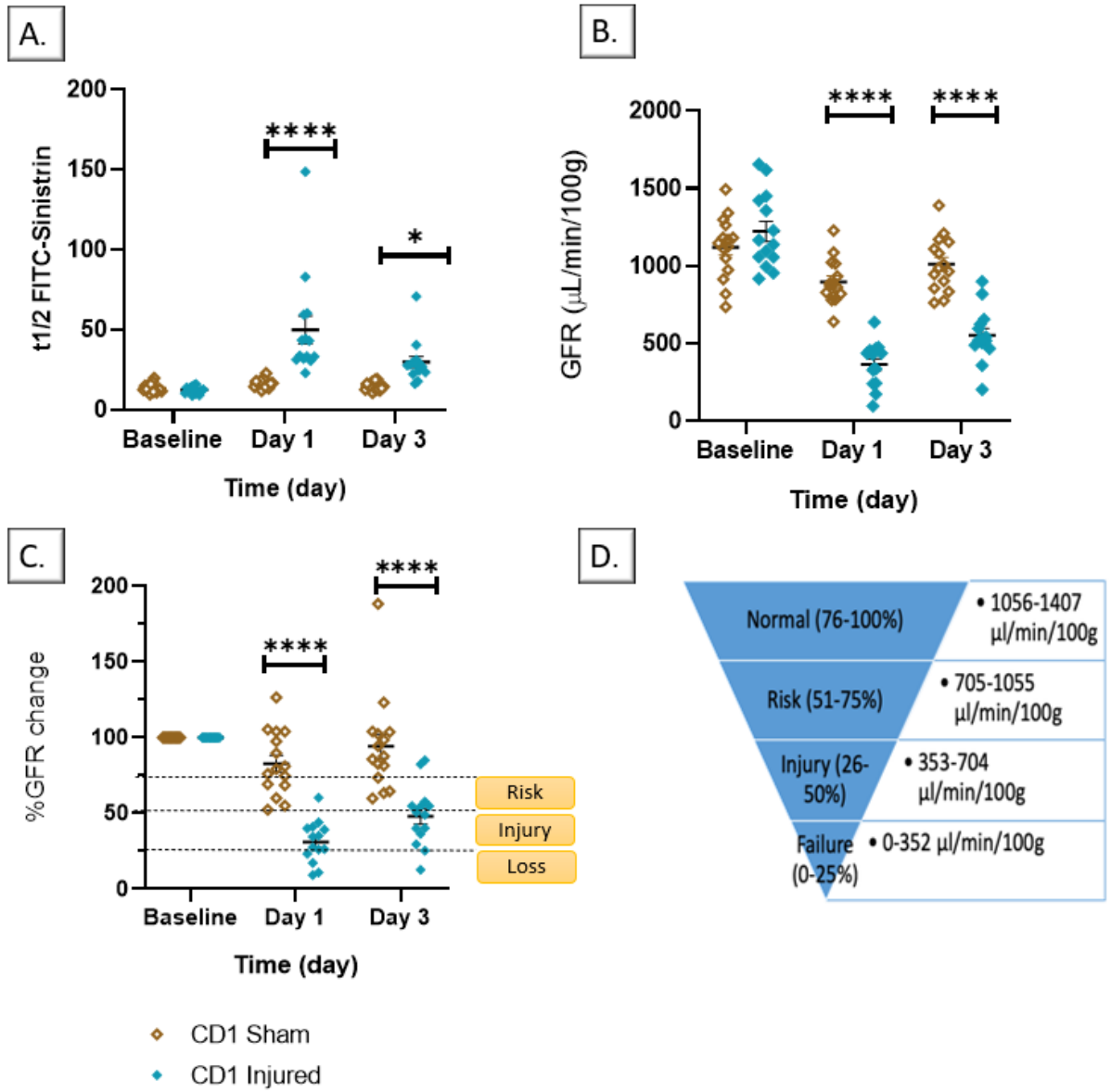

Figure 3.10: Changes in renal function in CD1 mice following bilateral R-IRI. Renal function was assessed at baseline and on days 1 and 3 after R-IRI, and compared to sham-operated animals (with no R-IRI) by **(A)** FITC-Sinistrin half-life. **(B)** FITC-Sinistrin half-life was used, along with body weight, to calculate absolute changes in GFR after R-IRI. **(C)** Proportional change in GFR following R-IRI with 'RIFLE' criteria representation. **(D)** ADQI 'RIFLE' criteria. **n=17** injured mice and **n=15** sham-operated animals; n = 2 animals were excluded from the final results due to either surgery complications or exceeding severity limits. All data points represent

individual animals and error bars represent mean ± SEM. Significant differences between injured and sham-operated animals with: *p=0.018 and ****p<0.0001.

When comparing changes in body weight in CD1 mice following R-IRI, there were extremely significant differences between injured and sham groups with a less than 0.066% chance of randomly observing an effect this large (or larger) in an experiment of this size. Bilateral R-IRI led to a significant decline in body weight on days 1 and 2 (with statistically significant differences at day 2 between the two groups), however, by day 3 injured mice started regaining weight (Figure 3.11). At the study end-point (day 3), there were still statistically significant differences in body weight between injured and sham-operated groups (**p= 0.0066). There was no correlation between changes in renal function and changes in body weight following R-IRI.

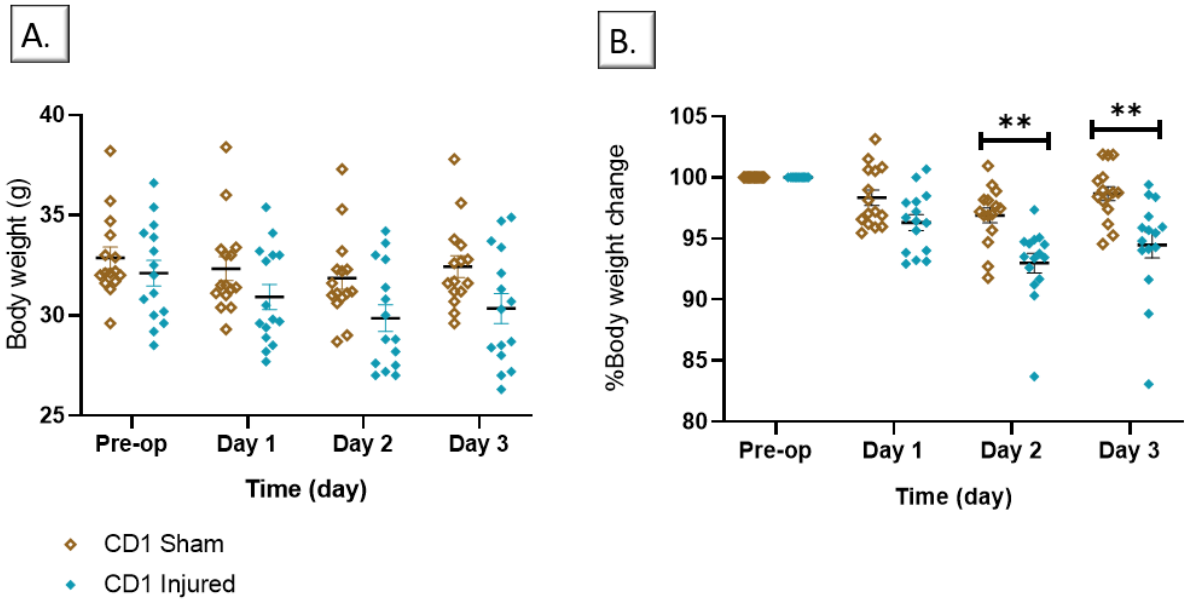

Figure 3.11: Changes in body weight in CD1 mice following bilateral R-IRI. (A) Body weight was measured at baseline and on days 1, 2 and 3 after R-IRI, and compared to sham-operated animals (with no R-IRI). **(B)** Proportional change in body weight following R-IRI. **n=17** injured mice and **n=15** sham-operated animals; n = 2 animals were excluded from the final results due to either surgery complications or exceeding severity limits. All data points represent individual animals and error bars represent mean ± SEM. Significant differences between injured and sham-operated animals with: *p=0.0314 and **p=0.0093.

3.5.6. The impact of regenerative medicine therapies on CD1 mice following R-IRI

Twenty-one male CD1 received 250,000 hUC-MSC through IV injection immediately after bilateral R-IRI, whereas fifteen CD1 received 100µL PBS; 4 animals did not survive the study and were excluded from the analysis (Figure 3.12 and Figure 3.13).

There were no statistically significant differences in renal function between treatment and PBS groups following bilateral R-IRI (Figure 3.12). The effect of hUC-MSC treatment on proportional GFR change was considered not significant with an 95% chance of randomly observing an effect this large (or larger) in an experiment this size, with mice in the hUC-MSC group displaying a higher degree of variability. At day 3 post-surgery, animals in both groups showed a recovery of renal function when compared to day 1 with no differences between the two groups. Differences in proportional recovery of renal function following treatment were also analysed (Figure 3.12D): while the hUC-MSC group had a slightly higher mean of recovery than the PBS group (2.41% difference between means), there were no statistically significant changes between the two groups.

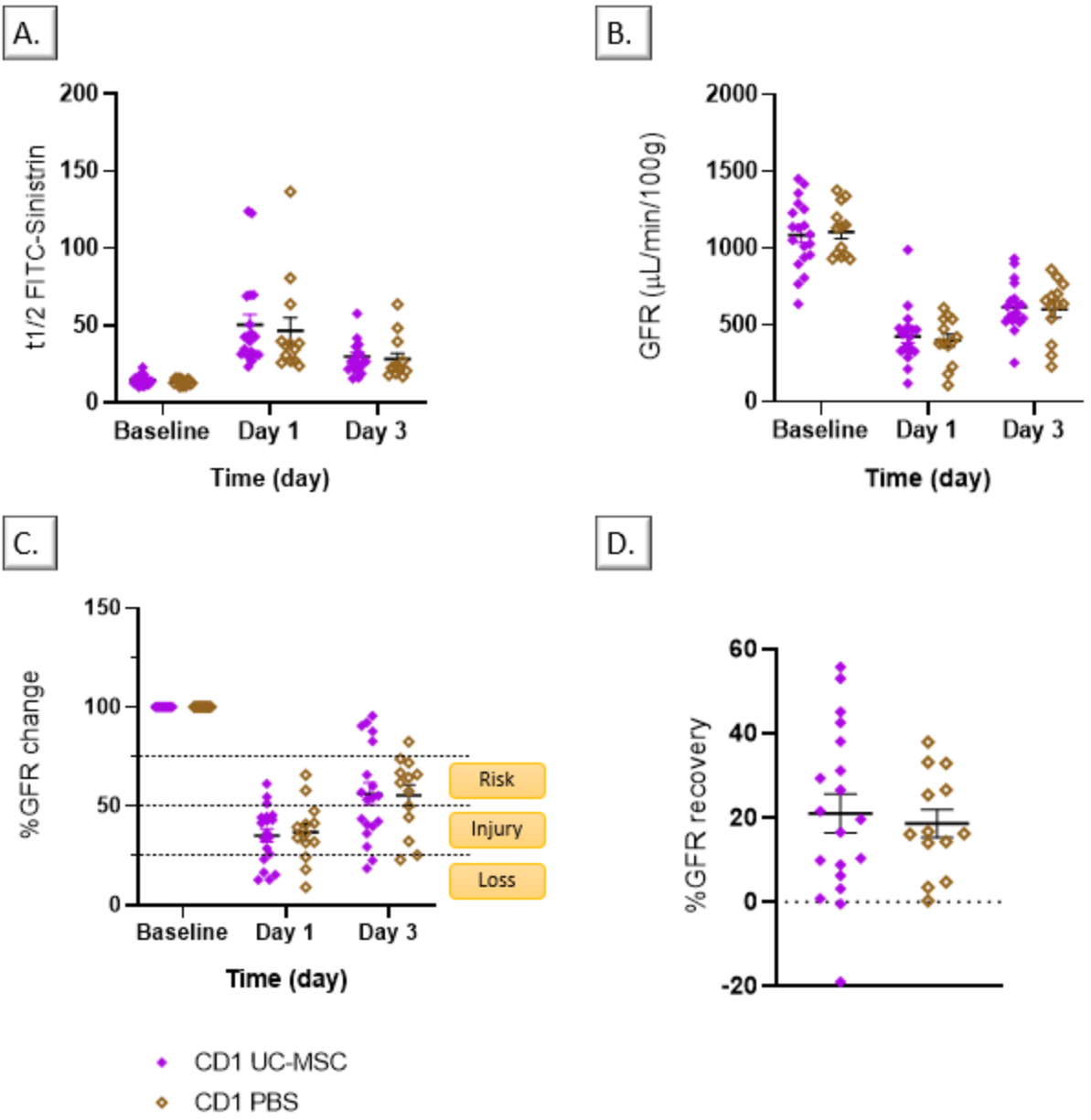

Figure 3.12: Changes in renal function in CD1 mice in response to hUC-MSC therapy following bilateral R-IRI. Renal function of animals receiving hUC-MSC therapy was assessed at baseline and on days 1 and 3 after R-IRI, and compared to animals that had received PBS by (A) FITC-Sinistrin half-life. (B) FITC-Sinistrin half-life was used, along with body weight, to calculate absolute changes in GFR after R-IRI. (C) Proportional change in GFR following R-IRI with 'RIFLE' criteria representation. **(D)** GFR recovery rate following R-IRI. **n=21** hUC-MSC group and **n=15** PBS group; n = 4 animals were excluded from the final results due to either surgery complications or exceeding severity limits. All data points represent individual animals and error bars represent mean ± SEM (A-C). Wide lines represent the mean and short lines represent SEM (D).

When comparing changes in body weight following R-IRI between PBS and hUC-MSC, there were no differences between the two groups (Figure 3.13). Mice showed a steady decrease in body weight post-surgery. On day 1 and day 2 post-surgery, mice in the hUC-MSC group lost proportionally more weight than those in the PBS group. On day 3, animals in both groups started regaining weight mice, however, mice that had received hUC-MSC treatment showed a slightly higher increase. As with changes in renal function, there was a high degree of variability in body weight following R-IRI regardless of treatment group.

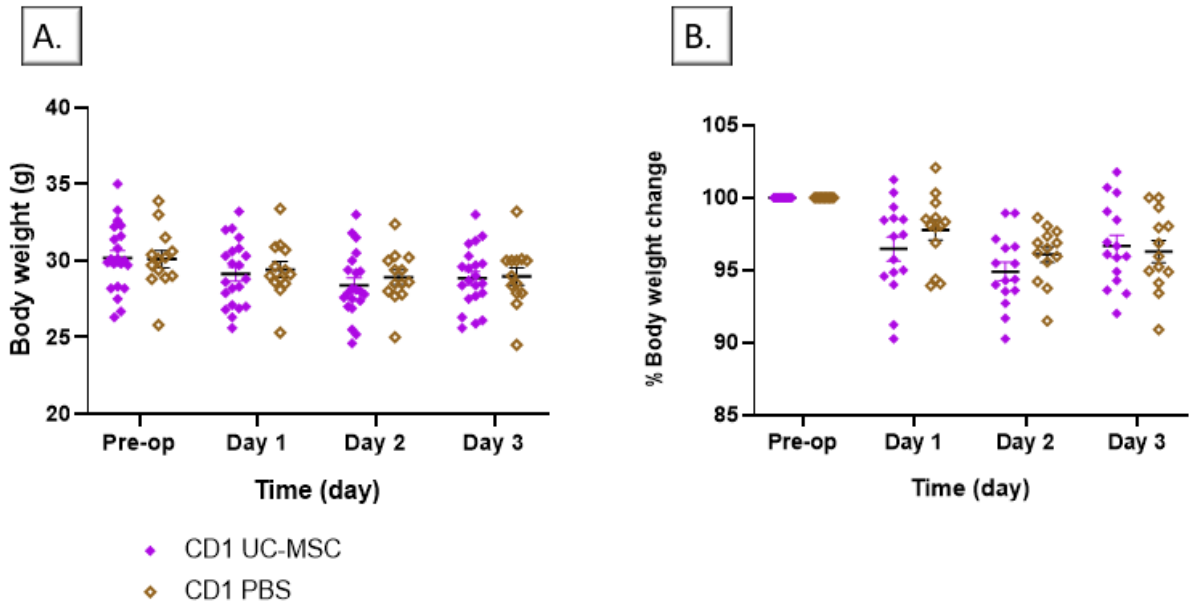

Figure 3.13: Changes in body weight in CD1 mice in response to hUC-MSC therapy following bilateral R-IRI. (A) Body weight of animals receiving hUC-MSC therapy was measured at baseline and on days 1, 2 and 3 after R-IRI, and compared to animals that had received PBS. **(B)** Proportional change in body weight following R-IRI. **n=21** hUC-MSC group and **n=21** PBS group; n = 4 animals were excluded from the final results due to either surgery complications or exceeding severity limits. All data points represent individual animals and error bars represent mean ± SEM.

3.5.7. Comparing the impact of R-IRI on different mouse strains

Comparing changes in renal function following sham procedure in three different mouse strains showed that animals displayed both differences in baseline renal function (not statistically significant) and also responded differently to the procedure (Figure 3.14 A and C). Statistical analysis showed that the strain of the mice had an extremely significant effect on renal function following sham procedure, with a 0.01% chance of randomly observing an effect this large (or larger) in an experiment of this size. Furthermore, proportional changes

in GFR indicated that both C57BL/6 alb and CD1 strains were more affected by the procedure, with a higher reduction in renal function when compared to the BALB/c strain. BALB/c mice showed a significantly less reduction in GFR following sham-operated procedure, with CD1 mice the most affected by the surgery; these effects were more pronounced on day 3 post-surgery. These results demonstrate that the sham surgery alone affected the animals to different degrees, based on their strain.

Comparing changes in renal function following bilateral renal IRI in the three different strains indicated that the animals also responded differently to kidney injury (Figure 3.14B and D). On day 1 post-surgery, C57BL/6 alb mice had the sharpest decline in renal function (mean GFR = 308 µL/min/100g and mean %GFR = 25%), followed by BALB/c mice (mean GFR = 392 µL/min/100g and mean %GFR = 29%) and CD1 mice (mean GFR = 395 µL/min/100g and mean %GFR = 33%); however, these differences were not statistically significant. By day 3 post-surgery, BALB/c mice showed the highest recovery after R-IRI procedure (mean GFR = 934 µL/min/100g and mean %GFR = 73%), followed by C57BL/6 alb mice (mean GFR = 709 µL/min/100g and mean %GFR = 61%) and CD1 mice (mean GFR = 582.7 µL/min/100g and mean %GFR = 49.8%) which recovered the least from the surgery.

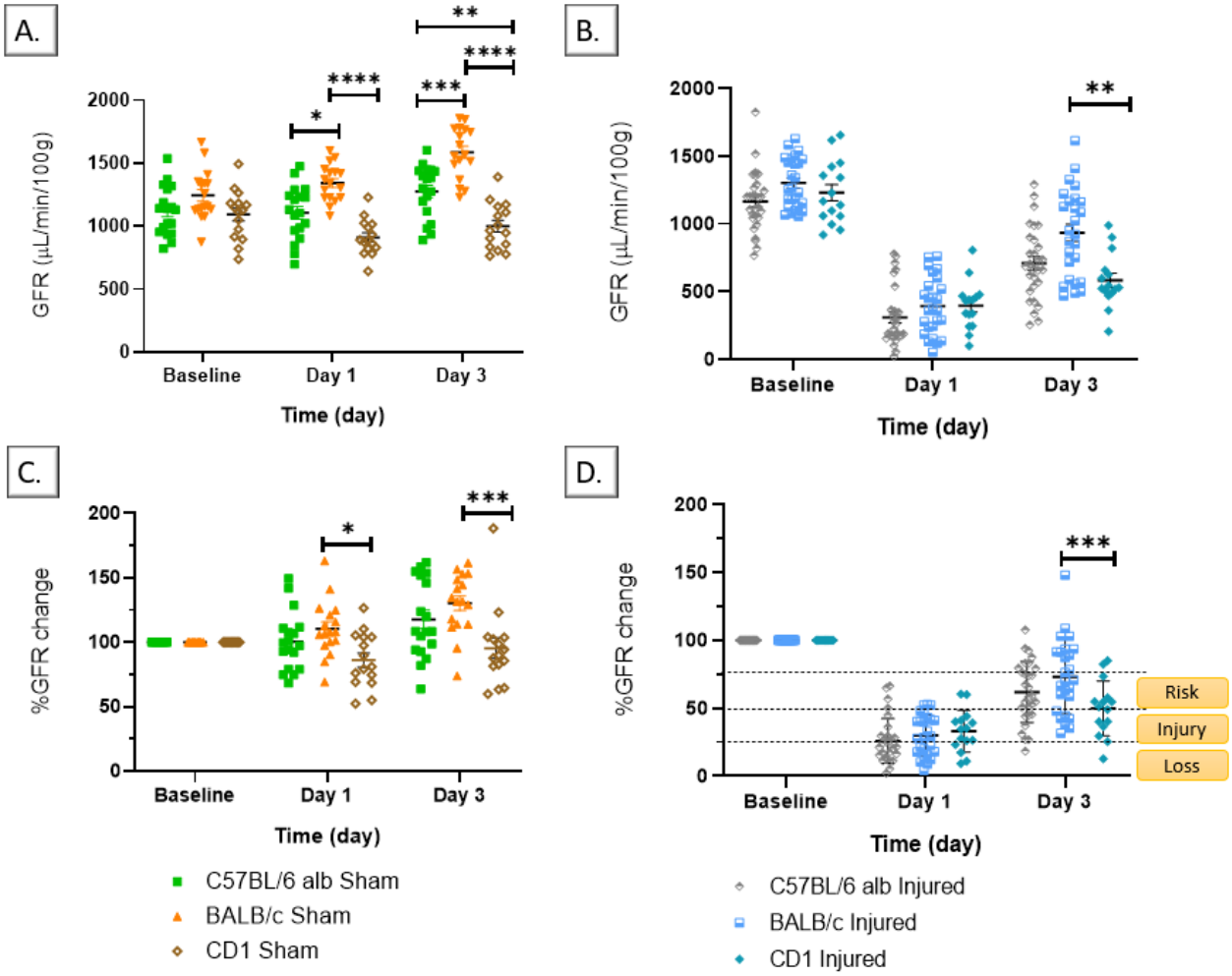

Figure 3.14: **Comparing changes in renal function in different mouse strains. (A)** GFR results of mice from three different strains that underwent sham procedure at baseline and days 1 and 3 after surgery. **(B)** GFR results of mice from three different strains following R-IRI procedure at baseline and days 1 and 3 after surgery. **(C)** Proportional change in GFR following sham procedure. **(D)** Proportional change in GFR following R-IRI with 'RIFLE' criteria representation. Significant differences between the three strains in response to surgery (both sham procedure and R-IRI). *p<0.05, **p<0.005, ***p<0.0005 and ****p<0.0001. All data points represent individual animals and error bars represent mean ± SEM.

As CD1 mice had significantly higher body weight at the start of the *in vivo* experiments, comparisons in body weight changes following bilateral R-IRI and sham procedure were done using proportional changes in weight (Figure 3.15). On day 1 post sham procedure (Figure 3.15A), all three strains lost approximately 2% of their baseline body weight. On day 2 post sham procedure, BALB/c and CD1 mice showed the highest reduction in body weight (approximately 4% loss) in comparison to C57BL/6 alb (approximately 2% loss). However, by day 3 post sham procedure, CD1 mice have lost the least amount of weight

(approximately 2% loss), followed by BALB/c and C57BL/6 alb mice (approximately 4% loss). Nevertheless, these differences in body weight loss following sham procedure were not statistically significant.

Comparisons between BALB/c, C57BL/6 alb and CD1 mice in body weight changes in response to bilateral R-IRI showed that strain had an extremely significant effect on body weight following renal IRI, with a 0.022% chance of randomly observing an effect this large (or larger) in an experiment of this size. Throughout the experiment, CD1 mice lost the least amount of body weight in response to bilateral R-IRI (Figure 3.15B), and by the study end-point, CD1 mice weighed significantly more than either BALB/c or C57BL/6 alb mice. BALB/c mice showed the strongest response to R-IRI, losing the most body weight (approximately 12.3% loss). These significant differences in body weight between strains in response to R-IRI were also displayed in the overall health of animals. By the end of the experiment, BALB/c mice were the most affected by the surgery, while C57BL/6 alb and CD1 mice showed the least physical distress.

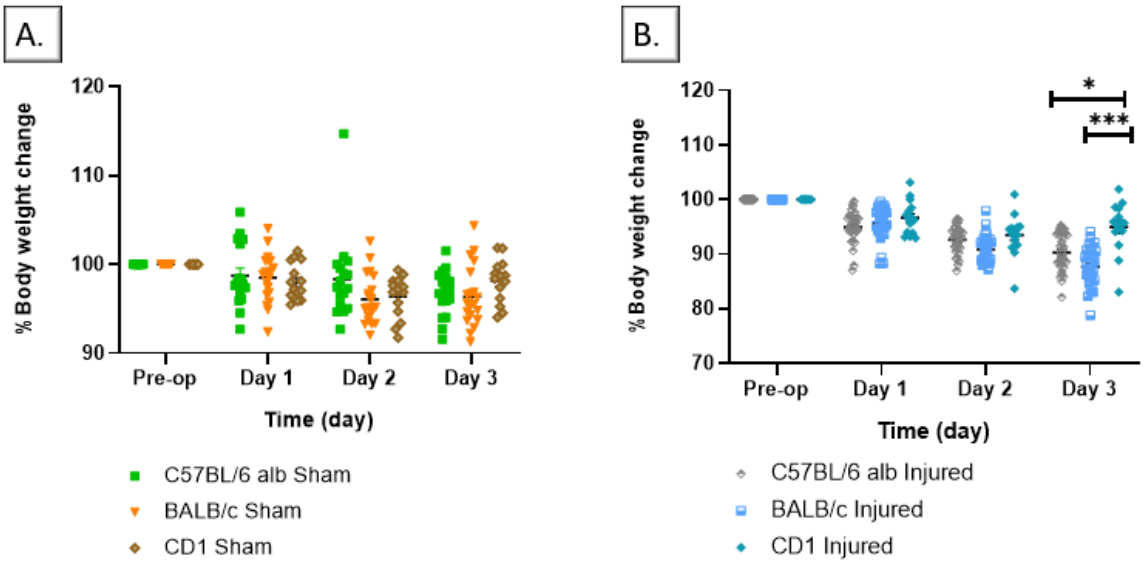

Figure 3.15: Comparing changes in body weight in different mouse strains. (A) Body weight of mice from three different strains that underwent sham procedure at baseline and days 1,2 and 3 after surgery. **(B)** Body weight of mice from three different strains following R-IRI procedure at baseline and days 1, 2 and 3 after surgery. **(C)** Proportional change in body weight following sham procedure. **(D)** Proportional change in body weight following R-IRI. All data points represent individual animals and error bars represent mean ± SEM.

3.5.8. Comparing the impact of regenerative medicine therapies on different mouse strains following R-IRI

Changes in renal function in response to bilateral R-IRI and PBS treatment between different strains were also analysed (Figure 3.16 A and C). PBS treatment led to a similar response to that of just the R-IRI procedure, without any injection proving the suitability of PBS as an internal control (Figure 3.14D): on day 3 post-surgery, BALB/c mice showed the highest rate of renal function recovery, while CD1 mice were the most affected by the procedure. Furthermore, strain effect on proportional changes in GFR (Figure 3.16C) following R-IRI and PBS treatment was considered very significant, with a 0.85% chance of randomly observing an effect this large (or larger) in an experiment of this size.

Comparing changes in renal function in response to bilateral renal IRI and hUC-MSC treatment (Figure 3.16 B and D) showed similar but less pronounced differences between the three strains: by day 3 of the study end-point, CD1 mice had significantly lower renal function, while BALB/c are the least injured by the procedure (Figure 3.16D). Furthermore, strain effect on proportional changes in GFR (Figure 3.16D) following R-IRI and PBS treatment was considered very significant, with a 0.91% chance of randomly observing an effect this large (or larger) in an experiment of this size.

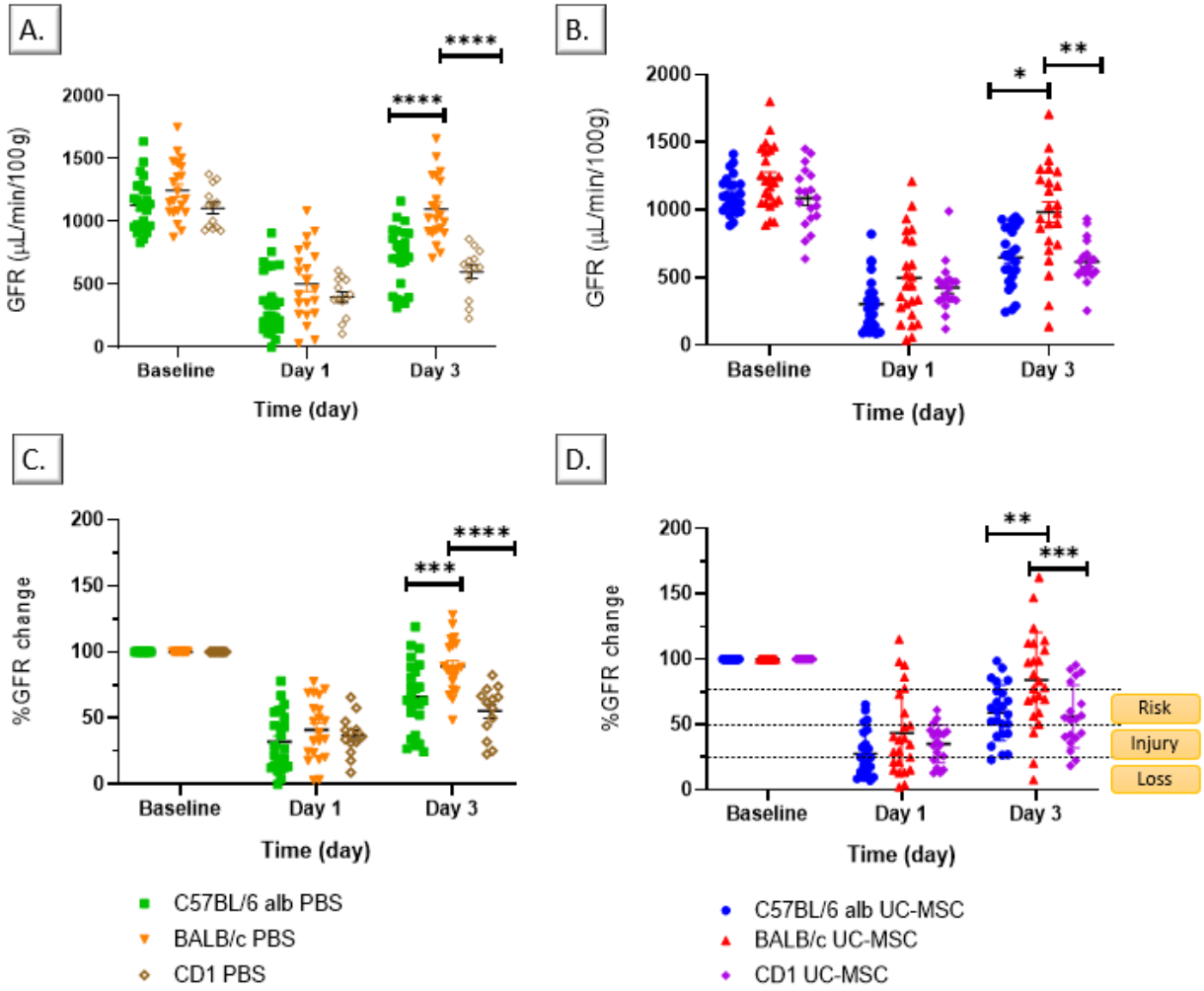

Figure 3.16: Comparing changes in renal function between BALB/c, C57BL/6 albino and CD1 strains following bilateral R-IRI and hUC-MSC/PBS treatment. (A) GFR results of mice from three different strains following R-IRI procedure and PBS treatment at baseline and days 1 and 3 after surgery. **(B)** GFR results of mice from three different strains following R-IRI procedure and hUC-MSC treatment at baseline and days 1 and 3 after surgery. **(C)** Proportional change in GFR following R-IRI in the PBS group. **(D)** Proportional change in GFR following R-IRI in the hUC-MSC group, with 'RIFLE' criteria representation. Significant differences between the three strains in response to surgery. *p<0.05, **p<0.005, ***p<0.0005 and ****p<0.0001. All data points represent individual animals and error bars represent mean ± SEM.

Comparisons in body weight changes between BALB/c, C57BL/6 alb and CD1 mice in response to bilateral R-IRI (Figure 3.17B) showed that strain has significant effects on body weight following renal IRI, however, this effect was more pronounced within the PBS groups (0.017% chance of randomly observing an effect this large in an experiment of this size) than in the hUC-MSC group (0.12% chance of randomly observing an effect this large in an experiment of this size). At the experiment end-point, BALB/c mice in both PBS and hUC-MSC

group were the most affected, losing approximately 10% of their body weight; CD1 mice were the least affected, losing approximately 4% body weight, followed by C57BL/6 alb with a mean body weight loss of 7%.

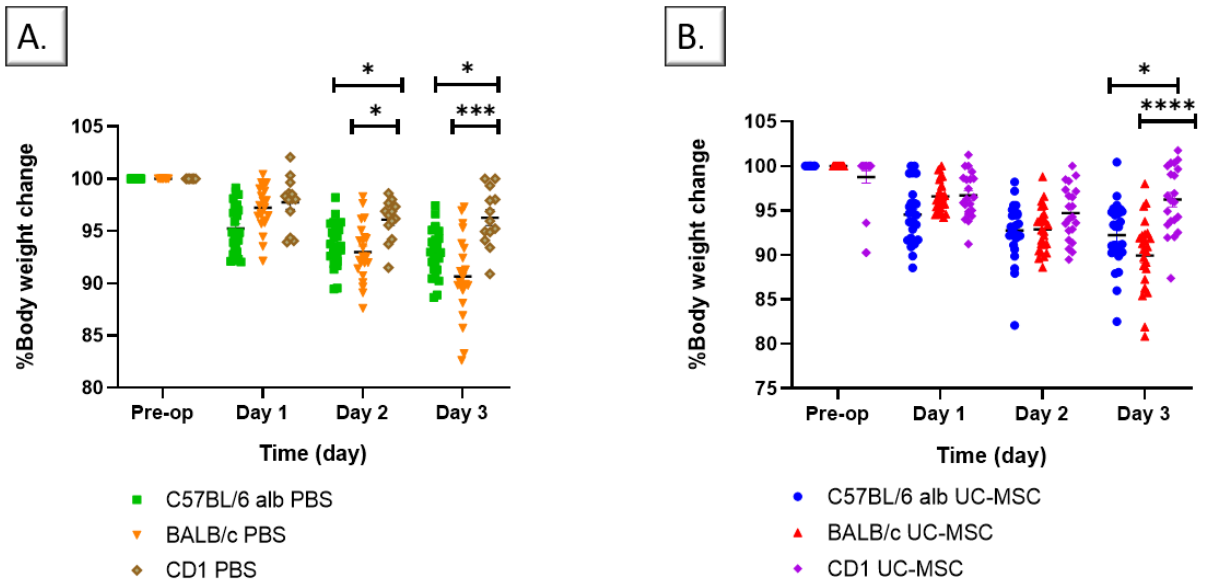

Figure 3.17: Comparing changes in body weight between BALB/c, C57BL/6 albino and CD1 strains following bilateral R-IRI and hUC-MSC/PBS treatment. (A) Body weight of mice from three different strains after R-IRI and PBS treatment at baseline and days 1, 2 and 3 after surgery. **(B)** Body weight of mice from three different strains following R-IRI, and hUC-MSC treatment at baseline and days 1, 2 and 3 after surgery. **(C)** Proportional change in body weight following R-IRI in the PBS group. **(D)** Proportional change in body weight following R-IRI n the hUC-MSC group. Significant differences between the three strains in response to surgery. *p<0.05 **p<0.005, ***p<0.0005 and ****p<0.0001. All data points represent individual animals and error bars represent mean ± SEM.

Strain	Procedure	Treatment	Time	%CV
BALB/c	Sham	N/A	Day 1	19.60%
			Day 3	18.03%
	IRI	N/A	Day 1	50.50%
			Day 3	37.74%
	IRI	hUC-MSC	Day 1	73.76%
			Day 3	43.19%
	IRI	PBS	Day 1	55.32%
			Day 3	22.17%
C57BL/6 alb	Sham	N/A	Day 1	22.46%
			Day 3	25.55%
	IRI	N/A	Day 1	63.65%
			Day 3	36.35%
	IRI	hUC-MSC	Day 1	64.66%
			Day 3	36.13%
	IRI	PBS	Day 1	67.60%
			Day 3	39.79%
CD1	Sham	N/A	Day 1	24.74%
			Day 3	32.44%
	IRI	N/A	Day 1	46.34%
			Day 3	40.65%
	IRI	hUC-MSC	Day 1	41.23%
			Day 3	42.83%
	IRI	PBS	Day 1	41.53%
			Day 3	34.53%

Table 3.1: Coefficient of variation from absolute GFR values. %CV was calculated from absolute GFR values following bilateral R-IRI or sham-operated procedure to compare the variability in renal function between strains.

3.6. Discussion

3.6.1. The bilateral renal ischaemia-reperfusion injury model is highly variable

The bilateral R-IRI model was used for this study as the majority of clinical AKI cases result from ischaemia-reperfusion injury and involve both kidneys[16,21,25,47,49,61,265]. However, the variability of the pre-clinical bilateral renal IRI model is a well-documented fact[16,21,25,47,49,61,265], and evidence of it can also be seen clearly in the experiments conducted within this thesis, regardless of the mouse strain studied. Previous experiments done within the group have shown that standardising the pre-surgical anaesthetic time to 30 minutes drastically reduces GFR variability following R-IRI[266,267]. Fluctuations in the body temperature of animals have also been linked to the IRI model's variability. As a result, animals were placed on a heat pad during the surgery and body temperature was maintained constant using a

rectal probe with a feedback-regulated system. Furthermore, previous optimisation experiments conducted in our group also showed that a clamp time of 27.5 minutes induced an injury level severe enough with a lower mortality rate whereas longer clamp time (i.e., 30 minutes) led to a too severe injury and animals were unable to reach the experimental end-point (i.e., survive for three days after injury induction without breaching the humane endpoints set)[267]. However, even with a pre-anaesthetic time, clamp time and body temperature standardised, the bilateral R-IRI model is highly variable, regardless of animal strain. Based on the ADQI 'RIFLE' classification, 47.14% of the total number of animals that underwent bilateral R-IRI in these experiments (no treatment) were classified within the 'Loss' category whereas 32.8% of animals were classified within the 'Injury' category.

3.6.2. Strain-dependent response to bilateral renal ischaemia-reperfusion injury

In order to determine whether response to bilateral R-IRI is strain-dependent, surgery was performed on three different mouse strains: BALB/c, C57BL/6 alb and CD1, that are characterised by different genetic backgrounds and immunological profiles.

Comparing baseline renal function data in three different mouse strains showed clear differences between strains, however, these differences were not statistically significant. Furthermore, these differences were consistent throughout the experiments and more pronounced once the animals underwent sham-operated procedure. Comparing percentage change in renal function in three different mouse strains following sham-procedure showed a similar pattern with the inbred mice (i.e., BALB/c and C57BL/6 alb) presenting an increase in GFR while the outbred animals (i.e., CD1) showed a decrease in GFR (Figure 3.14 A and B). These differences in renal function following sham-operated procedure highlight the impact a surgery, in the absence of injury, could have on the body, and it has important implications for future translational studies as it shows a strain-dependent response to such operations.

Kidney function was found to decline considerably following bilateral R-IRI (day 1) and partially recover in all three strains (day 3) revealing the kidneys significant capability to restore function after an episode of AKI (Figure 3.14 B and D). When comparing strain response to bilateral renal IRI, we observed a comparable pattern to the one seen following sham-operated procedure: by day 3, BALB/c mice were the least affected by the R-IRI procedure, displaying the least reduction in renal function when compared to C57BL/6 alb

and CD1 mice; these differences were consistent throughout the experiments (Figure 3.14 B and D). Previous experiments performed within the Wilm group pointed towards the opposite effect, with BALB/c mice more susceptible to injury when compared to C57BL/6 alb mice[267]. However, it is important to note that while in the current experiments BALB/c mice showed higher renal function following R-IRI surgery, they also displayed the highest degree of distress and reduction in mobility when compared to the other two strains. Furthermore, this was coupled with a higher loss/exclusion of BALB/c mice from experiments: n = 5 animals excluded from the R-IRI (no treatment) group, n = 4 animals excluded from the hUC-MSC, and n = 2 animals excluded from the PBS group. Interestingly, while C57BL/6 alb showed a lower reduction in renal function following bilateral R-IRI than BALB/c, they were also the most resilient and least affected physically by the procedure: n = 2 animals excluded from the R-IRI (no treatment) group, and n = 1 animals excluded from MSC group. Finally, the CD1 mice also presented with a high loss/exclusion of animals from experiments: n = 2 animals excluded from the R-IRI (no treatment) group, n = 2 animals excluded from the hUC-MSC, and n = 2 animals excluded from the PBS group. Exclusion of animals from the final results would have skewed the data towards a less injured model on the 'RIFLE' chart and points towards the limitations of the bilateral R-IRI model i.e., it is difficult to cause significant kidney damage without breaching the severity limits and preventing early animal death.

These differences once again emphasize the importance of strain on translational research: careful considerations need to be taken in understanding genotype-phenotype relationships and how these can affect experimental outcomes to improve our experimental designs and create better disease models.

3.6.3. Intravenous injection of hUC-MSC does not improve renal function after bilateral renal ischaemia-reperfusion injury

In pursuance of determining the efficacy of hUC-MSC therapies in ameliorating kidney injury in a mouse model of AKI, animals were administered the cells immediately after bilateral R-IRI surgery. The therapies were tested in three different mouse strains (i.e., BALB/c, C57BL/6 alb and CD1) that are characterised by distinct immunological profiles. Nonetheless, we were unable to demonstrate the efficacy of hUC-MSC cells in ameliorating kidney injury following bilateral renal IRI in any of the mouse strains by the study 3-day end-

point, and we were ineffective in detecting an impact of the different immunological profiles on the therapy-effect of hUC-MSC.

There were no differences in renal function between the control group (PBS) and cellular therapy groups on either day 1 or day 3 following bilateral R-IRI, regardless of strain. Similarly, there were no differences in weight changes following bilateral R-IRI between treatment and control groups, regardless of strain. While not statistically significant, both BALB/c (Figure 3.4D) and C57BL/6 alb mice (Figure 3.8D) in the hUC-MSC group show a slightly slower rate of recovery of renal function (approximately 3% mean difference) when compared to the control group. In contrast, CD1 mice in the hUC-MSC group show a slightly higher rate of recovery of renal function (approximately 3.6% mean difference) when compared to the control group (Figure 3.12D). However, it would be difficult to interpret whether these differences are clinically significant due to the short length of experiments (i.e., 3 days).

Previous research points towards the renoprotective effects of MSC therapy, capable of ameliorating kidney function and reducing tubular damage after injury[21,25,225–229,258–260,26,106,149,191–193,207,224]. These studies investigated the effects of MSC in rodent kidney injury models, using either mice (C57BL/6 and BALB/c)[25,106,259,260,149,191,193,224,225,227,229,258] or rats[21,26,192,207,226,228], and assessed kidney function using BUN and/or SCr levels; it is important to note that all these studies have used young animals, similar to the one used in the current experiments although the sex of the animals was variable. While the current experiments in this thesis used a transcutaneous device to assess kidney function instead of biochemical parameters, multiple studies have validated the use of this technique which allows for the measurement of GFR without any of the constraints of sCr or BUN assays[241,242]. Furthermore, previous work from a Doctoral student in the B. Wilm not only also showed that the transcutaneous device provides an accurate measurement of kidney injury when compared to sCr and BUN levels in serum, and was also unable the prove the amelioration of renal function using these two biomarkers[267]. These studies also used a variety of injury models, such as toxin-induced using adriamycin, cisplatin or glycerol, unilateral and bilateral ischaemia models, and unilateral urethral obstruction (UUO) models, and efficacy of cellular therapies was demonstrated in all of them. Furthermore, these investigations used a variety of MSC (e.g., UC-MSC, BM-MSC, cord blood MSC and adipose tissue MSC), administered through

various routes, such as intra-arterial, intra-venous or intra-peritoneal, and at different doses ($1 \times 10^5 – 2 \times 10^6$ cells/animal). Taking into consideration the variability in experimental design and type of animal used in the experiments, it raises the question of why we were unable to demonstrate efficacy in our experiments. One reason for the lack of efficacy in the current studies could be due to the exposure of MSCs to various cells and molecules following *in vivo* administration which could change their phenotype and subsequently impact their effectiveness. Additionally, the precise mode of action of these therapies is still largely unknown and which potential attributes of MSCs are necessary for their efficacy. For example, the HLA-G (human leukocyte antigen-G - a major histocompatibility complex class I antigen) molecule has been found to play a crucial role in the therapeutic effects of MSCs[178,268], however, its expression can vary between different MSC sources and batches[116,188]. As a result, further research is necessary into the molecules which are capable of ameliorating injury and promoting recovery so as to maximise the therapeutic potential of these cells.

While MSC therapies have shown promising results in pre-clinical models of kidney disease (both *in vitro* and *in vivo*), their translation to the clinic has not yielded conclusive results on the merit of these treatments. Phase I clinical trials assessing the safety of MSCs in various disease models have found these therapies to be safe when given to humans[157,195,233–237]. However, when assessing the effects of MSC therapy on disease outcomes, the results were not as positive. A phase II and a phase III clinical trials showed that intravenous infusions of allogeneic MSCs were effective in reducing fistulas in patients with Crohn's disease[235,236], whereas a phase II clinical trial using MSCs for the treatment of COPD showed no significant differences in patients' quality-of-life following therapy. Preliminary data from a phase I clinical trial testing the safety and efficacy of MSC therapy in patients that are at high risk of developing AKI after cardiac surgery suggests that both length of hospital stay and readmission rates were reduced by 40% with a 20% reduction in the number of patients that developed AKI in the treatment group when compared to the control[157]. However, a phase II clinical trial to determine the efficacy of MSC treatment in reducing the recovery time from AKI after cardiac surgery found no differences between the therapy and placebo groups[237]. Taking all of this previous research into consideration, it is crucial that further investigation is conducted into the mode of action of MSCs so as to better replicate the results seen in pre-clinical studies and to translate these into the clinic.

Chapter 4

Assessing the efficacy of regenerative medicine therapies in ameliorating acute kidney injury through macrophage modulation

4. Assessing the efficacy of regenerative medicine therapies in ameliorating acute kidney injury through macrophage modulation

4.1. Introduction

Regenerative medicine therapies using MSCs have been researched extensively both in pre-clinical and clinical studies to target a host of autoimmune and inflammatory conditions such as graft versus host disease (GVHD), Crohn's disease, kidney disease, diabetes, cardiovascular or neurodegenerative diseases[121,178–180,203,235,236,269,270].

In vitro and *in vivo* models have shown that these multi-potent, hypo-immunogenic cells are capable of ameliorating various auto-immune and inflammatory diseases through paracrine and endocrine signalling pathways, although these mechanisms are not completely understood. Extensive research points towards the MSCs exerting their effects through the secretion of bioactive molecules such as cytokines, growth factors and chemokines that alter the local environment, modulate inflammation, and stimulate angiogenesis and tissue repair[157,185,187,190,203]. MSCs constitutively express a multitude of receptors and signalling substances: cellular adhesion molecules such as VCAM-1 and ICAM-1, cell fate / transcription factors such as Sox2 and Oct4, pro-angiogenic molecules such as IL-8, HGF VEGF, and immune-stimulatory molecules such as MCP-1, IL-6, IDO, TGF-β and PGE2[6,16,207–210,22,26,45,187,188,204–206]. In addition, mass spectroscopy analysis of the secretome released by bone marrow-derived MSCs showed distinct differences in protein composition depending on physiological state, i.e. the environment which MSCs are introduced into leads to the release of regulatory substances that match the primary needs of the tissue[209]. To better illustrate this point, several research studies have shown that MSC pro-inflammatory preconditioning leads to the release of immune-modulatory molecules while hypoxia preconditioning leads to the release of various growth factors[119,181,183,190,212–214].

AKI, a common complication in hospitalised patients, can have multiple causes, from pre-renal to post-renal, and is characterised by a multifactorial and complex pathophysiology[4,5,50]. Regardless of its aetiology, inflammation plays a crucial role in AKI with several components of both innate and adaptive immunity implicated in disease progression[10,19,43]. A special role in this process is played by macrophages, and this thesis is focused on their contribution to AKI and their response to cellular therapies. Animal models

of AKI have shown that macrophages are one of the main cells involved in kidney disease where they play a dual role, in both the early injury phase and the resolution of inflammation[16,17,52,102,251]. Macrophages are classified into two main groups: M1 characterised by a Th1 profiles and M2 macrophages characterised by a Th2 profile[19,64]. Whereas M1 macrophages play a major role in the early stage of kidney injury[19,52,102], M2 macrophages are involved in the late injury phase characterised by tubular cell repair and proliferation[64,251].

In vivo models of kidney disease have shown that MSC treatment can improve renal function in response to injury, and lead to a decrease in both serum creatinine and blood urea nitrogen, both markers of kidney injury[21,26,227,228,271,42,149,191–193,224–226]. In particular, MSC therapy exerts its renoprotective effects by preserving the structural integrity of the kidney through a decrease in tubular cell death, podocyte and glomerular cell loss, and leukocyte infiltration[21,149,193]. In addition, MSC treatment has been shown to promote tissue regeneration and repair by inducing the proliferation of endogenous renal cells and increasing angiogenesis[149,192,193]. Treatment is thought to induce a Th2 anti-inflammatory environment with a decrease in ROS expression, anti-apoptotic molecules, and inflammatory biomarkers, such IL-1β, IL-6, TNF-α, ICAM and NF-κβ. Furthermore, MSC therapy stimulates the polarisation of macrophages into an M2 phenotype with an increase in the levels of eNOS, IL-4 and IL-10[42,150,192,193].

4.2. Aims

This research has focused on examining three different mouse strains, two inbred (BALB/c and C57BL/6 alb) and one outbred (CD1) which differ in their susceptibility to inflammatory diseases and infection. We have chosen to investigate different mouse strains due to multiple studies indicating variability in data attributed to differences in genetic backgrounds[36,238–240]. Both C57BL/6 and BALB/c strains have been commonly used in pre-clinical models of AKI; these two strains are characterised by a Th1 profile and a Th2 profile, respectively: C57BL/6 T-cells easily produce IFN-γ and stimulate macrophage towards an M1 pro-inflammatory phenotype, whereas BALB/c T-cells produce IL-4 and stimulate macrophage towards an M2 anti-inflammatory phenotype. C57BL/6 and BALB/c strains are ideal for research into conditions were the immune system plays an active role, however, not much

research has been conducted using the CD1 strain[25,89,120–126,95–97,106,116–119]. However, as CD1 are an outbred strain, its inclusion in translational research should be encouraged as the inter-individual genetic variation of CD1 mice would better mimic the response seen in the human populations.

We have attempted to examine the role of genetic background on macrophage levels in the kidney and spleen using the acute kidney injury model described in Chapter 2, with a standardised clamping time. The spleen was chosen because it is the largest secondary lymphoid organ, with both local and systemic effects of immune cell responses, and a reservoir of monocytes and macrophages. Furthermore, spleen monocytes have the ability to migrate to inflamed tissues during an episode of acute inflammation[76,84,133,137].

In vivo experiments presented within this chapter had three main aims:

(1) to assess the effect of R-IRI on spleen and kidney macrophages, in three different mouse strains;

(2) to determine the effect of regenerative medicine therapies on spleen and kidney macrophages, in three different mouse strains following R-IRI;

(3) to determine the effect of regenerative medicine therapies on pro- and anti-inflammatory cytokine levels in BALB/c mice.

4.3. Experimental Design

AKI was induced in healthy animals from three different mouse strains (BALB/c, C57BL/6 alb and CD1) through bilateral clamping of the renal pedicles which supply the kidney with blood (see section *2.3* for more information).

To assess the effect of hUC-MSC therapy on macrophage levels in the kidneys and spleen, mice were injected with 250,000 MSCs (in 100µL volume) through the tail vein immediately after surgery. Control mice were given 100µL PBS by IV injection. Organs and blood were collected on day 3 following surgery, dissociated on the same day, and analysed through cytofluorimetric analysis the following day. Macrophages were identified using the following markers (Table 4.1): F4/80+ as a pan-macrophage marker used to identify tissue macrophages, $F4/80^{+}CD86^{+}$ to identify M1-like macrophages, $F4/80^{+}CD163^{+}$ to identify M2-

like macrophages, and F4/80$^+$CD86$^+$CD163$^+$ to identify those cells that contain markers of both M1 and M2 macrophages[137,251,272–276]. Due to the extended nature of the flow cytometry analysis (approximately 6 hours run-time for 10 animals), it was not possible to analyse more than 80,000 live events per experiment.

Cell type	Marker
Macrophage	F4/80$^+$
M1 macrophage	F4/80$^+$CD86$^+$
M2 macrophage	F4/80$^+$CD163$^+$
Intermediate macrophage state	F4/80$^+$CD86$^+$CD163$^+$

Table 4.1: Cell surface markers used for the detection of macrophages in cytofluorimetric analysis.

Preliminary assessment of various pro- and anti-inflammatory cytokines was performed using kidney cell suspensions and plasma collected through cardiac puncture from BALB/c mice following bilateral R-IRI; samples were assessed in triplicate for the following analytes: monocyte chemoattractant protein-1 (MCP-1), IL-1β, IL-6, IL-13, M-CSF, IFN-γ, IL-4, IL-10, IL-17E/IL-25, and TNF-α.

Analyte	Role
MCP-1	Pro-inflammatory chemokine – manages leukocyte recruitment to the site of inflammation[19,20,57,63,94,116,187,245–247]
IL-1β	Pro-inflammatory cytokine by monocytes, macrophages and kidney cells during injury[25,52,61,63,86,248]
IL-6	Cytokine with both pro- and anti-inflammatory roles[63,78,91,249,250]
IL-13	Anti-inflammatory cytokine associated with M2 macrophage polarisation[52,86,90,93,107,251,252]
M-CSF	Pro-inflammatory cytokine capable of activating monocytes and macrophages [17,63,85,93,97,253–255]
IFN-γ	Pro-inflammatory cytokine associated with M1 macrophage activation[61,215]
IL-4	Anti-inflammatory cytokine associated with M2 macrophage polarisation[53,55,61,116,204]
IL-10	Anti-inflammatory cytokine capable of inhibiting leukocyte migration and pro-inflammatory cytokines release[117,256]
IL-17E/IL-25	Anti-inflammatory cytokine capable of promoting Th2 responses[257]
TNF-α	Pro-inflammatory cytokine produced by monocytes, macrophages and kidney cells during injury[15,122,256]

Table 4.2: Multiplex Cytokine Analysis of mouse plasma for common pro- and anti-inflammatory cytokines.

4.4. Statistical analysis

Two-way ANOVA with Geisser-Greenhouse correction was performed as sphericity was not assumed, i.e. I did not assume that data were sampled from populations where the standard deviation were identical in all of the groups at all the time points. Sidak's multiple comparisons correction test (for comparisons between two groups) and Tukey's multiple comparisons correction test (for comparisons between three groups), with individual variances computed for each comparison were used to analyse the percentage of positive events identified. The correlation analysis was performed using the Mann-Whitney U test for non-parametric data with two variables, i.e. cytokine assay data. All data is shown as mean (95% confidence interval) ± SEM.

Statistical analysis was performed using GraphPad Prism 8 for Windows (GraphPad, LLC). All data points represent individual animals and error bars represent mean ± SEM. Statistical significance is represented by values $p< 0.05$.

4.5. Results

4.5.1. The effect of R-IRI on macrophage populations in the kidneys and spleen of BALB/c mice

In order to determine the effect of R-IRI on macrophage populations in the kidneys and spleen of BALB/c mice, AKI was induced in 7 healthy BALB/c mice, and at day 3 post-R-IRI macrophage levels in the kidneys and spleen were compared against those in 6 sham-operated (control) mice (Figures 4.1 and 4.2).

My data showed that renal IRI led to a slight decrease in the percentage of live $F4/80^+$ and $F4/80^+CD86^+$ cells in the kidneys of BALB/c mice when compared to control animals, though these differences were not statistically significant (Figure 4.1A). There were no differences in the percentage of $F4/80^+CD163^+$ and $F4/80^+CD86^+CD163^+$ cells in the kidneys of control and injured BALB/c mice (Figure 4.1A). When comparing macrophage levels within the $F4/80^+$ kidney population, there was with statistical significance a higher percentage of $F4/80^+CD86^+$ cells in injured mice when compared to control mice (*p=0.0284) (Figure 4.1C). A large percentage of F4/80+ kidney cells were negative for both CD86 and CD163 markers (78% - 88%), however, this population was smaller in injured BALB/c mice (Figure 4.1D).

While there was no difference in the levels of $F4/80^{+}CD86^{+}$ cells in kidney cell suspensions between sham-operated and injured BALB/c animals, there was a significant decrease in the levels of $F4/80^{+}CD163^{+}$ expression intensity in injured mice when compared to control animals (Figure 4.1B). My data demonstrated that renal IRI had a significant effect on median fluorescence intensity, with a 2.6% chance of randomly observing an effect this large (or larger) in an experiment of this size.

Renal IRI resulted in no differences in the percentage of positive live $F4/80^{+}$ cells in the spleens of BALB/c mice when compared to sham-operated animals (Figure 4.2A). There were also no differences in the levels of $F4/80^{+}CD86^{+}$ or $F4/80^{+}CD163^{+}$ expression intensity between injured and control BALB/c mice spleens (Figure 4.2B). Furthermore, there were no differences when comparing macrophage levels within the $F4/80^{+}$ spleen population (Figure 4.2 C and D). Similar to the kidneys, the spleen has a population of $F4/80^{+}$ cells that are negative for both CD86- and $CD163^{-}$, however, this population is much smaller than in the kidney (13% - 15%) (Figure 4.2C).

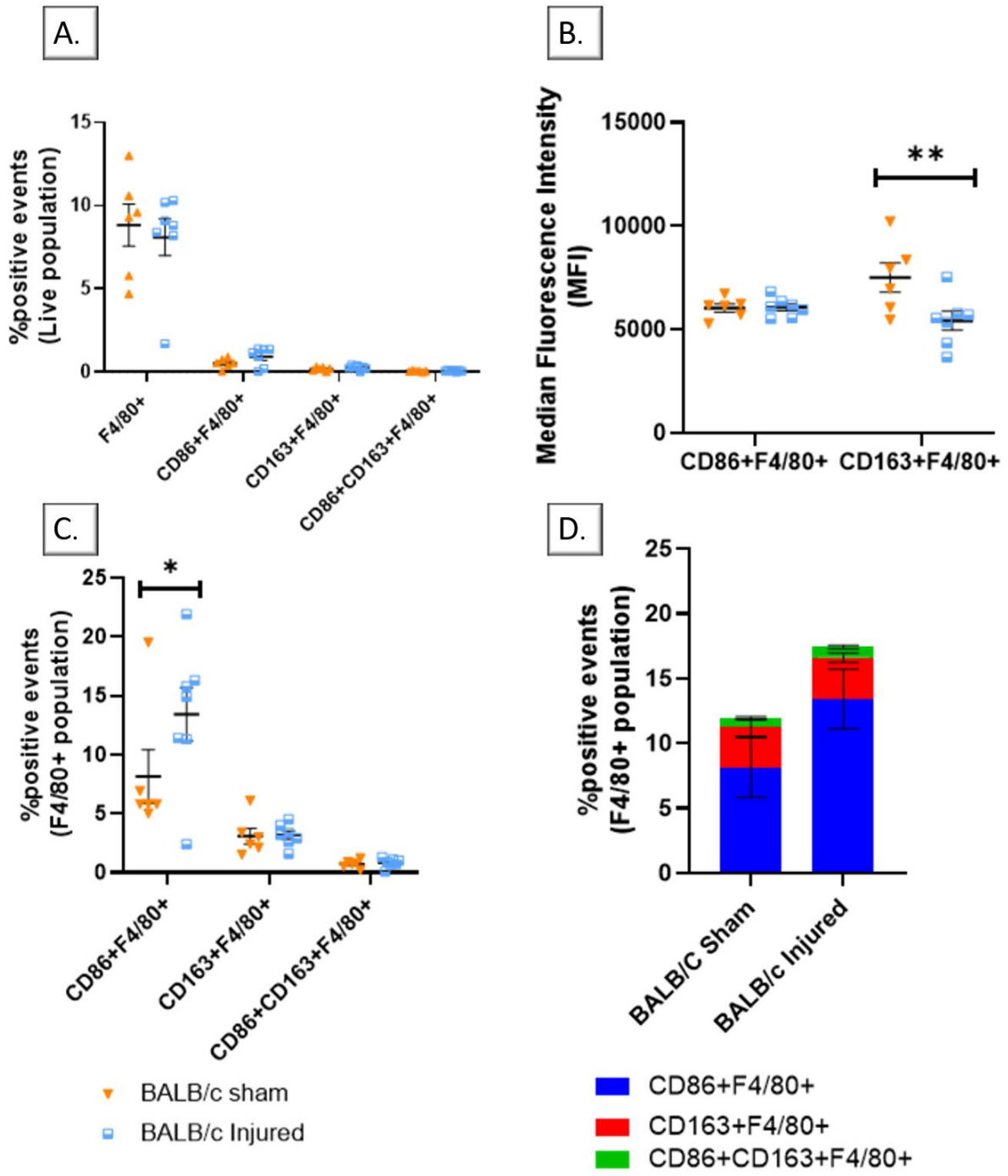

Figure 4.1: Changes in macrophage levels in BALB/c mice kidney cell suspensions following R-IRI. (**A**) The percentage of F4/80$^+$, F4/80$^+$CD86$^+$, F4/80$^+$CD163$^+$ and F4/80$^+$CD86$^+$CD163$^+$cells in kidney cell suspensions from BALB/c mice after R-IRI and compared to sham-operated mice; data showing the percentage of positive cells within the Live population. (**B**) Quantification of signal intensity of F4/80$^+$CD86$^+$ and F4/80$^+$CD163$^+$ cells in kidney cell suspensions from BALB/c mice after R-IRI and compared to sham-operated mice. (**C**) The percentage of F4/80$^+$CD86$^+$, F4/80$^+$CD163$^+$ and F4/80$^+$CD86$^+$CD163$^+$ cells in kidney cell suspensions from BALB/c mice after R-IRI and compared to sham-operated mice; data showing the percentage of positive cells within the F4/80+ population. (**D**) The percentage of F4/80$^+$CD86$^+$, F4/80$^+$CD163$^+$ and F4/80$^+$CD86$^+$CD163$^+$ cells in kidney cell suspensions from BALB/c mice after R-IRI and compared to sham-operated mice; data showing the percentage of positive cells within the

F4/80$^+$ population which are represented as ratios. **n=7** injured group and **n=6** sham group. Significant differences between injured and sham-operated animals. *p=0.0284 and **p=0.0048. All data points represent individual animals and error bars represent mean ± SEM.

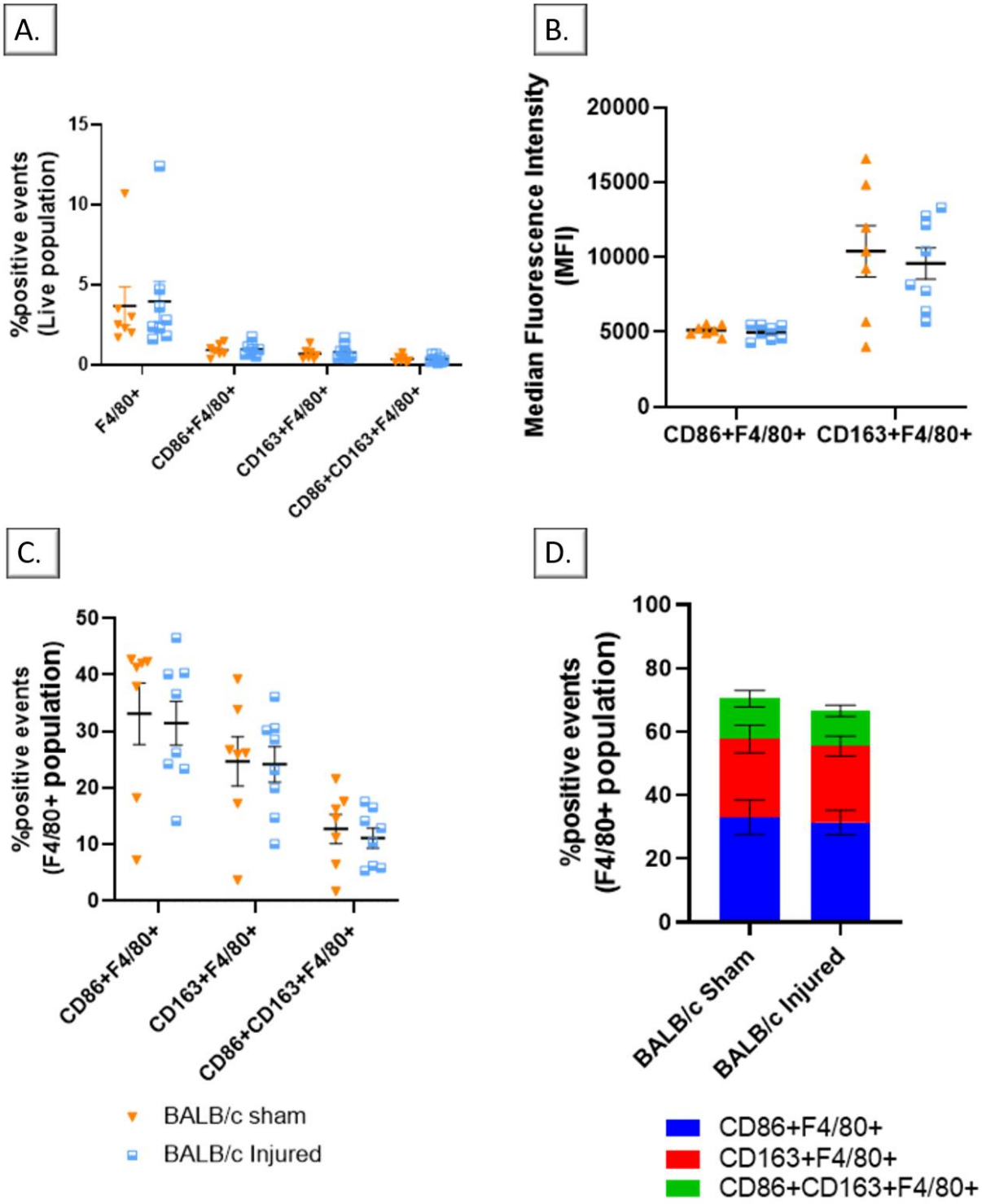

Figure 4.2: Changes in macrophage levels in BALB/c mice spleen cell suspensions following R-IRI. (A) The percentage of F4/80$^+$, F4/80$^+$CD86$^+$, F4/80$^+$CD163$^+$ and F4/80$^+$CD86$^+$CD163$^+$ cells in spleen cell suspensions from BALB/c mice after R-IRI and compared to sham-operated mice; data showing the percentage of positive cells within the Live population. **(B)**

Quantification of signal intensity of F4/80$^+$CD86$^+$ and F4/80$^+$CD163$^+$ cells in spleen cell suspensions from BALB/c mice after R-IRI and compared to sham-operated mice. **(C)** The percentage of F4/80$^+$CD86$^+$, F4/80$^+$CD163$^+$ and F4/80$^+$CD86$^+$CD163$^+$ cells in spleen cell suspensions from BALB/c mice after R-IRI and compared to sham-operated mice; data showing the percentage of positive cells within the F4/80$^+$ population. **(D)** The percentage of F4/80$^+$CD86$^+$, F4/80$^+$CD163$^+$ and F4/80$^+$CD86$^+$CD163$^+$ cells in spleen cell suspensions from BALB/c mice after R-IRI and compared to sham-operated mice; data showing the percentage of positive cells within the F4/80$^+$ population which are represented as ratios. **n=7** injured group and **n=6** sham group. All data points represent individual animals and error bars represent mean ± SEM.

4.5.2. The effect of regenerative medicine therapies on BALB/c mice following R-IRI

Next, I determined whether hUC-MSC as regenerative medicine therapies influenced the macrophage levels in the kidneys and spleens in BALB/c mice after R-IRI. Sixteen male BALB/c mice received 250,000 hUC-MSC through IV injection immediately after bilateral R-IRI, whereas thirteen BALB/c mice received 100µL PBS (Figure 4.3 and Figure 4.4).

Injured BALB/c mice that received hUC-MSC injections showed significantly lower percentage of live F4/80$^+$ cells in their kidneys when compared to the PBS group (*p=0.0393); there were no differences in the percentage of live F4/80$^+$CD86$^+$, F4/80$^+$CD163$^+$ and F4/80$^+$CD86$^+$CD163$^+$ in the kidneys of injured mice between treatment and PBS groups (Figure 4.3A). However, when comparing macrophage levels between injured animals that received PBS and those that had no injections (no hUC-MSC nor PBS, see section *4.5.1* for more information), there was a lower percentage of live F4/80$^+$ in the kidneys of BALB/c mice that received PBS, although this difference was not statistically significant (Figure 4.3B); this difference could be attributed to the high variability seen in the data as well as to the lower number of animals in the R-IRI no injection group. There were no differences in macrophage levels within the F4/80$^+$ kidney population (Figure 4.3 C and D) between treatment and PBS groups following bilateral R-IRI. Furthermore, there were no differences in the levels of either F4/80$^+$CD86$^+$ or F4/80$^+$CD163$^+$ antibody expression between treatment and PBS groups following R-IRI (Figure 4.3E).

In conclusion, intravenous injection of hUC-MSC led to minimal effects on macrophage responses in the kidneys of injured BALB/c mice.

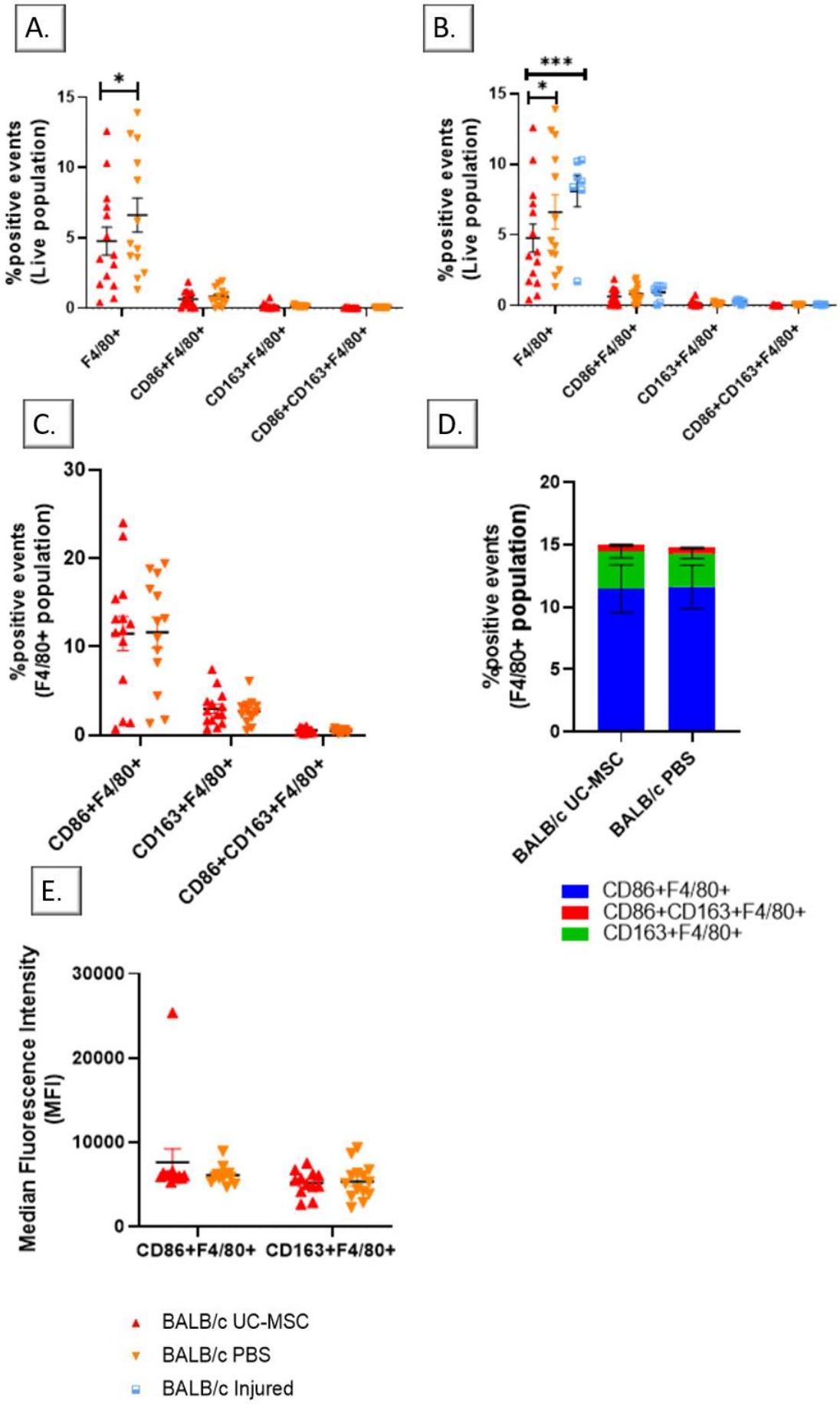
A.
B.
C.
D.
E.
%positive events (Live population)
F4/80+
CD86+F4/80+
CD163+F4/80+
CD86+CD163+F4/80+
%positive events (F4/80+ population)
BALB/c UC-MSC
BALB/c PBS
Median Fluorescence Intensity (MFI)
BALB/c Injured

Figure 4.3: Changes in macrophage levels in BALB/c mice kidney cell suspensions following R-IRI and hUC-MSC treatment. (**A**) The percentage of F4/80$^+$, F4/80$^+$CD86$^+$, F4/80$^+$CD163$^+$ and F4/80$^+$CD86$^+$CD163$^+$ cells in kidney cell suspensions from BALB/c mice after R-IRI and hUC-MSC therapy and compared to animals that had received PBS; data showing the percentage of positive cells within the Live population. (**B**) The percentage of F4/80$^+$, F4/80$^+$CD86$^+$, F4/80$^+$CD163$^+$ and F4/80$^+$CD86$^+$CD163$^+$ cells in kidney cell suspensions from BALB/c mice after R-IRI and hUC-MSC therapy and compared to animals that had received either PBS or no treatment; data showing the percentage of positive cells within the Live population. (**C**) The percentage of F4/80$^+$CD86$^+$, F4/80$^+$CD163$^+$ and F4/80$^+$CD86$^+$CD163$^+$ cells in kidney cell suspensions from BALB/c mice after R-IRI and hUC-MSC therapy and compared to animals that had received PBS; data showing the percentage of positive cells within the F4/80$^+$ population. (**D**) The percentage of F4/80$^+$CD86$^+$, F4/80$^+$CD163$^+$ and F4/80$^+$CD86$^+$CD163$^+$ cells in kidney cell suspensions from BALB/c mice after R-IRI and hUC-MSC therapy and compared to animals that had received PBS; data showing the percentage of positive cells within the F4/80+ population which are represented as ratios. (E) Quantification of signal intensity of F4/80$^+$CD86$^+$ and F4/80$^+$CD163$^+$ cells in kidney cell suspensions from BALB/c mice after R-IRI and hUC-MSC therapy and compared to animals that received PBS. **n=16** hUC-MCS group, **n=13** PBS group and **n=7** injured group (no treatment). Significant differences between treatment groups in the F4/80$^+$ population. *p=0.0393 and ***p=0.0009. All data points represent individual animals and error bars represent mean ± SEM.

There were no statistically significant differences in the percentage of positive live F4/80$^+$ cells in the spleens of BALB/c mice between treatment groups following bilateral R-IRI (Figure 4.4A). However, when comparing macrophage levels between injured animals that received treatment (both hUC-MSC and PBS) and no injections (no hUC-MSC or PBS, see section *4.5.1* for more information), there was a significantly higher percentage of live F4/80$^+$ in the spleens of BALB/c mice that had no injections (Figure 4.4B); this difference could be attributed to the high variability seen in the data as well as to the lower number of animals in the R-IRI no injection group. When comparing differences in macrophage levels within the F4/80$^+$ population in the spleen, hUC-MSC treatment led to a slightly lower percentage of F4/80$^+$CD163$^+$ and F4/80$^+$CD86$^+$CD163$^+$ cells following bilateral R-IRI, however, these differences were not statistically significant (Figure 4.4 C and D). There were also no differences in the levels of F4/80$^+$CD86$^+$ or F4/80$^+$CD163$^+$ antibody expression between treatment and PBS groups in injured BALB/c mice spleens (Figure 4.4E).

In conclusion, intravenous injection of hUC-MSC led to minimal effects on macrophage responses in the spleens of injured BALB/c mice, and these differences were not statistically significant.

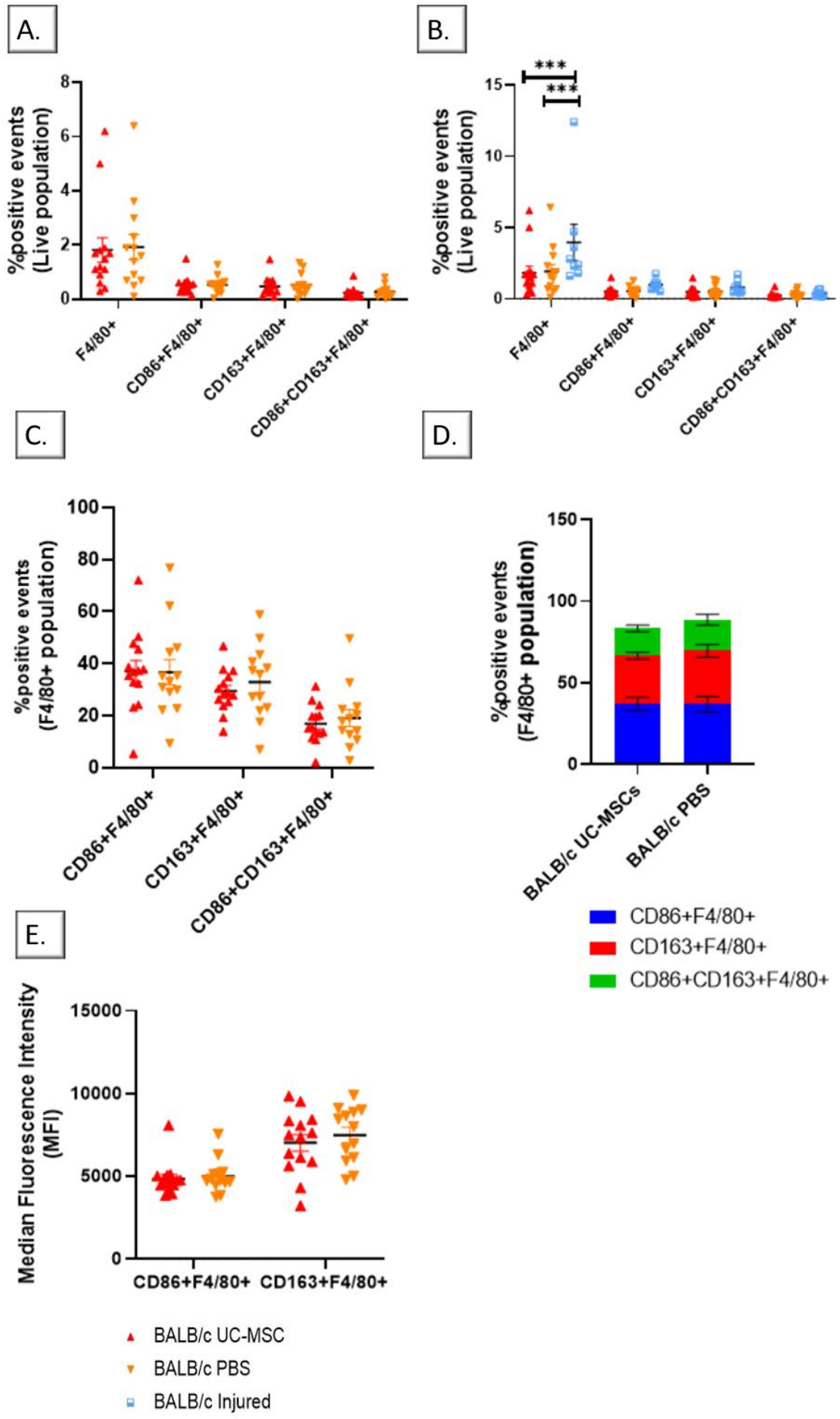
A.
%positive events (Live population)
F4/80+
CD86+F4/80+
CD163+F4/80+
CD86+CD163+F4/80+
B.
***
***
%positive events (Live population)
F4/80+
CD86+F4/80+
CD163+F4/80+
CD86+CD163+F4/80+
C.
%positive events (F4/80+ population)
CD86+F4/80+
CD163+F4/80+
CD86+CD163+F4/80+
D.
%positive events (F4/80+ population)
BALB/c UC-MSCs
BALB/c PBS
CD86+F4/80+
CD163+F4/80+
CD86+CD163+F4/80+
E.
Median Fluorescence Intensity (MFI)
CD86+F4/80+
CD163+F4/80+
BALB/c UC-MSC
BALB/c PBS
BALB/c Injured

Figure 4.4: Changes in macrophage levels in BALB/c mice spleen cell suspensions following R-IRI and hUC-MSC treatment. (**A**) The percentage of F4/80$^+$, F4/80$^+$CD86$^+$, F4/80$^+$CD163$^+$ and F4/80$^+$CD86$^+$CD163$^+$ cells in spleen cell suspensions from BALB/c mice after R-IRI and hUC-MSC therapy and compared to animals that had received PBS; data showing the percentage of positive cells within the Live population. (**B**) The percentage of F4/80$^+$, F4/80$^+$CD86$^+$, F4/80$^+$CD163$^+$ and F4/80$^+$CD86$^+$CD163$^+$ cells in spleen cell suspensions from BALB/c mice after R-IRI and hUC-MSC therapy and compared to animals that had received either PBS or no treatment; data showing the percentage of positive cells within the Live population. (**C**) The percentage of F4/80$^+$CD86$^+$, F4/80$^+$CD163$^+$ and F4/80$^+$CD86$^+$CD163$^+$ cells in spleen cell suspensions from BALB/c mice after R-IRI and hUC-MSC therapy and compared to animals that had received PBS; data showing the percentage of positive cells within the F4/80+ population. (**D**) The percentage of F4/80$^+$CD86$^+$, F4/80$^+$CD163$^+$ and F4/80$^+$CD86$^+$CD163$^+$ cells in spleen cell suspensions from BALB/c mice after R-IRI and hUC-MSC therapy and compared to animals that had received PBS; data showing the percentage of positive cells within the F4/80$^+$ population which are represented as ratios. (E) Quantification of signal intensity of F4/80$^+$CD86$^+$ and F4/80$^+$CD163$^+$ cells in spleen cell suspensions from BALB/c mice after R-IRI and hUC-MSC therapy and compared to animals that received PBS. **n=16** hUC-MCS group, **n=13** PBS group and **n=7** injured group (no treatment). Significant differences between treatment groups in the F4/80+ population. ***p<0.0004. All data points represent individual animals and error bars represent mean ± SEM.

4.5.3. The effect of R-IRI on C57BL/6 alb mice

AKI was induced in 8 healthy C57BL/6 alb mice, and injury level post-R-IRI was compared against 7 sham-operated (control) mice (Figures 4.5 and Figure 4.6).

Renal IRI led to a very significant increase in the percentage of live F4/80$^+$ cells in the kidneys of C57BL/6 alb mice when compared to control animals (***p=0.0001), with a 0.6% chance of randomly observing an effect this large (or larger) in an experiment of this size (Figure 4.5A). Bilateral R-IRI also led to a higher percentage of F4/80$^+$CD86$^+$ cells in the kidneys of C57BL/6 alb mice when compared to control mice, though the differences were not statistically significant (Figure 4.5A). There were no differences in the percentage of F4/80$^+$CD163$^+$ and F4/80$^+$CD86$^+$CD163$^+$ cells in the kidneys of control and injured C57BL/6 alb mice (Figure 4.5A). While there was no difference in the level of F4/80+CD86+ antibody expression between sham-operated and injured C57BL/6 alb animals, there was a lower median fluorescence intensity in F4/80$^+$CD163$^+$ antibody expression in injured mice when compared to control animals, although this difference was not statistically significant (Figure 4.5B). When comparing macrophage levels within the F4/80$^+$ population in the kidney, there was a statistically significant higher percentage of F4/80$^+$CD86$^+$ cells in injured mice when

compared to control mice (**p=0.0066) (Figure 4.5C). A large percentage of F4/80+ kidney cells were negative for both CD86 and CD163 markers (84% - 88%), however, this population was smaller in injured C57BL/6 alb mice (Figure 4.5D).

Renal IRI resulted in a significantly lower percentage of positive live $F4/80^+$ cells in the spleens of C57BL/6 alb mice when compared to sham-operated animals (*p=0.0114) (Figure 4.6A). Bilateral R-IRI also led to a slightly lower percentage of $F4/80^+CD86^+$ cells in the spleens of C57BL/6 alb mice when compared to control mice, though these differences were not statistically significant (Figure 4.6A). There were no differences in the percentage of live F4/80+CD163+ and $F4/80^+CD86^+CD163^+$ cells following bilateral R-IRI (Figure 4.6A). There were also no differences in the levels of $F4/80^+CD86^+$ or $F4/80^+CD163^+$ antibody expression between injured and control C57BL/6 alb mice spleens (Figure 4.6B). When comparing macrophage levels within the $F4/80^+$ spleen population, bilateral R-IRI led to a higher percentage of $F4/80^+CD86^+$ cells but a lower percentage of $F4/80^+CD163^+$ and $F4/80^+CD86^+CD163^+$ cells; however, these differences were not statistically significant (Figure 4.6 C and D). Similar to the kidneys, the spleens had a population of $F4/80^+$ cells that were negative for both $CD86^-$ and $CD163^-$, however, this population was smaller in the spleen and it decreased in response to injury (58% - 62%) (Figure 4.6C).

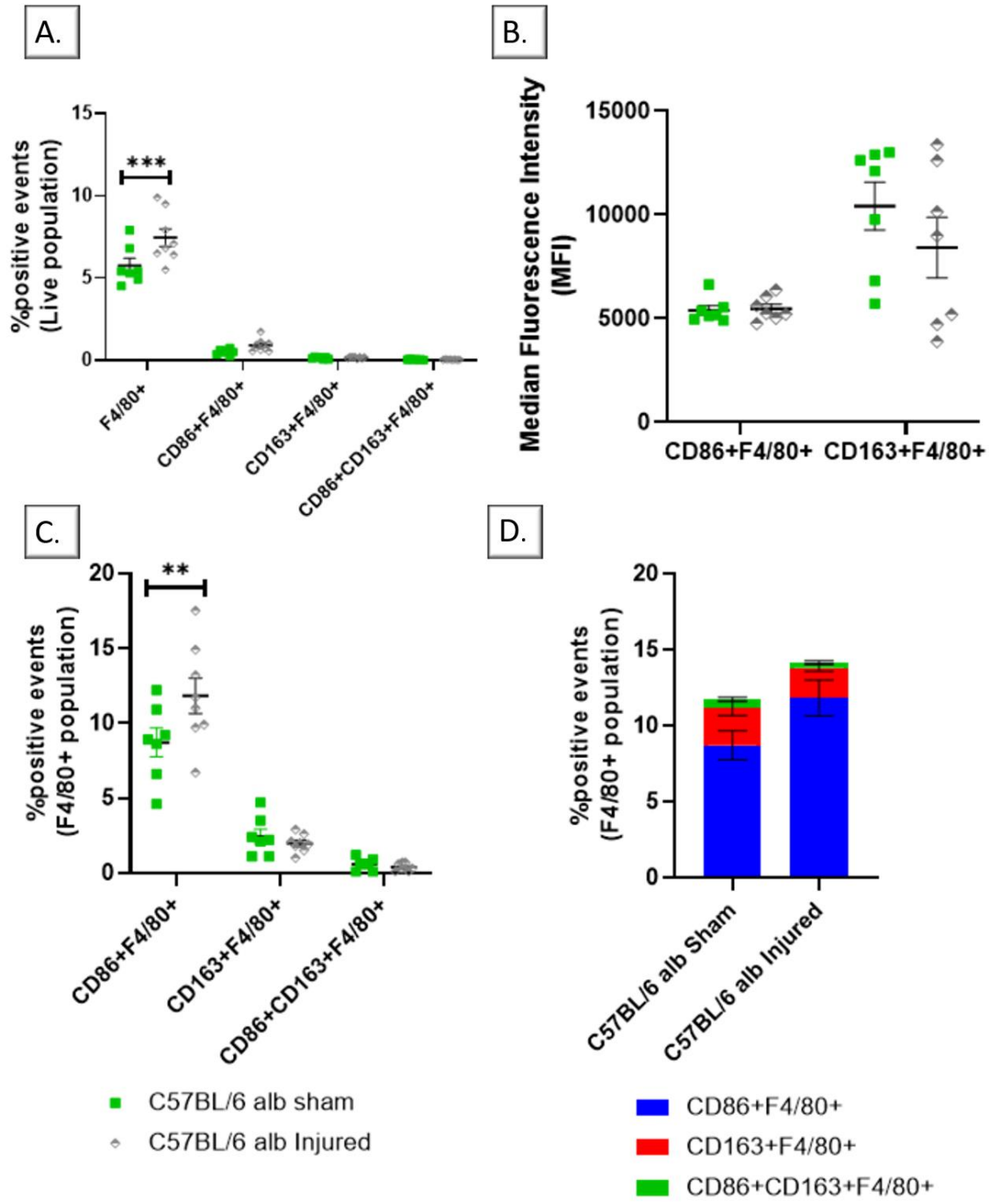

Figure 4.5: Changes in macrophage levels in C57BL/6 albino mice kidney cell suspensions following R-IRI. (A) The percentage of F4/80$^+$, F4/80$^+$CD86$^+$, F4/80$^+$CD163$^+$ and F4/80$^+$CD86$^+$CD163$^+$ cells in kidney cell suspensions from C57BL/6 alb mice after R-IRI and compared to sham-operated mice; data showing the percentage of positive cells within the Live population. **(B)** Quantification of signal intensity of F4/80$^+$CD86$^+$ and F4/80$^+$CD163$^+$ cells in kidney cell suspensions from C57BL/6 alb mice after R-IRI and compared to sham-operated mice. **(C)** The percentage of F4/80$^+$CD86$^+$, F4/80$^+$CD163$^+$ and F4/80$^+$CD86$^+$CD163$^+$ cells in kidney cell suspensions from C57BL/6 alb mice after R-IRI and compared to sham-operated mice; data showing the percentage of positive cells within the F4/80$^+$ population. **(D)** The percentage of F4/80$^+$CD86$^+$, F4/80$^+$CD163$^+$ and F4/80$^+$CD86$^+$CD163$^+$ cells in kidney cell

suspensions from BALB/c mice after R-IRI and compared to sham-operated mice; data showing the percentage of positive cells within the F4/80^{+} population which are represented as ratios. **n=8** injured group and **n=7** sham group. Significant differences between injured and sham-operated animals. **p=0.0066 and ***p=0.0001. All data points represent individual animals and error bars represent mean ± SEM.

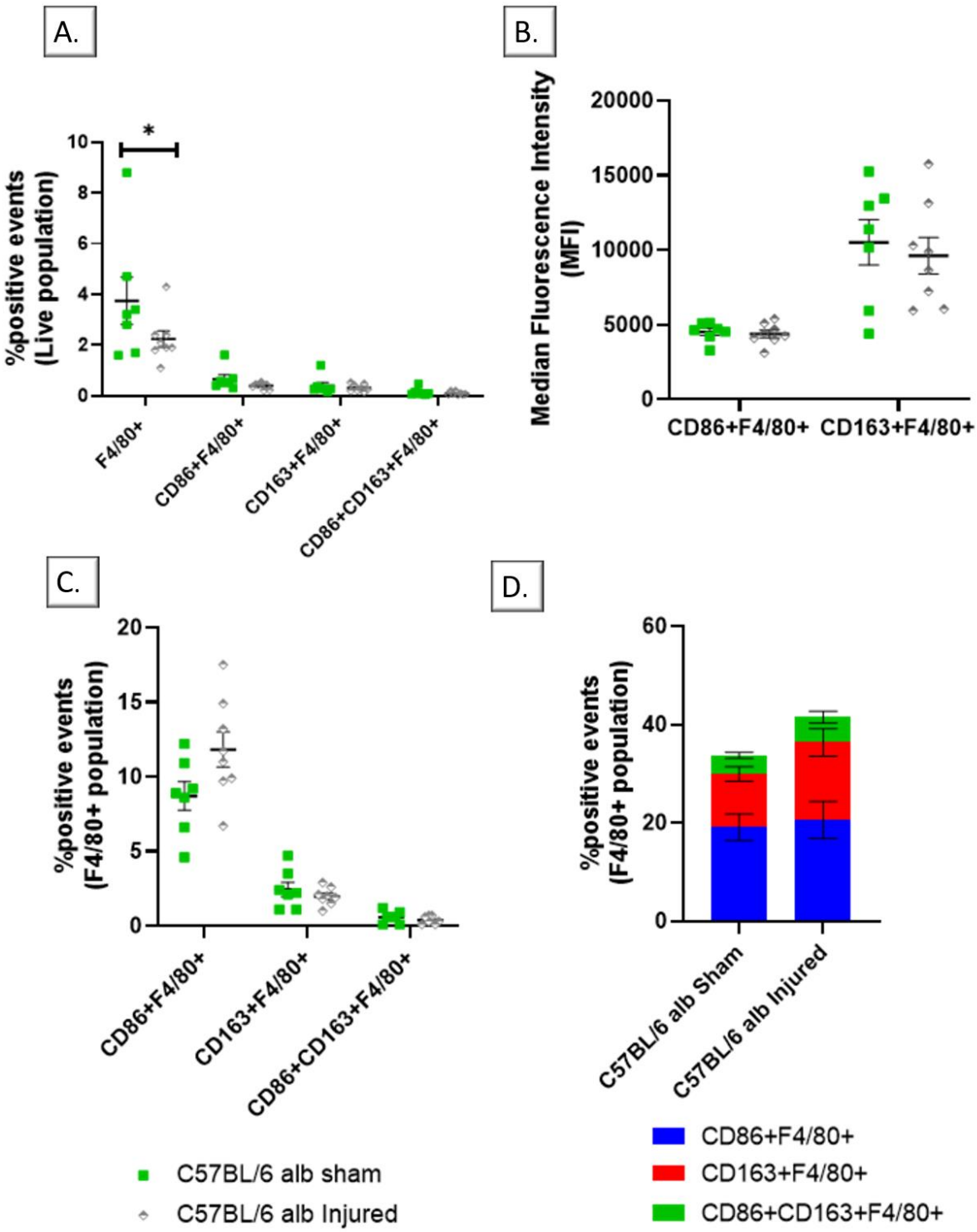

Figure 4.6: Changes in macrophage levels in C57BL/6 albino spleen cell suspensions following R-IRI. (A) The percentage of F4/80$^+$, F4/80$^+$CD86$^+$, F4/80$^+$CD163$^+$ and F4/80$^+$CD86$^+$CD163$^+$ cells in spleen cell suspensions from C57BL/6 alb mice after R-IRI and compared to sham-operated mice; data showing the percentage of positive cells within the Live population. **(B)** Quantification of signal intensity of F4/80$^+$CD86$^+$ and F4/80$^+$CD163$^+$ cells in spleen cell suspensions from C57BL/6 alb mice after R-IRI and compared to sham-operated mice. **(C)** The percentage of F4/80$^+$CD86$^+$, F4/80$^+$CD163$^+$ and F4/80$^+$CD86$^+$CD163$^+$ cells in spleen cell suspensions from C57BL/6 alb mice after R-IRI and compared to sham-operated

mice; data showing the percentage of positive cells within the F4/80$^+$ population. **(D)** The percentage of F4/80$^+$CD86$^+$, F4/80$^+$CD163$^+$ and F4/80$^+$CD86$^+$CD163$^+$ cells in spleen cell suspensions from BALB/c mice after R-IRI and compared to sham-operated mice; data showing the percentage of positive cells within the F4/80$^+$ population which are represented as ratios. **n=8** injured group and **n=7** sham group. Significant differences between injured and sham-operated animals. *p=0.0114. All data points represent individual animals and error bars represent mean ± SEM.

4.5.4. The effect of regenerative medicine therapies on C57BL/6 alb mice following R-IRI

Eleven male C57BL/6 alb mice received 250,000 hUC-MSC through IV injection immediately after bilateral R-IRI, whereas eleven C57BL/6 alb mice received 100µL PBS (Figure 4.7 and Figure 4.8).

There were no differences in the percentage of live F4/80$^+$, F4/80$^+$CD86$^+$, F4/80$^+$CD163$^+$ and F4/80$^+$CD86$^+$CD163$^+$ cells in the kidneys of injured mice between treatment and PBS groups (Figure 4.7A). However, when comparing macrophage levels between injured animals that received treatment (both hUC-MSC and PBS) and no injections (no hUC-MSC nor PBS, see section *4.5.3.* for more information), there was a significantly lower percentage of live F4/80$^+$ in the kidneys of C57BL/6 alb mice that had an injection (Figure 4.7B); this difference could be attributed to the high variability seen in the data as well as to the lower number of animals in the R-IRI no injection group. There were no differences when comparing macrophage levels within the F4/80$^+$ population in the kidney (Figure 4.7 C and D) between treatment groups in response to R-IRI. There were also no differences in the levels of F4/80$^+$CD86$^+$ or F4/80$^+$CD163$^+$ antibody expression between treatment groups following R-IRI (Figure 4.7E).

In conclusion, intravenous injection of hUC-MSC led to minimal effects on macrophage responses in the kidneys of injured C57BL/6 alb mice.

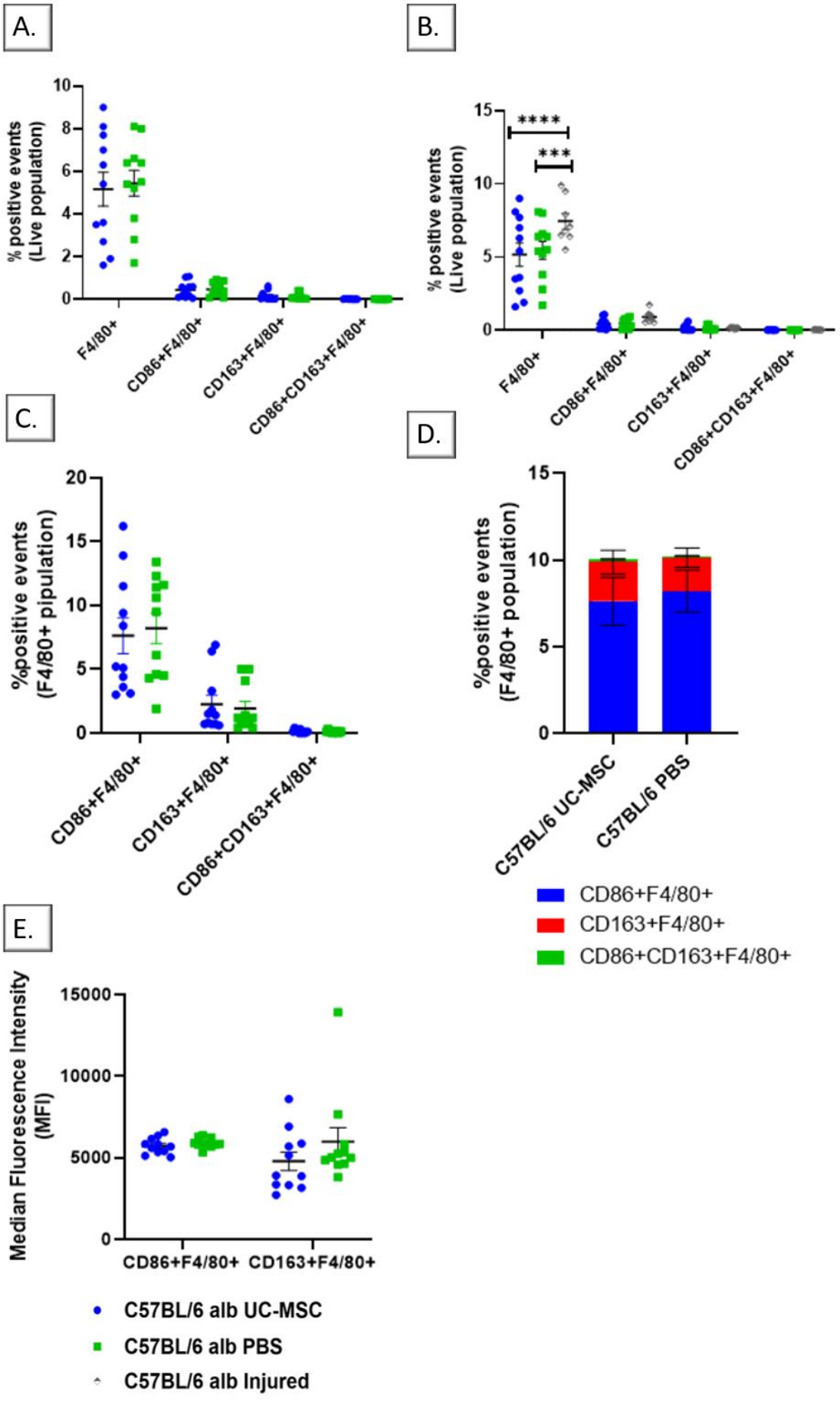
A.
% positive events (Live population)
F4/80+
CD86+F4/80+
CD163+F4/80+
CD86+CD163+F4/80+
B.
****
***
% positive events (Live population)
F4/80+
CD86+F4/80+
CD163+F4/80+
CD86+CD163+F4/80+
C.
%positive events (F4/80+ pipulation)
CD86+F4/80+
CD163+F4/80+
CD86+CD163+F4/80+
D.
%positive events (F4/80+ population)
C57BL/6 UC-MSC
C57BL/6 PBS
CD86+F4/80+
CD163+F4/80+
CD86+CD163+F4/80+
E.
Median Fluorescence Intensity (MFI)
CD86+F4/80+
CD163+F4/80+
C57BL/6 alb UC-MSC
C57BL/6 alb PBS
C57BL/6 alb Injured

Figure 4.7: Changes in macrophage levels in C57BL/6 albino mice kidneys cell suspensions following R-IRI and hUC-MSC treatment. (A) The percentage of F4/80$^+$, F4/80$^+$CD86$^+$, F4/80$^+$CD163$^+$ and F4/80$^+$CD86$^+$CD163$^+$ cells in kidney cell suspensions from C57BL/6 alb mice after R-IRI and hUC-MSC therapy and compared to animals that had received PBS; data showing the percentage of positive cells within the Live population. **(B)** The percentage of F4/80$^+$, F4/80$^+$CD86$^+$, F4/80$^+$CD163$^+$ and F4/80$^+$CD86$^+$CD163$^+$ cells in kidney cell suspensions from C57BL/6 alb mice after R-IRI and hUC-MSC therapy and compared to animals that had received either PBS or no treatment; data showing the percentage of positive cells within the Live population. **(C)** The percentage of F4/80$^+$CD86$^+$, F4/80$^+$CD163$^+$ and F4/80$^+$CD86$^+$CD163$^+$ cells in kidney cell suspensions from C57BL/6 alb mice after R-IRI and hUC-MSC therapy and compared to animals that had received PBS; data showing the percentage of positive cells within the F4/80+ population. **(D)** The percentage of F4/80$^+$CD86$^+$, F4/80$^+$CD163$^+$ and F4/80$^+$CD86$^+$CD163$^+$ cells in kidney cell suspensions from C57BL/6 alb mice after R-IRI and hUC-MSC therapy and compared to animals that had received PBS; data showing the percentage of positive cells within the F4/80$^+$ population which are represented as ratios. **(E)** Quantification of signal intensity of F F4/80$^+$CD86$^+$ and F4/80$^+$CD163$^+$ cells in kidney cell suspensions from C57BL/6 alb mice after R-IRI and hUC-MSC therapy and compared to animals that received PBS. **n=11** UC-MCS group, **n=11** PBS group and **n=8** injured group (no treatment). Significant differences between treatment groups in the F4/80$^+$ population. ***p=0.0004 and ****p<0.0001. All data points represent individual animals and error bars represent mean ± SEM.

Treatment with hUC-MSC led to a significantly lower percentage of live F4/80$^+$ cells in the spleens of injured C57BL/6 alb (*p= 0.0267), with a 3.7% chance of randomly observing an effect this large (or larger) in an experiment of this size (Figure 4.8A). When comparing macrophage levels between injured animals that received an injection and no injections (no hUC-MSC nor PBS, see section *4.5.3.* for more information), there were no differences between the PBS and no injection groups (Figure 4.8B). When comparing differences in macrophage levels within the F4/80$^+$ population in the spleen, hUC-MSC treatment led to a lower percentage of F4/80$^+$CD86$^+$ and F4/80$^+$CD86$^+$CD163$^+$ cells, and a slightly higher percentage of F4/80$^+$CD163$^+$ cells following bilateral R-IRI, however, these differences were not statistically significant (Figure 4.8 C and D). While there were no differences in the levels of F4/80$^+$CD86$^+$ antibody expression in the spleens of injured C57BL/6 alb mice, hUC-MSC treatment led to a reduced F4/80$^+$CD163$^+$ antibody expression when compared to PBS treatment (Figure 4.8E).

In conclusion, intravenous injection of hUC-MSC led to minimal effects on macrophage responses in the spleens of injured C57BL/6 alb mice.

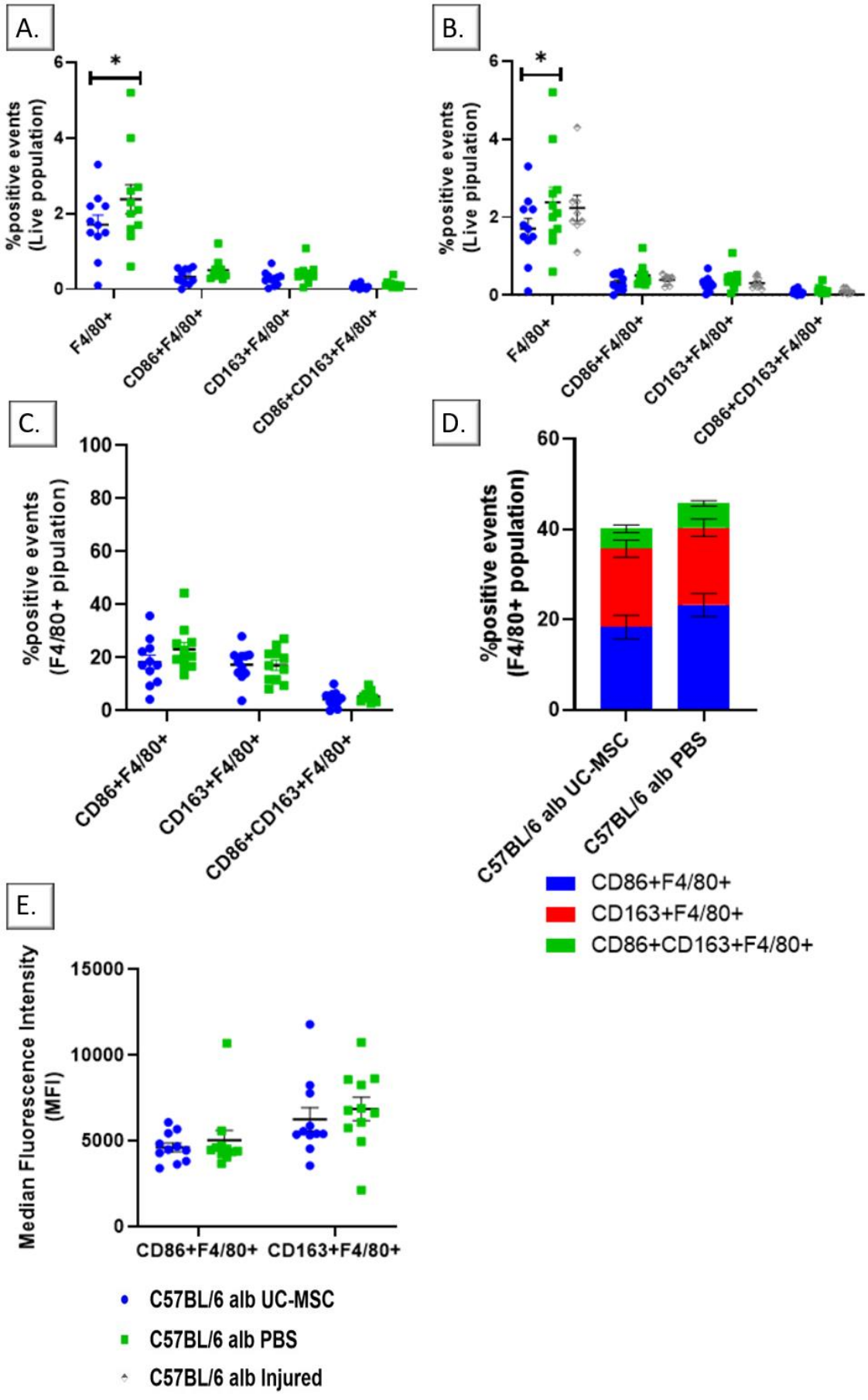
A.
%positive events (Live population)
F4/80+
CD86+F4/80+
CD163+F4/80+
CD86+CD163+F4/80+
B.
%positive events (Live pipulation)
C.
%positive events (F4/80+ pipulation)
D.
%positive events (F4/80+ population)
C57BL/6 alb UC-MSC
C57BL/6 alb PBS
CD86+F4/80+
CD163+F4/80+
CD86+CD163+F4/80+
E.
Median Fluorescence Intensity (MFI)
C57BL/6 alb UC-MSC
C57BL/6 alb PBS
C57BL/6 alb Injured

Figure 4.8: Changes in macrophage levels in C57BL/6 albino mice spleen cell suspensions following R-IRI and hUC-MSC treatment. (A) The percentage of F4/80$^+$, F4/80$^+$CD86$^+$, F4/80$^+$CD163$^+$ and F4/80$^+$CD86$^+$CD163$^+$ cells in spleen cell suspensions from BALB/c mice after R-IRI and hUC-MSC therapy and compared to animals that had received PBS; data showing the percentage of positive cells within the Live population. **(B)** The percentage of F4/80$^+$, F4/80$^+$CD86$^+$, F4/80$^+$CD163$^+$ and F4/80$^+$CD86$^+$CD163$^+$ cells in spleen cell suspensions from C57BL/6 alb mice after R-IRI and hUC-MSC therapy and compared to animals that had received either PBS or no treatment; data showing the percentage of positive cells within the Live population. **(C)** The percentage F4/80$^+$CD86$^+$, F4/80$^+$CD163$^+$ and F4/80$^+$CD86$^+$CD163$^+$ cells in spleen cell suspensions from C57BL/6 alb mice after R-IRI and hUC-MSC therapy and compared to animals that had received PBS; data showing the percentage of positive cells within the F4/80+ population. **(D)** The percentage of F4/80$^+$CD86$^+$, F4/80$^+$CD163$^+$ and F4/80$^+$CD86$^+$CD163$^+$ cells in spleen cell suspensions from C57BL/6 alb mice after R-IRI and hUC-MSC therapy and compared to animals that had received PBS; data showing the percentage of positive cells within the F4/80$^+$ population which are represented as ratios. **(E)** Quantification of signal intensity of F4/80$^+$CD86$^+$and F4/80$^+$CD163$^+$ cells in spleen cell suspensions from C57BL/6 alb mice after R-IRI and hUC-MSC therapy and compared to animals that received PBS. **n=11** UC-MCS group, **n=11** PBS group and **n=8** injured group (no treatment). Significant differences between treatment groups in the F4/80$^+$ population. *p<0.02. All data points represent individual animals and error bars represent mean ± SEM.

4.5.5. The effect of R-IRI on CD1 mice

AKI was induced in 7 healthy CD1 mice, and injury level post-R-IRI was compared against 7 sham-operated (control) mice (Figure 4.9 and Figure 4.10).

Renal IRI led to an significantly higher percentage of live F4/80$^+$ (****p<0.0001), F4/80$^+$CD86$^+$ (***p=0.0003) and F4/80$^+$CD163$^+$ (****p<0.0001) cells in the kidneys of CD1 mice when compared to control animals, with a 0.01% chance of randomly observing an effect this large (or larger) in an experiment of this size (Figure 4.9A). Bilateral R-IRI also led to a higher percentage of F4/80$^+$CD86$^+$CD163$^+$ cells in the kidneys of CD1 mice when compared to control mice, though the difference was not statistically significant (Figure 4.9A). Bilateral R-IRI led to a statistically significant lower median fluorescence intensity of F4/80$^+$CD86$^+$ antibody expression (*p=0.0344) and to a statistically significant higher median fluorescence intensity of F4/80$^+$CD163$^+$ antibody expression (*p= 0.0087) in injured mice when compared to control mice (Figure 4.9B). When comparing macrophage levels within the F4/80$^+$ population in the kidney, there was a statistically significant higher percentage of F4/80$^+$CD86$^+$ (**p<0.0001), F4/80$^+$CD163$^+$ (**p<0.0001) and F4/80$^+$CD86$^+$CD163$^+$ (**p=0.0096) cells in injured mice when compared to control mice (Figure 4.9 C and D). These differences in macrophage levels in response to R-IRI within the percentage of F4/80$^+$ in the

kidneys were considered extremely significant, with a 0.01% chance of randomly observing an effect this large (or larger) in an experiment of this size (Figure 4.9C). However, a large percentage of $F4/80^+$ kidney cells in sham-operated animals were negative for both $CD86^-$ and $CD163^-$ markers (approximately 38%) (Figure 4.9D).

Renal IRI resulted in a significantly lower percentage of positive live $F4/80^+$ cells in the spleens of CD1 mice when compared to control mice (*p=0.0411), however, the data showed a high degree of variability in the control group (Figure 4.10A). Bilateral R-IRI also led to a slightly lower percentage of $F4/80^+CD163^+$ cells in the spleens of CD1 mice when compared to control mice, though the differences were not statistically significant (Figure 4.10A). There were no differences in the percentage of live $F4/80^+CD86^+$ and $F4/80^+CD86^+CD163^+$ cells following bilateral R-IRI (Figure 4.10A). Bilateral R-IRI led to a higher median fluorescence intensity of $F4/80^+CD163^+$ antibody expression in the spleens of injured mice when compared to control mice, however, these differences were not statistically significant (Figure 4.10B). When comparing macrophage levels within the $F4/80^+$ spleen population, bilateral R-IRI led to an increase in the percentage of $F4/80^+CD86^+$, $F4/80^+CD163^+$ and $F4/80^+CD86^+CD163^+$ cells, however, these differences were not statistically significant (Figure 4.10 C and D). Similar to the kidneys, the spleen had a population of $F4/80^+$ cells that were negative for both $CD86^-$ and $CD163^-$ (15% - 22%), however, this population is smaller in CD1 sham mice (Figure 4.10C).

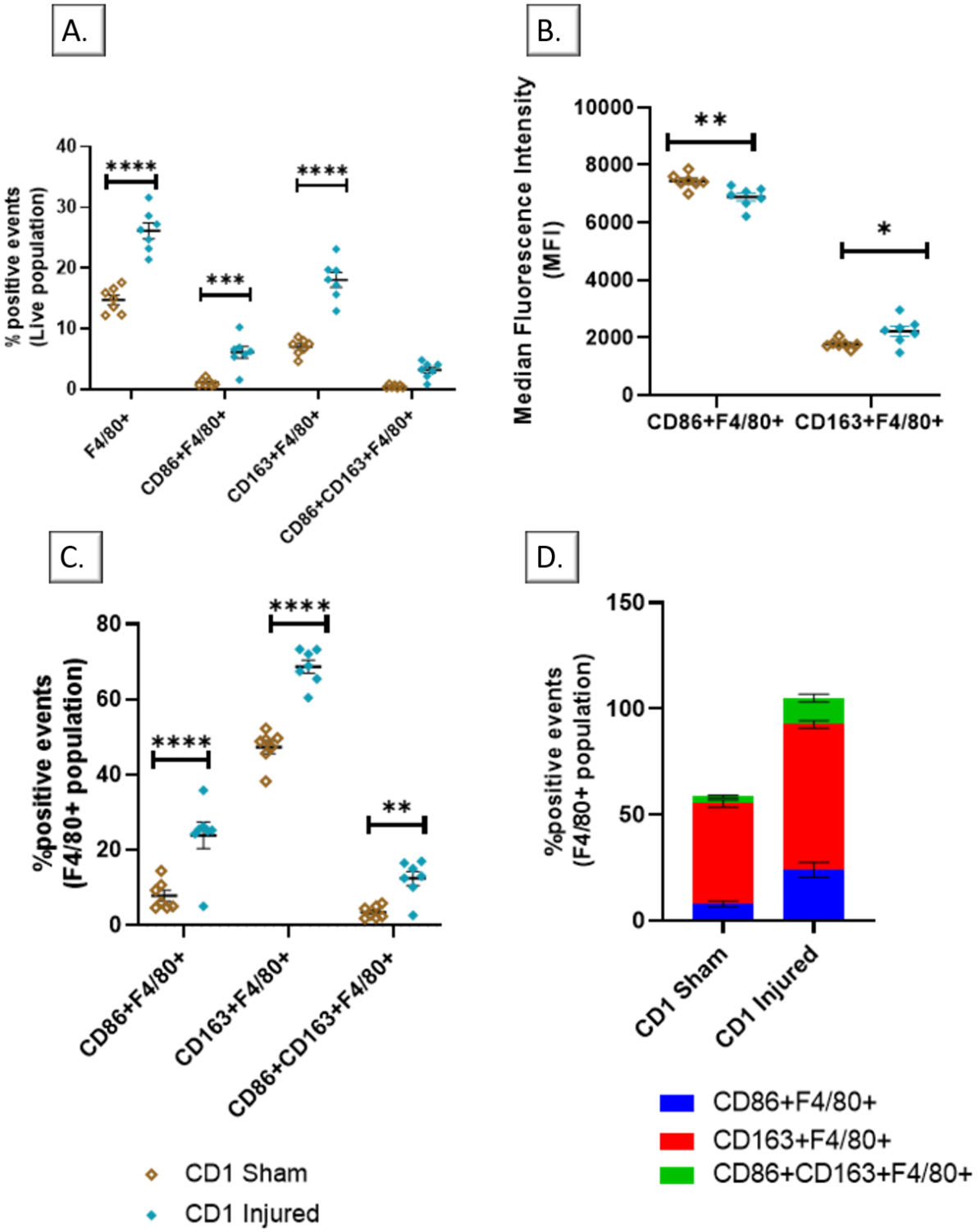

Figure 4.9: Changes in macrophage levels in CD1 mice kidney cell suspension following R-IRI. (A) The percentage of F4/80$^+$, F4/80$^+$CD86$^+$, F4/80$^+$CD163$^+$ and F4/80$^+$CD86$^+$CD163$^+$ cells in kidney cell suspensions from CD1 mice after R-IRI and compared to sham-operated mice; data showing the percentage of positive cells within the Live population. **(B)** Quantification of signal intensity of F4/80$^+$CD86$^+$ and F4/80$^+$CD163$^+$ cells in kidney cell suspensions from CD1mice after R-IRI and compared to sham-operated mice. **(C)** The percentage of F4/80$^+$CD86$^+$, F4/80$^+$CD163$^+$ and F4/80$^+$CD86$^+$CD163$^+$ cells in kidney cell suspensions from CD1 mice after R-IRI, and compared to sham-operated mice; data showing the percentage of

positive cells within the F4/80^{+} population. **(D)** The percentage of F4/80^{+}CD86^{+}, F4/80^{+}CD163^{+} and F4/80^{+}CD86^{+}CD163^{+} cells in kidney cell suspensions from CD1mice after R-IRI, and compared to sham-operated mice; data showing the percentage of positive cells within the F4/80^{+} population which are represented as ratios. **n=7** injured group and **n=7** sham group. Significant differences between injured and sham-operated animals. *p=0.0344, **p<0.0097, ***p=0.0003 and ****p<0.0001. All data points represent individual animals and error bars represent mean ± SEM.

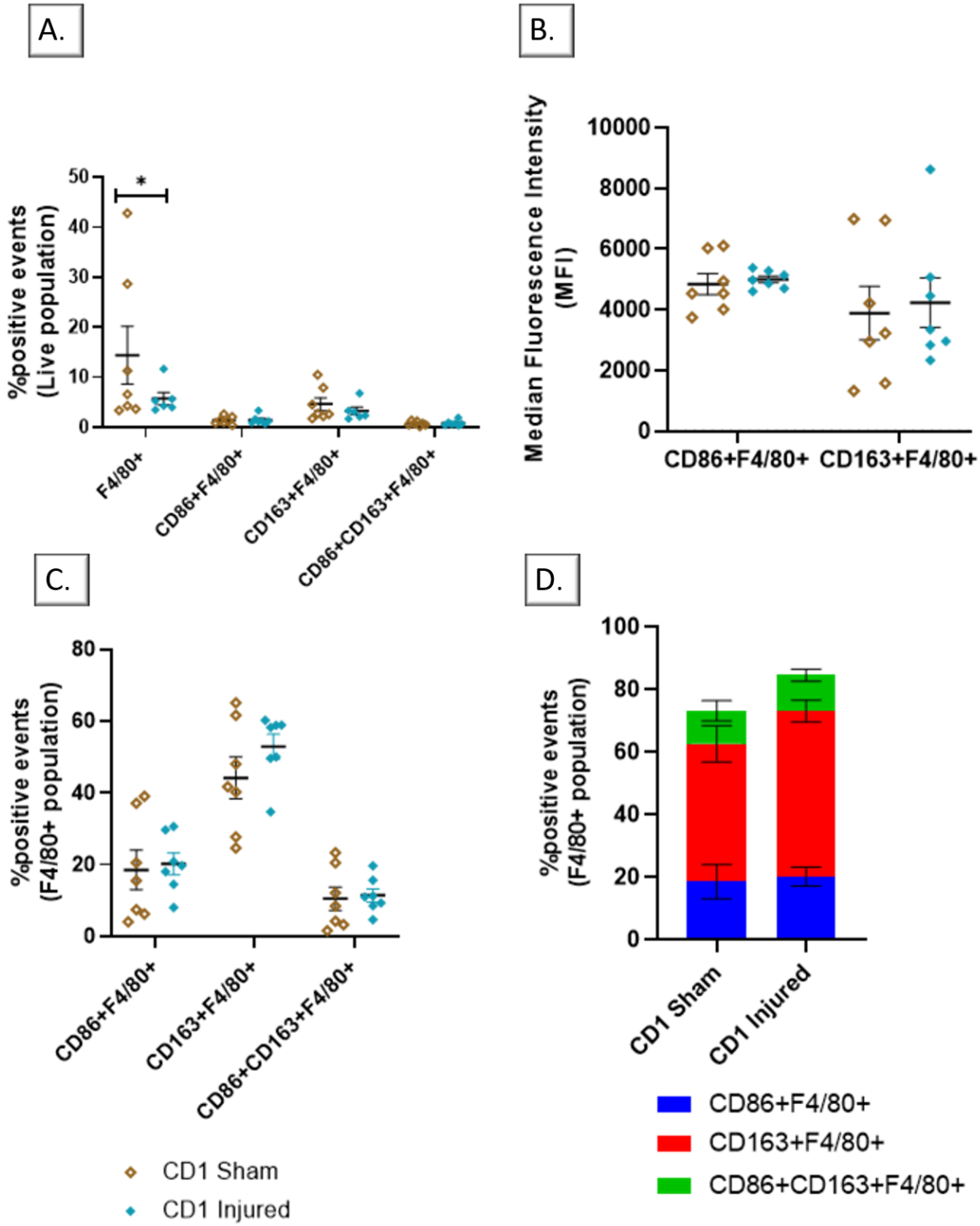

Figure 4.10: Changes in macrophage levels in CD1 albino spleen cell suspensions following R-IRI. (A) The percentage of F4/80$^+$, F4/80$^+$CD86$^+$, F4/80$^+$CD163$^+$ and F4/80$^+$CD86$^+$CD163$^+$ cells in spleen cell suspensions from CD1 mice after R-IRI, and compared to sham-operated mice; data showing the percentage of positive cells within the Live population. **(B)** Quantification of signal intensity of F4/80$^+$CD86$^+$ and F4/80$^+$CD163$^+$ cells in spleen cell suspensions from CD1 mice after R-IRI, and compared to sham-operated mice. **(C)** The percentage of F4/80$^+$CD86$^+$, F4/80$^+$CD163$^+$ and F4/80$^+$CD86$^+$CD163$^+$ cells in spleen cell suspensions from CD1 mice after R-IRI, and compared to sham-operated mice; data showing the percentage of positive cells within the F4/80$^+$ population. **(D)** The percentage of

F4/80^{+}CD86^{+}, F4/80^{+}CD163^{+} and F4/80^{+}CD86^{+}CD163^{+} cells in spleen cell suspensions from CD1 mice after R-IRI, and compared to sham-operated mice; data showing the percentage of positive cells within the F4/80^{+} population which are represented as ratios. **n=7** injured group and **n=7** sham group. Significant differences between injured and sham-operated animals. *p=0.0411. All data points represent individual animals and error bars represent mean ± SEM.

4.5.6. The effect of regenerative medicine therapies on CD1 mice following R-IRI

Fifteen male CD1 mice received 250,000 hUC-MSC through IV injection immediately after bilateral R-IRI, whereas thirteen CD1 mice received 100µL PBS (Figure 4.11 and Figure 4.12).

There were no differences in the percentage of F4/80^{+}, F4/80^{+}CD86^{+}, F4/80^{+}CD163^{+} and F4/80^{+}CD86^{+}CD163^{+} cells in the kidneys of injured mice between hUC-MSC and PBS treatment groups (Figure 4.11A). However, when comparing macrophage levels between injured animals that received an injection (both hUC-MSC and PBS) and no injections (no hUC-MSC nor PBS, see section *4.5.5* for more information), there was a lower percentage of live F4/80^{+} and F4/80^{+}CD163^{+} cells in the kidneys mice that had received an injection, however, these differences were not significant (Figure 4.11B); this difference could be attributed to the high variability seen in the data. When comparing differences in macrophage levels within the F4/80^{+} population in the kidney, there are no differences in the percentage of F4/80^{+}CD86^{+}, F4/80^{+}CD163^{+} and F4/80^{+}CD86^{+}CD163^{+} cells between treatment groups following bilateral R-IRI (Figure 4.11 C and D). There were no differences in the levels of F4/80^{+}CD163^{+} antibody expression between treatment groups following R-IRI, however, hUC-MSC treatment led to a higher the median fluorescence intensity of F4/80^{+}CD86^{+} antibody expression (Figure 4.11E).

In conclusion, intravenous injection of hUC-MSC led to minimal effects on macrophage responses in the kidneys of injured CD1 mice, and these differences were not statistically significant.

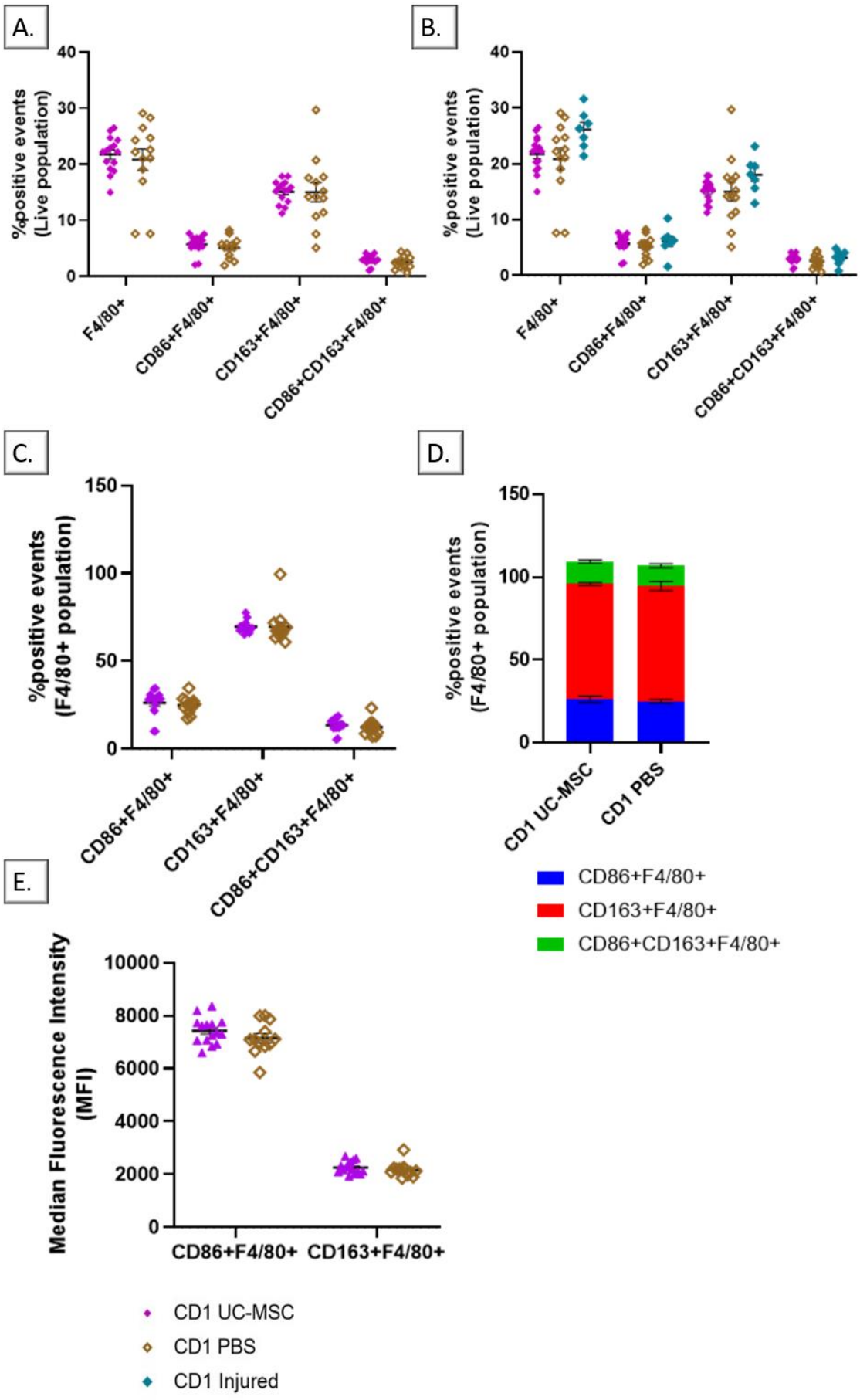
A.
%positive events (Live population)
40
30
20
10
0
F4/80+
CD86+F4/80+
CD163+F4/80+
CD86+CD163+F4/80+
B.
%positive events (Live population)
40
30
20
10
0
F4/80+
CD86+F4/80+
CD163+F4/80+
CD86+CD163+F4/80+
C.
%positive events (F4/80+ population)
150
100
50
0
CD86+F4/80+
CD163+F4/80+
CD86+CD163+F4/80+
D.
%positive events (F4/80+ population)
150
100
50
0
CD1 UC-MSC
CD1 PBS
CD86+F4/80+
CD163+F4/80+
CD86+CD163+F4/80+
E.
Median Fluorescence Intensity (MFI)
10000
8000
6000
4000
2000
0
CD86+F4/80+
CD163+F4/80+
CD1 UC-MSC
CD1 PBS
CD1 Injured

Figure 4.11: Changes in macrophage levels in CD1 mice kidney cell suspensions following R-IRI and hUC-MSC treatment. (A) The percentage of F4/80^{+}, F4/80^{+}CD86^{+}, F4/80^{+}CD163^{+} and F4/80^{+}CD86^{+}CD163^{+} cells in kidney cell suspensions from CD1 mice after R-IRI and hUC-MSC therapy, and compared to animals that had received PBS; data showing the percentage of positive cells within the Live population. **(B)** The percentage of F4/80^{+}, F4/80^{+}CD86^{+}, F4/80^{+}CD163^{+} and F4/80^{+}CD86^{+}CD163^{+} cells in kidney cell suspensions from CD1mice after R-IRI and hUC-MSC therapy, and compared to animals that had received either PBS or no treatment; data showing the percentage of positive cells within the Live population. **(C)** The percentage of F4/80^{+}CD86^{+}, F4/80^{+}CD163^{+} and F4/80^{+}CD86^{+}CD163^{+} cells in kidney cell suspensions from CD1 mice after R-IRI and hUC-MSC therapy, and compared to animals that had received PBS; data showing the percentage of positive cells within the F4/80^{+} population. **(D)** The percentage of F4/80^{+}CD86^{+}, F4/80^{+}CD163^{+} and F4/80^{+}CD86^{+}CD163^{+} cells in kidney cell suspensions from CD1mice after R-IRI and hUC-MSC therapy, and compared to animals that had received PBS; data showing the percentage of positive cells within the F4/80^{+} population which are represented as ratios. **(E)** Quantification of signal intensity of F4/80^{+}CD86^{+} and F4/80^{+}CD163^{+} cells in kidney cell suspensions from CD1mice after R-IRI and hUC-MSC therapy, and compared to animals that received PBS. **n=15** UC-MCS group, **n=13** PBS group and n=7 injured group (no treatment). All data points represent individual animals and error bars represent mean ± SEM.

Treatment with human UC-MSC led to a very significant lower percentage of live F4/80+ cells in the spleens injured CD1 mice (*p=0.0497), with a 0.59% chance of randomly observing an effect this large (or larger) in an experiment of this size (Figure 4.12A). An injection of hUC-MSC also led to a decrease in the percentage of F4/80^{+}CD86^{+}, F4/80^{+}CD163^{+} and F4/80^{+}CD86^{+}CD163^{+} cells in the spleens of injured mice, however, these differences were not statistically significant when compared to the PBS group. When comparing macrophage levels between injured animals that received PBS treatment and no injection (no hUC-MSC nor PBS, see section *4.5.5.* for more information), there was an increase in the percentage of live F4/80^{+} in the spleens of CD1 mice within the PBS group, however, the difference was not statistically significant (Figure 4.12B)); this difference could be attributed to the high variability seen in the data. When comparing differences in macrophage levels within the F4/80^{+} population in the spleen, hUC-MSC treatment led to a statistically significant higher percentage of F4/80^{+}CD86^{+} (*p=0.0153) and F4/80^{+}CD163^{+} (*p=0.0238*) cells, with a 0.03% chance of randomly observing an effect this large (or larger) in an experiment of this size. Treatment with human UC-MSC also led to a higher percentage of F4/80^{+}CD163^{+} cells following bilateral R-IRI, however, this change was not statistically significant (Figure 4.12 C and D). While there were no differences in the levels of F4/80^{+}CD86^{+} antibody expression in

the spleens of injured CD1 mice, hUC-MSC treatment led to an increase in $F4/80^{+}CD163^{+}$ antibody expression when compared to PBS treatment (Figure 4.12E).

In conclusion, intravenous injection of hUC-MSC led to minimal effects on macrophage responses in the spleens of injured CD1 mice.

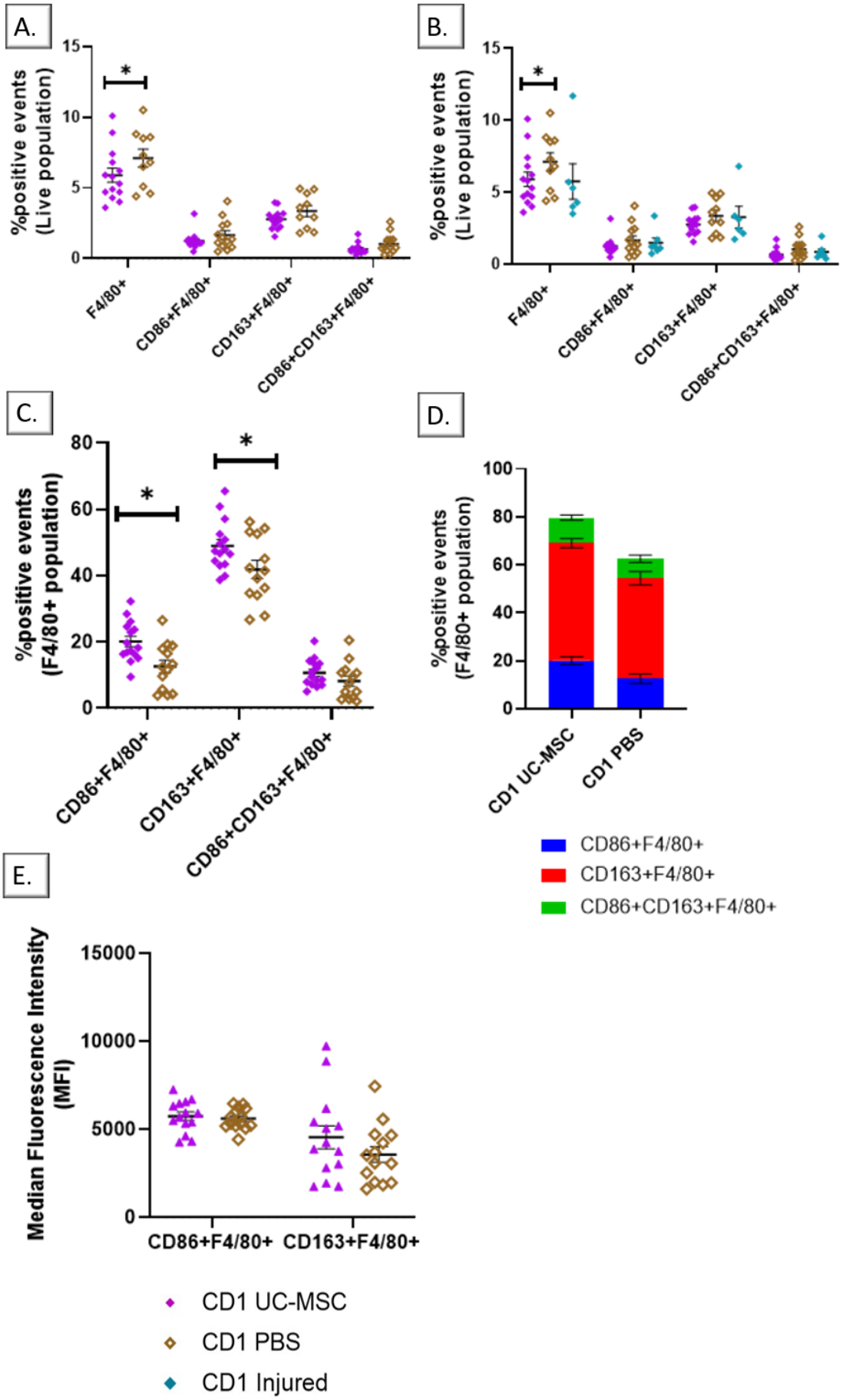
A.
%positive events (Live population)
15
10
5
0
*
F4/80+
CD86+F4/80+
CD163+F4/80+
CD86+CD163+F4/80+
B.
%positive events (Live population)
15
10
5
0
*
F4/80+
CD86+F4/80+
CD163+F4/80+
CD86+CD163+F4/80+
C.
%positive events (F4/80+ population)
80
60
40
20
0
*
*
CD86+F4/80+
CD163+F4/80+
CD86+CD163+F4/80+
D.
%positive events (F4/80+ population)
100
80
60
40
20
0
CD1 UC-MSC
CD1 PBS
CD86+F4/80+
CD163+F4/80+
CD86+CD163+F4/80+
E.
Median Fluorescence Intensity (MFI)
15000
10000
5000
0
CD86+F4/80+
CD163+F4/80+
CD1 UC-MSC
CD1 PBS
CD1 Injured

Figure 4.12: Changes in macrophage levels in CD1 mice spleen cell suspensions following R-IRI and hUC-MSC treatment. (A) The percentage of F4/80$^+$, F4/80$^+$CD86$^+$, F4/80$^+$CD163$^+$ and F4/80$^+$CD86$^+$CD163$^+$ cells in spleen cell suspensions from CD1 mice after R-IRI and hUC-MSC therapy, and compared to animals that had received PBS; data showing the percentage of positive cells within the Live population. **(B)** The percentage of F4/80$^+$, F4/80$^+$CD86$^+$, F4/80$^+$CD163$^+$ and F4/80$^+$CD86$^+$CD163$^+$ cells in spleen cell suspensions from CD1 mice after R-IRI and hUC-MSC therapy, and compared to animals that had received either PBS or no treatment; data showing the percentage of positive cells within the Live population. **(C)** The percentage of F4/80$^+$CD86$^+$, F4/80$^+$CD163$^+$ and F4/80$^+$CD86$^+$CD163$^+$ cells in spleen cell suspensions from CD1 mice after R-IRI and hUC-MSC therapy, and compared to animals that had received PBS; data showing the percentage of positive cells within the F4/80$^+$ population. **(D)** The percentage of F4/80$^+$CD86$^+$, F4/80$^+$CD163$^+$ and F4/80$^+$CD86$^+$CD163$^+$ cells in spleen cell suspensions from CD1 mice after R-IRI and hUC-MSC therapy, and compared to animals that had received PBS; data showing the percentage of positive cells within the F4/80+ population which are represented as ratios. **(E)** Quantification of signal intensity of F4/80$^+$CD86$^+$and F4/80$^+$CD163$^+$ cells in spleen cell suspensions from CD1 mice after R-IRI and hUC-MSC therapy, and compared to animals that received PBS. **n=15** UC-MCS group, **n=13** PBS group and n=7 injured group (no treatment). Significant differences between treatment groups in the F4/80$^+$ population. *p<0.05. All data points represent individual animals and error bars represent mean ± SEM.

4.5.7. Comparing the effect of R-IRI on different mouse strains

Comparing changes in macrophage levels in kidney cell suspensions following sham procedure in three different mouse strains indicated that the animals responded differently to the procedure (Figure 4.13). Statistical analysis showed that the variable 'strain' had an extremely significant effect on macrophage levels following sham-operated procedure, with a 0.01% chance of randomly observing an effect this large (or larger) in an experiment of this size. CD1 mice had significantly higher levels of F4/80$^+$ and F4/80$^+$CD163$^+$ cells in their injured kidneys when compared to both BALB/c and C57BL/6 alb mice (****p<0.0001) (Figure 4.13A). Furthermore, CD1 mice also had a larger population of F4/80$^+$CD86$^+$ and F4/80$^+$CD86$^+$CD163$^+$ cells, however, these differences were not statistically significant (Figure 4.13A). There were also significant differences between C57BL/6 alb and BALB/c mice: C57BL/6 alb mice showed a significantly lower percentage of F4/80$^+$ cells (***p=0.0009) (Figure 4.13A).

Comparisons in median fluorescence intensity and antibody expression between the three strains also showed extremely significant differences (Figure 4.13B). CD1 mice had significantly higher levels in F4/80$^+$CD86$^+$ antibody expression when compared to C57BL/6 alb mice (*p=0.0366), however, there were no differences between CD1 mice and BALB/c mice.

On the other hand, CD1 mice showed significantly lower levels in $F4/80^{+}CD163^{+}$ antibody expression when compared to both BALB/c and C57BL/6 alb mice (****$p<0.0001$). There were also significant differences in median fluorescence intensity between BALB/c and C57BL/6 alb mice: C57BL/6 alb mice displayed significantly higher levels in $F4/80^{+}CD163^{+}$ antibody expression (**$p=0.0033$).

When comparing differences in macrophage levels within the $F4/80^{+}$ population in the kidney after sham-operated procedure, there were no differences in the percentage of $F4/80^{+}CD86^{+}$ and $F4/80^{+}CD86^{+}CD163^{+}$ cells between the three strains. However, CD1 mice displayed significantly higher levels in the percentage of $F4/80^{+}CD163^{+}$ cells when compared to the other two strains (****$p<0.0001$) (Figure 4.13 C and D).

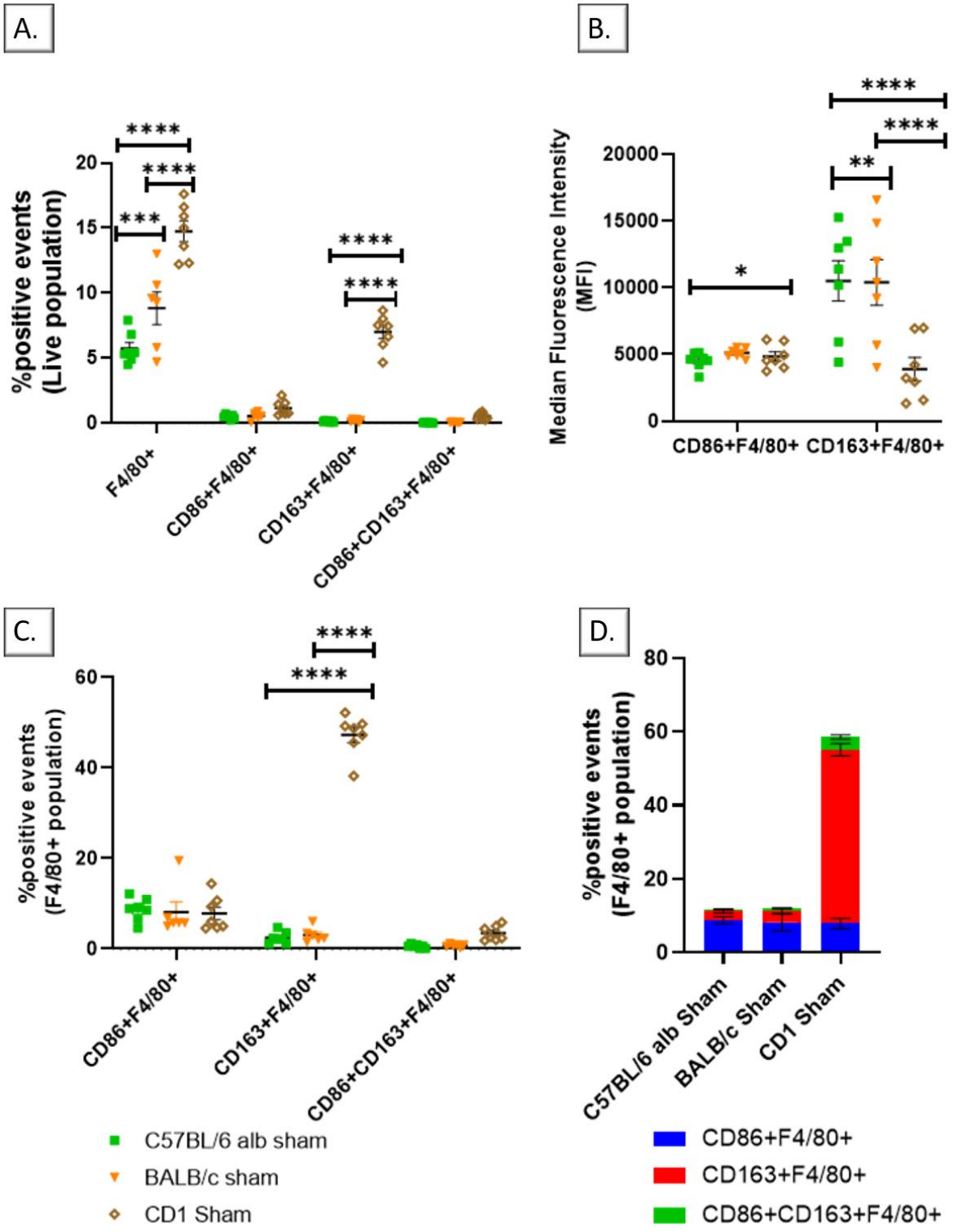

Figure 4.13: Comparing changes in macrophage levels in kidney cell suspensions of BALB/c, C57BL/6 albino and CD1 mice following sham procedure. (A) The percentage of F4/80$^+$, F4/80$^+$CD86$^+$, F4/80$^+$CD163$^+$ and F4/80$^+$CD86$^+$CD163$^+$ cells in kidney cell suspensions from animals that underwent sham-operated procedure, in three different mouse strains; data showing the percentage of positive cells within the Live population. **(B)** Quantification of signal intensity of F4/80$^+$CD86$^+$ and F4/80$^+$CD163$^+$ cells in kidney cell suspensions from animals that underwent sham-operated procedure, in three different mouse strains. **(C)** The

percentage of F4/80$^+$, F4/80$^+$CD86$^+$, F4/80$^+$CD163$^+$ and F4/80$^+$CD86$^+$CD163$^+$ cells in kidney cell suspensions from animals that underwent sham-operated procedure, in three different mouse strains; data showing the percentage of positive cells within the F4/80$^+$ population. **(D)** The percentage of F4/80$^+$, F4/80$^+$CD86$^+$, F4/80$^+$CD163$^+$ and F4/80$^+$CD86$^+$CD163$^+$ cells in kidney cell suspensions from animals that underwent sham-operated procedure, in three different mouse strains; data showing the percentage of positive cells within the F4/80$^+$ population which are represented as ratios. Significant differences between strains in response to sham-operated procedure. *p=0.0366, **p=0.0033, ***p=0.0009 and ****p<0.0001.

Adding on the previous analysis showed above (Figure 4.13) where we have demonstrated a strain-dependent response to the sham-operated procedure, we proceeded to assess the impact of bilateral R-IRI on macrophage levels in kidneys (Figure 4.14).

Comparing changes in macrophage levels in kidney cell suspensions following bilateral R-IRI in three different mouse strains indicates that the animals respond differently to the procedure (Figure 4.14). Statistical analysis shows that the variable 'strain' has an extremely significant effect on macrophage levels following bilateral R-IRI, with a 0.01% chance of randomly observing an effect this large (or larger) in an experiment of this size. CD1 mice showed a significantly higher percentage of F4/80$^+$, F4/80$^+$CD86$^+$ and F4/80$^+$CD163$^+$ cells (****p<0.0001) when compared to both BALB/c and C57BL/6 alb mice (Figure 4.14A). Furthermore, CD1 mice also showed a higher percentage in F4/80$^+$CD86$^+$CD163$^+$ cells, however, these differences were not statistically significant (Figure 4.14A). There were no differences in macrophage levels between C57BL/6 alb and BALB/c mice in response to renal IRI (Figure 4.14A).

Comparisons in median fluorescence intensity and antibody expression between the three strains also showed extremely significant differences. CD1 mice showed significantly lower levels in F4/80$^+$CD163$^+$ antibody expression when compared to both BALB/c (**p=0.0034) and C57BL/6 alb mice (****p<0.0001) (Figure 4.14B). There were also significant differences in median fluorescence intensity between BALB/c and C57BL/6 alb mice: C57BL/6 alb mice displayed significantly higher levels in F4/80$^+$CD163$^+$ antibody expression (**p=0.0062) (Figure 4.14B). On the other hand, CD1 mice showed higher levels in CD86+F4/80+ antibody expression when compared to both C57BL/6 alb and BALB/c mice, however, these differences were not statistically significant (Figure 4.14B). C57BL/6 alb mice

showed lower levels in CD86+F4/80+ antibody expression in response to R-IRI when compared to BALB/c mice, however, these differences were not statistically significant.

When comparing differences in macrophage levels within the F4/80+ population in the kidney following bilateral R-IRI, there were significantly higher levels of $F4/80^{+}CD86^{+}$, $F4/80^{+}CD163^{+}$ and $F4/80^{+}CD86^{+}CD163^{+}$ cells in CD1 mice when compared to the other two strains (**p=0.0013; ***p=0.0002; ****p<0.0001) (Figure 4.14 C and D).

When comparing changes in macrophage levels in the kidneys between the three strains, we detected a similar pattern between C57BL/6 alb (Figure 4.5A) and CD1 (Figure 4.9A) mice in response to bilateral renal IRI; both strains showed a higher percentage in the levels of $F4/80^{+}$ and $F4/80^{+}CD86^{+}$ cells whereas BALB/c mice showed the opposite pattern, i.e., a decrease in the $F4/80^{+}$ and $F4/80^{+}CD86^{+}$ cells (Figure 4.1A). Both BALB/c (Figure 4.1B) and C57BL/6 alb (Figure 4.5B) showed an increase in the levels of in $F4/80^{+}CD163^{+}$ antibody expression in kidney cell lysates while CD1 mice (Figure 4.9B) presented contrasting result in response to renal IRI. However, when comparing changes in macrophage levels within the $F4/80^{+}$ population in the kidney, all three strains showed a similar pattern of response characterised by an increase in the levels of $F4/80^{+}CD86^{+}$ cells following bilateral R-IRI (Figure 4.1C, Figure 4.5C and Figure 4.9C). In addition, in all three strains, R-IRI led to a decrease in the percentage of $F4/80^{+}$ that are negative for both $CD86^{-}$ and $CD163^{-}$ in the kidneys of injured mice (Figure 4.1D, Figure 4.5D and Figure 4.9D).

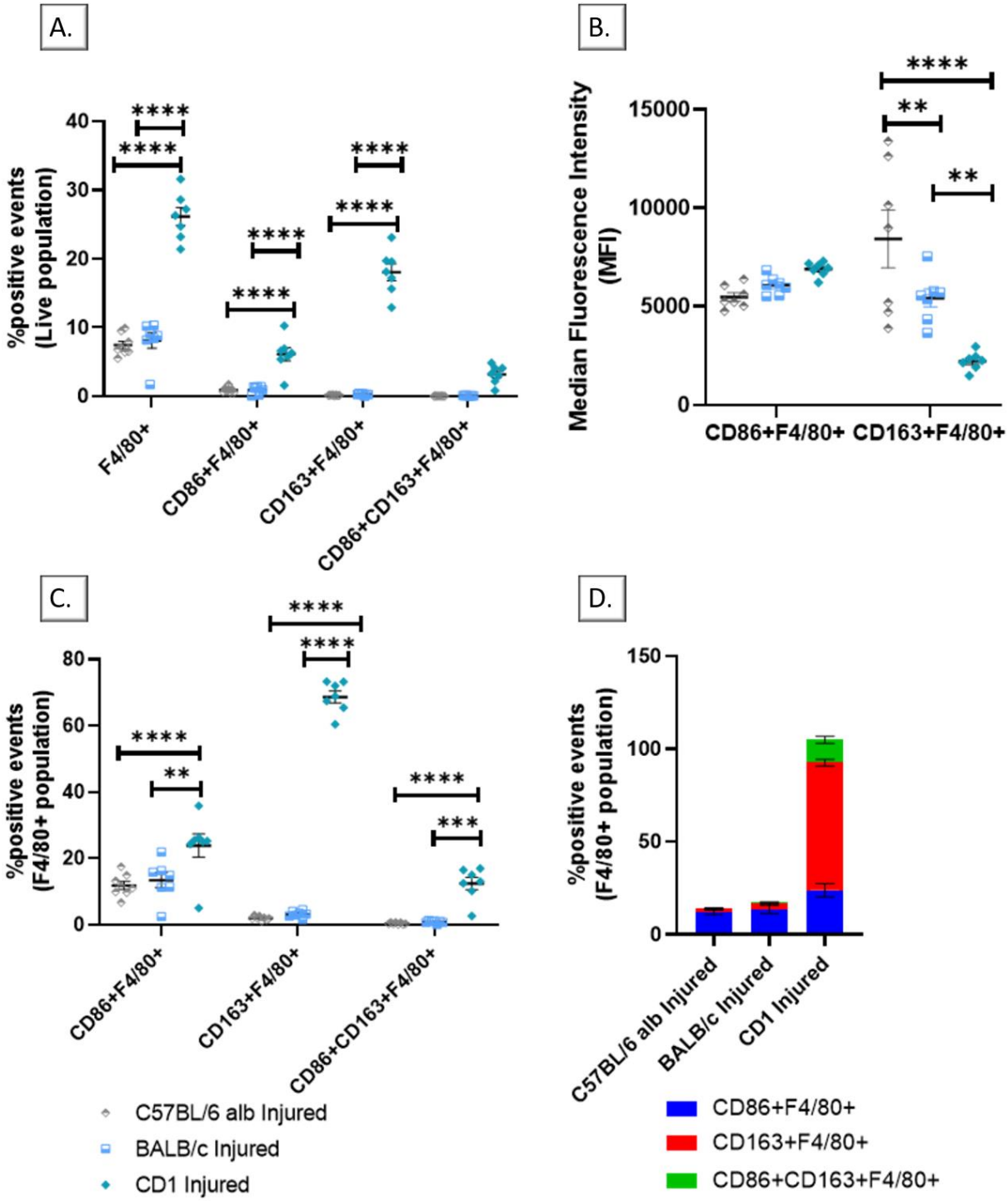

Figure 4.14: Comparing changes in macrophage levels in kidney cell suspensions of BALB/c, C57BL/6 albino and CD1 mice following bilateral R-IRI. (A) The percentage of F4/80$^+$, F4/80$^+$CD86$^+$, F4/80$^+$CD163$^+$ and F4/80$^+$CD86$^+$CD163$^+$ cells in kidney cell suspensions after bilateral R-IRI, in three different mouse strains; data showing the percentage of positive cells within the Live population. **(B)** Quantification of signal intensity of F4/80$^+$CD86$^+$ and F4/80$^+$CD163$^+$ cells in kidney cell suspensions after bilateral R-IRI, in three different mouse strains. **(C)** The percentage of F4/80$^+$, F4/80$^+$CD86$^+$, F4/80$^+$CD163$^+$ and F4/80$^+$CD86$^+$CD163$^+$ cells in kidney cell suspensions after bilateral R-IRI, in three different mouse strains; data showing the percentage of positive cells within the F4/80$^+$ population. **(D)** The percentage of

F4/80$^+$, F4/80$^+$CD86$^+$, F4/80$^+$CD163$^+$ and F4/80$^+$CD86$^+$CD163$^+$ cells in kidney cell suspensions after bilateral R-IRI, in three different mouse strains; data showing the percentage of positive cells within the F4/80$^+$ population which are represented as ratios. Significant differences between strains in response to bilateral R-IRI. **p<0.06, ***p=0.0002 and ****p<0.0001.

Comparing changes in macrophage levels in spleen cell suspensions following sham procedure in three different mouse strains indicates that the animals respond differently to the procedure (Figure 4.15). Statistical analysis shows that strain has a very significant effect on macrophage levels following sham-operated procedure, with a 0.21% chance of randomly observing an effect this large (or larger) in an experiment of this size. CD1 mice showed a significant increase in percentage of F4/80$^+$ cells when compared to both BALB/c (**p=0.0032) and C57BL/6 alb mice (**p=0.0035) (Figure 4.15A). Furthermore, CD1 mice also showed an increase in F4/80$^+$CD86$^+$, F4/80$^+$CD163$^+$ and F4/80$^+$CD86$^+$CD163$^+$ cells, however, these differences were not statistically significant (Figure 4.15A). There were also differences between C57BL/6 alb and BALB/c mice: C57BL/6 alb mice showed a decrease in the percentage of F4/80$^+$CD86$^+$ and F4/80$^+$CD163$^+$ cells, and an increase in the percentage F4/80$^+$CD86$^+$CD163$^+$ cells, however, these differences were not statistically significant (Figure 4.15A). Comparisons in median fluorescence intensity and antibody expression also showed differences between the three strains (Figure 4.15B). CD1 mice showed a significant decrease in F4/80$^+$CD163$^+$ antibody expression when compared to both BALB/c (***p=0.0002) and C57BL/6 alb mice (***p=0.0001). In contrast, BALB/c mice showed an increase in F4/80$^+$CD86$^+$ antibody expression when compared to both CD1 and C57BL/6 alb mice, however, these differences were not statistically significant. There were also significant differences in median fluorescence intensity between BALB/c and C57BL/6 alb mice: C57BL/6 alb mice displayed a significant increase in F4/80+CD163+ antibody expression (**p=0.0033) (Figure 4.15B). When comparing differences in macrophage levels within the F4/80+ population in the spleen after sham-operated procedure, BALB/c mice showed an increase in the percentage of F4/80$^+$CD86$^+$ and F4/80+CD86+CD163+ cells when compared to both C57BL/6 alb and CD1 mice, however these differences were not statistically significant. In contrast, C56BL/6 alb mice showed the lowest percentage in F4/80$^+$CD86$^+$, F4/80$^+$CD163$^+$ and F4/80$^+$CD86$^+$CD163$^+$ positive cells. (Figure 4.15 C and D). In addition, CD1 mice showed a significant increase in

F4/80⁺CD163⁺ cells when compared BALB/c (*p=0.0247) and C57BL/6 alb mice (****p<0.0001) (Figure 4.15 C and D).

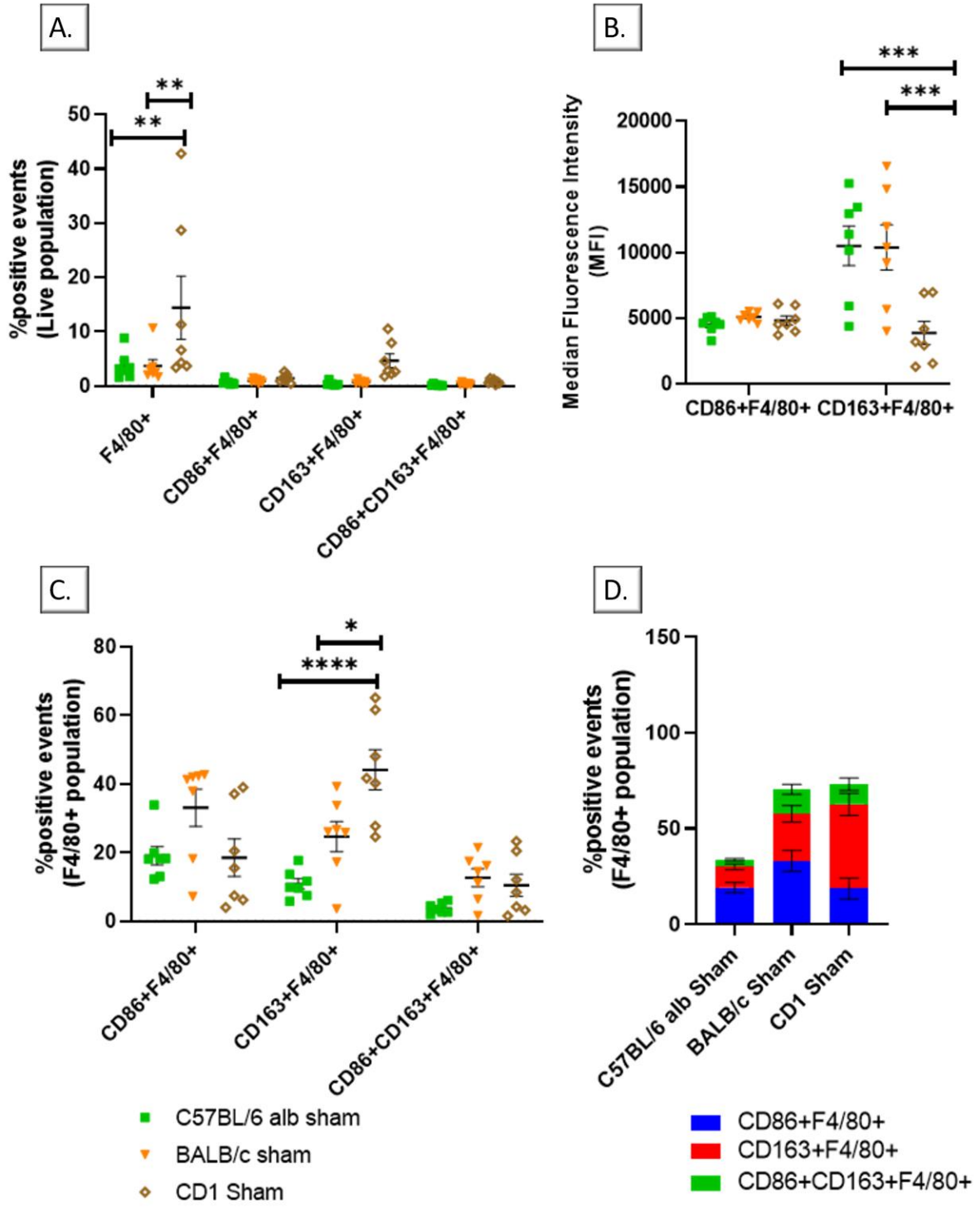

Figure 4.15: Comparing changes in macrophage levels in spleen cell suspensions of BALB/c, C57BL/6 albino and CD1 mice following sham procedure. (A) The percentage of F4/80⁺, F4/80⁺CD86⁺, F4/80⁺CD163⁺ and F4/80⁺CD86⁺CD163⁺ cells in spleen cell suspensions from animals that underwent sham-operated procedure, in three different mouse strains; data showing the percentage of positive cells within the Live population. **(B)** Quantification of

signal intensity of F4/80$^+$CD86$^+$ and F4/80$^+$CD163$^+$ cells in spleen cell suspensions from animals that underwent sham-operated procedure, in three different mouse strains. **(C)** The percentage of F4/80$^+$, F4/80$^+$CD86$^+$, F4/80$^+$CD163$^+$ and F4/80$^+$CD86$^+$CD163$^+$ cells in spleen cell suspensions from animals that underwent sham-operated procedure, in three different mouse strains; data showing the percentage of positive cells within the F4/80$^+$ population. **(D)** The percentage of F4/80$^+$, F4/80$^+$CD86$^+$, F4/80$^+$CD163$^+$ and F4/80$^+$CD86$^+$CD163$^+$ cells in spleen cell suspensions from animals that underwent sham-operated procedure, in three different mouse strains; data showing the percentage of positive cells within the F4/80$^+$ population which are represented as ratios. Significant differences between strains in response to sham-operated procedure. *p<0.017, **p=0.0086 and ****p<0.0001.

Adding on the previous analysis showed above (Figure 4.15) where we have demonstrated a strain-dependent response to the sham-operated procedure, we proceeded to assess the impact of bilateral R-IRI on macrophage levels in spleen (Figure 4.16).

Comparing changes in macrophage levels in spleen cell suspensions following bilateral R-IRI in three different mouse strains indicates that the animals respond differently to the procedure (Figure 4.16). Statistical analysis shows that strain has an extremely significant effect on macrophage levels following bilateral R-IRI, with a 0.01% chance of randomly observing an effect this large (or large) in an experiment of this size. CD1 mice showed a significant increase in percentage of F4/80$^+$ (**p=0.0016) and F4/80$^+$CD163$^+$ (*p=0.0172) cells when compared to C57BL/6 alb mice (Figure 4.16A). Furthermore, CD1 mice also showed an increase in percentage of F4/80$^+$ and F4/80$^+$CD163$^+$ cells when compared to BALB/c mice, however, these differences were not statistically significant. In addition, CD1 mice showed an increase in the percentage of F4/80$^+$CD86$^+$ and F4/80$^+$CD86$^+$CD163$^+$ cells when compared to the other two strains, however, these differences were not statistically significant (Figure 4.15A) There were also difference in macrophage levels between BALB/c and C57BL/6 mice: BALB/c mice showed an increase in F4/80$^+$, F4/80$^+$CD86$^+$and F4/80$^+$CD163$^+$ cells, however, these differences were not statistically significant. In contrast, C57BL/6 alb showed an increase in the percentage of F4/80$^+$CD86$^+$CD163$^+$ cells when compared to BALB/c mice (Figure 4.16A). Comparisons in median fluorescence intensity and antibody expression also showed differences between the three strains (Figure 4.16B). CD1 mice showed a significant decrease in F4/80$^+$CD163$^+$ antibody expression when compared to both BALB/c and C57BL/6 alb mice (****p<0.0001). There were no differences in F4/80$^+$CD163$^+$ antibody expression

following renal IRI between BALB/c and C57BL/6 alb mice. In contrast, C57BL/6 alb mice showed a slight decrease in F4/80^{+}CD86^{+} antibody expression when compared to both CD1 and BALB/c mice, however, these differences were not statistically significant. There were no differences in F4/80^{+}CD86^{+} antibody expression following bilateral R-IRI between BALB/c and CD1 mice (Figure 4.16B). When comparing differences in macrophage levels within the F4/80+ population in the spleen after bilateral R-IRI (Figure 4.16 C and D), CD1 mice showed significant in the percentage of F4/80^{+}CD163^{+} when compared to both C57BL/6 alb and BALB/c mice (****p<0.0001). BALB/c showed the highest percentage in CD86+F4/80+ within the F4/80+ population in the spleen when compared to CD1 and C57BL/6 alb mice, however, these differences were not statistically significant; there were no differences between CD1 and C57BL/6 alb mice in the percentage F4/80^{+}CD86^{+} cells, in response to renal IRI. In contrast, C56BL/6 alb mice showed the lowest percentage in F4/80^{+}CD86^{+}CD163^{+} positive cells (Figure 4.16 C and D).

When comparing changes in macrophage levels in the spleen between the three strains, we detected a similar pattern between C57BL/6 alb (Figure 4.5A) and CD1 (Figure 4.9A) mice in response to bilateral renal IRI; both strains showed a higher percentage in the levels of F4/80^{+} and F4/80^{+}CD86^{+} cells whereas BALB/c mice showed the opposite pattern, i.e., a decrease in the F4/80^{+} and F4/80^{+}CD86^{+} cells (Figure 4.1A). Both BALB/c (Figure 4.1B) and C57BL/6 alb (Figure 4.5B) showed an increase in the levels of in F4/80^{+}CD163^{+} antibody expression in kidney cell lysates while CD1 mice (Figure 4.9B) presented contrasting results in response to renal IRI. However, when comparing changes in macrophage levels within the F4/80^{+} population in the kidney, all three strains showed a similar pattern of response characterised by an increase in the levels of F4/80^{+}CD86^{+} cells following bilateral R-IRI (Figure 4.1C, Figure 4.5C and Figure 4.9C). In addition, in all three strains, R-IRI led to a decrease in the percentage of F4/80^{+} that are negative for both CD86^{-} and CD163^{-} in the kidneys of injured mice (Figure 4.1D, Figure 4.5D and Figure 4.9D).

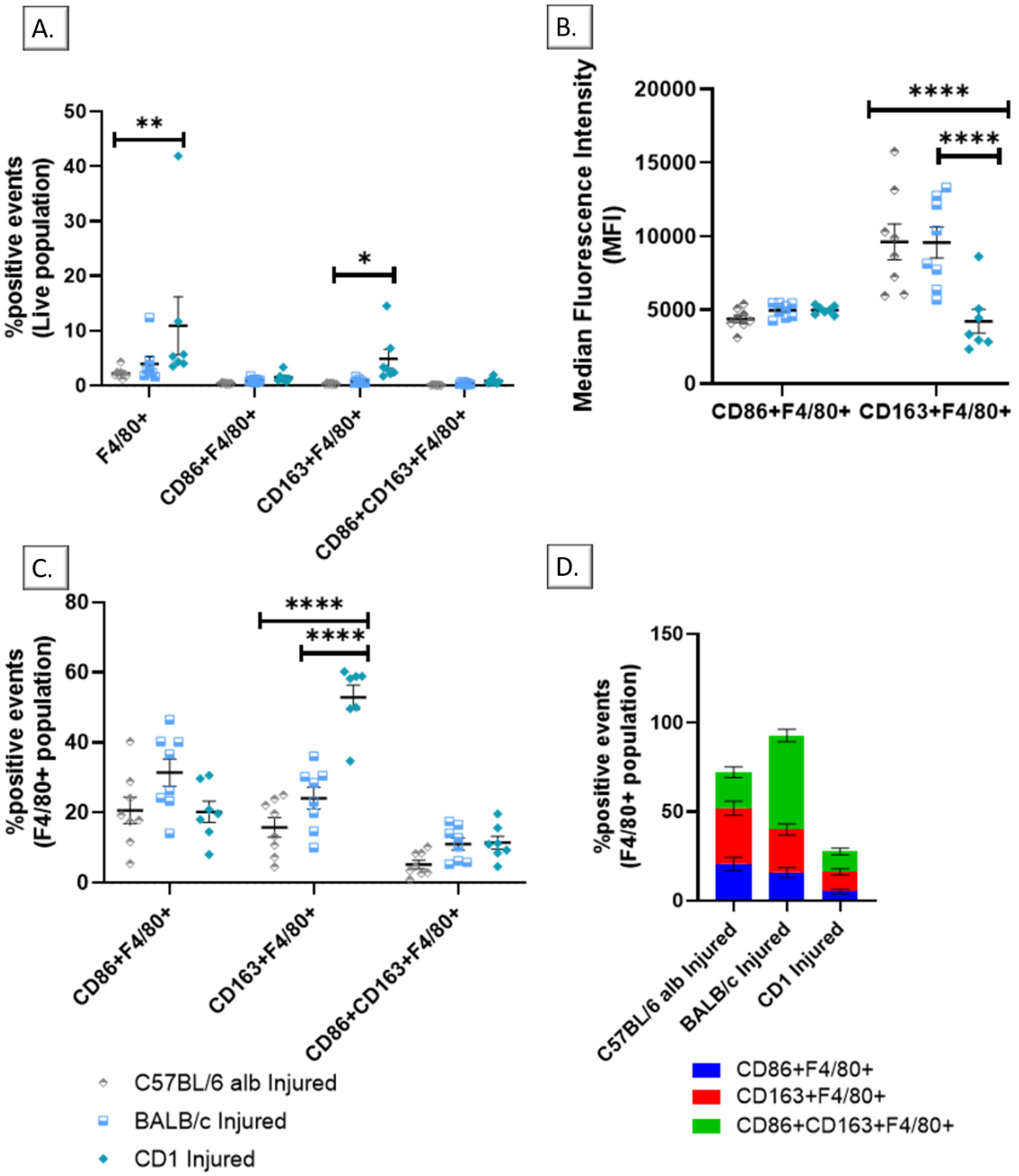

Figure 4.16: Comparing changes in macrophage levels in spleen cell suspensions of BALB/c, C57BL/6 albino and CD1 mice following bilateral R-IRI. (A) The percentage of F4/80$^+$, F4/80$^+$CD86$^+$, F4/80$^+$CD163$^+$ and F4/80$^+$CD86$^+$CD163$^+$ cells in spleen cell suspensions after bilateral R-IRI, in three different mouse strains; data showing the percentage of positive cells within the Live population. **(B)** Quantification of signal intensity of F4/80$^+$CD86$^+$ and F4/80$^+$CD163$^+$ cells in spleen cell suspensions after bilateral R-IRI, in three different mouse strains. **(C)** The percentage of F4/80$^+$, F4/80$^+$CD86$^+$, F4/80$^+$CD163$^+$ and F4/80$^+$CD86$^+$CD163$^+$ cells in spleen cell suspensions after bilateral R-IRI, in three different mouse strains; data showing the percentage of positive cells within the F4/80$^+$ population. **(D)** The percentage of F4/80$^+$, F4/80$^+$CD86$^+$, F4/80$^+$CD163$^+$ and F4/80$^+$CD86$^+$CD163$^+$ cells in spleen cell suspensions

after bilateral R-IRI, in three different mouse strains; data showing the percentage of positive cells within the F4/80^{+} population which are represented as ratios. Significant differences between strains in response to bilateral R-IRI. *p=0.0172, **p=0.0016 and ****p<0.0001.

4.5.8. Preliminary analysis on the effect of hUC-MSC therapy on cytokine levels following bilateral R-IRI in BALB/c mice

Levels of MCP-1, IL-1β, IL-6, IL-13, M-CSF, IFN-γ, IL-4, IL-10, IL-17E/IL-25, and TNF-α were below the limit of detection or extrapolated below LLOQ in BALB/c plasma for both hUC-MSC and PBS groups (Table 4.3).

Our preliminary data on the effects of hUC-MSC treatment on cytokine levels showed lower levels of IL-1β, IL-4 and IL-17E/IL-25 in the kidneys of injured BALB/c mice when compared to the PBS group, however, these results were not statistically significant (Figure 4.17). hUC-MSC treatment led to higher levels of MCP-1 and M-CSF in the kidneys of injured BALB/c mice when compared to the PBS group, with significant changes in the later (*p=0.0159). Levels of TNF-α, IL-6, IL-13, INF-γ and IL-10 were below the limit of detection or extrapolated below LLOQ in BALB/c kidney cell suspensions for both hUC-MSC and PBS groups (Table 4.4).

Cytokine	Level	hUC-MSC treatment	PBS treatment
MCP-1	LLOQ	✓	✓
IL-13	OOR<	✓	✓
IL-6	OOR<	✓	✓
M-CSF	OOR<	✓	✓
IFN-γ	OOR<	✓	✓
IL-1β	OOR<	✓	✓
IL-4	OOR<	✓	✓
IL-10	OOR<	✓	✓
IL-17E/IL-25	LLOQ	✓	✓
TNF-α	LLOQ	✓	✓

Table 4.3: Measurement of MCP-1, IL-1β, IL-6, IL-13, M-CSF, IFN-γ, IL-4, IL-10, IL-17E/IL-25, and TNF-α in plasma of injured BALB/c mice following hUC-MSC treatment or PBS injection. The upper and lower levels of quantification were: MCP-1 64,327.683 - 84.985 pg/mL, IL-1β 56,098.702 – 70.588 pg/mL, IL-6 6,155.229 – 24.893 pg/mL, IL-13 12,416.024 – 49.036 pg/mL, M-CSF 520.838 – 2.125 pg/mL, IFN-γ 3,223.254 – 12.481 pg/mL, IL-4 14,965.769 – 14.873 pg/mL, IL-10 3,362.301 – 13.667 pg/mL, IL-17E/IL-25 33,626.873 – 43.575 pg/mL, and TNF-α 591.633 – 0.775 pg/mL. **n=5** UC-MCS group, **n=4** PBS group. LLOQ = results were extrapolated below the lower limit of quantification. OOR< = cytokine levels were out of range below LLOQ.

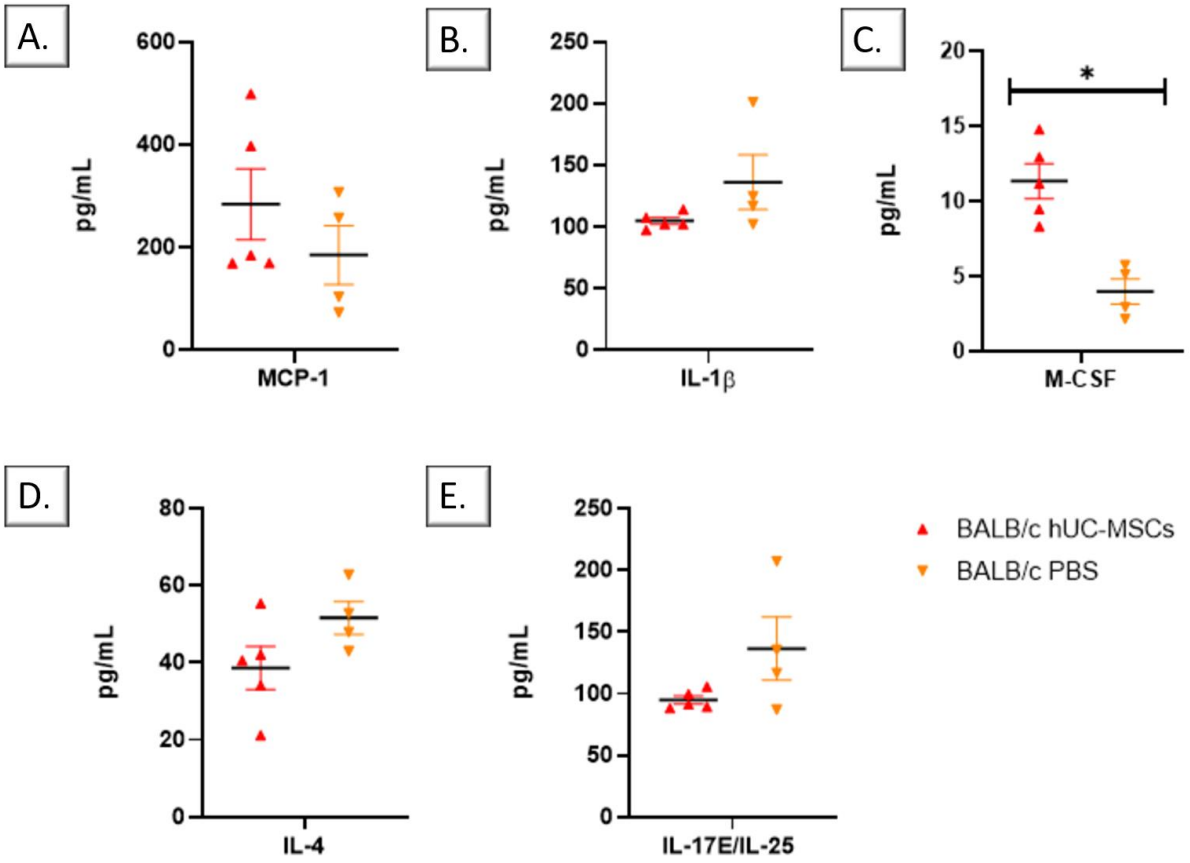

Figure 4.17: Measurement of MCP-1, IL-1β, M-CSF, IL-4, and IL-17E/IL-25 in kidney cell suspensions of injured BALB/c mice following hUC-MSC treatment or PBS injection. The upper and lower levels of quantification were: MCP-1 64,327.683 - 84.985 pg/mL, IL-1β 56,098.702 – 70.588 pg/mL, M-CSF 520.838 – 2.125 pg/mL, IL-4 14,965.769 – 14.873 pg/mL, and IL-17E/IL-25 33,626.873 – 43.575 pg/mL. **n=5** UC-MCS group, **n=4** PBS group. *p=0.0159

Cytokine	Level	hUC-MSC treatment	PBS treatment
IL-13	OOR<	✓	✓
IL-6	OOR<	✓	✓
IFN-γ	OOR<	✓	✓
IL-10	OOR<	✓	✓
TNF-α	LLOQ	✓	✓

Table 4.4: Measurement of IL-13, IL-6, IFN-γ, IL-10 and TNF-α in kidney cell suspensions of injured BALB/c mice following hUC-MSC treatment or PBS injection. The upper and lower levels of quantification were: IL-13 12,416.024 – 49.036 pg/mL, IL-6 6,155.229 – 24.893 pg/mL, IFN-γ 3,223.254 – 12.481 pg/mL, IL-10 3,362.301 – 13.667 pg/mL, and TNF-α 591.633 – 0.775 pg/mL. **n=5** UC-MCS group, **n=4** PBS group. LLOQ = results were extrapolated below the lower limit of quantification. OOR< = cytokine levels were below LLOQ. *p=0.0159

4.6. Discussion

4.6.1. Bilateral renal ischaemia-reperfusion leads to an increase in macrophage levels in the kidneys of injured mice, however, this response is strain-dependent

In the current experiments conducted within this thesis, we have for the first time assessed F4/80$^+$ macrophage changes in the kidney at day 3 following bilateral renal IRI, and attempted to categorise these macrophages into M1- and M2-like cells. Furthermore, we have attempted to distinguish whether these differences are strain specific by analysing macrophage responses in three different genetic mouse strains.

First and foremost, it is important to note that we were able to detect significant differences between the three strains when comparing macrophage levels in the kidneys following sham-operated procedure (Figure 4.13). These differences in macrophage levels following sham-operated procedure highlight the impact a surgery, in the absence of injury, could have on the body, and it has paramount implications for future translational studies as it shows a strain-dependent response to such operations. Nevertheless, further experiments should also be conducted to measure macrophage levels in control animals (i.e., animals that did not undergo any procedures) and compare whether these strain differences seen in the sham-operated animals are innate to the strain itself and would persist or whether it is a strain-dependent response to the surgery itself.

In the current experiments, renal injury induced by bilateral IRI led to a significant increase in the percentage of F4/80$^+$ cells in the kidneys of C57BL/6 alb and CD1 mice, however, we were unable to detect similar changes in the BALB/c strain where data showed the opposite trend between sham and injured kidneys. While neither C57BL/6 alb nor BALB/c mice showed any differences in M1- and M2-like levels following surgery (Figures 4.1A and Figure 4.5A), CD1 mice showed a significant increase in the levels of both pro- and anti-inflammatory macrophages at day 3 post injury (Figure 4.9A). We were also able to detect a significant increase in the levels of M1-like cells (within the F4/80$^+$ population) following R-IRI surgery in all three strains, although there were significant differences in strain response to injury, with CD1 mice showing the highest increase in the percentage of M1-like macrophages (Figures 4.1C, Figure 4.5C and Figure 4.9C). This data is mostly consistent with the literature

where renal IRI leads to an increase in the numbers of M1 macrophages during the injury phase and an increase in M2 macrophage levels during the repair phase[16,17,92–94,105,19,20,49,52,57,61,63,64]. Li *et al.* (2008) used a bilateral R-IRI model with a 32min clamp time and identified that the number of F4/80$^+$ macrophages peaks at 24h following injury induction and continues to be elevated until day 7; this group used a combination of FACS sorting and immunohistochemistry to identify macrophages in young male C57BL/6 and BALB/c mice but no distinction was made between the two strains[277]. Depletion studies during the injury phase of AKI have shown that F4/80$^+$ macrophages have a central role in the progression of disease whereas depletion during the repair phase has been associated with prolonged injury and an increase in inflammatory markers[52,64,79,83,278]. In another study by Lee *et al.* (2011), it was found that F4/80$^+$ macrophages iNOS expression (M1 marker) peaks at 24h after injury and declines by day 7 whereas Arg1 (M2 marker) starts being expressed at day 3 and its expression peaks at day 7; this group employed a unilateral 30min clamp model followed by immediate nephrectomy, and used both immunohistochemistry and FACS sorting to identify macrophages in young male C57BL/6 and BALB/c mice although no distinction was made between the two strains[52]. In contrast, Lu *et al.* (2012) employed a 24min bilateral R-IRI model and found no significant change in F4/80$^+$ cells between sham and injured groups at 24 hours after injury induction; this group used flow cytometry to identify macrophages in male wild-type C57BL/6 and BALB/c mice, however, no distinction was made between the two strains[279]. The differences in the data identified between the current experiments conducted within this thesis and research at other labs could be explained by a number of reasons, such as: 1) differences in the injury model and clamping time, 2) the lack of differentiation between strains in some experiments, 3) differences in the markers used to distinguish between M1 and M2 macrophages coupled with the fact that macrophages are a highly plastic population of cells capable of existing in various intermediate states[19,52,91,57,61,64,86–90], and 4) differences in the experimental end-points i.e., when macrophage levels were measured.

By day 3 following injury, previous research has shown that the injury phase has mostly ended and the organ enters a regeneration and repair period[17,52,55,57,64,65,280]. However, current data extracted from BALB/c and C57BL/6 alb experiments showed no differences in the levels of M2-like cells and only a slight increase in the levels of M1-like cells (although not statistically significant) between sham and injured animals. These discrepancies could be due

to the nature of the experimental design. As mentioned previously, it was only possible to read 80,000 Live events per experiment due to the extended length of time needed to prepare and run the samples (approximately 11.5 hours from organ collection until all the samples had been run through the flow cytometer). However, best practices state that to get more accurate data, one should read at least 10,000 positive events (i.e., 10,000 F4/80 positive events). Furthermore, one should also be mindful of only using three markers to distinguish between different populations of macrophages. While F4/80^{+} is considered a murine pan-macrophage marker, it can also be found on monocytes and dendritic cells (DCs), although at lower levels. As a result, an accurate analysis should first exclude these two populations using markers such as CD24^{+} for DCs and CD115^{+} for monocytes[281–284].

When trying to distinguish between M1- and M2-like cells within the F4/80^{+} population in the kidney, a high percentage of these cells were negative for both CD86 (M1) and CD163 (M2) markers. However, there was a decrease in the percentage of F4/80^{+}CD86^{-} CD163^{-} cells following R-IRI surgery, irrespective of strain, suggesting that this undefined population in the sham kidneys could maybe be characterised as macrophages in a naïve, M0, non-activated state which is neither pro-inflammatory nor anti-inflammatory[87]. Moreover, most macrophages activated during inflammation are derived from blood monocytes which, as mentioned previously, can also express the F4/80 murine pan-macrophage marker although on lower levels when compared to tissue macrophages. This could indicate that a percentage of the F4/80^{+}CD86^{-}CD163^{-} population could be comprised of inflammatory monocytes which have travelled to the site of injury where they would differentiate into macrophages[84,85,285,286]. In addition, we have also been able to identify a macrophage population that is positive for both CD86^{+} (M1) and CD163^{+} (M2) markers – i.e., F4/80^{+}CD86^{+}CD163^{+}. The presence of this population while negligible in both BALB/c and C57BL/6 alb, was quite high in CD1 mice and showed a significant increase in response to injury. Macrophages are a highly plastic and heterogenous population whose functions and roles are influenced by their environment, and it is possible for them to exhibit both pro- and anti-inflammatory signatures while they transition from one phenotype to another[61,64,77,86,90,91,95,287]. Furthermore, using only two markers to distinguish between M1- and M2-like cells is quite an oversimplification especially when M2 macrophages can be categorised into three different classes of macrophages (i.e. M2a, M2b and M2c), with the

M2b class capable of producing high levels of inflammatory cytokines[61,78]. Further tests would need to be conducted in order to accurately distinguish between M1 and M2 macrophages such as investigating how they metabolise arginine: M1 macrophages produce inducible nitric oxide synthase (iNOS) whereas M2 macrophages produce ornithine[86,93,97,272,288–290].

Taking into consideration some of the differences we have identified between the three different strains, both at baseline (i.e., following sham-operated procedure) and subsequent to bilateral renal IRI induction, the choice of genetic background in animal models is paramount when creating an experimental design. BALB/c and C57BL/6 mice are the standard choice as both strains are inbred which allows for more repeatable and uniform results. However, current experiments still point towards major differences in response not only between strain but also towards within-strain variation. Furthermore, by using multiple mouse strains for translational studies, one is better equipped to study and understand how macrophage responses to IRI can be translated into the clinic where human inter-individual variability still remains an extensive challenge[239].

It is also important to note that the CD1 mice presented with significantly higher levels of M2-like macrophages when compared to BALB/c and C57/BL6 alb mice, regardless of the experimental conditions. Due to time constraints, we were unable to perform extensive optimisation experiments for our choice of antibodies in the CD1 strain. As such, we propose that further experiments should be conducted to optimise the $CD163^{+}$ marker in this strain before proceeding with further investigations into the effect of hUC-MSC therapies in animal models of kidney injury.

4.6.2. Bilateral renal ischaemia-reperfusion leads to minimal changes in macrophage levels in the spleens of injured mice

Bilateral R-IRI led to minimal changes in macrophage levels in the spleens of injured mice at day 3 following surgery (Figure 4.2, Figure 4.6 and Figure 4.10). Current literature on the role of the spleen during AKI shows discrepancy between research conducted at different laboratories, suggesting that the spleen could have both beneficial and deleterious effects on animal models of kidney disease depending on: 1) the injury level, and 2) the timing of the splenectomy in the experimental design[140,291–293]. While this may be the case, these studies have only investigated cytokine levels in the spleen up to 24 hours after injury induction. In

the current experimental design, we have for the first time assessed F4/80^{+} macrophage changes at day 3 following bilateral renal IRI, and attempted to categorise these macrophages into M1- and M2-like cells. We have shown that by day 3 following AKI induction, there was a significant decrease in the percentage of F4/80^{+} cells in the spleens of C57BL/6 alb (Figure 4.6) and CD1 mice (Figure 4.10), however, we were unable to detect similar changes in the BALB/c strain where data showed no differences between sham and injured spleens (Figure 4.2). There was also an increase in the percentage of M2-like cells within the F4/80^{+} population in the spleen of CD1 injured mice (Figure 4.10C), nevertheless, these differences were not statistically significant when compared to sham-operated animals.

Interestingly, we detected an increase in F4/80^{+}CD163^{+} antibody expression in CD1 mice following bilateral renal IRI (Figure 4.10B), whereas both BALB/c and C57BL/6 mice showed the opposite trend i.e., a decrease in F4/80^{+}CD163^{+} antibody expression (Figure 4.2B and Figure 4.6B). Nonetheless, CD1 mice displayed significantly lower F4/80^{+}CD163^{+} antibody expression when compared to the other two strain, regardless of whether they were injured or not (Figure 4.15B and Figure 4.16B).

Similar to the kidney, the spleen also presented with a population of cells positive for all three markers used (i.e., F4/80^{+}CD86^{+}CD163^{+}). Unlike in the kidney, the F4/80^{+}CD86^{+}CD163^{+} population was much higher in the spleen for both BALB/c and CD1 mice, with C57BL/6 alb mice showing approximately 4-times less triple positive cells when compared to BALB/c mice (not statistically significant) regardless of the procedure. As the population of F4/80^{+}CD86^{+}CD163^{+} cells was higher in the spleen than in the kidneys irrespective of strain, we were able to detect a lower percentages of F4/80^{+}CD86^{-}CD163^{-} cells in the spleen of mice when compared to the kidneys. The spleen is an organ that is rich in macrophages, with 4 different subpopulations having been detected so far[135,136,294]. As mentioned previously, macrophages are characterised by a high degree of plasticity and heterogeneity and distinguishing between different macrophage subpopulations using only three markers is highly problematic, especially when the spleen, in particular, presents with tissue macrophages negative for the F4/80 marker but positive for markers such as CD68^{+}, CD11b^{+} and CD11c^{+}, which can also be found on DCs[61,64,77,86,90,91,95,287,295]. Nonetheless, this is the first side-by-side comparison in three different mouse strains looking to identify changes

in macrophage levels in the spleen in response to bilateral renal IRI, and the data presented here indicates a role of the spleen in kidney disease and emphasises the role of genetic background in animal models of disease.

4.6.3. Intravenous injection of hUC-MSC has minimal effects on macrophage levels in the kidney following bilateral renal ischaemia-reperfusion injury

Intravenous injection of hUC-MSC led to minimal effects on macrophage responses in the kidneys of injured mice, regardless of strain. We were only able to detect a significant decrease in the percentage of F4/80$^+$ cells in the BALB/c mice that underwent bilateral R-IRI surgery and received therapy (Figure 4.3A) which is consistent with the current literature[25,60]. Interestingly, when comparing macrophage levels between injured animals that received PBS treatment and no therapy (no hUC-MSC nor PBS), there was a decrease in the percentage of live F4/80$^+$ in the PBS, regardless of strain (Figure 4.3B, Figure 4.5B and Figure 4.9B). This difference could be explained by high degree of variability of data and the low number of animals used for the injured/no treatment group. Nevertheless, hUC-MSC treatment had no effect on the levels of M1- or M2-like cells in all three strains; there was also no effect detected on the levels of F4/80$^+$ cells in either C57BL/6 alb or CD1 strains. Nevertheless, the effects of hUC-MSC injection on macrophage levels in the kidneys following bilateral renal IRI in the experiments conducted within this thesis where consistent between the three strains investigated.

These results were unexpected as current literature points towards MSCs having the ability to increase the levels of M2-like macrophages in injured kidneys[25,78,82,92,98,149,181,259]. Li *et al.* (2013) have shown a decrease in the levels of F4/80$^+$ cells and an increase in the numbers of CD206$^+$ cells (M2 marker) infiltrating the damaged kidney following hUC-MSC treatment; the group induced bilateral renal IRI in C57BL/6 mice using a 30 minute clamp time[25]. Geng *et al.* (2014) showed that autologous BM-MSC treatment can lead to an increase in the numbers of CD206$^+$ cells in injured kidneys; the group induced AKI in C57BL/6 using a glycerol injection[259]. However, it is also important to note that the aforementioned studies measured macrophage levels at day 5 following surgery and used a higher dose of MSC as treatment (10^6 – 2 x 10^6 cells per animal) which could provide an explanation to the discrepancy seen in our current results. In contrast, other studies have also shown that hUC-MSC treatments leads to no differences in the numbers of leukocytes in injured kidneys when

compared to control animals[246,296]. Jang *et al.* (2014) induced bilateral R-IRI in C57BL/6 mice, and treated them with two IP injections of hUC-MSC (10^6 cells/animal) 24 hours before injury and during reperfusion. However, they were unable to detect any differences in the numbers of $CD45^+$ leukocytes in injured kidneys, and only minimal changes in cytokine levels at day 1 and day 2 following injury induction[246]. Park *et al.* (2017) induced AKI in C57BL/6 mice using a cisplatin model; the groups were unable to detect any differences in macrophage levels between hUC-MSC and control groups at day 3 following injury induction[296].

Taking into consideration the substantial differences identified between current literature and our data, it is necessary to better understand the mechanisms by which these cellular therapies exert their effects to ameliorate injury and promote tissue repair and regeneration so as to develop efficacious therapeutic interventions.

4.6.4. Intravenous injection of hUC-MSC has minimal effect on macrophage levels in the spleen following bilateral renal ischaemia-reperfusion injury

Intravenous injection of hUC-MSC led to minimal effects on macrophage responses in the spleens of injured mice, regardless of strain. We were only able to detect a significant decrease in the percentage of $F4/80^+$ cells in the C57BL/6 alb and CD1 mice that underwent bilateral R-IRI surgery and received therapy (Figure 4.4A and Figure 4.10A). Interestingly, when comparing macrophage levels between injured animals that received PBS treatment and no therapy (no hUC-MSC or PBS), there is a decrease in the percentage of live $F4/80^+$ in the no therapy group in the C57BL/6 alb (Figure 4.4B) and CD1 (Figure 4.10B) strain while the BALB/c mice showed the opposite trend (Figure 4.4B). This difference could be explained by high degree of variability of data and the low number of animals used for the injured/no treatment group.

While hUC-MSC treatment leads to minimal effects in the spleen of BALB/c and C57BL/6 alb mice, we were able to measure a stronger effect in the CD1 strain. Cellular therapy led to a decrease in the levels of $F4/80^+$ cells in injured spleens (Figure 4.10A). Furthermore, a closer look at the F4/80+ population in the spleens also indicated a significant increase in the levels of both M1- and M2-like cells in the CD1 treatment group. As mentioned previously, the spleen is a primary lymphoid organ and a reservoir for monocytes and

macrophages, housing four distinct macrophage populations[84,134–136]. Multiple studies have shown that the spleen plays a central role in AKI where MSCs accumulate after 24h and are capable of ameliorating injury through the induction of regulatory T cells and a decrease in IFN-γ producing T cells[117,120,194,200,297,298]. In a different study, Akiyama *et al.* (2012) have shown that Treg generation is mediated by T-cell MSC-induced apoptosis and macrophages in the spleen: MSC injection leads to T-cell death, and an increase in macrophage and TGF-β levels in the spleen which triggers Treg induction[101].

4.6.5. Preliminary data points towards intravenous injection of hUC-MSC having minimal effects on cytokine levels following bilateral renal ischaemia-reperfusion injury

Inflammation plays a major role in kidney injury and current research has shown that leukocyte infiltration in the kidney is mediated by an increase in cytokine and chemokine levels[10,15,19,43,55,59,60,144].

We were able to detect a significant increase in the levels of M-CSF in kidney cell suspensions of the hUC-MSC treatment group when compared to the PBS group where M-CSF levels were bellow LLOQ (Figure 4.17C). M-CSF is a key regulator of macrophage proliferation, differentiation and survival, and is constitutively expressed by MSCs in their secretome[17,63,85,93,97,253–255,299]. *In vitro* studies have demonstrated a significant role of this molecule in the expansion and polarisation of M2 macrophages and, while we were unable to detect any changes in M2-like macrophages at day 3 between treatment and PBS groups in BALB/c mice, a longitudinal study assessing macrophage levels throughout a longer experimental design would be necessary before establishing whether these cellular therapies are successful or not[25,300–302].

We also detected an increase in the levels of MCP-1 in kidney cell suspensions from BALB/c mice that received hUC-MSC therapy when compared to PBS group, although the differences were not statistically significant (Figure 4.17A). MCP-1, a monocyte and macrophage chemoattractant molecule that stimulates IL-4 release from T-cells, is another cytokine that is constitutively expressed by MSCs in culture supernatants[187,303,304]. Furthermore, MCP-1 can also be used as a biomarker for AKI induction, as its urinary levels

increase shortly after the onset of injury[305]. MCP-1 plays a major role in recruiting monocytes to the damaged tissue, and in conjunction with M-CSF which can stimulate their differentiation into M2 macrophages play a primary role in inflammation. MCP-1 expression can also be induced after exposure to inflammatory stimuli such as M-CSF[18,19,61,217,306,307].

hUC-MSC treatment also led to a decrease in the levels of the pro-inflammatory cytokine IL-1β in injured kidneys when compared to the PBS group, however, these differences were not statistically significant (Figure 4.17B). These results are consistent with multiple studies investigating the effect of cellular therapies on modulating inflammatory markers during kidney injury[21,25,42,258,308]. Unexpectedly, we also observed a decrease in the levels of the anti-inflammatory cytokines IL-4 and IL-17E/IL-25 in the hUC-MSC (Figure 4.17D and Figure 4.17E), and were unable to measure any TNF-α, IL-6, IL-13, IFN-γ and IL-10 in kidney cell suspensions as levels were bellow LLOQ (Table 4.4). Whereas the cited studies and the experiments performed in this thesis measured protein levels in the organs of interest, the seen discrepancies could be due to the timeline of the experimental design: most studies have focused on measuring cytokine levels either at day 1 or day 5 following injury induction. Furthermore, the current analysis only included a small number of animals, focusing on the BALB/c strain while the aforementioned studies were performed on C57BL/6 mice.

Finally, we are unable to measure any cytokines in plasma in response to injury, regardless of whether the animals received therapy or not (Table 4.3). Previous research analysing cytokine levels in the blood in response to kidney injury, indicated a decrease in inflammatory cytokines, such as IL-1β, IL-12, IL-6 and TNF-α in response to cellular therapy; however, these studies analysed inflammatory molecules levels at 24h after injury whereas the current experiments assessed cytokine levels at 72h[124,258,302].

Further investigation is necessary in order to ascertain the impact of MSC therapies on cytokine levels in the kidney, as the current experiments only investigated differences in BALB/c mice and used a limited number of animals. However, our ability to measure an increase in M-CSF and MCP-1 levels in the hUC-MSC group when compared to control group at day 3, suggests that these therapies could be capable of stimulating macrophages towards an anti-inflammatory phenotype which is consistent with the current literature. As a result, additional experiments with extended end-points (i.e., day 5 and day 7) should be conducted

to examine the impact of cellular therapies on macrophage levels in kidneys and spleens following bilateral renal IRI.

Chapter 5

Final discussion and conclusions

5. Discussion

The *in vivo* experiments presented within this thesis had four main aims:

(1) assess the impact of R-IRI on renal function in three different mouse strains;

(2) compare the impact of R-IRI on renal function between three different mouse strains;

(3) assess the impact of regenerative medicine therapies on renal function in three different mouse strains following R-IRI;

(4) compare the impact of regenerative medicine therapies on renal function in three different mouse strains following R-IRI;

(5) assess the effect of R-IRI on spleen and kidney macrophages, in three different mouse strains;

(6) determine the effect of regenerative medicine therapies on spleen and kidney macrophages, in three different mouse strains following R-IRI;

(7) determine the effect of regenerative medicine therapies on pro- and anti-inflammatory cytokine levels in BALB/c mice.

5.1. Bilateral renal IRI leads to strain-dependent responses

We have demonstrated throughout this thesis that bilateral renal IRI leads to strain-dependent responses. We have employed a series of experiments that assessed renal function, weight and macrophage levels in kidneys and spleens to characterise and compare the effect of bilateral renal IRI has on three different mouse strains – BALB/c, C56BL/6 alb and CD1. We have chosen a bilateral renal IRI model as it is the most clinically relevant model of AKI although it is highly variable[16,21,25,47,49,61,265], as we have demonstrated throughout this thesis; the need for standardisation is paramount so as to minimise this variability as much as possible, and our research group has performed extensive work in this area[267,309]. We have used a standardised 30 minute pre-surgical anaesthetic time and a clamp time of 27.5 minutes, and ensured a constant body temperature throughout the surgical procedure so as to get a disease model that was severe enough to cause kidney injury without causing animal

death due to acute uraemia[111,267]. When choosing a strain to characterise, we selected BALB/c and C57BL/6 strains as they are two of the most commonly used mouse strains in pre-clinical research[25,95-97,106,116–126]. While both these strains are inbred, they are also characterised by different immunological profiles and, as such, they are ideal choice of animal model when investigating conditions such as AKI where the immune system plays a central role[25,95-97,106,116–126]. Regardless of the initial cause, AKI is characterised by an inflammatory response which involves multiple components of the immune system, with macrophages playing a central role[16,17,19,20,52,55,57,59,82,83]. As previously mentioned, BALB/c and C57BL/6 strains are characterised by T cell profiles and readily activate M2 and M1 macrophages, respectively, when stimulated with antigen[96,97,127,128]. As a result, one of our aims was to investigate if there are any differences in response to renal IRI between these strains. Finally, we have also chosen to characterise the response of CD1 mice to bilateral renal IRI as they are an outbred strain defined by inter-individual genetic variation which provides us with invaluable data when translating this research into the clinic.

Bilateral renal IRI led to a significant decrease in renal function and weight, regardless of strain. However, while all three strains underwent surgery in comparable conditions, reduction in renal function following surgery was significantly strain-dependent: by day 3, CD1 mice were the most affected by the procedure while BALB/c mice had the highest mean renal function; C57BL/6 alb mice displayed a higher reduction in renal function when compared to BALB/c mice, however, they were less injured than CD1 mice. In contrast, we saw a more significant reduction in body weight in BALB/c mice when compared to CD1 and C57BL/6 alb mice, with CD1 mice showing the least decrease in weight even though they had the highest loss of renal function. However, it is important to note that changes in body weight and the differences we have seen between strains can be attributed loss of muscle / fat weight and / or dehydration.

To assess whether differences in immune responses could be responsible for the differences in physiological effects following bilateral R-IRI, we investigated macrophage levels in kidneys and spleens. In the current experiments, renal injury induced by IRI led to a an increase in the percentage of F4/80^{+} cells in the kidneys of C57BL/6 alb and CD1 mice, consistent with the literature, however, we were unable to detect similar changes in the BALB/c strain where data showed the opposite trend between sham and injured kidneys i.e.,

a slight decrease in the percentage of F4/80$^+$ cells in the kidney, although differences were not significant[16,17,20,49,52,57,61,63,105]. The differences seen in the BALB/c strain when comparing the percentage of F4/80$^+$ cells in the kidney are unexpected, however, they could be explained by the inter-strain variability, low number of animals used (i.e., n < 7) as well as other limitations of the current experimental design (see section *5.3.* for further information). Nevertheless, bilateral R-IRI led to an increase in the levels of M1-like cells (within the live and F4/80$^+$ population) following R-IRI surgery in all three strains, although there were significant differences in strain response to injury, with CD1 mice showing the highest increase in the percentage of M1-like macrophages. As CD1 mice showed the highest reduction in renal function following surgery, the cellular changes seen in this strain could be correlated with the high degree of injury and low recovery of function seen within this strain. Surprisingly, we were only able to detect a significant increase in M2-like macrophage levels in CD1 mice but not in BALB/c and C57BL/6 alb mice. By day 3, all strains had recovered at least half of the renal function when compared to baseline pre-surgery levels with BALB/c and C57BL/6 alb mice showing the highest rate of recovery, however, we were unable to detect any differences in M2 anti-inflammatory macrophages in the inbred strains. Interestingly, while BALB/c and C57BL/6 alb mice are characterised by distinct T cell/macrophage profiles, they displayed a similar response in F4/80$^+$CD163$^+$ antibody expression: bilateral renal IRI led to a significant decrease in median fluorescence intensity of F4/80$^+$CD163$^+$ antibody expression in injured mice when compared to sham mice whereas CD1 mice followed the opposite trend i.e., an increase in median fluorescence intensity of F4/80$^+$CD163$^+$ antibody expression in injured mice when compared to sham mice.

We also assessed, for the first time, macrophage levels in the spleen at day 3 following bilateral renal IRI as this organ is a primary reservoir of macrophages, dendritic cells and monocytes, the latter capable of migrating to injured organs during sterile inflammation[76,84,133,137]. Bilateral R-IRI led to minimal changes in macrophage levels in the spleens of injured mice: we were only capable of detecting a significant decrease in the percentage of F4/80$^+$ cells in the spleens of injured C57BL/6 alb and CD1 mice, but no changes in injured BALB/c mice. Similar to the kidney, BALB/c and C57BL/6 alb mice displayed a similar response in F4/80$^+$CD163$^+$ antibody expression: bilateral renal IRI led to a decrease in median fluorescence intensity of F4/80$^+$CD163$^+$ antibody expression in injured mice when compared

to sham mice whereas CD1 mice followed the opposite trend i.e., an increase in median fluorescence intensity of F4/80^{+}CD163^{+} antibody expression in injured mice when compared to sham mice.

It is worth noting that we observed a high degree of inter-strain variability when trying to determine the percentage of macrophages in the organs of interest, regardless of strain. One would assume that this variability could be indicative of the variability associated with the bilateral R-IRI model, however, as macrophage levels were variable in both sham and injured groups, it cannot be attributed to the injury model. This variability could be attributed to some of the limitations of the current experimental design (see section *5.3.* for further information).

5.2. hUC-MSC therapies show no efficacy in ameliorating kidney injury following bilateral renal IRI

One of the main aims of this thesis was to establish the efficacy of MSC therapies in ameliorating kidney injury in mouse models of AKI, and to investigate their mechanisms of action. Nonetheless, we were not capable of establishing the efficacy of hUC-MSC therapies, administered immediately after bilateral renal IRI, in improving renal function. The experiments described within this thesis directly contradict the extensive pre-clinical literature that has been published within the last two decades, which has demonstrated a direct role of MSC therapies in ameliorating renal function after an episode of AKI[21,23,26,47,149,191–193,224–228]. Nonetheless, we were capable of determining a slight therapy-effect of hUC-MSC correlating with different immunological profiles when investigating the effect of cellular treatment on the immune system. Most notably: 1) hUC-MSC injection led to a significant decrease in the percentage of F4/80^{+} cells in the kidneys of injured BALB/c when compared to PBS (control) group (Figure 4.3A), 2) hUC-MSC injection led to a significant decrease in the percentage of F4/80^{+} cells in the spleens of injured C57BL/6 alb (Figure 4.4A) and CD1 (Figure 4.10A) mice when compared to PBS group, 3) hUC-MSC injection led to an increase in the levels of M-CSF and MCP-1 cytokines the kidneys of injured BALB/c when compared to PBS group, and 4) hUC-MSC injection led to a decrease in the levels of IL-1β cytokine in the kidneys of injured BALB/c when compared to PBS group. While these effects

on the immune system are consistent with the current literature, they were not replicated across all three strains[18,19,21,25,42,60,61,217,258,306-308]. Nevertheless, a decrease in inflammatory macrophages and/or IL-1β in the kidney following renal IRI have been associated with improved outcomes following AKI[21,25,149,302]. Surprisingly, we were unable to detect an increase in M2-like anti-inflammatory macrophages in the kidneys following hUC-MSC injection, however, increases in M-CSF and MCP-1 cytokines at day 3 after injury induction suggest a positive impact of treatment as these two cytokines play a key role in recruiting monocytes to the site of injury and stimulating their differentiation into M2 macrophages[18,19,61,217,306,307].

Taking into account the contrasting effects hUC-MSC therapies have been shown to have in these three strains, we would suggest that a longitudinal study to assess renal function and quantify macrophage and cytokine levels is required before determining whether these therapies could directly improve kidney function after AKI. One of the main difficulties when investigating the efficacy of MSCs is the lack of understanding of their mechanisms of action. Multiple studies point towards MSCs exerting their effects through the release of soluble molecules capable of modulating the various components of the immune system, stimulating angiogenesis and tissue repair (Table 1.3)[25,101,190,203,157,178,181–187]. However, several studies have also indicated that MSC donor variability and inter-laboratory culture differences are important aspects and can greatly influence their potency[213,310,311]. In addition, the MSCs' secretome composition has been shown to depend on the physiological needs of the tissue while MSC pre-activation using hypoxia or other molecules has been demonstrated to enhance their efficacy[119,181,183,190,209,212–214].

Additionally, a comprehensive analysis would also need to explore different levels of injury by varying the ischaemia period, and testing animals' responses to hUC-MSC therapies in these experimental conditions. These experiments would provide context into the underlying biological processes that contribute to injury and repair, and how cellular therapies respond in this microenvironment while also determining the optimal window for efficacy. Varying ischaemia levels would also be particularly relevant when translating these findings into the clinic where patients would present with a diverse spectrum of injury

severities. Lastly, injury level would also have an effect on the dose-response relationship and as such influence the cell dose required for therapeutic efficacy.

Furthermore, this data should be supplemented by immunohistochemical analysis to observe and compare the structural changes that occur within the kidney following bilateral renal IRI. A thorough examination of cellular morphology and tissue architecture following hUC-MSC treatment after kidney injury could capture changes otherwise missed through flow cytometry or GFR measurements. Furthermore, histology would supplement the FITC-Sinistrin experiments conducted and allow us to visually assess the level of injury following bilateral R-IRI, by assessing the levels of cellular death and measuring fibrosis. Furthermore, histology would provide us with the ability identify and quantify macrophages, as well as display the spatial relationship between macrophages and various cellular components of the kidney. Preliminary work showed that F4/80^{+} cells were localised within the interstitium, surrounding the injured tubules (Supplementary Figure 3). It is important to note that the histology assessment we have performed has been greatly hindered by the presence and accumulation of FITC-Sinistrin in the damaged tubules as the injured kidneys are unable of filtering and secreting the substance (Supplementary Figure 1F and Supplementary Figure 3D). As such, both flow cytometry and immunohistochemistry on frozen sections were greatly limited by the number of antibodies (and fluorochromes) that could be tested against.

5.3. Limitations of current work

The work presented within this thesis is subject to interpretation, and the experimental design employed comes with some severe limitations.

The pre-clinical bilateral renal IRI model is highly variable as it is extremely difficult to induce identical levels of injury in both kidneys, it depends on the skill of the surgeon performing the procedure, and surgical trauma can often occur which will inadvertently skew the results. This variability in the model is also associated with a lack of reproducibility and difficulties in comparing results between different studies. Furthermore, while the bilateral renal IRI model is more relevant in mimicking human renal pathophysiology, it is highly dependent on temperature and the duration of ischaemic period with slight variation in these two variables capable of resulting in significant changes in the severity of the

model[16,21,25,47,49,61,262,265,312,313]. The high variability in renal function following surgical procedure could also be explained, in part, to the use of isoflurane as an anaesthetic. Isoflurane conditioning has been shown to provide protection against various neural, cardio and renal procedures and introduce variability in the data. As a result, the duration of exposure, concentration and its effect on physiological parameters should be carefully considered when using isoflurane as an anaesthetic[8,314–317]. Moreover, one should also consider a 'running mean' approach to guide the number of animals needed within each experimental group. This would allow for the ability to dynamically adjust the animal sample size based on ongoing GFR measurement data and ensure that the study is adequately powered, and potentially minimise variability. The inter-strain variability observed within these experiments could also be attributed to microbiome differences. The gut microbiota presents a highly diverse ecosystem with a central role in modulating the mammalian immune system and other physiological processes, and microbiome differences between different animals have been shown to play a key role in inter-strain variability and their susceptibility to injury[240,318–324].

Finally, the inter-strain variability detected could also be associated with the current experimental design for macrophage detection and analysis. Due to the number of experiments performed at the end of the study (i.e., GFR measurements, cardiac puncture and plasma preparation, organ collection and dissociation, and cellular staining) coupled with the extensive time length needed to run the samples through the flow cytometer (i.e., 6 hours per 10 animals per experiment), it was not possible to read more than 80,000 Live events per experiment. Nonetheless, reading a minimum of 10,000 positive events (i.e., 10,000 F4/80 positive events) is the gold standard in order to get more accurate and reliable results. Furthermore, our study used only three markers to distinguish between M1 and M2 macrophages: F4/80$^+$ as a murine pan-macrophage marker, F4/80$^+$CD86$^+$ as an M1 marker and F4/80$^+$CD163$^+$ as a M2 marker. Nevertheless, the F4/80 marker can also be found, though at lower levels, on monocytes and DCs. Therefore, one should first exclude these two populations using markers such as CD24$^+$ for DCs and CD115$^+$ for monocytes[281–284]. Macrophage plasticity and heterogeneity has been extensively documented in addition to their ability to exist in intermediate subsets, which we have also proven within the current

work with existence of a F4/80^{+}CD86^{+}CD163^{+} triple stained population[19,52,91,57,61,64,86–90]. As a result, further experiments should be performed to distinguish between M1 and M2 macrophages by using a mixture of intra- and extracellular markers. Additionally, a ratio analysis of the flow cytometry data should also be explored rather than looking at overall numbers / percentages. Ratios are particularly useful for normalising data where variability is high thus providing a more accurate representation of relative changes within distinct macrophage populations. This would allow for comparison of macrophage subtypes from the same animal or from different animals and therefore a potentially better assessment of the efficacy of hUC-MSC therapies in modulating macrophage levels following bilateral renal IRI.

Another limitation of the current experimental design is attributed to the age of the animals utilised in the experiments. Our study, and most pre-clinical studies in literature, are carried out on young, healthy mice which is not representative of the population for which these cellular therapies targeted for. Prevalence of AKI has been shown to increase with age with several epidemiological studies indicating an increase in the number of elderly patients on dialysis[272]. This has been attributed to the presence of comorbidities and physiological changes in the ageing kidney. The treatment of comorbidities such as hypertension or cardiovascular disease often involves medication regimens that are either nephrotoxic or disturb renal haemodynamics[5,6,22,325]. Furthermore, the ageing kidney is characterised by further alterations in renal haemodynamics and chronic low-grade inflammation as well as cellular senescence[272]. Studies performed on sham aged mice show a marked increase in macrophage and pro-inflammatory levels when compared to sham young mice. As a result, it is paramount that these differences are taken into consideration when designing pre-clinical studies as it will drastically affect their translation into the clinic.

Next, it is important to look at the design of our experiments: in this thesis we have focused on **male** mice, used only **one dose** of **un-primed hUC-MSC** given **immediately** after surgery. First, it is important to explore the dose-response relationship as the effectiveness of therapy can vary with different doses and affect the impact it has on injury. As such, varying dosage levels would be necessary to establish whether this cellular therapy has ameliorating effects on kidney function following an episode of AKI. Secondly, focusing on a single route of administration can have limiting effects as different routes of administration would have

different effects on cellular biodistribution and thus efficacy. This is particularly important when translating these results to clinical settings where the most efficacious route of administration could vary based on the disease being investigated[21,23,26,44,47,71,98,179,183,194–202]. Thirdly, focusing on a single cell type might prevent us from identifying the most effective therapy going forward: MSC can be isolated from almost all tissues[26,181–186]. As such, comparing the effect of MSCs obtained from different sources would allow for a better understanding of their therapeutic effects. Fourth, the studies in this thesis had a 3-day experimental endpoint which might not have been enough to capture the possible delayed responses of hUC-MSC. It is important to extend the duration of these experiments to observe the long-term effects of these therapies and to create a more comprehensive view of the complexities around the mode of action of these cells. Fifth, excluding females from a study means that one would have a limited understanding of sex differences in disease mechanisms and their responses to treatment while also contributing to gender bias in research. Sixth, it is worth investigating whether multiple doses of hUC-MSC at different time points would have a beneficial effect. Furthermore, treatment doses given at later time points i.e., after the induction of surgery would better translate in the clinic where patients do not have access to therapies immediately after the onset of injury. Finally, multiple studies have shown that priming cells with various cytokines or growth factors before administering them as therapy could enhance their efficacy, modulate immune response and promote tissue regeneration[119,181,183,190,212–214].

This work could have also been supported by a series of *in vitro* experiments investigating the relationships between hUC-MSC and bone marrow-derived macrophages from all three strains. This would have allowed for a quicker and more effective way to test the effects cellular therapies on macrophages, and explore the cellular interactions under standardised conditions, without the presence of other biological and physiological factors. Finally, *in vitro* experiments would have allowed for a side-by-side comparison of macrophages responses and behaviours from three different mouse strains. These experiments could have also been accompanied by high throughput screening to better study biological interactions in a range of experimental conditions. Finally, both *in vitro* and *in vivo* experiments would have benefitted from integrating RNA sequencing to perform large-scale

analysis that profiles the whole transcriptome, from gene expression to non-coding RNAs. RNA sequencing would have provided a more an in-depth view of the distinct macrophage populations found in the kidneys and spleen, and the temporal dynamics that are involved in the macrophage transition from one phenotype to another.

5.4. Final conclusions

In conclusion, despite extensive *in vivo* testing, we were unable to demonstrate the efficacy of human UC-MSC therapies in ameliorating kidney injury when administered intravenously immediately after bilateral renal IRI, regardless of mouse strain. We were able to demonstrate that hUC-MSC treatment can marginally modulate macrophages in kidney and spleen, and influence cytokine levels in the kidney. However, these effects were not replicated across the three strains and displayed high inter-strain variability. The predominant limitations to this body of work have been explored, and a more comprehensive analysis is proposed to ascertain whether these differences are clinically significant. Nevertheless, this study has provided the first in-depth analysis that aimed to examine the role of genetic background in macrophage modulation using a bilateral renal IRI model. This study will provide a strong foundation for future pre-clinical research looking to uncouple the role of genetic variation in models of kidney disease, and how to better mitigate these differences to ensure conclusive and reproducible results. Accurate understanding of these genetic differences will have significant implications for the design of novel therapies for the treatment and prevention of AKI.

Supplementary Materials & Methods

Immunofluorescence on frozen tissue sections

To optimise the R-IRI model and to assess the effect of injury in the kidneys, the organs were prepared for immunohistochemistry. Briefly, the organs were collected and washed with ice-cold PBS, cleaned of any residual fat and cut in half. The tissue was fixed with 4% paraformaldehyde (PFA; Sigma-Aldrich, Germany, Cat. Number 30525-89-4) at 4°C for 30min, followed by 3x washes with PBS, 15min each. The organs were preserved overnight in 30% sucrose (Sigma-Aldrich, Germany, Cat. Number 57-50-1), at 4°C. The following day, the organs were removed from sucrose, mounted in OCT embedding compound (CryoMatrix, Fisher Scientific, UK, Cat. Number 12542716) in peel-a-ways molds (Fisher Scientific, UK, Cat. Number 12647736), frozen on dry ice, and stored at -80°C. The organs were cut into 7µM thick tissue sections using a cryostat, mounted onto gelatin-coated histological slides (SuperFrost Plus Adhesion, Fisher Scientific, UK, Cat Number 10149870), and stored at -20°C for analysis.

To perform immunofluorescence on frozen tissue sections, the slides were removed from the freezer and thawed at room temperature, for 10 - 20min; all further steps were performed in a humid chamber. The sections were washed 3x with PBS at room temperature, for 5min each wash. Next, the tissue sections were permeabilized with 0.25% Triton (Sigma-Aldrich, Germany, Cat. Number 9036-19-5) in PBS, for 10min at room temperature, and once again washed 3x with PBS, for 5min at room temperature. After the final wash, tissue sections were blocked with 2% BSA in PBS, for 1h at room temperature, followed by overnight incubation with the primary antibody (Supplementary Table 1) diluted in 2% BSA, at 4°C. The following day, sections were washed 2x in quick succession and then 3x in PBS at room temperature, for 5min. Next, the tissue sections were incubated with the secondary antibody (Supplementary Table 1) and DAPI (Abcam, Cat Number ab228549), diluted in 2% BSA for 1h at room temperature, in the dark. Finally, the sections were washed 4x in PBS, at room temperature for 5min. The slides were then mounted with anti-fade mounting media (GelMount, Sigma-Aldrich, Germany, Cat. Number G 0918), covered with a glass coverslip, and sealed with clear nail polish. Images of tissue sections were taken using a Zeiss ApoTome.2.

Antibody	Supplier	Isotype	Dilution
KIM-1	Novus, UK, Cat. Number AF1750	Goat / IgG polyclonal	1 : 100
Ki-67	Abcam, UK, Cat. Number ab78494	Rabbit / IgG polyclonal	1 : 100
CD31	ThermoFisher, UK, Cat. Number 14-0311-82	Rat / IgG2a, kappa	1 : 200
F4/80	Abcam, UK, Cat. Number ab16911	Rat / IgG2a, kappa	1 : 100
Alexa Fluor® 594	Abcam, UK, Cat. Number ab150132	Donkey Anti-Goat IgG	1 : 500
Alexa Fluor® 647	BioLegend, UK, Cat. Number 407512	Anti-Rat IgG2a	1 : 500
Alexa Fluor® 647	Abcam, UK, Cat. Number ab150075	Donkey Anti-Rabbit IgG	1 : 500

Supplementary Table 1: Primary and secondary antibodies used for immunofluorescence on frozen sections.

Tissue sections were stained for KIM-1 and CD31 (Supplementary Figure 1). KIM-1 is a transmembrane protein whose expression is strongly upregulated in injured kidneys (Supplementary Figure 1A) and is considered a strong biomarker of tubular injury whereas CD31 is a vascular marker of differentiation (Supplementary Figure 1B), and it can be seen upregulated in the injured areas (Supplementary Figure 1C). Important to note is the strong background we can observe in the FITC-488 channel (Supplementary Figure 1F) due to the accumulation of FITC-Sinistrin in injured tubules, and the kidneys inability to filter the substance.

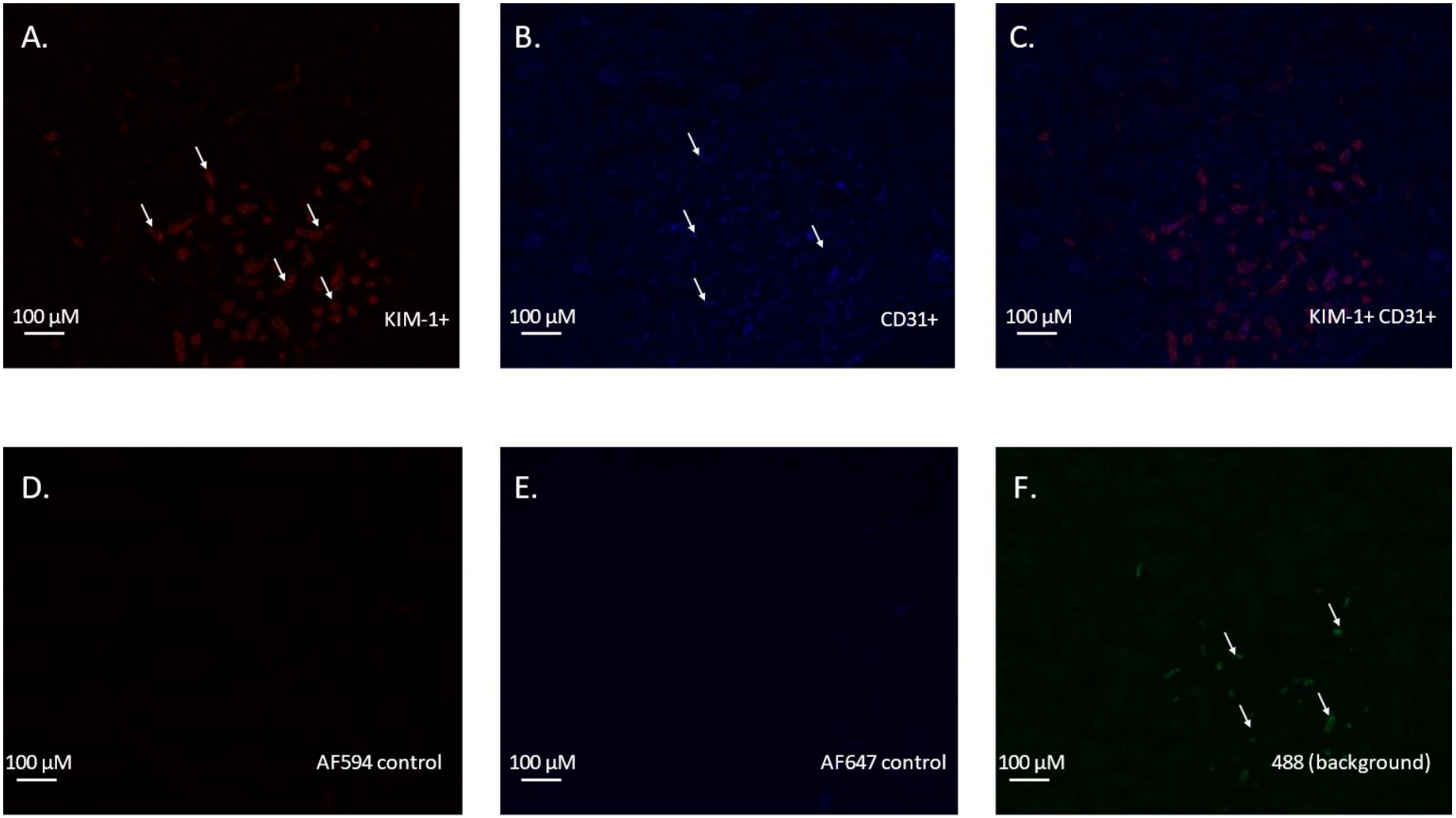

Supplementary Figure 1: KIM-1$^+$ and CD31$^+$ immunofluorescence staining on frozen tissue sections. Representative images of A. KIM-1$^+$ cells, B. CD31$^+$ cells, and C. Merged images of double-stained CD31$^+$ and KIM-1$^+$ cells in injured kidney of BALB/c mice; D. AlexaFluor 594 negative control, E. AlexaFluor 647 negative control, and F. Representative image taken using the 488 channel to showcase the strong visible background due to the accumulation of FITC-Sinistrin in injured tubules following GFR measurements. Abbreviations: AF - AlexaFluor

Tissue sections were stained for Ki-67 (Supplementary Figure 2). Ki-67 is a nuclear protein upregulated in all phases of the cell cycle.

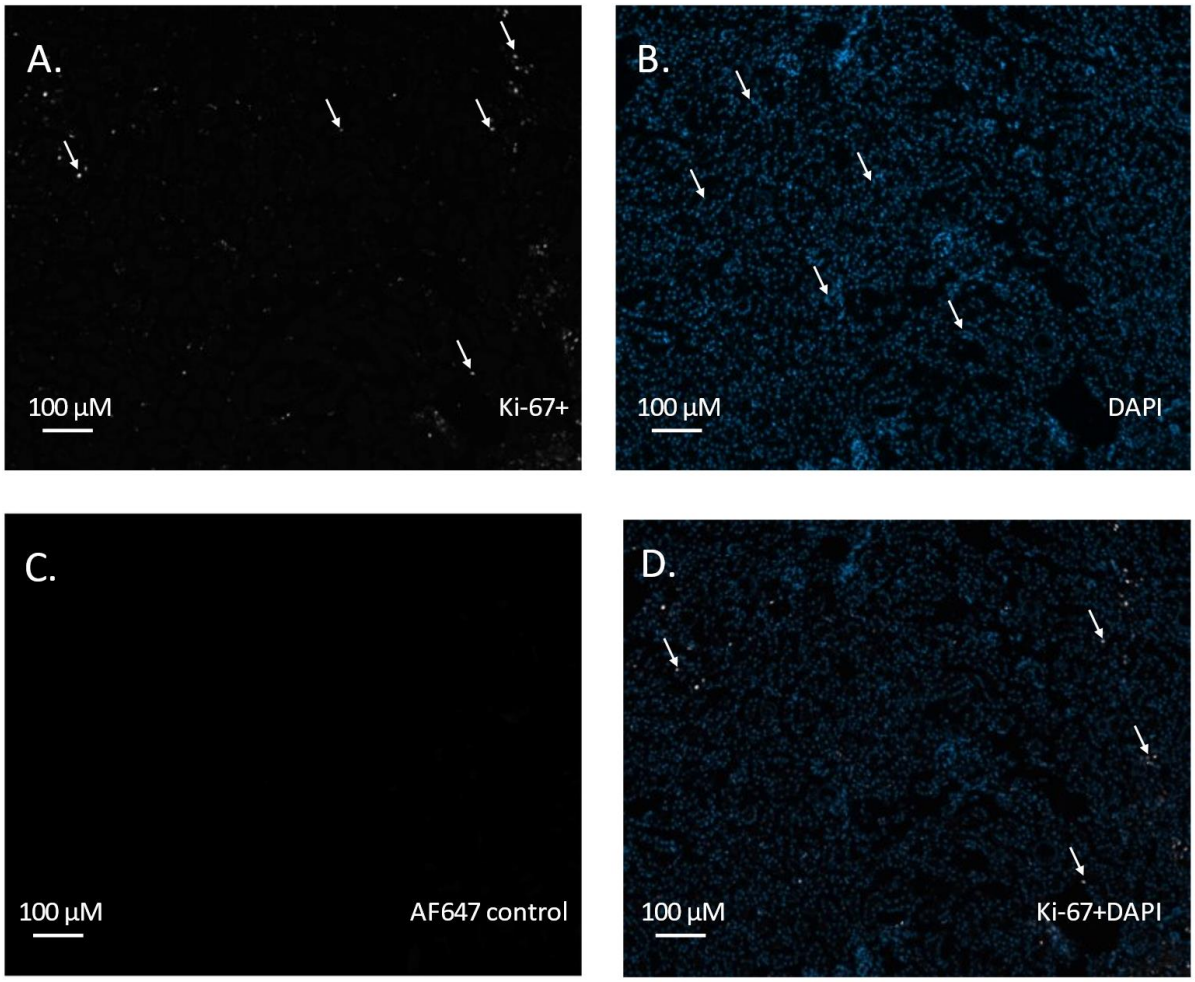

Supplementary Figure 2: Ki-67^{+} and DAPI immunofluorescence staining on frozen tissue sections. Representative images of A. Ki-67^{+} cells, B. DAPI stained nuclei, and D. Merged images of double-stained Ki-67^{+} and DAPI nuclei in injured kidney of BALB/c mice; C. AlexaFluor 647 negative control. Abbreviations: AF – AlexaFluor.

Tissue sections were stained with F4/80 (Supplementary Figure 3) to identify macrophages in kidneys. F4/80+ cells can be seen located in the interstitium of the kidney, and surrounding the injured tubules where FITC-Sinistrin can be seen accumulated (Supplementary Figure 3B).

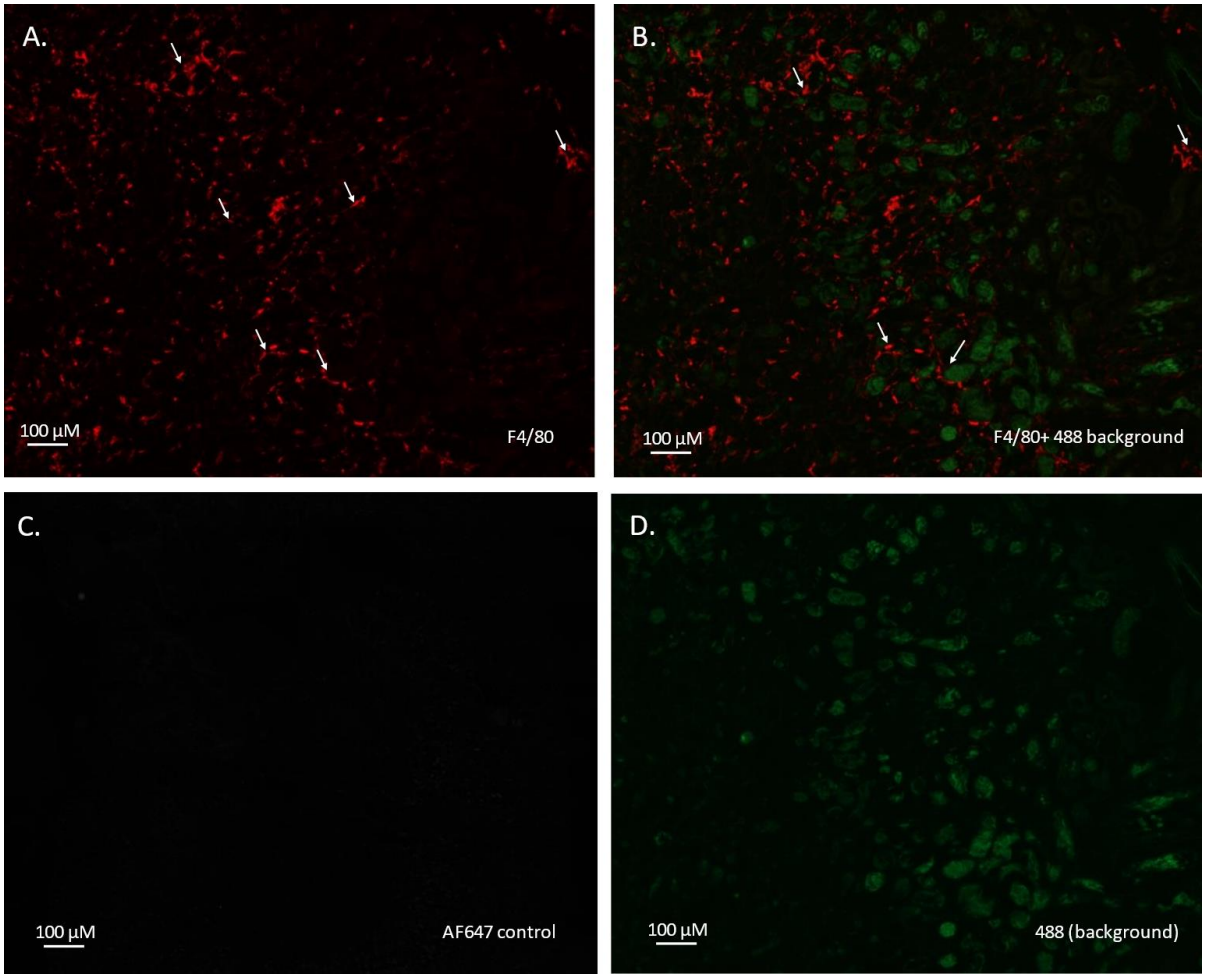

Supplementary Figure 3: F4/80$^+$ immunofluorescence staining on frozen tissue sections. Representative images of A. F4/80$^+$ cells, B. F4/80$^+$ cells in the interstitium surrounding injured tubules, and C. AlexaFluor 594 negative control, D. Representative image taken using the 488 channel to showcase the strong visible background due to the accumulation of FITC-Sinistrin in injured tubules following GFR measurements. Abbreviations: AF – AlexaFluor.

Due to time limitations and lack of funding, it was not possible to go past the optimization stage of the immunohistochemistry protocol discussed above.

Bibliography

1. Reece, J.B., Urry, L.A., Cain, M.L., Wasserman, S.A., Minorsky, P.V., Jackson, R.B. & Waserman, S.B. *Campbell Biology. 9th Edition*. pg 968 - 971 (2009).

2. Tortora, G. J. *& Derrickson, Brian. Principles of Anatomy and Physiology*. pg 1018 - 1055 (2009).

3. Martini, F. H., Nath, J. L. & Bartholomew, E. F. *Fundametals of Anatomy&Physiology*. *Development*. pg 954 -992 (2012).

4. Liu, J., Krautzberger, A.M., Sui, .SH., Hofmann, O.M., Chen, Y., Baetscher, M., Grgic, I., Kumar, S., Humphreys, B.D., Hide, W.A. & McMahon, A.P. Cell-specific translational profiling in acute kidney injury. *J. Clin. Invest.* **124**, 1242–54 (2014).

5. Makris, K. & Spanou, L. Acute Kidney Injury: Definition, Pathophysiology and Clinical Phenotypes. *Clin. Biochem. Rev.* **37**, 85 (2016).

6. Ortiz, A., Sanchez,-Niño M.D., Izquierdo, M.C., Martin-Cleary, C., Garcia-Bermejo, L., Moreno, J.A., Ruiz-Ortega, M., Draibe, J., Cruzado, J.M., Garcia-Gonzalez, M.A., Lopez-Novoa, J.M., Soler, M.J. & Sanz, A.B. Translational value of animal models of kidney failure. *Eur. J. Pharmacol.* **759**, 205–220 (2015).

7. Official journal of the international society of nephrology KDIGO 2012 clinical practice guideline for the evaluation and management of chronic kidney disease.(2012). Available at: https://kdigo.org/wp-content/uploads/2017/02/KDIGO_2012_CKD_GL.pdf (Accessed: 3rd December 2022)

8. Gibbs, K. M., Izer, J. M., Reeves, W. B., Wilson, R. P. & Cooper, T. K. Effects of General Anesthesia on 2 Urinary Biomarkers of Kidney Injury-Hepatitis A Virus Cellular Receptor 1 and Lipocalin 2-in Male C57BL/6J Mice. *J. Am. Assoc. Lab. Anim. Sci.* **58**, 21–29 (2019).

9. Patel, S.S., Molnar, M.Z., Tayek, J.A., Ix, J.H., Noori, N., Benner, D., Heymsfield, S., Kopple, J.D., Kovesdy, C.P. % Kalantar-Zadeh, K. Serum creatinine as a marker of muscle mass in chronic kidney disease: results of a cross-sectional study and review of literature. *J. Cachexia. Sarcopenia Muscle* **4**, 19 (2013).

10. Vaidya, V. S., Ferguson, M. A. & Bonventre, J. V. Biomarkers of acute kidney injury. *Annu. Rev. Pharmacol. Toxicol.* **48**, 463–493 (2008).

11. Hosten, A. O. BUN and Creatinine. *Clin. Methods Hist. Phys. Lab. Exam.* (1990).

12. Han, W.K., Waikar, S.S., Johnson, A., Betensky, R.A., Dent, C.L., Devarajan, P. & Bonventre, J.V. Urinary biomarkers in the early diagnosis of acute kidney injury. *Kidney Int.* **73**, 863–869 (2008).

13. Ferguson, M. A. & Waikar, S. S. Established and emerging markers of kidney function. *Clin. Chem.* **58**, 680–689 (2012).

14. Chevalier, R. L. The proximal tubule is the primary target of injury and progression of kidney disease: role of the glomerulotubular junction. *Am. J. Physiol. - Ren. Physiol.* **311**, F145 (2016).

15. Holderied, A., Kraft, F., Marschner, J. A., Weidenbusch, M. & Anders, H. J. 'point of no return' in unilateral renal ischemia reperfusion injury in mice. *J. Biomed. Sci.* **27**, 1–15 (2020).

16. Huen, S. C. & Cantley, L. G. Macrophage-mediated injury and repair after ischemic kidney injury. *Pediatr. Nephrol.* **30**, 199–209 (2015).

17. Zhang, M.Z., Yao, B., Yang, S., Jiang, L., Wang, S., Fan, X., Yin, H., Wong, K., Miyazawa, T., Chen, J., Chang, I., Singh, A. & Harris R.C. CSF-1 signaling mediates recovery from acute kidney injury. *J. Clin. Invest.* **122**, 4519–32 (2012).

18. Jung, M., Brüne, B., Hotter, G. & Sola, A. Macrophage-derived Lipocalin-2 contributes to ischemic resistance mechanisms by protecting from renal injury. *Sci. Rep.* **6**, 1–13 (2016).

19. John, D. & Imig, M. J. R. Immune and Inflammatory Role in Renal Disease. **3**, 957–976 (2014).

20. Jang, H. R. & Rabb, H. Immune cells in experimental acute kidney injury. *Nat. Rev. Nephrol.* **11**, 88–101 (2015).

21. Cao, H., Qian, H., Xu, W., Zhu, W., Zhang, X., Chen, Y., Wang, M., Yan, Y. & Xie, Y. Mesenchymal stem cells derived from human umbilical cord ameliorate ischemia/reperfusion-induced acute renal failure in rats. *Biotechnol. Lett.* **32**, 725–732 (2010).

22. Sawhney, S. & Fraser, S. D. Epidemiology of AKI: Utilizing Large Databases to Determine the Burden of AKI. *Adv. Chronic Kidney Dis.* **24**, 194–204 (2017).

23. Santeramo, I., Herrera-Perez, Z., Illera, A., Taylor, A., Kenny, S., Murray, P., Wilm B. & Gretz N. Tissue-specific progenitor and stem cells Human Kidney-Derived Cells Ameliorate Acute Kidney Injury Without Engrafting into Renal Tissue. *Stem Cell Transl. Med.* **6**, 1373–1384 (2017).

24. NICE. Context | Acute kidney injury: prevention, detection and management | Guidance | NICE. (2019). Available at: https://www.nice.org.uk/guidance/ng148/chapter/Context#:~:text=The costs to the NHS,lung and skin cancer combined. (Accessed: 3rd December 2022)

25. Li, W., Zhang, Q., Wang, M., Wu, H., Mao, F., Zhang, B., Ji, R., Gao, S., Sun, Z., Zhu, W., Qian, H., Chen, Y. & Xu, W. Macrophages are involved in the protective role of human umbilical cord-derived stromal cells in renal ischemia–reperfusion injury. *Stem Cell Res.* **10**, 405–416 (2013).

26. Feng, Z., Ting, J., Alfonso, Z., Strem, B.M., Fraser, J.K., Rutenberg, J., Kuo, H.C. & Pinkernell, K. Fresh and cryopreserved, uncultured adipose tissue-derived stem and regenerative cells ameliorate ischemia–reperfusion-induced acute kidney injury. *Nephrol. Dial. Transplant.* **25**, 3874–3884 (2010).

27. Nakazawa, D., Kumar, S.V., Marschner, J., Desai, J., Holderied, A., Rath, L., Kraft, F., Lei, Y., Fukasawa, Y., Moeckel, G.W., Angelotti, M.L., Liapis, H. & Anders, H.J. Histones and Neutrophil Extracellular Traps Enhance Tubular Necrosis and Remote Organ Injury in Ischemic AKI. *J. Am. Soc. Nephrol.* **28**, 1753–1768 (2017).

28. Lopes, J. A. & Jorge, S. The RIFLE and AKIN classifications for acute kidney injury: a critical and comprehensive review. *Clin. Kidney J.* **6**, 8–14 (2013).

29. Ricci, Z., Cruz, D. & Ronco, C. The RIFLE criteria and mortality in acute kidney injury: A systematic review. *Kidney Int.* **73**, 538–546 (2008).

30. Hoste, E.A., Clermont, G., Kersten, A., Venkataraman, R., Angus, D.C., De Bacquer, D. & Kellum, J.A. RIFLE criteria for acute kidney injury are associated with hospital mortality in critically ill patients: a cohort analysis. *Crit. Care* **10**, R73 (2006).

31. Bagshaw, S.M., Uchino, S., Cruz, D., Bellomo, R., Morimatsu, H., Morger,a S., Schetz, M., Tan, I., Bouman, C., Macedo, E., Gibney, N., Tolwani, A., Oudemans-van Straaten, H.M., Ronco, C.

& Kellum, J.A. A comparison of observed versus estimated baseline creatinine for determination of RIFLE class in patients with acute kidney injury. *Nephrol. Dial. Transplant* **24**, 2739–2744 (2009).

32. Maccariello, E., Soares, M., Valente, C., Nogueira L., Valença R.V., Machado, J.E. & Rocha, E. RIFLE classification in patients with acute kidney injury in need of renal replacement therapy. *Intensive Care Med.* **33**, 597–605 (2007).

33. Bell, M., Liljestam, E., Granath, F., Fryckstedt, J., Ekbom, A. & Martling, C.R.. Optimal follow-up time after continuous renal replacement therapy in actual renal failure patients stratified with the RIFLE criteria. *Nephrol. Dial. Transplant* **20**, 354–360 (2005).

34. Mehta, R.L., Kellum, J.A., Shah, S.V., Molitoris, B.A., Ronco, C., Warnock, D.G. &, Levin, A. Acute Kidney Injury Network: report of an initiative to improve outcomes in acute kidney injury. *Crit. Care* **11**, (2007).

35. *KDIGO Clinical Practice Guideline for Acute Kidney Injury.* Available at: http://www.kidney-international.org (2012). (Accessed: 26th December 2022)

36. Scarfe, L., Menshikh, A., Newton, E., Zhu, Y., Delgado, R., Finney, C. & de Caestecker, M.P. Long-term outcomes in mouse models of ischemia-reperfusion-induced acute kidney injury. *Am. J. Physiol. - Ren. Physiol.* **317**, F1068–F1080 (2019).

37. Bellomo, R., Kellum, J. A. & Ronco, C. Acute kidney injury. *Lancet* **380**, 756–766 (2012).

38. Rewa, O. & Bagshaw, S. M. Acute kidney injury-epidemiology, outcomes and economics. *Nat. Rev. Nephrol.* **10**, 193–207 (2014).

39. Manzoor, H. & Bhatt, H. Prerenal Kidney Failure. *StatPearls* (2022).

40. Postrenal Acute Kidney Injury - Topic Overview. Available at: https://wa.kaiserpermanente.org/kbase/topic.jhtml?docId=aa115548. (Accessed: 26th December 2022)

41. Sun, C.-K., Zhang, X.Y., Sheard, P. W., Mabuchi, A. & Wheatley, A. M. Change in mitochondrial membrane potential is the key mechanism in early warm hepatic ischemia-reperfusion injury. *Microvasc. Res.* **70**, 102–110 (2005).

42. Semedo, P., Palasio, C.G., Oliveira, C.D., Feitoza, C.Q., Gonçalves, G.M., Cenedeze, M.A., Wang, P.M., Teixeira, V.P., Reis, M.A., Pacheco-Silva, A. & Câmara, N.O. Early modulation of inflammation by mesenchymal stem cell after acute kidney injury. *Int. Immunopharmacol.* **9**, 677–682 (2009).

43. Sharfuddin, A. A. & Molitoris, B. A. Pathophysiology of ischemic acute kidney injury. *Nat. Rev. Nephrol.* **7**, 189–200 (2011).

44. Lin, F., Moran, A. & Igarashi, P. Intrarenal cells, not bone marrow-derived cells, are the major source for regeneration in postischemic kidney. *J. Clin. Invest.* **115**, 1756–1764 (2005).

45. Tögel, F., Weiss, K., Yang, Y., Hu, Z., Zhang, P. & Westenfelder, C. Vasculotropic, paracrine actions of infused mesenchymal stem cells are important to the recovery from acute kidney injury. *Am. J. Physiol. Physiol.* **292**, F1626–F1635 (2007).

46. Basile, D. P. The endothelial cell in ischemic acute kidney injury: implications for acute and chronic function. *Kidney Int.* **72**, 151–156 (2007).

47. Behr, L., Hekmati, M., Fromont, G., Borenstein, N., Noel, L.H., Lelievre-Pegorier, M. &

Laborde, K. Intra Renal Arterial Injection of Autologous Mesenchymal Stem Cells in an Ovine Model in the Postischemic Kidney. *Nephron Physiol.* **107**, p65–p76 (2007).

48. Menke, J., Iwata, Y., Rabacal, W.A., Basu, R., Yeung, Y.G., Humphreys, B.D., Wada, T., Schwarting, A., Stanley, E.R. & Kelley, V.R. CSF-1 signals directly to renal tubular epithelial cells to mediate repair in mice. *J. Clin. Invest.* **119**, 2330–42 (2009).

49. Soares, R. O. S., Losada, D. M., Jordani, M. C., Évora, P. & Castro-E-Silva, O. Ischemia/Reperfusion Injury Revisited: An Overview of the Latest Pharmacological Strategies. *Int. J. Mol. Sci.* **20**, (2019).

50. Thadhani, R., Pascual, M. & Bonventre, J. V. Acute renal failure. *N. Engl. J. Med.* **334**, 1448–1460 (1996).

51. Prakash, J., de Borst, M.H., Lacombe, M., Opdam, F., Klok, P.A., van Goor, H., Meijer, D.K., Moolenaar, F., Poelstra, K. & Kok, R.J. Inhibition of Renal Rho Kinase Attenuates Ischemia/Reperfusion-Induced Injury. *J. Am. Soc. Nephrol.* **19**, 2086 (2008).

52. Lee, S., Huen, S., Nishio, H., Nishio, S., Lee, H.K., Choi, B.S., Ruhrberg, C. & Cantley, L.G. Distinct Macrophage Phenotypes Contribute to Kidney Injury and Repair. *J. Am. Soc. Nephrol.* **22**, 317–326 (2011).

53. Huen, S.C., Huynh, L., Marlier, A., Lee, Y., Moeckel, G.W. & Cantley, L.G. GM-CSF Promotes Macrophage Alternative Activation after Renal Ischemia / Reperfusion Injury. J Am Soc Nephrol. 2015 Jun;26(6):1334–1345 (2015). doi:10.1681/ASN.2014060612

54. Linkermann, A., Stockwell, B. R., Krautwald, S. & Anders, H. J. Regulated cell death and inflammation: an auto-amplification loop causes organ failure. *Nat. Rev. Immunol.* **14**, 759–767 (2014).

55. Bonavia, A. & Singbartl, K. A review of the role of immune cells in acute kidney injury. *Pediatr. Nephrol.* **33**, 1629–1639 (2018).

56. Afsar, B., Afsar, R.E., Dagel, T., Kaya, E., Erus, S., Ortiz, A., Covic, A. & Kanbay, M. Capillary rarefaction from the kidney point of view. *Clin. Kidney J.* **11**, 295–301 (2018).

57. Li, L. & Okusa, M. D. Macrophages, dendritic cells, and kidney ischemia-reperfusion injury. *Semin. Nephrol.* **30**, 268–277 (2010).

58. Situmorang, G. R. & Sheerin, N. S. Ischaemia reperfusion injury: mechanisms of progression to chronic graft dysfunction. *Pediatr. Nephrol.* **34**, 951–963 (2019).

59. Kimura, T., Isaka, Y. & Yoshimori, T. Autophagy and kidney inflammation. *Autophagy* **13**, 997 (2017).

60. Mulay, S. R., Linkermann, A. & Anders, H. J. Necroinflammation in Kidney Disease. *J. Am. Soc. Nephrol.* **27**, 27–39 (2016).

61. Tian, S. & Chen, S.-Y. Macrophage polarization in kidney diseases. *Macrophage* **2**, (2015).

62. da Silva, L. B. L., Palma, P. V. B., Cury, P. M. & Bueno, V. Evaluation of stem cell administration in a model of kidney ischemia-reperfusion injury. *Int. Immunopharmacol.* **7**, 1609–1616 (2007).

63. Scheller, J., Chalaris, A., Schmidt-Arras, D. & Rose-John, S. The pro- and anti-inflammatory properties of the cytokine interleukin-6. *Biochim. Biophys. Acta - Mol. Cell Res.* **1813**, 878–888 (2011).

64. Huen, S. C. *et al.* GM-CSF Promotes Macrophage Alternative Activation after Renal Ischemia/Reperfusion Injury. *J. Am. Soc. Nephrol.* **26**, 1334–1345 (2015).

65. Ferenbach, D. A. & Bonventre, J. V. ScienceDirect Acute kidney injury and chronic kidney disease : From the laboratory to the clinic §. 41–48 (2016).

66. Lazzeri, E. *et al.* Endocycle-related tubular cell hypertrophy and progenitor proliferation recover renal function after acute kidney injury. *Nat. Commun. 2018 91* **9**, 1–18 (2018).

67. Humphreys, B. D. *et al.* Intrinsic Epithelial Cells Repair the Kidney after Injury. *Cell Stem Cell* **2**, 284–291 (2008).

68. Anders, H. J. Immune system modulation of kidney regeneration - mechanisms and implications. *Nat. Rev. Nephrol.* **10**, 347–358 (2014).

69. Lazzeri, E., Angelotti, M.L., Peired, A., Conte, C., Marschner, J.A., Maggi, L., Mazzinghi, B., Lombardi, D., Melica, M.E., Nardi, S., Ronconi, E., Sisti, A., Antonelli, G., Becherucci, F., De Chiara, L., Guevara, R.R., Burger, A., Schaefer, B., Annunziato, F., Anders, H.J., Lasagni, L. & Romagnani, P. Endocycle-related tubular cell hypertrophy and progenitor proliferation recover renal function after acute kidney injury. doi:10.1038/s41467-018-03753-4

70. Chambers, B. E. & Wingert, R. A. Renal progenitors: Roles in kidney disease and regeneration. *World J. Stem Cells* **8**, 367 (2016).

71. Duffield, J. S. & Bonventre, J. V. Kidney tubular epithelium is restored without replacement with bone marrow-derived cells during repair after ischemic injury. *Kidney Int.* **68**, 1956–1961 (2005).

72. Witzgall, R., Brown, D., Schwarz, C. & Bonventre, J. V. Localization of proliferating cell nuclear antigen, vimentin, c-Fos, and clusterin in the postischemic kidney. Evidence for a heterogenous genetic response among nephron segments, and a large pool of mitotically active and dedifferentiated cells. *J. Clin. Invest.* **93**, 2175–88 (1994).

73. Bonventre, J. V. & Yang, L. Cellular pathophysiology of ischemic acute kidney injury. *J. Clin. Invest.* **121**, 4210–4221 (2011).

74. Oliver, J. A., Maarouf, O., Cheema, F. H., Martens, T. P. & Al-Awqati, Q. The renal papilla is a niche for adult kidney stem cells. *J. Clin. Invest.* **114**, 795–804 (2004).

75. Rath, M., Müller, I., Kropf, P., Closs, E. I. & Munder, M. Metabolism via Arginase or Nitric Oxide Synthase: Two Competing Arginine Pathways in Macrophages. *Front. Immunol.* **5**, (2014).

76. Mu, X., Li, Y. & Fan, G. C. TISSUE-RESIDENT MACROPHAGES IN THE CONTROL OF INFECTION AND RESOLUTION OF INFLAMMATION. *Shock* **55**, 14 (2021).

77. Jang, H. R. & Rabb, H. Immune cells in experimental acute kidney injury. *Nat. Rev. Nephrol.* **11**, 88–101 (2015).

78. Kim, J. & Hematti, P. Mesenchymal stem cell-educated macrophages: a novel type of alternatively activated macrophages. *Exp. Hematol.* **37**, 1445–53 (2009).

79. Duffield, J.S., Forbes, S.J., Constandinou, C.M., Clay, S., Partolina, M., Vuthoori, S., Wu, S., Lang, R. & Iredale, J.P. Selective depletion of macrophages reveals distinct, opposing roles during liver injury and repair. *J. Clin. Invest.* **115**, 56–65 (2005).

80. Lavin, Y., Mortha, A., Rahman, A. & Merad, M. Regulation of macrophage development and

function in peripheral tissues. *Nat. Rev. Immunol. 2015 1512* **15**, 731–744 (2015).

81. Lahmar, Q. *et al.* Tissue-resident versus monocyte-derived macrophages in the tumor microenvironment. *Biochim. Biophys. Acta* **1865**, 23–34 (2016).

82. Ko, J. H., Kim, H. J., Jeong, H. J., Lee, H. J. & Oh, J. Y. Mesenchymal Stem and Stromal Cells Harness Macrophage-Derived Amphiregulin to Maintain Tissue Homeostasis. *Cell Rep.* **30**, 3806-3820.e6 (2020).

83. Day, Y. J., Huang, L., Ye, H., Linden, J. & Okusa, M. D. Renal ischemia-reperfusion injury and adenosine 2A receptor-mediated tissue protection: role of macrophages. *Am. J. Physiol. Renal Physiol.* **288**, (2005).

84. Swirski, F.K., Nahrendorf, M., Etzrodt, M., Wildgruber, M., Cortez-Retamozo, V., Panizzi, P., Figueiredo, J.L., Kohler, R.H., Chudnovskiy, A., Waterman, P., Aikawa, E., Mempel, T.R., Libby, P., Weissleder R. & Pittet, M.J. Identification of splenic reservoir monocytes and their deployment to inflammatory sites. *Science (80-.).* **325**, 612–616 (2009).

85. Zhang, X., Goncalves, R. & Mosser, D. M. The isolation and characterization of murine macrophages. *Curr. Protoc. Immunol.* **Chapter 14**, Unit 14.1 (2008).

86. Chinetti-Gbaguidi, G. & Staels, B. Current Opinion in Lipidology Macrophage polarization in metabolic disorders : functions and regulation. *Curr. Opin. Lipidol.* **22**, 365–372 (2011).

87. Orekhov, A.N., Orekhova, N.A., Nikiforov, N.G., Myasoedova, V.A., Grechko, A.V., Romanenko, E.B., Zhang, D., and Chistiakov, D.A. Monocyte differentiation and macrophage polarization. *Vessel Plus* **3**, 10 (2019).

88. Mosser, D. M. & Edwards, J. P. Exploring the full spectrum of macrophage activation. *Nat. Rev. Immunol. 2008 812* **8**, 958–969 (2008).

89. Mills, C. D. Anatomy of a discovery: M1 and M2 macrophages. *Front. Immunol.* **6**, 212 (2015).

90. Wang, N., Liang, H. & Zen, K. Molecular mechanisms that influence the macrophage m1-m2 polarization balance. *Front. Immunol.* **5**, 614 (2014).

91. Chen, L., Wang, S., Wang, Y., Zhang, W., Ma, K., Hu, C., Zhu, H., Liang, S., Liu, M. & Xu N. IL-6 influences the polarization of macrophages and the formation and growth of colorectal tumor. *Oncotarget* **9**, 17443–17454 (2018).

92. Vasandan, A.B., Jahnavi, S., Shashan,k C., Prasad, P., Kumar, A. & Prasanna, S.J. Human Mesenchymal stem cells program macrophage plasticity by altering their metabolic status via a PGE 2-dependent mechanism OPEN. *Nat. Publ. Gr.* (2016). doi:10.1038/srep38308

93. Mantovani, A., Sica, A., Sozzani, S., Allavena, P., Vecchi, A. & Locati M. The chemokine system in diverse forms of macrophage activation and polarization. *Trends Immunol.* **25**, 677–686 (2004).

94. Meng, X.-M., Tang, P. M.-K., Li, J. & Lan, H. Y. Macrophage Phenotype in Kidney Injury and Repair. *Kidney Dis.* **1**, 138–146 (2015).

95. Mills, C. D., Kincaid, K., Alt, J. M., Heilman, M. J. & Hill, A. M. M-1/M-2 macrophages and the Th1/Th2 paradigm. *J. Immunol.* **164**, 6166–6173 (2000).

96. Kuroda, E., Sugiura, T., Zeki, K., Yoshida, Y. & Yamashita, U. Sensitivity Difference to the Suppressive Effect of Prostaglandin E2 Among Mouse Strains: A Possible Mechanism to Polarize Th2 Type Response in BALB/c Mice. *J. Immunol.* **164**, 2386–2395 (2000).

97. Orecchioni, M., Ghosheh, Y., Pramod, A. B. & Ley, K. Macrophage Polarization: Different Gene Signatures in M1(LPS+) vs. Classically and M2(LPS-) vs. Alternatively Activated Macrophages. *Front. Immunol.* **10**, (2019).

98. Leibacher, J. & Henschler, R. Biodistribution, migration and homing of systemically applied mesenchymal stem/stromal cells Mesenchymal Stem/Stromal Cells - An update. *Stem Cell Res. Ther.* **7**, 1–12 (2016).

99. Mosser, D. M. The many faces of macrophage activation. *J. Leukoc. Biol.* **73**, 209–212 (2003).

100. Lorenzi, W., Goncalves, F.D.C., Scheider, N., Silva, E.F., Paz, A.H.D.R. & Saueressig, M.G.Effect of repeated administration of adipocyte-derived mesenchymal stem cells on a murine model of bronchiolitis obliterans. *Interact. Cardiovasc. Thorac. Surg.* **19**, S86–S86 (2014).

101. Kiyama, K., Chen, C., Wang, D., Xu, X., Qu, C., Yamaza, T., Cai, T., Chen, W., Sun, L. & Shi, S. Mesenchymal-stem-cell-induced immunoregulation involves FAS-ligand-/FAS-mediated T cell apoptosis. *Cell Stem Cell* **10**, 544–55 (2012).

102. Anders, H. J. & Ryu, M. Renal microenvironments and macrophage phenotypes determine progression or resolution of renal inflammation and fibrosis. *Kidney Int.* **80**, 915–925 (2011).

103. Italiani, P. & Boraschi, D. From Monocytes to M1/M2 Macrophages: Phenotypical vs. Functional Differentiation. *Front. Immunol.* **5**, (2014).

104. Shaw, I., Rider, S., Mullins, J., Hughes, J. & Péault, B. Pericytes in the renal vasculature: roles in health and disease. *Nat. Rev. Nephrol. 2018 148* **14**, 521–534 (2018).

105. Ferenbach, D. A. & Bonventre, J. V. Acute kidney injury and chronic kidney disease: From the laboratory to the clinic. *Nephrol. Ther.* **12 Suppl 1**, S41–S48 (2016).

106. Hauser, P.V., De Fazio, R., Bruno, S., Sdei, S., Grange, C., Bussolati, B., Benedetto, C. & Camussi, G. Stem cells derived from human amniotic fluid contribute to acute kidney injury recovery. *Am. J. Pathol.* **177**, 2011–21 (2010).

107. Martinez, F. O., Sica, A., Mantovani, A. & Locati, M. Macrophage activation and polarization. *Front. Biosci.* **13**, 453–461 (2008).

108. Edwards, J. P., Zhang, X. & Mosser, D. M. The expression of heparin-binding epidermal growth factor-like growth factor by regulatory macrophages. *J. Immunol.* **182**, 1929–39 (2009).

109. Sanz, A. B., Sanchez-Niño, M. D., Martín-Cleary, C., Ortiz, A. & Ramos, A. M. Progress in the development of animal models of acute kidney injury and its impact on drug discovery. *Expert Opin. Drug Discov.* **8**, 879–895 (2013).

110. Hosszu, A., Kaucsar, T., Seeliger, E. & Fekete, A. Animal Models of Renal Pathophysiology and Disease. *Methods Mol. Biol.* **2216**, 27–44 (2021).

111. Zager, R. A. Progression from acute kidney injury to chronic kidney disease: clinical and experimental insights and queries. *Nephron. Clin. Pract.* **127**, 46–50 (2014).

112. Basile, D. P., Donohoe, D., Roethe, K. & Osborn, J. L. Renal ischemic injury results in permanent damage to peritubular capillaries and influences long-term function. *Am. J. Physiol. Renal Physiol.* **281**, F887–F899 (2001).

113. Basile, D.P., Friedrich, J.L., Spahic, J., Knipe, N., Mang, H., Leonard, E.C., Changizi-Ashtiyani, S., Bacallao, R.L., Molitoris, B.A. & Sutton, T.A. Impaired endothelial proliferation and mesenchymal transition contribute to vascular rarefaction following acute kidney injury. *Am.*

J. Physiol. Renal Physiol. **300**, (2011).

114. Scarfe, L., Menshikh, A., Newton, E., Zhu, Y., Delgado, R., Finney, C. & de Caestecker, M.P. Long-term outcomes in mouse models of ischemia-reperfusion-induced acute kidney injury. *Am J Physiol Ren. Physiol* **317**, 1068–1080 (2019).

115. What is a mouse model? Available at: https://www.jax.org/why-the-mouse/model. (Accessed: 11th February 2023)

116. Deusem, T., Stubbendorff, M., Tang-Quan, K., Phillips, N., Kay, M.A., Eiermann, T., Phan, T.T., Volk, H.D., Reichenspurner, H., Robbins, R.C. & Schrepfer, S. Immunogenicity and immunomodulatory properties of umbilical cord lining mesenchymal stem cells. *Cell Transplant.* **20**, 655–667 (2011).

117. Németh, K., Leelahavanichkul, A., Yuen, P.S., Mayer, B., Parmelee, A., Doi, K., Robey, P.G., Leelahavanichkul, K., Koller, B.H., Brown, J.M., Hu, X., Jelinek, I., Star, R.A. & Mezey, E. Bone marrow stromal cells attenuate sepsis via prostaglandin E2–dependent reprogramming of host macrophages to increase their interleukin-10 production. *Nat. Med.* **15**, 42–49 (2009).

118. Sharkey, J., Ressel, L., Brillant, N., Scarfe, L., Wilm, B., Park, B.K. & Murray, P. A Noninvasive Imaging Toolbox Indicates Limited Therapeutic Potential of Conditionally Activated Macrophages in a Mouse Model of Multiple Organ Dysfunction. *Stem Cells Int.* **2019**, (2019).

119. Jang, M.J., You, D., Park, J.Y., Kim, K., Aum, J., Lee, C., Song, G., Shin, H.C., Suh, N., Kim, Y.M. & Kim, C.S. Hypoxic Preconditioned Mesenchymal Stromal Cell Therapy in a Rat Model of Renal Ischemia-reperfusion Injury: Development of Optimal Protocol to Potentiate Therapeutic Efficacy. *Int. J. stem cells* **11**, 157–167 (2018).

120. Hu, J., Zhang, L., Wang, N., Ding, R., Cui, S., Zhu, F., Xie, Y., Sun, X., Wu, D., Hong, Q., Li, Q., Shi, S., Liu, X. & Chen, X. Mesenchymal stem cells attenuate ischemic acute kidney injury by inducing regulatory T cells through splenocyte interactions. *Kidney Int.* **84**, 521–531 (2013).

121. Ohtaki, H., Ylostalo, J.H., Foraker, J.E., Robinson, A.P., Reger, R.L., Shioda, S. & Prockop, D.J. Stem/progenitor cells from bone marrow decrease neuronal death in global ischemia by modulation of inflammatory/immune responses. *Proc. Natl. Acad. Sci. U. S. A.* **105**, 14638–43 (2008).

122. Ren, Y., Xie, Y., Jiang, G., Fan, J., Yeung, J., Li, W., Tam, P.K. & Savill, J. Apoptotic Cells Protect Mice against Lipopolysaccharide-Induced Shock. *J. Immunol.* **180**, 4978–4985 (2008).

123. Sanmarco, L.M., Ponce, N.E., Visconti, L.M., Eberhardt, N., Theumer, M.G., Minguez, Á.R. & Aoki, M.P. IL-6 promotes M2 macrophage polarization by modulating purinergic signaling and regulates the lethal release of nitric oxide during Trypanosoma cruzi infection. *Biochim. Biophys. Acta - Mol. Basis Dis.* **1863**, 857–869 (2017).

124. Geng, Y., Zhang, L., Fu, B., Zhang, J., Hong, Q., Hu, J., Li, D., Luo, C., Cui, S., Zhu, F. & Chen, X. Mesenchymal stem cells ameliorate rhabdomyolysis-induced acute kidney injury via the activation of M2 macrophages. *Stem Cell Res. Ther.* **5**, (2014).

125. Jaworska, K., Ratajczak, J., Huang, L., Whalen, K., Yang, M., Stevens, B.K. & Kinsey, G.R. Both PD-1 Ligands Protect the Kidney from Ischemia Reperfusion Injury. *J. Immunol.* **194**, 325–333 (2015).

126. Lee, H., Nho, D., Chung, H.S., Lee, H., Shin, M.K., Kim, S.H. & Bae, H. CD4+CD25+ regulatory T cells attenuate cisplatin-induced nephrotoxicity in mice. *Kidney Int.* **78**, 1100–1109 (2010).

127. Mills, C. D., Kincaid, K., Alt, J. M., Heilman, M. J. & Hill, A. M. M-1/M-2 Macrophages and the Th1/Th2 Paradigm. *J. Immunol.* **164**, 6166–6173 (2000).

128. Sellers, R. S., Clifford, C. B., Treuting, P. M. & Brayton, C. Immunological variation between inbred laboratory mouse strains: Points to consider in phenotyping genetically immunomodified mice. *Vet. Pathol.* **49**, 32–43 (2012).

129. Whalen, H., Shiels, P., Littlejohn, M. & Clancy, M. A novel rodent model of severe renal ischemia reperfusion injury. *Ren. Fail.* **38**, 1694–1701 (2016).

130. Packialakshmi, B., Stewart, I. J., Burmeister, D. M., Chung, K. K. & Zhou, X. Large animal models for translational research in acute kidney injury. *Ren. Fail.* **42**, 1042 (2020).

131. de Caestecker, M. & Harris, R. Translating Knowledge Into Therapy for Acute Kidney Injury. *Semin. Nephrol.* **38**, 88–97 (2018).

132. Skrypnyk, N. I., Siskind, L. J., Faube, S. & de Caestecker, M. P. Bridging translation for acute kidney injury with better preclinical modeling of human disease. *https://doi.org/10.1152/ajprenal.00552.2015* **310**, F972–F984 (2016).

133. Li, L., Wei, W., Li, Z., Chen, H., Li, Y., Jiang, W., Chen, W., Kong, G., Yang, J. & Li Z. The spleen promotes the secretion of CCL2 and supports an M1 dominant phenotype in hepatic macrophages during liver fibrosis. *Cell. Physiol. Biochem.* **51**, 557–574 (2018).

134. Den Haan, J. M. M. & Kraal, G. Innate Immune Functions of Macrophage Subpopulations in the Spleen. *J. Innate Immun.* **4**, 437 (2012).

135. Borges da Silva, H., Fonseca, R., Pereira, R.M., Cassado Ados, A., Álvarez, J.M. & D'Império Lima, M.R. Splenic macrophage subsets and their function during blood-borne infections. *Front. Immunol.* **6**, 480 (2015).

136. A-Gonzalez, N. & Castrillo, A. Origin and specialization of splenic macrophages. *Cell. Immunol.* **330**, 151–158 (2018).

137. Gordon, S. & Plüddemann, A. Tissue macrophages: heterogeneity and functions. *BMC Biol.* **15**, (2017).

138. Andrés-Hernando, A., Altmann, C., Ahuja, N., Lanaspa, M.A., Nemenoff, R., He, Z., Ishimoto, T., Simpson, P.A., Weiser-Evans, M.C., Bacalja, J. & Faubel, S. Splenectomy exacerbates lung injury after ischemic acute kidney injury in mice. *Am. J. Physiol. - Ren. Physiol.* **301**, F907 (2011).

139. Kim, E., Yang, J., D Beltran, C. & Cho, S. Role of spleen-derived monocytes/macrophages in acute ischemic brain injury. *J. Cereb. Blood Flow Metab.* **34**, 1411 (2014).

140. Gigliotti, J. C. & Okusa, M. D. The Spleen: The Forgotten Organ in Acute Kidney Injury of Critical Illness. *Nephron. Clin. Pract.* **127**, 153 (2014).

141. Platts, M. M., Anastassiades, E., Sheriff, S., Smith, S. & Bartolo, D. C. Spleen size in chronic renal failure. *Br. Med. J. (Clin. Res. Ed).* **289**, 1415 (1984).

142. Hoste, E.A.J., Kellum, J.A., Selby, N.M., Zarbock, A., Palevsky, P.M., Bagshaw, S.M., Goldstein, S.L., Cerdá, J. & Chawla, L.S. Global epidemiology and outcomes of acute kidney injury. *Nat. Rev. Nephrol. 2018 1410* **14**, 607–625 (2018).

143. Chawla, L.S., Bellomo, R., Bihorac, A,. Goldstein, S.L., Siew, E.D., Bagshaw, S.M., Bittleman, D., Cruz, D., Endre, Z., Fitzgerald, R.L., Forni, L., Kane-Gill, S.L., Hoste, E., Koyner, J., Liu, K.D.,

Macedo, E., Mehta, R., Murray, P. & Nadim, M. Acute kidney disease and renal recovery: consensus report of the Acute Disease Quality Initiative (ADQI) 16 Workgroup. *Nat. Rev. Nephrol. 2017 134* **13**, 241–257 (2017).

144. Jin, H., Zhang, Y., Din,g Q., Wang, S.S., Rastogi, P., Dai, D.F., Lu, D., Purvis, M., Cao, C., Wang, A., Liu, D., Ren, C., Elhadi, S., Hu, M.C., Chai, Y., Zepeda-Orozco, D., Campisi, J. & Attanasio, M. Epithelial innate immunity mediates tubular cell senescence after kidney injury. *JCI Insight* **4**, (2019).

145. Bucaloiu, I. D., Kirchner, H. L., Norfolk, E. R., Hartle, J. E. & Perkins, R. M. Increased risk of death and de novo chronic kidney disease following reversible acute kidney injury. *Kidney Int.* **81**, 477–485 (2012).

146. CKD Stages | The UK Kidney Association. Available at: https://ukkidney.org/health-professionals/information-resources/uk-eckd-guide/ckd-stages. (Accessed: 27th December 2022)

147. Yang, L., Besschetnova, T. Y., Brooks, C. R., Shah, J. V. & Bonventre, J. V. Epithelial cell cycle arrest in G2/M mediates kidney fibrosis after injury. *Nat. Med.* **16**, 535 (2010).

148. Diagnosis | Diagnosis | Chronic kidney disease | CKS | NICE. Available at: https://cks.nice.org.uk/topics/chronic-kidney-disease/diagnosis/diagnosis/. (Accessed: 27th December 2022)

149. Rota, C., Morigi, M., Cerullo, D., Introna, M., Colpani, O., Corna, D., Capelli, C., Rabelink, T.J., Leuning, D.G., Rottoli, D., Benigni, A., Zoja, C. & Remuzzi, G. Therapeutic potential of stromal cells of non-renal or renal origin in experimental chronic kidney disease. *Stem Cell Res. Ther.* **9**, (2018).

150. Lee, H., Fessler, M. B., Qu, P., Heymann, J. & Kopp, J. B. Macrophage polarization in innate immune responses contributing to pathogenesis of chronic kidney disease. *BMC Nephrol.* **21**, (2020).

151. Carney, E. F. The impact of chronic kidney disease on global health. *Nat. Rev. Nephrol.* **16**, (2020).

152. GBD Chronic Kidney Disease Collaboration. Global, regional, and national burden of chronic kidney disease, 1990–2017: a systematic analysis for the Global Burden of Disease Study 2017. *Lancet* **395**, 709–733 (2020).

153. Rapa, S. F., Di Iorio, B. R., Campiglia, P., Heidland, A. & Marzocco, S. Inflammation and Oxidative Stress in Chronic Kidney Disease—Potential Therapeutic Role of Minerals, Vitamins and Plant-Derived Metabolites. *Int. J. Mol. Sci.* **21**, (2020).

154. Akchurin, O. M. & Kaskel, F. Update on Inflammation in Chronic Kidney Disease. *Blood Purif.* **39**, 84–92 (2015).

155. Hsu, R. K. & Hsu, C. yuan. The Role of Acute Kidney Injury in Chronic Kidney Disease. *Semin. Nephrol.* **36**, 283–292 (2016).

156. Jones, J., Holmen, J., De Graauw, .J, Jovanovich, A., Thornton, S. & Chonchol, M. Association of complete recovery from acute kidney injury with incident CKD stage 3 and all-cause mortality. *Am. J. Kidney Dis.* **60**, 402–408 (2012).

157. Tögel, F. E. & Westenfelder, C. Mesenchymal stem cells: a new therapeutic tool for AKI. *Nat. Rev. Nephrol.* **6**, 179–183 (2010).

158. Parikh, C. R., Coca, S. G., Wang, Y., Masoudi, F. A. & Krumholz, H. M. Long-term prognosis of acute kidney injury after acute myocardial infarction. *Arch. Intern. Med.* **168**, 987–995 (2008).

159. Newsome, B.B., Warnock, D.G., McClellan, W.M., Herzog, C.A., Kiefe, C.I., Eggers, P.W. & Allison, J.J. Long-term risk of mortality and end-stage renal disease among the elderly after small increases in serum creatinine level during hospitalization for acute myocardial infarction. *Arch. Intern. Med.* **168**, 609–616 (2008).

160. Lo, L.J., Go, A.S., Chertow, G.M., McCulloch, C.E., Fan, D., Ordoñez, J.D. & Hsu, C.Y. Dialysis-requiring acute renal failure increases the risk of progressive chronic kidney disease. *Kidney Int.* **76**, 893 (2009).

161. Hsu, C.Y., Chertow, G.M., McCulloch, C.E., Fan, D., Ordoñez, J.D. & Go A.S. Nonrecovery of kidney function and death after acute on chronic renal failure. *Clin. J. Am. Soc. Nephrol.* **4**, 891–898 (2009).

162. Thakar, C. V., Christianson, A., Himmelfarb, J. & Leonard, A. C. Acute kidney injury episodes and chronic kidney disease risk in diabetes mellitus. *Clin. J. Am. Soc. Nephrol.* **6**, 2567–2572 (2011).

163. James, M.T., Hemmelgarn, B.R., Wiebe, N., Pannu, N., Manns, B.J., Klarenbach, S.W. & Tonelli, M. Alberta Kidney Disease Network. Glomerular filtration rate, proteinuria, and the incidence and consequences of acute kidney injury: a cohort study. *Lancet (London, England)* **376**, 2096–2103 (2010).

164. Hsu, C.Y., Ordoñez, J.D., Chertow, G.M., Fan, D., McCulloch, C.E. & Go, A.S. The risk of acute renal failure in patients with chronic kidney disease. *Kidney Int.* **74**, 101–107 (2008).

165. Li, W., Zhang, Q., Wang, M., Wu, H., Mao, F., Zhang, B., Ji, R., Gao, S., Sun, Z., Zhu, W., Qian, H., Chen, Y. & Xu, W. Macrophages are involved in the protective role of human umbilical cord-derived stromal cells in renal ischemia–reperfusion injury. *Stem Cell Res.* **10**, 405–416 (2013).

166. Bhatraju, P.K., Zelnick, L.R., Chinchilli, V.M., Moledina, D.G., Coca, S.G., Parikh, C.R., Garg, A.X., Hsu, C.Y., Go, A.S., Liu, K.D., Ikizler, T.A., Siew, E.D., Kaufman, J.S., Kimmel, P.L., Himmelfarb, J. & Wurfel, M.M. Association Between Early Recovery of Kidney Function After Acute Kidney Injury and Long-term Clinical Outcomes. *JAMA Netw. Open* **3**, e202682–e202682 (2020).

167. Nash, D. M., Przech, S., Wald, R. & O'Reilly, D. Systematic review and meta-analysis of renal replacement therapy modalities for acute kidney injury in the intensive care unit. *J. Crit. Care* **41**, 138–144 (2017).

168. Gilbert, J., Lovibond, K., Mooney, A. & Dudley, J. Renal replacement therapy: summary of NICE guidance. *BMJ* **363**, (2018).

169. NICE. Overview | Renal replacement therapy and conservative management | Guidance | NICE. (2018). Available at: https://www.nice.org.uk/guidance/ng107. (Accessed: 3rd December 2022)

170. NICE. Immunosuppressive therapy for kidney transplant in adults. (2022). Available at: https://www.nice.org.uk/guidance/ta481/resources/immunosuppressive-therapy-for-kidney-transplant-in-adults-pdf-82605021450181#:~:text=It%20recommended%20basiliximab%2C%20daclizumab%2C%20tacrolimus,for%20kidney%20transplant%20in%20adults.. (Accessed: 3rd December 2022)

171. Suarez-Pierre, A., Choudhury, R., Carroll, A.M., King, R.W., Iguidbashian, J., Cotton, J., Colborn, K.L., Kennealey, P.T., Cleveland, J.C., Pomfret, E. & Fullerton, D.A. Measuring the effect of the COVID-19 pandemic on solid organ transplantation. *Am. J. Surg.* **224**, 437 (2022).

172. Legeai, C., Savoye, E., Cantrelle, C., Jasseron, C., Santin, G., Brousse, G., Duman, M., Foubert, F., Mahmoudi, R., Deshayes, A., Antoine, C. & Kerbaul, F. Impact of COVID-19 on 2020 transplant activity and waiting lists in France. *J. Liver Transplant.* **5**, 100051 (2022).

173. Sharma, V., Shaw., A., Lowe, M., Summers, A., van Dellen, D. & Augustine, T. The impact of the COVID-19 pandemic on renal transplantation in the UK. *Clin. Med. (Northfield. Il).* **20**, e82 (2020).

174. Department of Health & Social Care. Organs and tissues to be excluded from the opt-out organ donation system – quick read - GOV.UK. (2020). Available at: https://www.gov.uk/government/consultations/opt-out-organ-donation-organs-and-tissues-excluded-from-the-new-system/organs-and-tissues-to-be-excluded-from-the-opt-out-organ-donation-system-quick-read. (Accessed: 28th December 2022)

175. Ravaioli M, De Pace V, Angeletti A, Comai G, Vasuri F, Baldassarre M, Maroni L, Odaldi F, Fallani G, Caraceni P, Germinario G, Donadei C, Malvi D, Del Gaudio M, Bertuzzo VR, Siniscalchi A, Ranieri VM, D'Errico A, Pasquinelli G, Morelli MC, Pinna AD, Cescon M, La Manna G. Hypothermic Oxygenated New Machine Perfusion System in Liver and Kidney Transplantation of Extended Criteria Donors:First Italian Clinical Trial. *Sci. Reports 2020 101* **10**, 1–11 (2020).

176. NHS Organ Donation. New UK strategy sets out ambition to be world leaders in organ donation and transplantation - NHS Organ Donation. (2021). Available at: https://www.organdonation.nhs.uk/get-involved/news/new-uk-strategy-sets-out-ambition-to-be-world-leaders-in-organ-donation-and-transplantation/. (Accessed: 28th December 2022)

177. NIH - National Institute of Diabetes and Digestive and Kidney Diseases. Conservative Management for Kidney Failure | NIDDK. (2018). Available at: https://www.niddk.nih.gov/health-information/kidney-disease/kidney-failure/conservative-management. (Accessed: 28th December 2022)

178. Selmani, Z., Naji, A., Zidi, I., Favier, B., Gaiffe, E., Obert, L., Borg, C., Saas, P., Tiberghien, P., Rouas-Freiss, N., Carosella, E.D. & Deschaseaux, F. Human Leukocyte Antigen-G5 Secretion by Human Mesenchymal Stem Cells Is Required to Suppress T Lymphocyte and Natural Killer Function and to Induce CD4 $^{+}$ CD25 ^{high} FOXP3 $^{+}$ Regulatory T Cells. *Stem Cells* **26**, 212–222 (2008).

179. Furlani, D., Ugurlucan, M., Ong, L., Bieback, K., Pittermann, E., Westien, I., Wang, W., Yerebakan, C., Li, W., Gaebel, R., Li, R.K., Vollmar, B., Steinhoff, G. & Ma, N. Is the intravascular administration of mesenchymal stem cells safe?: Mesenchymal stem cells and intravital microscopy. *Microvasc. Res.* **77**, 370–376 (2009).

180. Taha, S., Volkme,r E., Haas, E., Alberton, P., Straub, T., David-Rus, D., Aszodi, A., Giunta, R. & Saller, M.M. Differences in the Inflammatory Response of White Adipose Tissue and Adipose-Derived Stem Cells. *Int. J. Mol. Sci.* **21**, 1086 (2020).

181. Le Blanc, K. & Mougiakakos, D. Multipotent mesenchymal stromal cells and the innate immune system. *Nat. Rev. Immunol.* **12**, 383–396 (2012).

182. Lee, J. W., Fang, X., Krasnodembskaya, A., Howard, J. P. & Matthay, M. A. Concise review:

Mesenchymal stem cells for acute lung injury: role of paracrine soluble factors. *Stem Cells* **29**, 913–9 (2011).

183. Khan, R. S. & Newsome, P. N. A comparison of phenotypic and functional properties of mesenchymal stromal cells and multipotent adult progenitor cells. *Front. Immunol.* **10**, 1952 (2019).

184. Li, X., Bai, J., Ji, X., Li, R., Xuan, Y. & Wang, Y. Comprehensive characterization of four different populations of human mesenchymal stem cells as regards their immune properties, proliferation and differentiation. *Int. J. Mol. Med.* **34**, 695–704 (2014).

185. Nancarrow-Lei, R., Mafi, P., Mafi, R. & Khan, W. A Systemic Review of Adult Mesenchymal Stem Cell Sources and their Multilineage Differentiation Potential Relevant to Musculoskeletal Tissue Repair and Regeneration. *Curr. Stem Cell Res. Ther.* **12**, (2017).

186. Roemeling-van Rhijn, M., Khairoun, M., Korevaar, S.S., Lievers, E., Leuning, D.G., Ijzermans, J.N., Betjes, M.G., Genever, P.G., van Kooten, C., de Fijter, H.J., Rabelink, T.J., Baan, C.C., Weimar, W., Roelofs, H., Hoogduijn, M.J. & Reinders, M.E. Human Bone Marrow- and Adipose Tissue-derived Mesenchymal Stromal Cells are Immunosuppressive *In vitro* and in a Humanized Allograft Rejection Model. *J. Stem Cell Res. Ther.* **Suppl 6**, 20780–20780 (2013).

187. Kozlowska, U., Krawczenko., A, Futoma., K., Jurek, T., Rorat, M., Patrzalek, D. & Klimczak, A. Similarities and differences between mesenchymal stem/progenitor cells derived from various human tissues. *World J. Stem Cells* **11**, 347–374 (2019).

188. Wan,g Q., Yang, Q., Wang, Z., Tong, H., Ma, L., Zhang, Y., Shan, F., Meng, Y. & Yuan, Z. Comparative analysis of human mesenchymal stem cells from fetal-bone marrow, adipose tissue, and Warton's jelly as sources of cell immunomodulatory therapy. *Hum. Vaccin. Immunother.* **12**, 85–96 (2016).

189. Baksh, D., Yao, R. & Tuan, R. S. Comparison of proliferative and multilineage differentiation potential of human mesenchymal stem cells derived from umbilical cord and bone marrow. *Stem Cells* **25**, 1384–1392 (2007).

190. Kaundal, U., Bagai, U. & Rakha, A. Immunomodulatory plasticity of mesenchymal stem cells: a potential key to successful solid organ transplantation. *J. Transl. Med. 2018 161* **16**, 1–16 (2018).

191. Imberti, B., Morigi, M., Tomasoni, S., Rota, C., Corna, D., Longaretti, L., Rottoli, D., Valsecchi, F., Benigni, A., Wang, J., Abbate, M., Zoja, C. & Remuzzi, G. Insulin-like growth factor-1 sustains stem cell mediated renal repair. *J. Am. Soc. Nephrol.* **18**, 2921–8 (2007).

192. Chen, Y.T., Sun, C.K., Lin, Y.C., Chang, L.T., Chen, Y.L., Tsai, T.H., Chung, S.Y., Chua, S., Kao, Y.H., Yen, C.H., Shao, P.L., Chang, K.C., Leu, S. & Yip, H.K. Adipose-derived mesenchymal stem cell protects kidneys against ischemia-reperfusion injury through suppressing oxidative stress and inflammatory reaction. *J. Transl. Med.* **9**, (2011).

193. Morigi, M., Rota, C., Montemurro, T., Montelatici, E., Lo Cicero, V., Imberti, B., Abbate, M., Zoja, C., Cassis, P., Longaretti, L., Rebulla, P., Introna, M., Capelli, C., Benigni, A., Remuzzi, G. & Lazzari, L. Life-sparing effect of human cord blood-mesenchymal stem cells in experimental acute kidney injury. *Stem Cells* **28**, 513–522 (2010).

194. Sanchez-Diaz, M., Quiñones-Vico, M.I., Sanabria de la Torre, R., Montero-Vílchez, T., Sierra-Sánchez, A., Molina-Leyva, A. & Arias-Santiago, S. Biodistribution of Mesenchymal Stromal Cells after Administration in Animal Models and Humans: A Systematic Review. *J. Clin. Med.*

10, 2925 (2021).

195. Khedoe, P.P.S.J., de Kleijn, S., van Oeveren-Rietdijk, A.M., Plomp, J.J., de Boer, H.C., van Pel, M., Rensen, P.C.N., Berbée, J.F.P. & Hiemstra, P.S. Acute and chronic effects of treatment with mesenchymal stromal cells on LPS-induced pulmonary inflammation, emphysema and atherosclerosis development. *PLoS One* **12**, e0183741 (2017).

196. Leibacher, J., Dauber, K., Ehser ,S., Brixner, V., Kollar, K., Vogel, A., Spoh,n G., Schäfer, R., Seifried, E. & Henschler, R. Human mesenchymal stromal cells undergo apoptosis and fragmentation after intravenous application in immune-competent mice. *Cytotherapy* **19**, 61–74 (2017).

197. Leibacher, J. & Henschler, R. Biodistribution, migration and homing of systemically applied mesenchymal stem/stromal cells. *Stem Cell Res. Ther.* **7**, (2016).

198. Eggenhofer, E., Benseler, V., Kroemer, A., Popp, F.C., Geissler, E.K., Schlitt, H.J., Baan, C.C., Dahlke, M.H. & Hoogduijn, M.J. Mesenchymal stem cells are short-lived and do not migrate beyond the lungs after intravenous infusion. *Front. Immunol.* **3**, 1–8 (2012).

199. Lee, R.H., Pulin, A.A., Seo, M.J., Kota, D.J., Ylostalo, J., Larson, B.L., Semprun-Prieto, L., Delafontaine, P. & Prockop, D.J. Intravenous hMSCs improve myocardial infarction in mice because cells embolized in lung are activated to secrete the anti-inflammatory protein TSG-6. *Cell Stem Cell* **5**, 54–63 (2009).

200. Mäkelä, T., Takalo, R., Arvola, O., Haapanen, H., Yannopoulos, F., Blanco, R., Ahvenjärvi, L., Kiviluoma, K., Kerkelä, E., Nystedt, J., Juvonen, T. & Lehenkari, P. Safety and biodistribution study of bone marrow–derived mesenchymal stromal cells and mononuclear cells and the impact of the administration route in an intact porcine model. *Cytotherapy* **17**, 392–402 (2015).

201. Walczak, P., Zhang, J., Gilad, A.A., Kedziorek, D.A., Ruiz-Cabello, J., Young, R.G., Pittenger, M.F., van Zijl, P.C., Huang, J. & Bulte, J.W. Dual-modality monitoring of targeted intraarterial delivery of mesenchymal stem cells after transient ischemia. *Stroke* **39**, 1569–74 (2008).

202. Toupet, K., Maumus, M., Peyrafitte, J.A., Bourin, P., van Lent, P.L., Ferreira, R., Orsetti, B., Pirot, N., Casteilla, L., Jorgensen, C.. & Noël, D. Long-Term Detection of Human Adipose-Derived Mesenchymal Stem Cells After Intraarticular Injection in SCID Mice. *Arthritis Rheum.* **65**, 1786–1794 (2013).

203. Tobin, L. M., Healy, M. E., English, K. & Mahon, B. P. Human mesenchymal stem cells suppress donor CD4(+) T cell proliferation and reduce pathology in a humanized mouse model of acute graft-versus-host disease. *Clin. Exp. Immunol.* **172**, 333–348 (2013).

204. Aggarwal, S. & Pittenger, M. F. Human mesenchymal stem cells modulate allogeneic immune cell responses. *Blood* **105**, 1815–1822 (2005).

205. Dabrowska, S., Andrzejewska, A., Janowski, M. & Lukomska, B. Immunomodulatory and Regenerative Effects of Mesenchymal Stem Cells and Extracellular Vesicles: Therapeutic Outlook for Inflammatory and Degenerative Diseases. *Front. Immunol.* **11**, 3809 (2021).

206. Banas, A., Teratani, T., Yamamoto, Y., Tokuhara,, M., Takeshita F., Osaki, M., Kawamata, M., Kato, T., Okochi, H. & Ochiya, T. IFATS Collection: In Vivo Therapeutic Potential of Human Adipose Tissue Mesenchymal Stem Cells After Transplantation into Mice with Liver Injury. *Stem Cells* **26**, 2705–2712 (2008).

207. Tögel, F., Cohen, A., Zhang, P., Yan,g Y., Hu, Z. & Westenfelder, C. Autologous and allogeneic

marrow stromal cells are safe and effective for the treatment of acute kidney injury. *Stem Cells Dev.* **18**, 475–85 (2009).

208. Zhang, Q., Yang, Y.J., Wang, H., Dong, Q.T., Wang, T.J., Qian, H.Y. & Xu, H. Autophagy activation: a novel mechanism of atorvastatin to protect mesenchymal stem cells from hypoxia and serum deprivation via AMP-activated protein kinase/mammalian target of rapamycin pathway. *Stem Cells Dev.* **21**, 1321–32 (2012).

209. Wangler, S., Kamali, .A, Wapp, C., Wuertz-Kozak, K., Häckel, S., Fortes, C., Benneker, L.M., Haglund, L., Richards, R.G., Alini, M., Peroglio, M. & Grad, S. Uncovering the secretome of mesenchymal stromal cells exposed to healthy, traumatic, and degenerative intervertebral discs: a proteomic analysis. *Stem Cell Res. Ther.* **12**, 1–17 (2021).

210. Kang, J., Zhang, L., Luo, X., Ma, X., Wang, G., Yang, Y., Yan, Y., Qian, H., Zhang, X., Xu, W. & Mao, F. Systematic Exposition of Mesenchymal Stem Cell for Inflammatory Bowel Disease and Its Associated Colorectal Cancer. *Biomed Res. Int.* **2018**, (2018).

211. Spaggiari, G.M., Capobianco, A., Abdelrazik, H., Becchetti, F., Mingari, M.C. & Moretta, L. Mesenchymal stem cells inhibit natural killer-cell proliferation, cytotoxicity, and cytokine production: role of indoleamine 2,3-dioxygenase and prostaglandin E2. *Blood* **111**, 1327–33 (2008).

212. François, M., Romieu-Mourez, R., Li, M. & Galipeau, J. Human MSC Suppression Correlates With Cytokine Induction of Indoleamine 2,3-Dioxygenase and Bystander M2 Macrophage Differentiation. *Mol. Ther.* **20**, 187–195 (2012).

213. Gray, A., Schloss, R. S. & Yarmush, M. Donor variability among anti-inflammatory pre-activated mesenchymal stromal cells. *Technology* **4**, 201–215 (2016).

214. Liu, X.B., Chen, H., Chen, H.Q., Zhu, M.F., Hu, X.Y., Wang, Y.P., Jiang, Z., Xu, Y.C., Xiang, M.X. & Wang, J.A. Angiopoietin-1 preconditioning enhances survival and functional recovery of mesenchymal stem cell transplantation. *J. Zhejiang Univ. Sci. B* **13**, 616–23 (2012).

215. Maggini, J., Mirkin, G., Bognanni, I., Holmberg, J., Piazzón, I.M., Nepomnaschy, I., Costa, H., Cañones, C., Raiden, S., Vermeulen, M. & Geffner, J.R. Mouse bone marrow-derived mesenchymal stromal cells turn activated macrophages into a regulatory-like profile. *PLoS One* **5**, e9252 (2010).

216. François, M., Romieu-Mourez, R., Li, M. & Galipeau, J. Human MSC suppression correlates with cytokine induction of indoleamine 2,3-dioxygenase and bystander M2 macrophage differentiation. *Mol. Ther.* **20**, 187–195 (2012).

217. Akiyama, K., Chen, C,. Wang, D., Xu, X., Qu, C., Yamaza, T., Cai, T., Chen, W., Sun, L., Shi, S. Mesenchymal-stem-cell-induced immunoregulation involves FAS-ligand-/FAS-mediated T cell apoptosis. *Cell Stem Cell* **10**, 544–555 (2012).

218. Melief, S.M., Schrama, E., Brugman, M.H., Tiemessen, M.M., Hoogduijn, M.J., Fibbe, W.E. & Roelofs, H. Multipotent stromal cells induce human regulatory T cells through a novel pathway involving skewing of monocytes toward anti-inflammatory macrophages. *Stem Cells* **31**, 1980–1991 (2013).

219. Spaggiari, G. M., Abdelrazik, H., Becchetti, F. & Moretta, L. MSCs inhibit monocyte-derived DC maturation and function by selectively interfering with the generation of immature DCs: central role of MSC-derived prostaglandin E2. *Blood* **113**, 6576–83 (2009).

220. Ramasamy, R., Tong, C. K., Seow, H. F., Vidyadaran, S. & Dazzi, F. The immunosuppressive

effects of human bone marrow-derived mesenchymal stem cells target T cell proliferation but not its effector function. *Cell. Immunol.* **251**, 131–136 (2008).

221. Glennie, S., Soeiro, I., Dyson, P. J., Lam, E. W. F. & Dazzi, F. Bone marrow mesenchymal stem cells induce division arrest anergy of activated T cells. *Blood* **105**, 2821–2827 (2005).

222. Tse, W. T., Pendleton, J. D., Beyer, W. M., Egalka, M. C. & Guinan, E. C. Suppression of allogeneic T-cell proliferation by human marrow stromal cells: implications in transplantation. *Transplantation* **75**, 389–397 (2003).

223. Rozenberg, A., Rezk, A., Boivin, M.N., Darlington, P.J., Nyirenda, M., Li, R., Jalili, F., Winer, R., Artsy, E.A., Uccelli, A., Reese, J.S., Planchon, S.M., Cohen, J.A. & Bar-Or, A. Human Mesenchymal Stem Cells Impact Th17 and Th1 Responses Through a Prostaglandin E2 and Myeloid-Dependent Mechanism. *Stem Cells Transl. Med.* **5**, 1506–1514 (2016).

224. Morigi, M., Introna, M., Imberti, B., Corna, D., Abbate, M., Rota, C., Rottoli, D., Benigni, A., Perico, N., Zoja, C., Rambaldi, A., Remuzzi, A. & Remuzzi, G. Human bone marrow mesenchymal stem cells accelerate recovery of acute renal injury and prolong survival in mice. *Stem Cells* **26**, 2075–2082 (2008).

225. Morigi, M., Imberti, B., Zoja, C., Corna, D., Tomasoni, S., Abbate, M., Rottoli, D., Angioletti, S., Benigni, A., Perico, N., Alison, M. & Remuzzi, G. Mesenchymal stem cells are renotropic, helping to repair the kidney and improve function in acute renal failure. *J. Am. Soc. Nephrol.* **15**, 1794–804 (2004).

226. Kinomura, M., Kitamura, S., Tanabe, K., Ichinose, K., Hirokoshi, K., Takazawa, Y., Kitayama, H., Nasu, T., Sugiyama, H., Yamasaki, Y., Sugaya, T., Maeshima, Y. & Makino, H. Amelioration of Cisplatin-Induced Acute Renal Injury by Renal Progenitor-Like Cells Derived From the Adult Rat Kidney. *Cell Transplant.* **17**, 143–158 (2008).

227. Cao, H., Cheng, Y., Gao, H., Zhuang, J., Zhang, W., Bian, Q., Wang, F., Du, Y., Li Z., Kong, D., Ding, D. & Wang, Y. In Vivo Tracking of Mesenchymal Stem Cell-Derived Extracellular Vesicles Improving Mitochondrial Function in Renal Ischemia-Reperfusion Injury. *ACS Nano* **14**, 4014–4026 (2020).

228. da Silva, A. F., Silva, K., Reis, L. A., Teixeira, V. P. C. & Schor, N. Bone Marrow-Derived Mesenchymal Stem Cells and Their Conditioned Medium Attenuate Fibrosis in an Irreversible Model of Unilateral Ureteral Obstruction. *Cell Transplant.* **24**, 2657–2666 (2015).

229. Bi, B., Schmitt, R., Israilova, M., Nishio, H. & Cantley, L. G. Stromal cells protect against acute tubular injury via an endocrine effect. *J. Am. Soc. Nephrol.* **18**, 2486–96 (2007).

230. Morelli, A. E. & Larregina, A. T. Concise Review: Mechanisms behind apoptotic cell-based therapies against transplant rejection and graft versus host disease. *Stem Cells* **34**, 1142–1150 (2016).

231. Freire-de-Lima, C.G., Xiao, Y.Q., Gardai, S.J., Bratton, D.L., Schiemann, W.P. & Henson, P.M. Apoptotic cells, through transforming growth factor-beta, coordinately induce anti-inflammatory and suppress pro-inflammatory eicosanoid and NO synthesis in murine macrophages. *J. Biol. Chem.* **281**, 38376–84 (2006).

232. Bruno, S., Grange, C., Deregibus, M.C., Calogero, R.A., Saviozzi, S., Collino, F., Morando, L., Busca, A., Falda, M., Bussolati, B., Tetta, C. & Camussi, G. Mesenchymal stem cell-derived microvesicles protect against acute tubular injury. *J. Am. Soc. Nephrol.* **20**, 1053–67 (2009).

233. Stolk, J., Broekman, W., Mauad, T., Zwaginga, J.J., Roelofs, H., Fibbe ,W.E., Oostendorp, J.,

Bajema, I., Versteegh, M.I., Taube, C. & Hiemstra, P.S. A phase I study for intravenous autologous mesenchymal stromal cell administration to patients with severe emphysema. *QJM An Int. J. Med.* **109**, 331–336 (2016).

234. Weiss, D. J., Casaburi, R., Flannery, R., LeRoux-Williams, M. & Tashkin, D. P. A Placebo-Controlled, Randomized Trial of Mesenchymal Stem Cells in COPD. *Chest* **143**, 1590–1598 (2013).

235. Panés, J., García-Olmo, D., Van Assche, G., Colombel, J.F., Reinisch, W., Baumgart D.C., Dignass, A., Nachury, M., Ferrante, M., Kazemi-Shirazi, L., Grimaud, J.C., de la Portilla, F., Goldin, E., Richard, M.P., Leselbaum, A. & Danese, S.; ADMIRE CD Study Group Collaborators. Expanded allogeneic adipose-derived mesenchymal stem cells (Cx601) for complex perianal fistulas in Crohn's disease: a phase 3 randomised, double-blind controlled trial. *Lancet (London, England)* **388**, 1281–1290 (2016).

236. Forbes, G.M., Sturm, M.J., Leong, R.W., Sparrow, M.P., Segarajasingam, D., Cummins, A.G., Phillips, M. & Herrmann, R.P. A phase 2 study of allogeneic mesenchymal stromal cells for luminal Crohn's disease refractory to biologic therapy. *Clin. Gastroenterol. Hepatol.* **12**, 64–71 (2014).

237. Swaminathan, M., Stafford-Smith, M., Chertow, G.M., Warnock D.G., Paragamian, V., Brenner, R.M., Lellouche, F., Fox-Robichaud, A., Atta, M.G., Melby, S., Mehta, R.L., Wald, R., Verma, S. & Mazer, C.D; ACT-AKI investigators. Allogeneic mesenchymal stem cells for treatment of AKI after cardiac surgery. *J. Am. Soc. Nephrol.* **29**, 260–267 (2018).

238. Hartner, A., Cordasic, N., Klanke, B., Veelken, R. & Hilgers, K. F. Strain differences in the development of hypertension and glomerular lesions induced by deoxycorticosterone acetate salt in mice. *Nephrol. Dial. Transplant.* **18**, 1999–2004 (2003).

239. Hoover-Plow, J.L., Gong, Y., Shchurin, A., Busuttil, S.J., Schneeman, T.A. & Hart, E. Strain and model dependent differences in inflammatory cell recruitment in mice. *Inflamm. Res.* **57**, 457 (2008).

240. Scarfe, L., Rak-Raszewska, A., Geraci, S., Darssan, D., Sharkey, J., Huang, J., Burton, N.C., Mason, D., Ranjzad, P., Kenny, S., Gretz, N., Lévy, R., Kevin Park, B., García-Fiñana, M., Woolf, A.S., Murray, P. & Wilm, B. Measures of kidney function by minimally invasive techniques correlate with histological glomerular damage in SCID mice with adriamycin-induced nephropathy. *Sci. Reports 2015 51* **5**, 1–13 (2015).

241. Harwood, R., Bridge, J., Ressel, L., Scarfe, L., Sharkey, J., Czanner, G., Kalra, P., Odudu, A., Kenny, S., Wilm, B. & Murray, P. Murine models of renal ischaemia reperfusion injury: An opportunity for refinement using non-invasive monitoring methods. *bioRxiv* 2019.12.17.879742 (2019). doi:10.1101/2019.12.17.879742

242. Scarfe, L., Schock-Kusch, D., Ressel, L., Friedemann, J., Shulhevich, Y., Murray, P., Wilm, B. & de Caestecker, M. Transdermal Measurement of Glomerular Filtration Rate in Mice. *J. Vis. Exp.* **2018**, (2018).

243. Friedemann, J., Heinrich, R., Shulhevich, Y., Raedle M., William-Olsson, L., Pill, J. & Schock-Kusch, D. Improved kinetic model for the transcutaneous measurement of glomerular filtration rate in experimental animals. *Kidney Int.* **90**, 1377–1385 (2016).

244. Schreiber, A., Shulhevich, Y., Geraci, S., Hesser, J., Stsepankou, D., Neudecker, S., Koenig, S., Heinrich, R., Hoecklin, F., Pill, J., Friedemann, J., Schweda, F., Gretz, N. & Schock-Kusch, D. Transcutaneous measurement of renal function in conscious mice. *Am. J. Physiol. Renal*

Physiol. **303**, (2012).

245. Lim, J.P., Leung, B.P., Ding, Y.Y., Tay, L., Ismail, N.H., Yeo, A., Yew, S. & Chong, M.S. Monocyte chemoattractant protein-1: a proinflammatory cytokine elevated in sarcopenic obesity. *Clin. Interv. Aging* **10**, 605 (2015).

246. Jang, H.R., Park, J.H., Kwon, G.Y., Lee, J.E., Huh, W., Jin, H.J., Choi, S.J., Oh, W., Oh, H.Y. & Kim, Y.G. Effect of preemptive treatment with human umbilical cord blood-derived mesenchymal stem cells on the development of renal ischemia-reperfusion injury in mice. *Am. J. Physiol. Renal Physiol.* **307**, F1149–F1161 (2014).

247. WERNER, S. & GROSE, R. Regulation of Wound Healing by Growth Factors and Cytokines. *Physiol. Rev.* **83**, 835–870 (2003).

248. Cho, D.I., Kim, M.R., Jeong, H.Y., Jeong, H.C., Jeong, M.H., Yoon, S.H., Kim, Y.S. & Ahn, Y. Mesenchymal stem cells reciprocally regulate the M1 / M2 balance in mouse bone marrow-derived macrophages. **46**, e70-9 (2014).

249. Gallucci, R.M., Sugawara, T., Yucesoy, B., Berryann, K., Simeonova, P.P., Matheson, J.M. & Luster, M.I. Interleukin-6 Treatment Augments Cutaneous Wound Healing in Immunosuppressed Mice. *J. Interf. Cytokine Res.* **21**, 603–609 (2001).

250. Gallucci, R.M., Simeonova, P.P., Matheson, J.M., Kommineni, C., Guriel, J.L., Sugawara, T. & Luster, M.I. Impaired cutaneous wound healing in interleukin-6–deficient and immunosuppressed mice. *FASEB J.* **14**, 2525–2531 (2000).

251. Lu, J., Cao, Q., Zheng, D., Sun, Y., Wang, C., Yu, X., Wang, Y., Lee, V.W., Zheng, G., Tan, T.K., Wang, X., Alexander, S.I., Harris, D.C. & Wang, Y. Discrete functions of M2a and M2c macrophage subsets determine their relative efficacy in treating chronic kidney disease. *Kidney Int.* **84**, 745–755 (2013).

252. Menzies, F. M., Henriquez, F. L., Alexander, J. & Roberts, C. W. Sequential expression of macrophage anti-microbial/inflammatory and wound healing markers following innate, alternative and classical activation. *Clin. Exp. Immunol.* **160**, 369–79 (2010).

253. Le Meur, Y., Fixe, P., Aldigier, J. C., Leroux-Robert, C. & Praloran, V. Macrophage colony stimulating factor involvement in uremic patients. *Kidney Int.* **50**, 1007–1012 (1996).

254. Fang, T. C., Pang, C. Y., Chiu, S. C., Ding, D. C. & Tsai, R. K. Renoprotective effect of human umbilical cord-derived mesenchymal stem cells in immunodeficient mice suffering from acute kidney injury. *PLoS One* **7**, (2012).

255. Zhang, Q.Z., Su, W.R., Shi, S.H., Wilder-Smith, P., Xiang, A.P., Wong, A., Nguyen, A.L., Kwon, C.W. & Le A.D. Human gingiva-derived mesenchymal stem cells elicit polarization of m2 macrophages and enhance cutaneous wound healing. *Stem Cells* **28**, 1856–68 (2010).

256. Deng, J., Kohda, Y., Chiao, H., Wang, Y., Hu, X., Hewitt, S.M., Miyaji, T., McLeroy, P., Nibhanupudy, B., Li, S. & Star, R.A. Interleukin-10 inhibits ischemic and cisplatin-induced acute renal injury. *Kidney Int.* **60**, 2118–2128 (2001).

257. Kleinschek, M.A., Owyang, A.M., Joyce-Shaikh, B., Langrish, C.L., Chen, Y., Gorman, D.M., Blumenschein, W.M., McClanahan, T., Brombacher, F., Hurst, S.D., Kastelein, R.A. & Cua, D.J. IL-25 regulates Th17 function in autoimmune inflammation. *J. Exp. Med.* **204**, 161 (2007).

258. Donizetti-Oliveira, C., Semedo, P., Burgos-Silva, M., Cenedeze, M.A., Malheiros, D.M., Reis, M.A., Pacheco-Silva, A. & Câmara, N.O. Adipose Tissue-Derived Stem Cell Treatment Prevents

Renal Disease Progression. *Cell Transplant.* **21**, 1727–1741 (2012).

259. Geng, Y., Zhang, L., Fu, B., Zhang, J., Hong, Q., Hu, J., Li, D., Luo, C., Cui, S., Zhu, F. & Chen, X. Mesenchymal stem cells ameliorate rhabdomyolysis-induced acute kidney injury via the activation of M2 macrophages. *Stem Cell Res. Ther.* **5**, 1–14 (2014).

260. Herrera, M.B., Bussolati, B., Bruno, S., Morando, L., Mauriello-Romanazzi, G., Sanavio, F., Stamenkovic, I., Biancone, L. & Camussi, G. Exogenous mesenchymal stem cells localize to the kidney by means of CD44 following acute tubular injury. *Kidney Int.* **72**, 430–441 (2007).

261. Hesketh, E.E., Czopek, A., Clay, M., Borthwick, G., Ferenbach, D., Kluth, D. & Hughes, J. Renal ischaemia reperfusion injury: a mouse model of injury and regeneration. *J. Vis. Exp.* (2014). doi:10.3791/51816

262. Skrypnyk, N. I., Harris, R. C. & de Caestecker, M. P. Ischemia-reperfusion Model of Acute Kidney Injury and Post Injury Fibrosis in Mice. *J. Vis. Exp.* 50495 (2013). doi:10.3791/50495

263. Guan, Y., Nakano, D., Zhang, Y., Li, L., Tian, Y. & Nishiyama, A. A mouse model of renal fibrosis to overcome the technical variability in ischaemia/reperfusion injury among operators. *Sci. Reports 2019 91* **9**, 1–9 (2019).

264. Wang, H. E., Jain, G., Glassock, R. J. & Warnock, D. G. Comparison of absolute serum creatinine changes versus Kidney Disease: Improving Global Outcomes consensus definitions for characterizing stages of acute kidney injury. *Nephrol. Dial. Transplant* **28**, 1447–1454 (2013).

265. Wei, Q. & Dong, Z. Mouse model of ischemic acute kidney injury: technical notes and tricks. *Am. J. Physiol. Renal Physiol.* **303**, (2012).

266. Harwood, R., Bridge, J., Ressel, L., Scarfe, L., Sharkey, J., Czanner, G., Kalra, P.A., Odudu, A., Kenny, S., Wilm, B. & Murray, P. Murine models of renal ischemia reperfusion injury: An opportunity for refinement using noninvasive monitoring methods. *Physiol. Rep.* **10**, (2022).

267. Harwood, R. Investigating the physiology of ischaemia reperfusion injury of the mouse kidney and the efficacy of regenerative medicine therapies after acute kidney injury. (2021). PhD thesis, University of Liverpool.

268. Zoehler, B., Fracaro, L., Boldrini-Leite, L.M., da Silva, J.S., Travers, P.J., Brofman, P.R.S., Bicalho, M.D.G. & Senegaglia, A.C. HLA-G and CD152 Expression Levels Encourage the Use of Umbilical Cord Tissue-Derived Mesenchymal Stromal Cells as an Alternative for Immunosuppressive Therapy. *Cells* **11**, (2022).

269. Munoz, J. R., Stoutenger, B. R., Robinson, A. P., Spees, J. L. & Prockop, D. J. Human stem/progenitor cells from bone marrow promote neurogenesis of endogenous neural stem cells in the hippocampus of mice. *Proc. Natl. Acad. Sci. U. S. A.* **102**, 18171–6 (2005).

270. Bernardo, M.E., Ball, L.M., Cometa, A.M., Roelofs, H., Zecca, M., Avanzini, M.A., Bertaina, A., Vinti, L., Lankester, A., Maccario, R., Ringden, O., Le Blanc, K., Egeler, R.M., Fibbe, W.E. & Locatelli, F. Co-infusion of ex vivo-expanded, parental MSCs prevents life-threatening acute GVHD, but does not reduce the risk of graft failure in pediatric patients undergoing allogeneic umbilical cord blood transplantation. *Bone Marrow Transplant.* **46**, 200–207 (2011).

271. Duffield, J.S., Park, K.M., Hsiao L.L., Kelley, V.R., Scadden, D.T., Ichimura, T. & Bonventre, J.V. Restoration of tubular epithelial cells during repair of the postischemic kidney occurs independently of bone marrow-derived stem cells. *J. Clin. Invest.* **115**, 1743 (2005).

272. Kim, M.G., Yang, J., Ko, Y.S., Lee, H.Y., Oh, S.W., Cho, W.Y. & Jo, S.K. Impact of aging on transition of acute kidney injury to chronic kidney disease. *Sci. Reports 2019 91* **9**, 1–11 (2019).

273. Olmes, G., Büttner-Herold, M., Ferrazzi, F., Distel, L., Amann, K. & Daniel, C. CD163+ M2c-like macrophages predominate in renal biopsies from patients with lupus nephritis. *Arthritis Res. Ther.* **18**, 1–16 (2016).

274. Cao, Q., Harris, D. C. H. & Wang, Y. Macrophages in kidney injury, inflammation, and fibrosis. *Physiology (Bethesda).* **30**, 183–194 (2015).

275. Martinez, F. O., Helming, L. & Gordon, S. Alternative activation of macrophages: an immunologic functional perspective. *Annu. Rev. Immunol.* **27**, 451–483 (2009).

276. dos Anjos Cassado, A. F4/80 as a major macrophage marker: The case of the peritoneum and spleen. *Results Probl. Cell Differ.* **62**, 161–179 (2017).

277. Li, L., Huang, L., Sung, S.S., Vergis, A.L., Rosin, D.L., Rose, C.E. Jr, Lobo, P.I. & Okusa, M.D. The chemokine receptors CCR2 and CX3CR1 mediate monocyte/macrophage trafficking in kidney ischemia–reperfusion injury. *Kidney Int.* **74**, 1526 (2008).

278. Guo, S., Wietecha, T.A., Hudkins, K.L, Kida, Y. & Spencer, MW, Pichaiwong W, Kojima I, Duffield JS, Alpers CE. Macrophages are essential contributors to kidney injury in murine cryoglobulinemic membranoproliferative glomerulonephritis. *Kidney Int.* **80**, 946–958 (2011).

279. Lu, L., Faubel, S., He, Z., Andres Hernando, A., Jani, A., Kedl, R. & Edelstein, C.L. Depletion of Macrophages and Dendritic Cells in Ischemic Acute Kidney Injury. *Am. J. Nephrol.* **35**, 181–190 (2012).

280. Lumeng, C. N., Delproposto, J. B., Westcott, D. J. & Saltiel, A. R. Phenotypic switching of adipose tissue macrophages with obesity is generated by spatiotemporal differences in macrophage subtypes. *Diabetes* **57**, 3239–3246 (2008).

281. Yu, Y.R., O'Koren., E.G., Hotten, D.F., Kan, M.J., Kopin, D., Nelson, E.R., Que, L. & Gunn, M.D. A Protocol for the Comprehensive Flow Cytometric Analysis of Immune Cells in Normal and Inflamed Murine Non-Lymphoid Tissues. *PLoS One* **11**, e0150606 (2016).

282. Askew, D. & Clifford, V. Antigen processing and CD 24 expression determine antigen presentation by splenic CD 4 + and CD 8 + dendritic cells. doi:10.1111/j.1365-2567.2007.02711.x

283. Porta, C., Riboldi, E., Ippolito, A. & Sica, A. Molecular and epigenetic basis of macrophage polarized activation. *Semin. Immunol.* **27**, 237–248 (2015).

284. Ingersoll, M.A., Spanbroek, R., Lottaz, C., Gautier, E.L., Frankenberger, M., Hoffmann, R., Lang, R., Haniffa, M., Collin, M., Tacke, F., Habenicht, A.J., Ziegler-Heitbrock, L. & Randolph, G.J. Comparison of gene expression profiles between human and mouse monocyte subsets. *Blood* **115**, e10 (2010).

285. Macrophages & their Markers | Bio-Rad. Available at: https://www.bio-rad-antibodies.com/macrophage-m1-m2-tam-tcr-cd169-cd-markers-antibodies.html. (Accessed: 19th October 2018)

286. Nahrendorf, M., Swirski, F.K., Aikawa, E., Stangenberg, L., Wurdinger, T., Figueiredo, J.L., Libby, P., Weissleder, R. & Pittet, M.J. The healing myocardium sequentially mobilizes two monocyte subsets with divergent and complementary functions. *J. Exp. Med.* **204**, 3037–47

(2007).

287. Martinez, F. O. & Gordon, S. The M1 and M2 paradigm of macrophage activation: time for reassessment. *F1000Prime Rep.* **6**, (2014).

288. Basile, D. P., Donohoe, D. L., Roethe, K. & Mattson, D. L. Chronic renal hypoxia after acute ischemic injury: effects of l -arginine on hypoxia and secondary damage. *Am. J. Physiol. Physiol.* **284**, F338–F348 (2003).

289. Basile, D. P. The endothelial cell in ischemic acute kidney injury: implications for acute and chronic function. *Kidney Int.* **72**, 151–156 (2007).

290. Whyte, C.S., Bishop, E.T., Rückerl, D., Gaspar-Pereira, S., Barker, R.N., Allen, J.E., Rees, A.J. & Wilson, H.M. Suppressor of cytokine signaling (SOCS)1 is a key determinant of differential macrophage activation and function. *J. Leukoc. Biol.* **90**, 845–854 (2011).

291. Kinsey, G. R. The spleen as a bidirectional signal transducer in acute kidney injury. *Kidney Int.* **91**, 1001–1003 (2017).

292. Hiroyoshi, T., Tsuchida, M., Uchiyama, K., Fujikawa, K., Komatsu, T., Kanaoka, Y. & Matsuyama, H. Splenectomy protects the kidneys against ischemic reperfusion injury in the rat. *Transpl. Immunol.* **27**, 8–11 (2012).

293. Gigliotti, J.C., Huang, L., Ye, H., Bajwa, A., Chattrabhuti, K., Lee, S., Klibanov, A.L., Kalantari, K., Rosin, D.L. & Okusa, M.D. Ultrasound prevents renal ischemia-reperfusion injury by stimulating the splenic cholinergic anti-inflammatory pathway. *J. Am. Soc. Nephrol.* **24**, 1451–1460 (2013).

294. Hey, Y. Y. & O'Neill, H. C. Murine spleen contains a diversity of myeloid and dendritic cells distinct in antigen presenting function. *J. Cell. Mol. Med.* **16**, 2611–9 (2012).

295. Lloyd, C. M., Phillips, A. R. J., Cooper, G. J. S. & Dunbar, P. R. Three-colour fluorescence immunohistochemistry reveals the diversity of cells staining for macrophage markers in murine spleen and liver. *J. Immunol. Methods* **334**, 70–81 (2008).

296. Park, J.H., Jang, H.R., Kim, D.H., Kwon, G.Y., Lee, J.E., Huh, W., Choi, S.J., Oh, W., Oh, H.Y. & Kim, Y.G. Early, but not late, treatment with human umbilical cord blood-derived mesenchymal stem cells attenuates cisplatin nephrotoxicity through immunomodulation. *Am. J. Physiol. - Ren. Physiol.* **313**, F984–F996 (2017).

297. Toupet, K., Maumus, M., Luz-Crawford, P., Lombardo, E., Lopez-Belmonte, J., van Lent, P., Garin, M.I, van den Berg, W., Dalemans, W., Jorgensen, C.& Noël, D. Survival and biodistribution of xenogenic adipose mesenchymal stem cells is not affected by the degree of inflammation in arthritis. *PLoS One* **10**, e0114962 (2015).

298. Park, M.J., Lee, S.H., Moon, S.J., Lee, J.A., Lee, E.J., Kim, E.K., Park, J.S., Lee, J., Min, J.K., Kim, S.J., Park, S.H. & Cho, M.L. Overexpression of soluble RAGE in mesenchymal stem cells enhances their immunoregulatory potential for cellular therapy in autoimmune arthritis. *Sci. Rep.* **6**, 35933 (2016).

299. Majumdar, M. K., Thiede, M. A., Haynesworth, S. E., Bruder, S. P. & Gerson, S. L. Human marrow-derived mesenchymal stem cells (MSCs) express hematopoietic cytokines and support long-term hematopoiesis when differentiated toward stromal and osteogenic lineages. *J. Hematother. Stem Cell Res.* **9**, 841–848 (2000).

300. Takizawa, N., Okubo, N., Kamo, M., Chosa, N., Mikami, T., Suzuki, K., Yokota, S., Ibi, M.,

Ohtsuka, M., Taira, M., Yaegashi, T., Ishisaki, A. & Kyakumoto, S. Bone marrow-derived mesenchymal stem cells propagate immunosuppressive/anti-inflammatory macrophages in cell-to-cell contact-independent and -dependent manners under hypoxic culture. *Exp. Cell Res.* **358**, 411–420 (2017).

301. Chen, Y.T., Sun, C.K., Lin, Y.C., Chang, L.T., Chen, Y.L., Tsai, T.H., Chung, S.Y., Chua, S., Kao, Y.H., Yen, C.H., Shao, P.L., Chang, K.C., Leu, S. & Yip, H.K. Adipose-derived mesenchymal stem cell protects kidneys against ischemia-reperfusion injury through suppressing oxidative stress and inflammatory reaction. *J. Transl. Med.* **9**, 51 (2011).

302. Eirin, A., Zhu, X.Y., Krier, J.D., Tang, H., Jordan, K.L., Grande, J.P., Lerman, A., Textor, S.C. & Lerman, L.O. Adipose tissue-derived mesenchymal stem cells improve revascularization outcomes to restore renal function in swine atherosclerotic renal artery stenosis. *Stem Cells* **30**, 1030–41 (2012).

303. Boomsma, R. A. & Geenen, D. L. Mesenchymal Stem Cells Secrete Multiple Cytokines That Promote Angiogenesis and Have Contrasting Effects on Chemotaxis and Apoptosis. *PLoS One* **7**, 35685 (2012).

304. Cao, C., Tarlé, S. & Kaigler, D. Characterization of the immunomodulatory properties of alveolar bone-derived mesenchymal stem cells. *Stem Cell Res. Ther.* **11**, 1–13 (2020).

305. Munshi, R., Johnson, A., Siew, E.D., Ikizler, .TA., Ware, L.B., Wurfel, M.M., Himmelfarb, J. & Zager, R.A. MCP-1 Gene Activation Marks Acute Kidney Injury. *J. Am. Soc. Nephrol.* **22**, 165 (2011).

306. Gschwandtner, M., Derler, R. & Midwood, K. S. More Than Just Attractive: How CCL2 Influences Myeloid Cell Behavior Beyond Chemotaxis. *Front. Immunol.* **10**, 2759 (2019).

307. Bender, A. T., Ostenson, C. L., Giordano, D. & Beavo, J. A. Differentiation of human monocytes in vitro with granulocyte–macrophage colony-stimulating factor and macrophage colony-stimulating factor produces distinct changes in cGMP phosphodiesterase expression. *Cell. Signal.* **16**, 365–374 (2004).

308. Tögel, F., Hu, Z., Weiss, K., Isaac, J., Lange, C. & Westenfelder, C. Administered mesenchymal stem cells protect against ischemic acute renal failure through differentiation-independent mechanisms. *Am. J. Physiol. Physiol.* **289**, F31–F42 (2005).

309. Harwood, R., Bridge, J., Ressel, L., Scarfe, L., Sharkey, J., Czanner, G., Kalra, P.A., Odudu, A., Kenny, S., Wilm, B. & Murray, P. Murine models of renal ischemia reperfusion injury: An opportunity for refinement using noninvasive monitoring methods. *Physiol. Rep.* **10**, (2022).

310. Kim, M., Erickson, I.E., Huang, A.H., Garrity, S.T. & Mauck, R.L, Steinberg, DR. Donor Variation and Optimization of Human Mesenchymal Stem Cell Chondrogenesis in Hyaluronic Acid. *Tissue Eng. Part A* **24**, 1693 (2018).

311. Stroncek, D.F., Jin, P., McKenna, D.H., Takanashi, M., Fontaine, M.J., Pati, S., Schäfer, R., Peterson, E., Benedetti, E. & Reems, J.A. Human Mesenchymal Stromal Cell (MSC) Characteristics Vary Among Laboratories When Manufactured From the Same Source Material: A Report by the Cellular Therapy Team of the Biomedical Excellence for Safer Transfusion (BEST) Collaborative. *Front. Cell Dev. Biol.* **8**, 458 (2020).

312. Fu, Y., Tang, C., Cai, J., Chen, G., Zhang, D. & Dong, Z. Mechanism and Treatment of Renal Fibrosis: Rodent models of AKI-CKD transition. *Am. J. Physiol. - Ren. Physiol.* **315**, F1098 (2018).

313. Harwood, R., Bridge, J., Ressel, L., Scarfe, L., Sharkey, J., Czanner, G., Kalra, P.A., Odudu, A., Kenny, S., Wilm, B. & Murray, P. Murine models of renal ischemia reperfusion injury: An opportunity for refinement using noninvasive monitoring methods. *Physiol. Rep.* **10**, (2022).

314. Lee, H.T., Kim, M., Kim, M., Kim, N., Billings, F.T. 4th, D'Agati, V.D. & Emala, C.W Sr. Isoflurane protects against renal ischemia and reperfusion injury and modulates leukocyte infiltration in mice. *Am. J. Physiol. Renal Physiol.* **293**, (2007).

315. Athiraman, U., Dhar, R., Jayaraman, K., Karanikolas, M., Helsten, D., Yuan, J., Lele, A.V., Rath, G.P., Tempelhoff, R., Roth, S. & Zipfel, G.J. Conditioning Effect of Inhalational Anesthetics on Delayed Cerebral Ischemia After Aneurysmal Subarachnoid Hemorrhage. *Neurosurgery* **88**, 394 (2021).

316. Constantinides, C., Mean, R. & Janssen, B. J. Effects of Isoflurane Anesthesia on the Cardiovascular Function of the C57BL/6 Mouse. *ILAR J.* **52**, e21 (2011).

317. Kim, M., Ham, A., Kim, J.Y., Brown, K.M., D'Agati, V.D. & Lee, H.T. The volatile anesthetic isoflurane induces ecto-5'-nucleotidase (CD73) to protect against renal ischemia and reperfusion injury. *Kidney Int.* **84**, 90–103 (2013).

318. Belkaid, Y. & Hand, T. W. Role of the Microbiota in Immunity and inflammation. *Cell* **157**, 121 (2014).

319. Wu, H. J. & Wu, E. The role of gut microbiota in immune homeostasis and autoimmunity. *Gut Microbes* **3**, 4 (2012).

320. Zheng, D., Liwinski, T. & Elinav, E. Interaction between microbiota and immunity in health and disease. *Cell Res. 2020 306* **30**, 492–506 (2020).

321. Org, E. & Lusis, A. J. Using the natural variation of mouse populations to understand host-gut microbiome interactions. *Drug Discov. Today. Dis. Models* **28**, 61 (2018).

322. Hufeldt, M. R., Nielsen, D. S., Vogensen, F. K., Midtvedt, T. & Hansen, A. K. Variation in the Gut Microbiota of Laboratory Mice Is Related to Both Genetic and Environmental Factors. *Comp. Med.* **60**, 336 (2010).

323. Nakade, Y., Iwata, Y., Furuichi, K., Mita, M., Hamase, K., Konno, R., Miyake, T., Sakai, N., Kitajima, S., Toyama, T., Shinozaki, Y., Sagara, A., Miyagawa, T., Hara, A., Shimizu, M., Kamikawa, Y., Sato, K., Oshima, M., Yoneda-Nakagawa, S., Yamamura, Y., Kaneko, S., Miyamoto, T., Katane, M., Homma, H., Morita, H., Suda, W., Hattori, M. & Wada, T. Gut microbiota–derived D-serine protects against acute kidney injury. *JCI Insight* **3**, (2018).

324. Gong, J., Noel, S., Pluznick, J. L., Hamad, A. R. A. & Rabb, H. Gut microbiota-kidney cross-talk in acute kidney injury. *Semin. Nephrol.* **39**, 107 (2019).

325. Sato, Y. & Yanagita, M. Immune cells and inflammation in AKI to CKD progression. *Am. J. Physiol. Renal Physiol.* **315**, F1501–F1512 (2018).

326. Borges da Silva, Tamiris (2021*) Investigation of the immunomodulatory effects of MSC-derived extracellular vesicles on human monocyte-derived macrophages*. PhD thesis, University of Liverpool.

.